Titre: Title:	Small-Scale Fire Resistance Evaluation of Carbon Fibers and their Composites
Auteur: Author:	Pablo Chavez Gomez
Date:	2022
Type:	Mémoire ou thèse / Dissertation or Thesis
Référence: Citation:	Chavez Gomez, P. (2022). Small-Scale Fire Resistance Evaluation of Carbon Fibers and their Composites [Thèse de doctorat, Polytechnique Montréal]. PolyPublie. https://publications.polymtl.ca/10523/

URL de PolyPublie: PolyPublie URL:	https://publications.polymtl.ca/10523/
Directeurs de recherche: Advisors:	Louis Laberge Lebel, & Étienne Robert
Programme: Program:	PhD.

POLYTECHNIQUE MONTRÉAL
affiliée à l'Université de Montréal

Small-scale fire resistance evaluation of carbon fibers and their composites

PABLO CHAVEZ GOMEZ
Département de génie mécanique

Thèse présentée en vue de l'obtention du diplôme de *Philosophiæ Doctor*
Génie mécanique

Août 2022

POLYTECHNIQUE MONTRÉAL
affiliée à l'Université de Montréal

Cette thèse intitulée :

Small-scale fire resistance evaluation of carbon fibers and their composites

présentée par **Pablo CHAVEZ GOMEZ**
en vue de l'obtention du diplôme de *Philosophiæ Doctor*
a été dûment acceptée par le jury d'examen constitué de :

Myriam BROCHU, présidente
Louis LABERGE LEBEL, membre et directeur de recherche
Étienne ROBERT, membre et codirecteur de recherche
Gabriel LAPLANTE, membre
Baljinder KANDOLA, membre externe

DEDICATION

. . . Not I, not any one else can travel that road for you,
You must travel it for yourself...

Walt Whitman, Song of Myself, 46

ACKNOWLEDGEMENTS

First and foremost, I would like to thank my thesis director and co-director, professors Louis Laberge Lebel and Étienne Robert. Their continuous support, guidance and patience have been key players in this research project. Every time that I had an idea, whichever it was, I was given nothing but encouragement and constructive feedback. It is a honour for me to be evaluated by professors Myriam Brochu, Baljinder Kandola, and Gabriel LaPlante. Thanks for accepting to be part of the Jury that evaluates the present dissertation. I am also extremely grateful to the Consejo Nacional de Ciencia y Tecnología (CONACYT) from Mexico for funding my graduate studies with a scholarship that started a couple of years before the beginning of the doctoral project until December 2020.

I also want to thank the partners of the CRIAQ/CARIC ENV-708 project for supporting this project, specially to people that I had the chance to interact with on a constant basis: Barry Barnett and Jason Hamp from Pratt & Whitney Canada, Billy Cheng from COMTEK Advanced Structures, Clyde Sharpe, Paulo Arruda, Alain Richer and Émilie Maillet from Elasto Proxy, and Simon Hind from the National Research Council Canada (NRC). This research project also pushed me to knock several doors while exploring materials as wells as fabrication and characterization techniques. I would like to thank Robin Dubé, Bruno Croteau-Labouly and Alexandre Chagnon from the Centre Technologique en Aérospatiale (CTA) for supporting the fabrication of composite laminates, which were possible thanks to the donation of prepreg rolls by Kevin Dupuis from Bombardier Aerospace. Moreover, thanks a lot to the *endless* list of material suppliers that donated material samples, making this project possible.

Thanks to Polytechnique staff for providing support in challenging technical tasks: Christian-Charles Martel for helping me with the fabrication and machining of composites, and Philippe Massé for his continuous support and advice in the combustion lab. Thanks to the secretaries Jacinthe Dubé, Hélène Coulibaly and Fadila Filali as well as the staff from the reception dock Gilbert Trudeau, Alain Papineau, François Bellemare and Philippe Latreille who helped me to order, ship and receive materials & tools on a constant basis. I am also grateful to Marie-Noëlle Fleury, who saved us several times with carpentry tasks. Thanks to the research associates Isabelle Nowlan, Kambiz Chizari, Matthieu Gauthier, Roland Fotsing (from Polytechnique); Hatem Titi, Lucy Riffard and Petr Fiurasek (from McGill). You all helped me to complete my experimental plan. I apologize for the equipment that, in some cases and *by sheer coincidence*, broke down while I was around. Go figure!

I would like to thank Julieta Barroeta and Behnam Ashrafi from the NRC for recently giving me the opportunity to collaborate with them on very cool research topics while working on this dissertation in parallel. Their patience and support are highly appreciated.

Thanks a lot to the folks from the ACFSLab and LÉMUR groups. A *ginormous* shout-out to Tanja Pelzmann and Jean Langot for their friendship and support throughout our shared research project, as well as to Cristian Boantă, a.k.a. *santo padre* (ironic). The beers, trips, experimental sessions, philosophical discussions, and infinite coffee made these last years unforgettable. Un gros merci à Olivier Jobin et Benoît Dumas, for sharing their knowledge about rockets and their *passion* for kitschy graphical abstracts, weird ISO standards and teaching me some cool experimental techniques. Shokran Elie Antar and Antonella Succar for the ping pong sessions. Elie, please remember that there is no such thing as a stupid question. Thanks to Felix Lessard for the enriching discussions about composites and stuff that simply did not work in our experimental plans. To the rest of the gang in both labs, I apologize for not mentioning individual names. Otherwise, the acknowledgements would be as long as Article #1 (!!!). Thank you all for making every day an awesome day!

From other labs and groups from academia, thanks to Benjamin Barrouillet and Stefane Sved for the squash sessions. I am grateful to the members of the CREPEC student committee (Mélanie Girard, Fatma Ben Dieb, Mahdi Mejri, Manon Favre, Floriane Miquet-Westphal, Simon Sánchez Díaz, Sidharth Sarojini Narayana, Saoussen Gammoudi, Camille Verne) for their support while organizing events, as well as Carole-Anne de Caroufel and Diane Héroux for supporting such activities. A shout-out to Adam Smith (the composites man, not the economic theorist) for pushing me out of my comfort zone. Danke schön Martin Luckabauer for the nice discussions about airplanes. Merci Jacques Lengaigne for cracking the whip while I was working on this thesis.

Thanks to my friends in Mexico and in Montreal for putting up with my erratic schedules. Special thanks to my former flatmates: Julio Mendez, for turning the idea of pursuing a PhD into reality, and Ryley Evans, for sharing stories, bagels and beers. I have gotten the right to call people "mate"!

I will be forever indebted to my family, papá, mamá & Nancy. Your love and support have been a lighthouse in this storm called life. Hopefully we will meet again in another time/galaxy/dimension. To the rest of my family, ¡muchas gracias!. Your continuous support and love have made this possible. Last, but never the least, I would like to thank my wife, Diana. Her love, patience and support have helped me to become a better person and to bring this project to fruition. Gracias por hacerme crecer. Te amo, Hermosa.

RÉSUMÉ

De nos jours, l'utilisation des matériaux composites à matrice organique (CMO) en aéronautique est bien établie. La possibilité d'ajuster leurs propriétés leur donne un avantage sur les alliages traditionnels, permettant aux concepteurs d'avions de concevoir des structures de plus en plus légères. Cependant, la plupart de leurs constituants sont intrinsèquement inflammables ou sensibles aux températures élevées et, surtout, aux conditions oxydantes. Il est donc impératif de comprendre le comportement des CMO et de leurs éléments constitutifs dans les conditions agressives rencontrées lors des incendies d'avion. Ces conditions constituent une menace sérieuse pour la navigabilité et, par conséquent, la sécurité des passagers.

Compte tenu de l'omniprésence des CMO dans les avions modernes, en particulier les structures à base de fibre de carbone (FC), deux principaux défis ont été identifiés concernant leur résistance au feu. Premièrement, les réglementations et les normes d'évaluation spécifient la température de la flamme, le flux de chaleur, le type de combustible et la durée pour diverses applications finales, mais l'influence de la chimie de la flamme n'est que rarement prise en compte. A cet égard, la recherche fondamentale sur l'oxydation des matériaux à base de carbone s'est majoritairement appuyée sur des techniques thermoanalytiques, fours ou réacteurs sous atmosphères contrôlées. Par conséquent, la connaissance détaillée du comportement oxydatif des FC dans des conditions d'incendie réelles est rare. Deuxièmement, on ne connait toujours pas quelles caractéristiques de conception des structures CMO jouent un rôle essentiel dans leur résistance au feu. Pour répondre à ces enjeux, ce travail s'intéresse aux phénomènes physico-chimiques et mécaniques impliqués dans l'interaction CMO/feu à différentes échelles. Trois objectifs ont été définis en conséquence : (1) développer une méthodologie de conception et d'évaluation à faible coût pour les CMO résistants au feu validée par des tests à petite échelle, (2) déterminer l'effet du feu et des charges mécaniques sur la défaillance des FC, et (3) identifier les paramètres clés du processus d'endommagement des FC lorsqu'elles sont exposées au feu.

La thèse traite du premier objectif de manière pratique. Une méthodologie en quatre étapes a été proposée pour la conception et l'évaluation de configurations CMO légères et résistantes au feu. Pour la phase initiale, c'est-à-dire le design conceptuel, l'approche connue sous le nom de *conception axiomatique* a été introduite comme un outil pour traduire les besoins du client en exigences fonctionnelles, puis en paramètres de conception et de processus nécessaires pour obtenir le produit final. La deuxième étape, la sélection initiale des matériaux,

est basée sur des pratiques de conception standard et résumée dans un ensemble de directives de conception. La troisième étape, étant clé de la méthodologie, a présenté une approche d'évaluation thermomécanique à petite échelle. La dernière étape concernait la mise en œuvre de la logique floue pour gérer à la fois des exigences et critères d'évaluation précis et vagues, c'est-à-dire des données quantitatives et qualitatives, ainsi qu'un outil d'aide à la décision (OAD) multicritère pour classer les candidats tout en tenant compte de la préférence du concepteur. Ce dernier ensemble d'outils a permis de sélectionner le meilleur matériau candidat en tenant compte de plusieurs critères et priorités hétérogènes. Une étude de cas d'un carter de moteur d'avion a été présentée comme exemple d'application de cette méthodologie.

Le deuxième objectif a été couvert par l'étude du rôle de la chimie de la flamme et de la microstructure des fibres dans le processus de rupture des mèches de FC à base de polyacrylonitrile chargées en traction. Un brûleur à flamme plate (BFP) fournissant des flammes prémélangées en méthane/air avec différents rapports de mélange combustible/oxydant (ϕ) a été utilisé pour déterminer le temps de défaillance (TDD), sélectionné comme indicateur de résistance au feu. Les valeurs de TDD ont considérablement varié entre les flammes sous de faibles charges de traction, les différences devenant moins importantes avec l'augmentation des charges. Le mélange stœchiométrique ($\phi = 1.0$) a produit la condition la moins agressive, suivi de la flamme riche ($\phi = 1.2$) qui a modérément accéléré la rupture des mèches. Contrairement au mélange stœchiométrique, la flamme pauvre a donné des valeurs de TDD jusqu'à $\sim$50 % inférieures, confirmant l'agressivité accrue des flammes riches en oxygène. Les résultats ont également révélé une résistance à l'oxydation significativement plus élevée des FC à module élevé par rapport à leurs homologues à module inférieur, grâce à une différence d'un ordre de grandeur dans le TDD. Les données thermoanalytiques n'ont pas montré une différence aussi radicale. Les analyses au microscope électronique à balayage (MEB) ont suggéré l'influence de la corrosion par piqûres, ou *pitting*, sur la rapidité de défaillance, les piqûres visibles dépassant la taille critique des défauts.

Le troisième objectif a été abordé en approfondissant le processus d'oxydation des FC induite par la flamme. L'influence du feu et des impuretés sur le *pitting* a été étudiée au moyen d'insertions contrôlées et séquentielles de fibres dans les flammes suivies d'analyses au MEB, révélant deux mécanismes supplémentaires : la création des canaux, ou *channelling*, et l'endommagement amorphe. Les taux de croissance du *pitting* ont été déterminés en suivant des groupes de piqûres sélectionnés. Leur origine a été attribuée à des défauts structuraux et, surtout, à des impuretés hautement réactives détectées par activation neutronique et confirmées par spectroscopie de rayons X à dispersion d'énergie. Les résultats mettent en évidence les différences de taux d'oxydation entre la flamme et les conditions d'atmosphère contrôlée, ainsi que les différents effets des impuretés sur l'oxydation des fibres, c'est-à-dire la catalyse,

la mobilité et la stabilisation.

L'impact attendu de ce travail est multiple. Les concepteurs d'avions ont maintenant à leur disposition une méthodologie de conception et d'évaluation à faible coût des matériaux composites ignifuges. Les résultats devraient également déclencher des discussions significatives au sein de la communauté de la sécurité incendie des aéronefs, soulignant l'importance de la chimie de la flamme, de la microstructure et composition des FC ainsi que de la configuration des matériaux composites dans la résistance au feu. Du point de vue de la recherche appliquée, les modèles informatiques peuvent bénéficier des nouvelles connaissances sur le processus d'endommagement des FC pour des prédictions plus précises. De plus, le cadre d'évaluation des matériaux fournira aux concepteurs d'aéronefs un ensemble d'outils pour la sélection de configurations composites résistantes au feu. Des structures légères avec une résistance au feu améliorée peuvent désormais être conçues en utilisant une approche systématique et à bas coût.

ABSTRACT

Polymer matrix composites (PMCs) have revolutionized the aviation industry. The ability to customize their properties gives them an advantage over traditional alloys, enabling aircraft designers to conceive increasingly lighter structures. However, most of their constituents are inherently flammable or susceptible to high temperatures and oxidizing conditions. Since fire poses a serious threat to airworthiness and, consequently, passenger safety, it is crucial to understand the behavior of PMCs and their constitutive elements under the highly aggressive conditions encountered during fires.

Given the ubiquity of PMCs in modern aircraft, especially carbon fiber (CF)-based structures, two main challenges were identified pertaining to their fire resistance. First, regulations and evaluation standards specify the flame temperature, heat flux, fuel type, and duration for various final applications, yet the influence of the flame chemistry is only rarely considered. In this regard, basic research on the oxidation of carbonaceous materials has mostly relied on thermoanalytical techniques, furnaces or reactors under controlled atmospheres. Consequently, detailed knowledge of the oxidative behavior of CFs in true fire conditions is scarce. Second, it remains unclear which design features of PMC laminates play a critical role in their fire resistance. To address these challenges, this work focuses on the physicochemical and mechanical phenomena involved in the PMC/fire interaction at different length scales. Three objectives were defined as a result: (1) develop a resource-efficient design & evaluation methodology for fire-resistant PMCs validated by small-scale tests, (2) determine the effect of fire and mechanical loads on CF failure, and (3) identify the key parameters of the CF damage process when exposed to fire.

The thesis deals with the first objective in a practical manner. A four-stage methodology was proposed towards the design & evaluation of lightweight and fire-resistant PMC configurations. For the initial phase, i.e., conceptual design, Axiomatic Design (AD) was introduced as a tool to translate the customer needs into functional requirements, and subsequently into the design and processes parameters required to achieve the final product. The second stage, initial material screening, is based on standard design practices and summarized in a set of guidelines. The third and key stage of the methodology presented a small-scale evaluation approach. The last stage involved the implementation of fuzzy sets to handle both crisp and vague requirements and scores, i.e., quantitative and qualitative data, as well as a multi-criteria decision making (MCDM) method to rank the candidates while considering the designer's preference. This last set of tools enabled the selection of the best material can-

didate considering several heterogeneous criteria and priorities. A case study of an aircraft engine casing was presented as an application example for the methodology.

The second objective was covered by studying the role of flame chemistry and fiber microstructure in the failure process of loaded polyacrylonitrile (PAN)-based CF bundles. A flat flame burner (FFB) supplying premixed methane/air flames with different fuel/oxidizer ratios (ϕ) was used to determine the time-to-failure (TTF), selected as the indicator of fire resistance. TTF values varied markedly between flames under low tensile loads, with differences becoming less significant with increasing loads. The stoichiometric mixture ($\phi = 1.0$) yielded the least aggressive condition, followed by the fuel-rich flame ($\phi = 1.2$) which moderately accelerated the bundle failure. In contrast with stoichiometric flames, fuel-lean conditions ($\phi = 0.7$) yielded up to $\sim$50 % lower TTF values, confirming the enhanced aggressiveness of oxygen-rich flames. The results also revealed a significantly higher oxidative resistance of high modulus CFs with respect to their lower modulus counterparts, through a one order-of-magnitude difference in TTF. The thermoanalytical data did not show such a radical difference. Scanning electron microscopy (SEM) analyses suggested the influence of pitting on the failure promptness, with visible pits exceeding the critical flaw size.

The third objective was addressed by delving into the flame-induced CF oxidation process. The influence of fire and impurities on pitting was studied by means of controlled and sequential fiber insertion into flames followed by SEM analyses, revealing two additional mechanisms: channelling and amorphous damage. Pit growth rates were determined by tracking selected pit clusters. Their origin was attributed to structural defects and, to a greater extent, highly reactive impurities detected via neutron activation analysis (NAA), and confirmed by energy dispersive X-ray spectroscopy (EDS). The results highlight the differences in oxidation rates between flame and controlled-atmosphere conditions, as well as the different effects of impurities upon fiber oxidation, i.e., catalysis, mobility and hindrance.

The expected impact of this research is manifold. Aircraft designers are now presented with a resource-efficient design and material evaluation methodology. It is also expected to trigger meaningful discussions within the aircraft fire safety community, highlighting the importance of flame chemistry, CF microstructure/composition as well as material composite configuration in fire resistance. From an applied research point of view, computational models can benefit from the new insights into fiber damage towards more accurate predictions. Moreover, the material evaluation framework will provide aircraft designers with a set of tools towards the selection of fire-resistant composite configurations. Lightweight structures with improved and customized fire resistance can be now conceived using a systematic and resource-efficient approach. Ultimately, passengers will benefit from these improvements.

TABLE OF CONTENTS

LIST OF TABLES

LIST OF FIGURES

LIST OF SYMBOLS AND ACRONYMS

AC	advisory circular
ACEE	Aircraft Energy Efficiency
AD	Axiomatic Design
AHP	analytical hierarchy process
APU	auxiliary power unit
AFM	atomic force microscopy
ASA	active surface area
BET	Brunauer-Emmett-Teller
BMI	bismaleimide
BSU	basic structural unit
BT	burn-through
CA	customer attribute
CC	cone calorimeter
CI	confidence interval
CF	carbon fiber
CFR	Code of Federal Regulations
CFRP	carbon fibre reinforced polymer
CMC	ceramic matrix composite
CNT	carbon nanotube
CSM	chopped strand mat
CTA	Centre Technologique en Aérospatiale
d_{002}	interlayer spacing
d_i	internal shell diameter
DP	design parameter
DSC	differential scanning calorimetry
CF	carbon fiber

E_a	activation energy
EASA	European Union Aviation Safety Agency
EDS	energy dispersive X-ray spectroscopy
ESEM	environmental scanning electron microscopy
ETEM	environmental transmission electron microscopy
FAA	Federal Aviation Administration
FFB	flat flame burner
FRP	fiber reinforced polymer
FR	functional requirement
FST	flame, smoke and toxicity
GF	glass fiber
GMM	geometric mean method
GFRP	glass fiber reinforced polymer
HOPG	highly ordered pyrolytic graphite
HRR	heat release rate
HT-SEM	high temperature environmental scanning electron microscopy
HTT	heat treatment temperature
HUR	heat-up rate
HVOF	high velocity oxy Fuel
IF	Impact Factor
ISO	International Organization for Standardization
L_a	lateral size
L_c	stacking height
LCA	life cycle analysis
LOI	limiting oxygen index
LR	load realease
$\mu(x)$	membership function
$\mu_{\tilde{n}}(x)$	membership function
$\mu_{\sqcap}(x)$	trapezoidal membership function

$\mu_{\wedge}(x)$	triangular membership function
MADM	multi-attribute decision making
MCDM	multi-criteria decision making
MCC	micro combustion calorimeter
MDOF	multi-degree of freedom
MGI	Materials Genome Initiative
MMC	metal matrix composite
MWCNT	multi-walled carbon nanotube
NAA	neutron activation analysis
NASA	National Aeronautics and Space Administration
NRC	National Research Council Canada
OEM	original equipment manufacturer
OSU	Ohio State University
P_i	internal pressure
PAN	polyacrylonitrile
PBO	poly(p-phenylene-2,6- benzobisoxazole)
PC	polycarbonate
PEEK	polyether ether ketone
PEI	polyetherimide
PEKK	polyether ketone ketone
PES	poly ether sulphone
PI	polyimide
PIPD	polyhydroquinone-diimidazopyridine
PMC	polymer matrix composite
PPS	poly phenylene sulphide
PP	polypropylene
PV	process variable
PVF	polyvinyl fluoride
PW	plain weave

q	heat flux density
QI	quasi-isotropic
RTM	resin transfer moulding
σ_h	hoop stress
σ_l	longitudinal stress
SDOF	single-degree of freedom
SEM	scanning electron microscopy
SLOWPOKE-2	Safe LOW-POwer Kritical Experiment
SS	stainless steel
STA	simultaneous thermal analysis
STEM	scanning transmission electron microscopy
STM	scanning tunneling microscopy
SWCNT	wingle-walled carbon nanotube
t	shell thickness
T	temperature
T_{ad}	adiabatic temperature
TC	thermocouple
T_{CARS}	non-adiabatic temperature
TEM	transmission electron microscopy
T_g	glass transition temperature
TGA	thermogravimetric analysis
THR	total heat release
T_m	melting point
T_{max}	temperature corresponding to the maximum oxidation rate
$T_{0.5}$	temperature attained at 0.5 fractional burn-off
TOPSIS	Technique for Order of Preference by Similarity to Ideal Solution
TPS	thermal protection system
TSA	total surface area
TRL	technology readiness level

T_{Ta}	Tammann temperature
TTF	time-to-failure
TTI	time-to-ignition
UD	unidirectional
UL	Underwriters Laboratories
UTM	universal testing machine
UTS	ultimate tensile strength
$\mathbf{UTS}_{eq}$	equivalent ultimate tensile strength
VBB	vertical Bunsen burner
VE	vinyl ester
V_f	fiber volume fraction
XRD	X-ray diffraction

LIST OF APPENDICES

CHAPTER 1 INTRODUCTION

Aircraft are the extraordinary result of human ingenuity and, arguably, works of art[1]. However, unlike art, they are the product of a systematic design process driven by performance, cost, safety, manufacturing and, more than ever, environmental considerations. In this regard, the impact of aviation as part of humanity's environmental footprint [2] has brought a set of design constraints that have gained momentum in the conception and fabrication processes of transport aircraft [3]. In the end, due to certification regulations and the airlines' needs, aircraft manufacturers aim for products with the lowest operating cost and highest performance with minimal pollutant generation, without compromising on safety.

The desire for a more efficient aircraft inevitably entails weight reduction, among improvements in other disciplines (e.g., aerodynamics, propulsion). In this quest, manufacturers increasingly rely on polymer matrix composites (PMCs) to design civil and military aircraft. Their properties can be customized to meet structural requirements with lower weight penalties and part counts compared to traditional metallic constructions, hence their extensive use in modern transport aircraft [4, 5]. Nevertheless, some of their major drawbacks include reduced performance at high temperature (T) and inherent flammability for most of their constituents [6]. Their utilization is restricted to low T applications and, in the case of engines, to their "cold" zone [7]. Paradoxically, some PMC-based components need to act as firewalls in case of emergency. Heavy and nonstructural protective means are typically necessary to improve properties under fire, limiting potential weight saving compared to metal construction, and thus reducing fuel efficiency.

With an increasing need for lightweight, cost-efficient and environmentally-friendly PMC-based aircraft structures, several challenges pertaining to fire-safe designs remain to be addressed. The aircraft design process deals with often-conflicting criteria, seeking a compromise solution obtained through iterations. Material selection using standardized fire certification procedures is prohibitively expensive but a systematic design methodology based on a small-scale tests can accelerate the identification of potential solutions using a fraction of the resources. Thermomechanical modelling of PMCs under simulated fire conditions is improving rapidly, although predictive capabilities for the failure mechanisms are still needed. In particular, weakly-reactive reinforcement materials such as carbon fibers (CFs) are often controlling this failure and their behaviour under open flame attack is poorly understood.

[1] "There is a view, held by engineers as different as Brunel and Barnes Wallis, that a design which is functional is automatically beautiful" [1].

1.1 Challenges in the design of fire-resistant PMCs

The types of structures with fire resistance requirements are varied but aircraft powerplants are of special interest. The nature and geometry of their structure is generally restricted by aerodynamic considerations (not applicable to auxiliary power units (APUs)) and Ts encountered within their enclosures, typically leaving little room for protection. Furthermore, the continuous operation of powerplants has to be ensured in certain critical phases, such as take-off and climb, allowing the aircraft to gain altitude and land safely. Accordingly, operation at full thrust is needed, yielding complex mechanical stresses [7]. The specific problem at hand is the fire resistance of sandwich acoustic liners that are required to act as firewalls in case of an accidental in-flight fire, as previously discussed by Hamp and Caulfeild [8]. Fig. 1.1a shows the location of such panels in the fan inlet (hatched area) and the by-pass duct's outer surface (red area). Depending on the desired level of sound attenuation, such panels can have different configurations. Fig. 1.1 shows two typical configurations, i.e., single (SDOF) or multi-degree of freedom (MDOF), featuring one or more honeycomb layers, respectively.

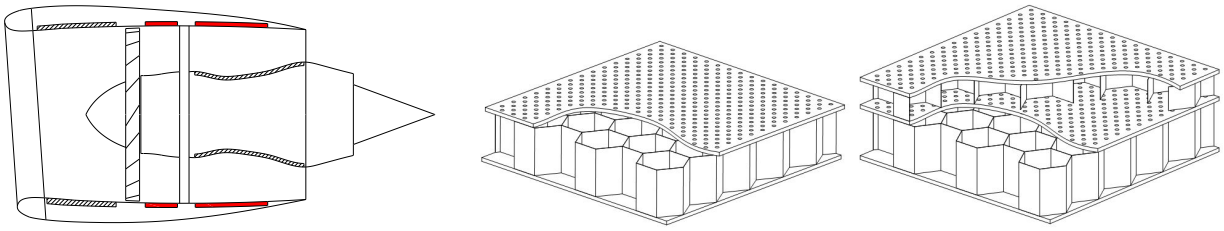

(a) (b)

Figure 1.1 Simplified schematic representation of a turbofan engine and its bypass duct acoustic liners. (b) Typical Configuration of Sandwich Acoustic Panels: SDOF (left) and MDOF (right).

Two main challenges have been identified with respect to the fire resistance of PMCs and, more specifically, of carbon fibre reinforced polymer (CFRP) composites. The first comes from an engineering design standpoint, related to the need for evaluating, selecting and ranking lightweight designs in a resource-efficient fashion. The second relates to a basic research need: understanding the oxidation of CFs-based composites by open flames and the resulting damage process causing subsequent mechanical failure.

1.2 General objectives & expected impact

The objective of this thesis is to enable the development of fire-resistant PMCs by taking advantage of small-scale tests. The challenges presented in §1.1 call for dedicated research spanning different length scales. In the first place, taking into account the different fire resistance requirements that will be described in §2.1.2, it becomes evident that there is no "one size fits all" solution for the selection of fire resistant material systems. Moreover, with current environmental considerations it very important to develop a material selection procedure that can consider relevant criteria, in addition to the more traditional cost-related and technical challenges. These three categories bring different requirements, with levels of importance depending on the stakeholders involved in the design process. Most importantly, as with any design activity, a compromise must be made between conflicting criteria. Thus, a systematic design and evaluation approach that integrates the aforementioned domains is highly desirable and is developed here. Recent works focusing on the design of load-carrying PMCs with improved fire-resistance in electric powerplants [9] illustrate the growing relevance of the topic. These challenges are ubiquitous in any design phase, regardless of the type of organization, and valid in the contexts of fire protection of means of transport, energy, building and infrastructure. Therefore, the impact of the aforementioned methodology is expected to extend beyond aerospace to other engineering domains dealing with the conceptual design of fire-resistant structures.

Second, the present work highlights the necessity of understanding the phenomena involved in the fire resistance of CFRP composites, while addressing the effect of several factors namely flame chemistry, CF type and microstructure, impurity contents, and mechanical loads. The closest related work focusing on fire-induced CF damage dates back to the late 1970s and early 1980s [10–13]. However, those efforts tackled a diametrically opposed problem to fire resistance, i.e., large-scale tests focusing on the complete combustion of CF in a post-crash fire scenario, to alleviate electric and health hazards. Therefore, a research need exists to characterize the thermal degradation of CF under open flame attack, both to understand the chemical and physical changes in the microstructure as well as to quantify the resulting evolution of macroscopic mechanical properties.

1.3 Organization of the thesis

The present thesis comprises eight chapters. The introduction concluding here, i.e, Chapter 1, provides an overview of the challenges faced when designing fire-resistant PMC-based structures. The general engineering and scientific challenges are identified, followed by the

general objectives of the thesis and the structure of the thesis. Chapter 2 starts off by giving an overview of composites, their use in aircraft, and the fire resistance requirements of PMCs considering an aircraft certification context. It reviews the relevant literature on the several aspects pertaining to the fire behavior of PMCs and the phenomena involved. Subsequently, composites design, certification and material selection strategies are presented from aircraft certification and general design standpoints, respectively. The oxidation and combustion of several carbonaceous materials are then extensively analyzed prior to addressing the CF-oxidation problem. The research objectives and the coherence of the subsequent chapters are detailed in Chapter 3. Chapters 4, 5, 6 contain the major findings of the thesis while tackling the challenges presented in §1.1. These Chapters are presented in the form of three peer-reviewed journal articles. Chapter 4 addresses the design of fire-resistant PMCs with focus on small-scale testing, and presents a holistic methodology comprising conceptual design, screening, evaluation and ranking. Delving into smaller scales, Chapters 5 and 6 address the research challenges related to CF oxidation under open flame attack, complementing each other. Conclusions are finally drawn in Chapter 8, complemented by a discussion of the limitations of the present work and opportunities for future research.

CHAPTER 2 LITERATURE REVIEW

The literature review is divided in four major sections. The first part (§2.1) begins by providing a historical perspective of composites and their use in aircraft. Fire safety is subsequently addressed, followed by the fire resistance of PMC-based structures and the evaluation needed as part of the aircraft certification process. The general behavior of PMCs when exposed to fire or heat sources is addressed. It covers the thermal, chemical and physical processes involved in the combustion of PMCs, as well as their thermomechanical behaviour. An overview of fire testing approaches for PMCs is given, focusing on the small-scale evaluation methods aiming at reproducing the conditions described in §2.1.2. Fire protection approaches are subsequently discussed, including integral and parasitic fireproofing means while discussing the traditional approaches to impart fire/high temperature protection. The review includes high-temperature or fireproof material systems deemed capable of replacing or being incorporated into structural components.

The second part (§2.2) addresses the design aspects deemed necessary in the conception of fire-resistant PMCs to be used in aircraft construction. Relevant design and material selection paradigms are reviewed, considering the evaluation aspects of composite-based structures in an aircraft certification context. Tools capable of capturing the vagueness of certain design requirements and evaluation criteria are presented, to enable the fairest selection of design concepts with heterogeneous criteria. Relevant methods and applications of decision-making methods and fuzzy sets are reviewed.

The third part (§2.3) reviews the manufacturing and physical properties of CFs, including the main precursors used for their fabrication, the processing parameters, and the resulting microstructure. These aspects are analyzed towards drawing conclusions about their possible influence in the oxidation at high temperatures in non-inert atmospheres. This part also explores the tensile behavior of CFs, which is the relevant mechanical property when no reinforcing matrix is left, for instance, when its pyrolysis has been completed.

Finally, the fourth part (§2.4) surveys CF oxidation and the phenomena involved in their combustion. The carbon oxidation process is analyzed considering its kinetics and the regimes involved. This information sheds light on the oxidation of the different carbon forms contained in CFs, in contrast to most of the available literature that focuses on other forms of carbon. The role of oxidizing species is presented, followed by the impurities that have an effect on the oxidation process, either enhancing or hindering it. The review ends with the presentation of fire-induced damage and its effects on the mechanical properties of CFs.

2.1 Composites, aircraft and fire

2.1.1 Composites in aircraft structures

An overview of composites used in aircraft is presented in this section together with the associated fire safety issues. The basic concepts of composite materials and their use in aircraft are accompanied by a historical overview. The fire threat in aviation is subsequently addressed, followed by the applicable certification process and the evaluation methods employed therein.

Composite materials

A composite material is the result of joining two or more materials, with bulk properties that differ from those of its individual constituents [14]. Due to their versatility and potential to obtain high specific properties, they have found applications not only in aviation [5], but in diverse domains such as space exploration (e.g. satellite structures, rocket nozzles, thermal protection systems (TPSs)), other transportation sectors (e.g. naval, automotive, rail), energy (e.g. wind turbines and offshore oil platforms), civil infrastructure & architecture (e.g. bridges, building siding), sports (e.g. hockey sticks, ski gear) and musical instruments (e.g. guitars), to name a few [15–17]. They enable designers to achieve form and function that could not be achieved with isotropic materials [18, 19].

PMCs[1] used in structural applications typically contain two basic constituents: reinforcement and a polymer matrix. The role of the reinforcement is to carry the load either in tension or compression, while the function of the matrix is to hold the fibers together, distribute the loads and, in the case of compression, prevent fiber buckling. A third constituent can be found in sandwich configurations where a core is used to increase specific flexural stiffness, energy absorption and impact resistance. Fig. 2.1 shows the evolution of composite materials in history, from the first man-made composites in the mesolithic based on straw and clay to advanced structures relying on polymeric, ceramic and metallic matrices. It also shows that metals were increasingly used for centuries until the 1960s, displacing natural and man-made composites. Since then, ceramics, polymers, and their composites have been gaining momentum owing to improved strength and stiffness at a fraction of the weight of common metals or alloys.

Theoretically, composites can have any custom set of physical properties by mixing two or

[1] This work primarily focuses on polymer matrix composites (PMCs). Composite materials used in aerospace are usually classified based on the nature of their matrix, i.e., polymeric (PMC), ceramic (CMC), or metallic (MMC). Several concepts from CMCs will be extensively borrowed here due to their inherent resistance to high temperature and oxidative conditions.

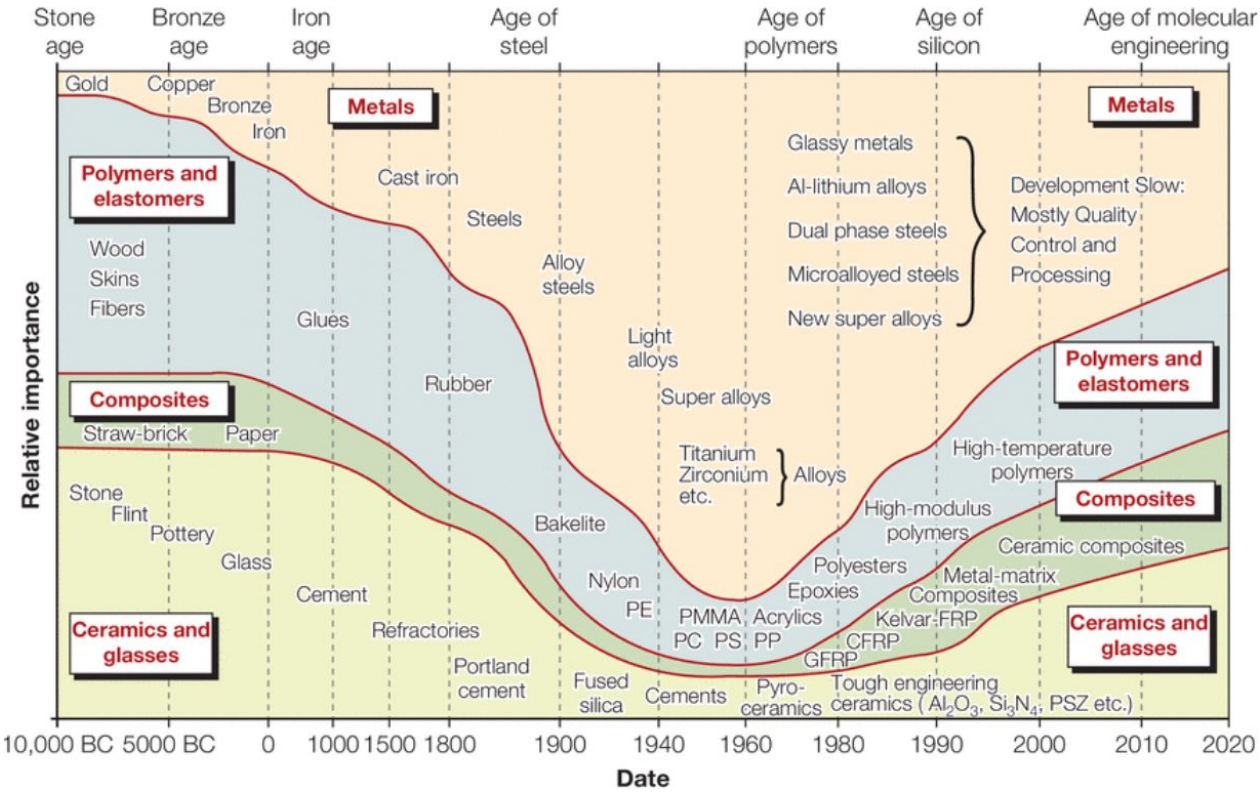

Figure 2.1 The evolution of materials with time (Reprinted from [20], with permission from Elsevier). Composite materials include the first man-made straw-clay blocks through advanced composites with polymer, ceramic and metallic matrices.

more materials [14], though physical and technical limitations exist. Considering the very large number of existing materials, estimated a decade ago to be on the order of $\sim 10^5$ [4, 21], the possible combinations towards useful composites are immense. Furthermore, with the Materials Genome Initiative (MGI) [22], the number of materials available is expected to increase at a high pace. Nonetheless, the design of aircraft structures is highly constrained, for instance by mechanical (strength, stiffness, toughness, fatigue), environmental (corrosion, wear, hygrothermal), manufacturing (material behavior, fabrication method, production volume & rate, tooling) and costs factors (raw materials, processing methods and materials). These constraints result in a significantly smaller pool of materials readily available for aerospace applications.

Composites in aviation

Early aircraft manufacturers relied on composite materials through their use of wood, the natural composite *par excellence* for structural applications. Wood, steel guy wires and

fabrics dominated the aircraft construction in the beginning of modern aviation before the rise of metallic structures, i.e., the first years of the 20th century [23]. Around the same time, in 1907 L. H. Baekeland filed a patent application for a method to affordably produce a phenol formaldehyde resin, later known as Bakelite. This marked not only a turning point towards bonded structures and aircraft composites, but also the beginning of the age of plastics [24]. The concept of bonded primary aircraft structures was later developed through the pioneering work of de Bruyne [25], in search of simpler joining methods. The introduction of PMCs into aircraft structures had to wait until World War II, when concerns about the supply of metals motivated the development of man-made composites [26]. Fig. 2.2a shows the fuselage of a Supermarine Spitfire prototype using a flax fibre / phenolic matrix (Bakelite) system known as 'Gordon Aerolite' [26–28], considered the earliest known application of PMCs in an aircraft structure. The potential of composites was not initially realized, hence the similarity of this design with metallic configurations. Inorganic fibers were later introduced. Some of the earliest examples of these include the asbestos/phenolic matrix prototype wing of the Fairey Delta E10/47 [26] or the Vultee BT-15 trainer which was one of the first aircraft known to incorporate fiberglass/ balsa wood sandwich panels [29].

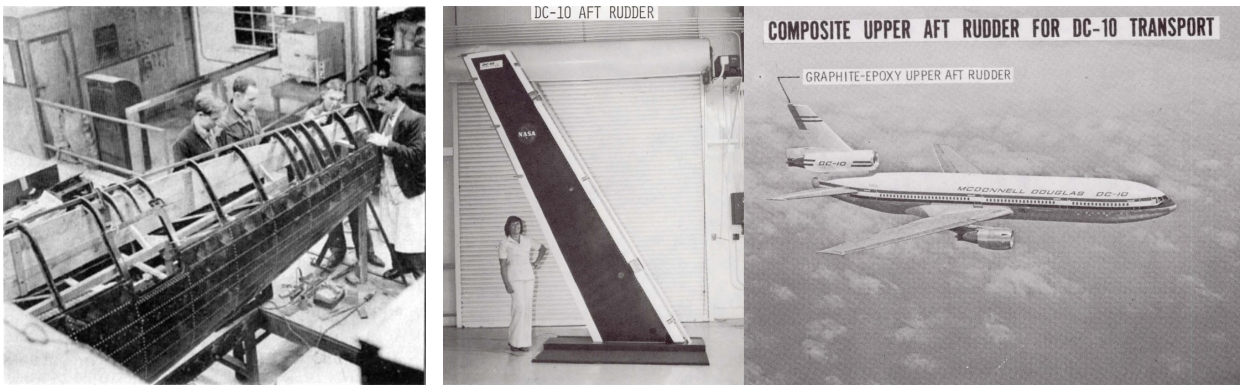

(a) (b)

Figure 2.2 Examples of pioneering composite applications in aircraft: (a) Prototype structure of a Supermarine Spitfire (military) aircraft based on Gordon Aerolite (flax/phenolic) *ca.* 1940 (Reprinted from [28], with permission from Elsevier). (b) Aft rudder of the Douglas DC-10 (commercial) aircraft vertical stabilizer (from [30]).

Boldly used in a military context therefrom, PMCs were gradually integrated into civil aircraft structures. Initially as non-structural components, PMCs made their way to primary structures by the early 1970s [26,27,31–33]. Owing to high oil prices, the National Aeronautics and Space Administration (NASA)-funded program Aircraft Energy Efficiency (ACEE) helped to boost the integration of composites in aircraft structures. Selected aircraft from Lockheed

(L-1011), Douglas (DC-10) and Boeing (B737, and later B727) incorporated graphite[2]/epoxy in their secondary structure [30, 35]. In Europe, Airbus decided to incorporate composites in the secondary structure of its two first aircraft, the A300 and the A310 [26], paving the way for their future aircraft to feature composites-intensive structures. Only several years later did Soviet commercial aircraft also started to incorporate PMCs in some Ilyushin (Il-86/Il-96) and Tupolev (Tu-204) models [36], although related details are somewhat scarce. An extensive usage of PMCs was observed since the mid 1970s in general aviation and rotorcraft. This is in contrast with the evolution of composites shown in Fig. 2.3, which shows a different trend in larger military and commercial aircraft. Partly owing to the aforementioned previous extensive validation campaigns of composite structures, nowadays PMCs can account for approximately half of the structural weight of the most recent aircraft: in the wide-body category, the Airbus A350 (∼52 %) and Boeing 787 (∼50 %), followed by the slightly lower fraction (∼40 %) attained in the Airbus A220.

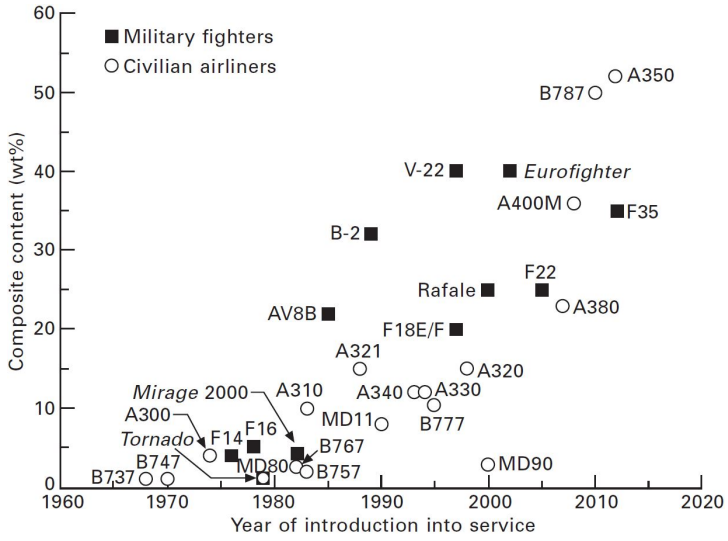

Figure 2.3 Amount of composite materials (structural wt%) military and commercial aircraft (Reprinted from [37], with permission from Elsevier).

Aircraft engine manufacturers have also ventured in the use of PMCs, following a similar sequential introduction. Rolls Royce initially introduced fiberglass blades in the compressor of their RB108 engine as early as in 1959, followed by their RB162 model [38]. Later, Hyfil carbon fiber/epoxy blades were incorporated in their RB211 engine in the late 1960s and early 1970s. Intended for the Lockheed L-1011 Tristar, these blades were aerodynamically sound, although manufacturing issues (e.g. repeatability) as well as poor performance upon

[2] *Graphite fiber* has been used to describe carbon fibers, although there seems to be a consensus that this usage is improper [34]. Carbon fibers typically have both amorphous and graphitic phases.

bird strike resulted in an unsustainable burden [39, 40]. Related technical and financial challenges forced Rolls Royce to file for bankruptcy in 1971 [41] and subsequently cancel the L-1011 Tristar program in 1981 [42]. This highlights the importance of technology maturity in decision making, which will be addressed in the article dealing with material selection (§4). Almost two decades later, the first successful major use of PMCs in commercial aircraft engines was made in the GE90 turbofan engine, intended for the Boeing 777. This engine incorporated fan blades fabricated via resin transfer moulding (RTM). Subsequently, turbofan engines have seen the implementation of PMCs for the most part in fan blades, casings, by-pass ducts or acoustic liners, thrust reversers and bracketry.

When used in engine applications, PMCs need to withstand demanding operating conditions such as hygrothermal cycling, complex mechanical loading and fatigue [7]. Their use is limited to the cold section, where the temperature does not exceed the wet glass transition temperature (T_g) of such material systems. Despite seemingly adverse operating conditions, the increasingly larger bypass ratios of modern aircraft engines further justifies the adoption of PMCs. For instance, the latest turbofan engines can reach a bypass ratio[3] of 10:1. In the near future, bypass ratios are expected to reach 12:1, leading to still larger fan sections and cold sections of the structure representing ∼35% of the engine's weight [7], hence the great potential of PMCs in these components.

Certification of composite aircraft structures

Aviation authorities, including the American Federal Aviation Administration (FAA) and the European Union Aviation Safety Agency (EASA)[4], guide the design of aircraft and certify their airworthiness. In North America, and more specifically in the U.S., the Title 14, Chapter I, Subchapter C, Part 25 of the Code of Federal Regulations (CFR) [43] dictates the airworthiness standards that any transport category aircraft must follow. Moreover, Part 33 [44] provides the specific requirements that engine manufacturers should fulfill in order to obtain type certification for their design. To comply with such regulations, prescriptive guidelines are used as means to ensure proper performance and minimize the risk of a catastrophic failure, involving loss of human lives and equipment.

Aircraft manufacturers have relied on inter-program feedback and lessons learned to evolve their designs based on proven technologies [45,46]. In the case of PMCs, for instance, Boeing's incremental use of composites in primary structures allowed to achieve a composites-intensive

[3]Mass flow rate of air circumventing the engine divided by the mass flow rate of air entering the engine's core.

[4]There is a high level of harmonization between regulatory organizations, including national entities, e.g., Transport Canada. Thus, FAA's is largely mentioned in this work for the sake of brevity.

design, the 787 Dreamliner, of which ∼50% of the structural weight is composites. At the same time, the knowledge acquired on composites during the 787 program has allowed to increase their usage in new designs of, e.g., 777X. The same goes for Airbus which since their initial model, the A300, has ventured further into the use of these materials [26, 46]. Nevertheless, economical, technological and safety concerns have always existed [47].

Current aircraft design practices enable a service life of 20+ years for commercial transport aircraft while fulfilling the operators' requirements [48]. The prevailing paradigm in aircraft certification when composite materials are used involves the use of the *building-block* approach [49, 50] shown in Fig. 2.4. The pyramid describes the types of specimens require to certify a composite structure. At the base, coupons have to be evaluated to obtain mechanical properties under different conditions. Elements or features such as flanges, solid and hollow sections are found in the second level. The data obtained from characterization at the two aforementioned levels are used to build databases for the sizing of details, first in sub-components and finally in large components. The idea is to test only a handful of components (last level) and the results are used to validated structural models.

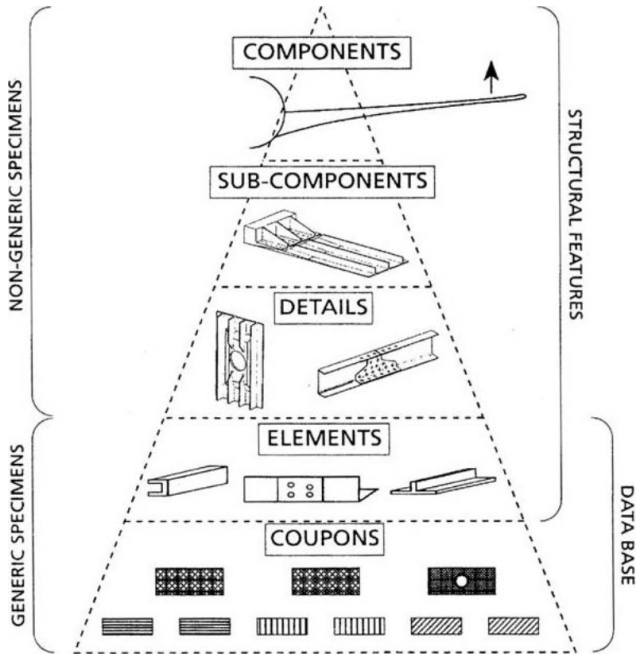

Figure 2.4 Aircraft certification paradigm for composite materials: the building-block approach (from [49]).

Aircraft certification is a long and costly process, especially for composites-based structures [51, 52] for which extensive testing is needed considering normal operating conditions [49]. For instance, it was reported that the certification of a CF/epoxy system used

extensively in the empennage of Boeing's 777 required more than 8000 and 300 tests at coupon/element and subcomponent levels, respectively [51]. The evaluation of PMCs needing to fulfill either *fireproof* or *fire resistant* roles is costly due to the size of test specimens needed for such endeavor (see §2.1.3). Additionally, challenges may be faced several years after certification due to unforeseen risk conditions such as updated fire regulations [53] or stringent environmental regulations [54].

2.1.2 Aircraft and fire safety

Fire safety is a general concern in civil, energy or transportation infrastructure [55]. This is especially true in manned enclosures with little room for manoeuvring and safe egress is virtually impossible, e.g., aircraft [56], submarines [15] and space vessels [57]. Accidental fires have been considered a threat to airworthiness since the dawn of modern aviation, from the psychological effects on crew and passengers to the structural damages and, consequently, reduced airworthiness [56,58–60]. During World War I and II, this threat was ever present due to enemy fire and the ensuing fuel or oil leaks. Regulating agencies knew that undetected fires were particularly dangerous, as pilots typically have less than 2 min to assess the developing threat and react accordingly. In most cases after this short period, the structural soundness of the aircraft is already severely compromised and it is already too late to put out the fire. Gradually, these threats were tackled with active suppression means, dominated by halogenated compounds. The development of effective fire suppression agents received much attention. Subsequently, the leap from piston to turbojet engines meant an improvement to the aircraft safety, mainly due to the decoupling of the engine from the fuselage and a modular design consisting of wing mounted engines [58–60].

For modern aircraft, several incidents and accidents have demonstrated that fire threat is still significant [61]. From a materials standpoint, Swissair's MD-11 accident near Peggy's Cove, Nova Scotia, Canada, in 1998 [62] is a vivid reminder of this. The accident investigation points at thermal/acoustic insulating materials as the main cause. Some of these materials were certified on an individual basis in terms of flammability, yet their synergistic behavior paved the way for thermal runaway. Even if materials are individually deemed safe, it is still essential to perform tests in conditions as close as possible to those found in aircraft operation. This is extremely relevant given that some researchers estimate that half of the accidents in aviation can be traced to the design phase and flawed assumptions [63].

Until the early 2000s, the composites certification process mainly focused on structural aspects and variability of the mechanical properties, for which some key aspects were identified, e.g., material sourcing, environmental effects and damage tolerance [32,35,64]. In view of the

increasing usage of PMCs in structural applications, dedicated studies were deemed necessary by the regulating entities [65]. Specific CFRP configurations were considered as fire-safe for extensive structural applications. However, the second example shown in Fig. 2.5b which took place in 2013, brought the fire safety of PMCs back under the spotlight after a ground fire incident involving the aft portion of a Boeing 787, which has a full-composite fuselage [66].

The examples demonstrate that fire is still a big threat to passenger safety. This is highly relevant in light of increasing aircraft electrification, considering the fact that electrical systems lie at the root of approximately two thirds of aircraft fires [61]. Therefore, it is important to understand the processes involved in the combustion of PMCs.

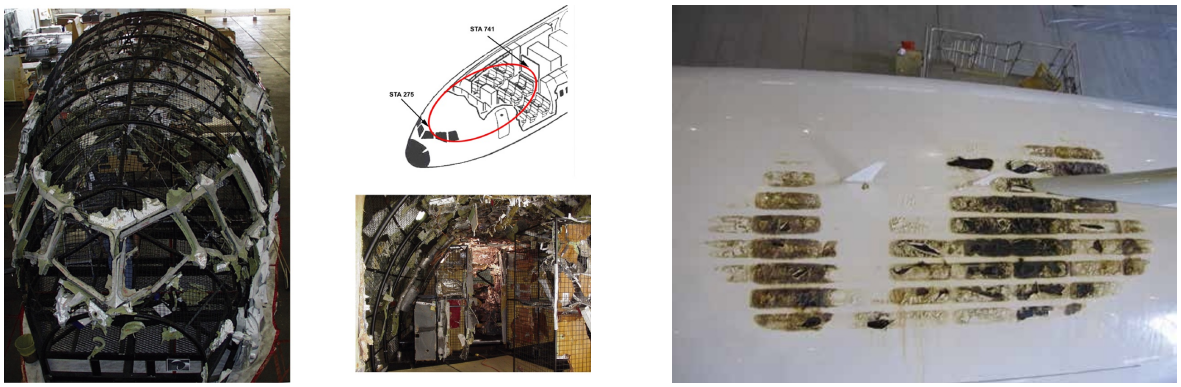

(a) (b)

Figure 2.5 Fire-related events where polymeric materials and/or their composites were involved: (a) Reconstruction mock-up of Swissair's MD-11 crashed near Peggy's Cove, Nova Scotia, Canada, on Sep. 2, 1998 (from [62]) (b) External view of fuselage damage of Ethiopian Airlines' Boeing 787 after fire at London Heathrow Airport (LHR), on Jul. 12, 2013 (from [66]).

Fire resistance of PMCs

Aircraft and engines have to be certified in terms of fire safety. In this regard, the concept of flammability is defined by the capability of a material to burn under certain conditions, which mainly depends on its intrinsic properties. Fire resistance has rather been defined as the ability of a component to withstand fire and provide protection for a certain period [67]. In an aviation context, two different designations are typically employed, i.e., *fireproof* and *fire resistant*, per 14 CFR §1.1 [68]. On the one hand, the *fireproof* term typically refers to components found in designated fire zones, i.e., mostly powerplants. This classification applies to materials and parts used to confine fire, i.e., firewalls, that need to withstand an

external flame attack, providing the same protection (or better) as steel. On the other hand, other materials and parts without fire-blocking functions must be able to withstand heat without catching fire uncontrollably. Thus, the *fire-resistant* classification is applicable to sheet or structural components that need to withstand heat to the same level (or better) as an aluminum alloy[5]. Their applicability depends on the function of the component and duration of flame exposure.

Evaluation of fire resistance

Structures expected to be *fire resistant* must retain their integrity when exposed to open flames. Such conditions are relevant to post-crash fire scenarios where fuselage skins can be exposed to flames due to damaged fuel tanks and subsequent spills. Fig. 2.6a shows an example of a post-crash fire, where an Airbus A340-313E skidded down the runway and fire ensued at Toronto Pearson Airport (YYZ), in August 2005. Owing to proper material protection and prompt evacuation, no fatalities were reported [70]. The general goal in such scenarios is to provide sufficient time for passengers egress in the safest way possible. In addition to their purpose under normal operating conditions, thermal/acoustic insulation blankets are also often used for the aforementioned fire-blocking purposes. Although the example above did not involve an aircraft with CFRP-based fuselage skins, the scenario is more relevant than ever to modern aircraft (see §2.1.1). The burn-through requirements for thermal/acoustic insulation materials and related test guidance are specified in 14 CFR §25.856 and the advisory circular (AC) 25.856-2A [71], respectively. The regulations mandate the use of an oil burner yielding a 1900 ± 100 °F (1038 ± 56 °C) flame with a $\dot{Q}$ of 16.0 ± 0.8 BTU ft^{-2} s^{-1} (182 ± 9 kW m^{-2}). The principal criteria are that no flame penetration should occur within a 4 min test, and that the heat flux density on the backside should not exceed 2.0 BTU ft^{-2} s^{-1} (22.7 kW m^{-2}) measured at a distance of 12 inches (30.5 cm). The dimension of each test specimen must be 16.0 ± 0.1 inches x 24.0 ± 0.1 inches (406 ± 3 mm x 610 ± 3 mm). The test specimen is placed at 30° with respect to the vertical, while the oil burner is kept (normally oriented) at 12 inches (30.5 cm) normal to the specimen's surface. Additional guidance is provided in FAA's Aircraft Materials Fire Test Handbook [72] Chapter 24.

A different classification pertains to components that need to be *fireproof*. An example is depicted in Fig. 2.6b, which shows the aftermath of the right turbofan engine of a Boeing 777-222 involved in an in-flight fire in February 2021. During the climb phase after taking off from Denver Intl. airport (DEN), the fracture of two fan blades caused a fire in the engine's accessory compartment, among other damages. Despite the fire, the engine was kept running

[5]No specific grade is considered, although Al alloys can behave very differently at high temperatures [69]

(a)

(b)

Figure 2.6 Fire-related accidents with no casualties where *fire resistant* and *fireproof* materials were involved, respectively: (a) Flames engulfing the fuselage of an Air France Airbus A340-313E after skidding down the runway at Toronto L. B. Pearson Airport (YYZ), on Aug. 2, 2005 (from [70]). (b) Aftermath of the in-flight fire that engulfed the turbofan engine of a Boeing 777 after taking off from Denver Intl. Airport (DEN), on Feb. 20, 2021 (from [73]).

to gain altitude and ensure a safe landing. This scenario is relevant to components found in designated fire zones of the "cold section" of modern turbofan engines which extensively rely on PMCs (see §2.1.1). According to 14 CFR §25.1181, these zones are the engine's power and accessory sections, powerplant compartments with no insulation found between the aforementioned sections, any APU compartment, fuel-burning heaters, compressor and accessory sections of turbine engines, as well as combustor, turbine and tailpipe sections of turbine engine installations that contain fuel or oil lines. Moreover, 14 CFR §25.1191 specifies that these fire zones must be isolated from the rest of the airplane by firewalls, shrouds or equivalent means, whereas 14 CFR §33.17 requires that firewalls must be *fireproof*, corrosion-protected and prevent any hazardous quantity of air, fluid or flame to pass around or through them.

Evaluation guidance is provided in AC20-135 (with Change 1) [53], AC33-13A [74] and Chapter 12 of [72]. For evaluation proposes, the use of an oil-based burner is mandated, capable of delivering a 2000 ± 150 °F (1093 ± 83 °C) flame with a $\dot{Q}$ of 9.3 BTU ft^{-2} s^{-1} (105.6 kW m^{-2}) or 4500 BTU h^{-1} (1.318 kW). Each test specimen must measure 24 inches x 24 inches (610 mm x 610 mm), although smaller samples of 10 inches x 10 inches (305 mm x 305 mm) may be used provided that all the design features are included. The test specimen is typically placed vertically in front of the oil burner, at the distance where calibration was performed. To be deemed *fireproof*, components found within designated fire zones, e.g., firewalls, need to withstand the flame impingement for 15 min showing no signs of flame penetration nor

exhibiting backside ignition while fulfilling their design purpose. Additionally, the specimen must not keep burning after the test flame is removed, no burn-through holes must be detected, and no attachment or fire seal point on the periphery can fail. Air flow and vibratory conditions may be needed to recreate the fire conditions expected in the final application. Components outside, yet adjacent to designated fire zones only need to be *fire resistant*. As such, they must fulfill the same burn-through and backside ignition criteria but only for 5 min. Flammable fluid-carrying components shall be *fire resistant* while flammable fluid tanks must meet the *fireproof* criteria per 14 CFR §25.1183. While these are typically of metallic construction, elastomeric/fibrous materials sharing characteristics with PMCs may be used as protective means, hence their relevance.

The last relevant scenario to PMC with lower structural demand pertains to cargo liners. The 14 CFR §25.857 and the Appendix F to Part 25 [75] specify that certain cargo liners must withstand the attack of a 1700 ± 100 °F (927 ± 38 °C) flame (or hotter) with a $\dot{Q}$ of 8.0 ± 0.5 BTU ft^{-2} s^{-1} (91 ± 6 kW m^{-2}). There must be no flame penetration within 5 min of the test and the measured T must not exceed 400 °F (204 °C) 4 inches (102 mm) away from the surface. Specimens must be of the same size as those for thermal/acoustic used for fuselage burn-through protection, i.e., 16.0 ± 0.1 inches x 24.0 ± 0.1 inches (406 ± 3 mm x 610 ± 3 mm). The test specimen is placed horizontally above the oil burner. Guidance is provided in the Chapter 8 [72]. This is especially relevant for cargo sections which may contain hazardous materials or that cannot be easily reached.

2.1.3 PMCs under fire attack

The effect of fire on PMCs can be summarized as thermal degradation, or reduction of physical properties, followed by thermal decomposition, which involves physico-chemical reactions triggered by high temperatures. Depending on their nature, polymers will soften when their T_g is reached and exceeded (applicable to thermosets and amorphous thermoplastics), followed by melting (only applicable to most of the thermoplastics). After heating and the onset of combustion, both micro- (decomposition, pyrolysis and oxidation) and macroscale (delamination, ignition and flame spread) phenomena are observed [6]. Polymer thermal decomposition under inert conditions, hereafter referred to as *pyrolysis*, takes place at early stages of the combustion process. On a molecular scale, carbon-based chains break down into smaller molecules through the following processes [6]:

- *End-chain scission* (or unzipping): group release from the chain's ends (typical process).
- *Random chain scission*: polymer chains break at random points along their length.

- *Chain stripping*: groups found in side chains attached to the backbone leave as stable molecules.

Fig. 2.7 shows the combustion process of PMCs due to a heat source in the macro scale, where the matrix and (organic) reinforcements typically undergo a series of physico-chemical changes depending on their chemical composition. The heating of the PMCs leads to the creation of flammable gaseous products, i.e., volatiles, and non-flammable species (non-combustible gases, solid residues such as fragmented fibers and char). The former can contribute as a heat source when they burn close to the surface and thus promote the combustion process, whereas the latter may contribute towards protecting the substrate or simply mix with the surrounding environment. To a lesser extent, char also can react in case of diffusion of an oxidizer, e.g., air, and contribute in the feedback loop, although it may also have desirable insulating properties given its high porosity. The loop ends when all the combustible material has been completely degraded or when endothermic chemical reactions do not provide enough heat to sustain the combustion process [6]. To understand the effect of fire on PMCs' behavior, the different constituents and their contribution to fire phenomena need to be individually assessed.

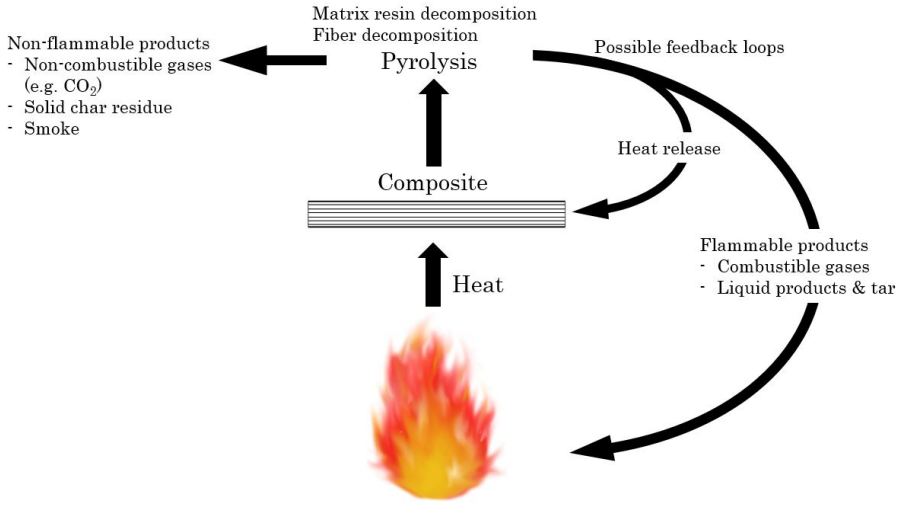

Figure 2.7 Mechanisms involved in the decomposition of PMCs during their combustion (adapted from [6]).

Generalities of fire evaluation

There is a plethora of tests that can be used to determine the evolution of the properties of PMCs under fire conditions [6, 76]. Each method provides different fire properties depending

on the test conditions. These methods can be grouped into different categories depending on their purpose. For example, calorimetry-based tests help to determine the heat release rate (HRR) of a specimen, whereas volatiles can be analyzed by means of spectrometric techniques. These data help to understand the basic phenomena involved, although differences are likely to be found when compared to flame-based tests. The decomposition footprints, i.e., spectra, can be obtained for the materials in question and these results can be linked to their chemical composition or volatilization scheme [77]. For example, Chetehouna *et al.* [78] analyzed three different CF-based composites with different matrices, i.e., epoxy, phenolic and polyether ketone ketone (PEKK). Upon pyrolysis of the specimens at different target temperatures, they reported multiple compounds roughly divided in phenols, furans, brominated compounds, ketones and diverse hydrocarbons. The temperatures used in their study had a major impact on the percentages for each of the resins.

For post-fire analysis, optical microscopy provides straightforward means to assess the material after fire testing. SEM/EDS-spectrometry can be employed to characterize the structure of the residual material, its concentration as well as material ablation and mass transport. Thus, the study of the residues can provide a good insight of the protection imparted to the underlying substrate [79].

For aircraft certification purposes and depending on the final application, tests are done on a small- and intermediate-scale basis to meet flame, smoke and toxicity (FST) and burn-through requirements, respectively. FST requirements are usually assessed by means of the cone calorimeter (CC). It is accepted that the information obtained through this method is not representative of a real fire [80], yet it provides insight of the fundamental phenomena that take place in the initial phase of a fire. Additionally, it can be also useful for screening purposes along with other bench-scale tests [81].

Sources of uncertainty

The variability of results in fire testing of PMCs has been amply reported, yet there is a continuing necessity to understand them. Cadena *et al.* [82] summarized the uncertainty existing in fire safety engineering in three types: epistemic, aleatory, ambiguity. First, according to the authors, the *epistemic* uncertainty relates to a lack or incompleteness of knowledge, typically found in complex systems and phenomena. The way to tackle it is by means of new or improved experiment-based theories. Given the extreme complexity of fire phenomena and interactions, this type of uncertainty is unlikely to disappear. Second, the *aleatory* type, is due to natural variability which, in the context of this dissertation, is inherent to composite materials. It is observed in large populations and is typically treated in a statistical

fashion. Finally, *ambiguity* is the result of vagueness and linguistic descriptions. This is typically found in normative contexts and is specific to guidelines and regulations. This type of uncertainty is tackled via consensus and alternative interpretations.

Some of the experimental uncertainties can also be attributed to ventilation systems or burners used in fire resistance tests and their features. For instance, Abu Talib *et al.* [83] measured the heat flux density (q) distribution of the propane burner mandated in the ISO 2685 standard [84] with a thin film gauge developed by the authors. They compared the data with calibration runs performed with a Gardon gauge, reporting some significant differences. Among these, they showed that the Gardon gauge overestimated the heat load while showing with their method that the same flame did not meet the 116 kW m^{-2} requirement. Regarding oil-based tests, Boulet *et al.* [85] modelled the kerosene-based burner used for certification tests using Large-Eddy Simulation (LES). Their results point at the need for considering both convective and radiative heat transfer for accurate temperature predictions, since kerosene-based flames are typically sootier. This is in line with the problematic described by Le Neve [86] who points at the overall q differences between propane- and oil-based burners despite the calibrated value.

Flammability characterization

The evaluation of *flammability* fails to capture some of the relevant aspects of fire resistance [76, 80]. Nonetheless, without the assessment of properties such as HRR and its key role in fire sciences, the knowledge about the underlying phenomena of fire resistance would be nonexistent. It is important to review the methods used for its assessment since a large body of literature has focused on the thermomechanical behavior of PMCs relying on one of the main flammability assessment tools: the CC or, at least, a radiant heat source.

For aircraft certification purposes, the flammability of PMCs is mainly assessed at a small scale, using a CC [87, 88] (100 mm x 100 mm specimens) or an Ohio State University (OSU) calorimeter [72] (149 $\pm$ 1 mm x 149 $\pm$ 1 mm specimens), and flame spread setups [72]. The CC can impose a wide spectrum of heat fluxes (10–100 kW m^{-2}) on the sample and can easily accommodate any kind of PMC laminate or bulk material. Fig. 2.8 shows the general arrangement of a typical CC, with a specimen shown in the horizontal configuration. The apparatus can also accommodate specimens installed vertically, as depicted in the inset. This is highly relevant since the specimen orientation plays a key role in the flame spread process [89]. The main property obtained with the CC is the HRR which is calculated using the oxygen consumption calorimetry concept, i.e., the heat of combustion is calculated based on the oxygen depletion measured in the exhaust gases. The HRR, considered the

most relevant property when assessing a fire hazard [76], provides information about the capability of the material to sustain its own decomposition, closely related to ignition, mass loss rate and smoke generation [6,76]. Other properties that are obtained in such tests include time-to-ignition (TTI), smoke density and, if connected to a spectrometer, toxic gases. In a similar fashion, the OSU calorimeter has been used to test aircraft cabin [76] and structural components [65]. However, this thermopile-based test typically yields different results when compared to the CC [90].

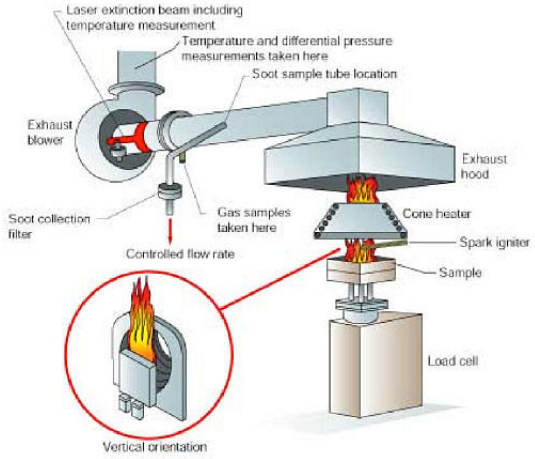

Figure 2.8 General arrangement of the CC (from [91]).

Toxicity and smoke behavior have been identified as key factors of passenger survival in both in-flight fires and post-crash scenarios [56, 61] which also have to be assessed to ensure reasonable levels in case of an aircraft fire scenario. In general terms, these assessments and the properties measured therein are well understood [6]. However, despite the large set of tools available for flammability assessment, some challenges still exist in their prediction due to the different length scales and factors involved [92–94]. Moreover, every single material configuration, heat flux and environmental factor will provide unique results in these setups [80]. In an effort to guide the selection of fire-safe configurations, the FAA conducted a comprehensive test campaign to determine the hazards from PMCs and associated polymers used in cabin applications [95]. Their results point at aromatic polymers as the best candidates owing to their high char yield.

There are other tests such as the Underwriters Laboratories (UL) 94 and the limiting oxygen index (LOI) tests, that rate the flammability of plastic materials. Such tests indicate whether the material is prone to keep burning (flame spread evaluation) and to emit large amounts of smoke or not, depending on the test atmosphere. Nonetheless, the outcome of such tests is somewhat irrelevant when mechanical properties are a concern. Additionally, TGA and DSC

can be used for thermal analyses to determine temperature-related mass evolution, and T_g or degree of crystallinity, respectively. The resulting data can be used in conjunction with other small-scale approaches (e.g. CC) to build fire models that help to predict the flammability and structural response of PMCs [96–98].

Some flammability assessments may be useful to predict pass/fail verdicts of certification tests based on bench-scale data. Lyon *et al.* [99, 100] developed a statistical approach called "phlogistic model"[6]. They tried to determine, from a probabilistic standpoint, whether a material would pass or fail a standardized small-scale fire test (namely FAA's vertical Bunsen burner (VBB) & HRR as well as UL'S UL-94 VBB tests) based on a reduced set of material properties obtained from a micro combustion calorimeter (MCC). They analyzed the results of hundreds of homogeneous/small-scale (5 ± 2 mg) samples and built their model therefrom. Their efforts were put on determining whether they were good predictors of pass/fail results of standardized testing procedures gathered from hundreds of polymeric materials tested over several years. They found out that some of the fire, thermal and combustion properties could be used as reliable indicator. Their approach considered the variability of fire test conditions caused by uncontrolled factors. However, it must be stressed again that flammability tests do not have the same length- nor time-scales needed for fire-resistance assessments.

Prior to the certification of the Boeing 787, the first commercial large-body aircraft to use CFRP skins, the FAA endeavored [65] to understand the flammability properties of CF/epoxy materials used in structural applications. They analyzed representative configurations using several techniques, namely CC, MCC, TGA, DSC, flame spread rig, OSU calorimeter and smoke density chamber. They reported that the material system burns in a similar manner to a charring material and that the CFs were essentially inert[7]. Their objective was to provide empirical data to be used for modelling of flammability and gaining more insights into aircraft fire scenarios.

Effects of constituents

The combustion of PMC is a complex process with several interconnected phenomena taking place simultaneously. Different research groups have focused on the individual effect of some physical factors such as reinforcement geometry, fiber type and volume fraction, panel thickness, and, in the case of sandwich panels, the effect of core. In this section, this information has been regrouped in three categories: matrix, reinforcement, and core.

It must be noted that the details regarding reinforcement and matrix are sometimes found

[6] portmanteau of *logistic model* and *phlogiston*, a fire-like element, popular in ancient Greece.
[7] Diametrically opposed to the CF oxidation-related phenomena discussed in this dissertation.

in the literature, when proprietary information is of no concern. However, most of the time, this information represents a competitive advantage and details can be scarce. Thus, it is not uncommon to find literature where the composite configuration is vaguely given as CF/epoxy.

Matrix The nature of the composites' matrix and their resin content as well as the effect of fillers and fire retardants have been investigated by several groups from a flammability standpoint.

For instance, Eibl [101] analyzed with TGA and CC the difference between two different epoxy-based composites, i.e., M18-1 and RTM6 epoxy resin systems (both from Hexcel), with the same woven CF reinforcement (4HS Satin standard modulus). M18-1 was an epoxy toughened with polyetherimide (PEI) incorporating $Mg(OH)_3$ and zinc borate as flame retardants, whereas RTM6 epoxy did not have toughener nor fire retardants. The specimens ranged from 1–8 mm in thickness. The resins, their individual constituents (epoxy and PEI) and composites were firstly analyzed via TGA in N_2 and air, yielding a small char yield improvement of 5 and 3 percent, respectively, for M18-1 with respect to RTM6. Considering a q of 60 kW m^{-2}, lower and wider HRRs curves were observed with increasing thickness (2–8 mm), being characteristic of thermally-thick specimens. Considering only a 2 mm-thick configuration, a significant difference on HRR was only observed at 20 kW m^{-2} where the HRR curve of the modified epoxy was shifted (delayed) owing to the action of the toughener and fire retardants. At higher irradiation levels, miminal shifting was observed, although the modified epoxy showed several small peaks, indicating sequential delaminations.

Dao *et al.* [102] studied the effect of fiber volume fraction (V_f) on the flammability of CF/epoxy laminates. They exposed two laminates with different V_f, i.e., 56 and 59 %, to several q values using a cone calorimeter. Even with minimal differences in V_f, they showed that higher values yielded lower HRR and total heat release (THR), TTI and mass loss. The variation of these properties is explained by the reduction of the available combustible material, i.e., the resin.

Carpier *et al.* [103], analyzed a CF/poly phenylene sulphide (PPS) system with a simultaneous thermomechanical approach using a CC while applying a tensile load on 200 mm-long dogbone specimens. They used two approaches. The first consisted in preloading the specimen, exposing it to a q of 40 or 60 kW m^{-2} for a 2 min, and then proceeded to test the specimen monotonically until failure. The backside temperature was measured throughout the process. They reported a temperature increase and lower final load as a result of higher loads. The second approach focused on the *creep* behavior, subjecting the specimen to a constant load, ranging from 12.5–50 %, while applying a q of 60 kW m^{-2}. They described a

protective-effect of CF plies (at ± 45°). They concluded that, even after PPS melting, CFs can withstand the tensile load as long as they do not get sufficiently oxidized.

The cited studies indicate that the resin composition and content has an impact on the flammability of composites structures. Moreover, it is suggested that the resin decomposition can be influenced by the nature of the reinforcement. However, there is still a need for research on the effects of matrix on the fire resistance of composite structures.

Reinforcement The nature of the reinforcing fibers plays a key role in the fire properties of composite structures. If organic fibers are employed, they will have minimal to no fire resistance, possibly contributing to aspects such as charring when aromatic polymers are considered, e.g., aramid. On the other hand, inert fibers may help towards preventing gas migration or working as insulators.

Bourbigot and Flambard [104] compared the heat resistance and reaction-to-fire of several high performance organic fibers with para-aramid (Kevlar®) fibers as baseline. They analyzed poly(p-phenylene-2,6- benzobisoxazole) (PBO) (Zylon®), copolymer p-aramid (Technora®), polyhydroquinone-diimidazopyridine (PIPD) (M5®), phenol-aldehide (Kynol®), melamine (Basofil®), polyamideimide (Kermel®) and recylced oxidized PAN fibers. Upon comparison of their thermal behavior determined by TGA and CC, they found out that Zylon® performed the best. They pointed at heterocyclic polymers as candidate materials for fire-safe application while keeping high mechanical properties. TGA/DSC and CC results point at better flammability properties of PBO fibers. It must be noted that these fibers are organic and expected to be fully pyrolysed and oxidized upon flame attack.

Bhat *et al.* [105] analyzed the fire resistance of basalt fiber reinforced polymers (FRPs) and compared their results against glass fiber reinforced polymer (GFRP). They found out that basalt-based composites have inferior fire resistance due to higher emissivity of the reinforcement. This translated into faster failure at lower loads. Both share a softening effect caused by high temperature. In a different study, Bhat *et al.* [106] studied three different plant-based fiber types, i.e, flax, hemp and jute, using fiber tows (or bundles) and vinyl ester (VE)-based laminates while using E-glass as baseline. They exposed fiber tows to heat using capstan grips and a heat gun, whereas slender specimens, i.e., 600 mm x 50 mm were exposed to a radiant heat source limited to a 100 mm long gauge length. Even at low temperatures ($T \leq 200\,^{\circ}\mathrm{C}$), the strength and modulus of natural fibers were severely degraded. Moreover, composites with natural fibers yielded a TTF one-order-of-magnitude shorter than their glass counterpart. However, the behavior of flax fibers was slightly superior.

It is evident that natural or organic fibers are unsuitable for fire-blocking applications. How-

ever, it must be highlighted that such fibers behave differently, owing to different levels of organic content. This is analogous to some other aspects analyzed in this dissertation, like the assumption about CFs behaving in the same way when exposed to fire, as it will be seen in §5 and §6.

Besides the nature of the reinforcing fibers, other aspects such as the reinforcement architecture and orientation have to be considered. Several groups have investigated, for instance, the differences between unidirectional tapes, woven fabrics and discontinuous reinforcements, as well as the effect of fiber alignment.

Brown and Mathys [107] analyzed polyester-, VE- and phenolic-based laminates. Reinforcement wise, they compared the reaction-to-fire of glass fiber chopped strand mat (CSM) and a woven architecture. They found that woven samples delaminated more than the laminates with randomly-oriented short fibers, i.e., CSM, most likely due to the fabric crimp which forces swelling. Resin layers and pockets induced by the woven architecture translated into higher peak HRR and faster TTI. CSM had a more homogeneous fiber distribution, which translated into broader curves. Moreover, the CSM configuration involved a polyester binder, which increased the smoke production and yielded higher THR. Phenolic-based samples performed best with woven architecture. Counter-intuitively, polyester-based laminates yielded better results with CSM, due to the high thermal stress cracking of phenolics.

Ghazzawi *et al.* [108] compared the effect of woven (plain weave (PW) and Twill 2x2) and unidirectional (UD) glass reinforcements using polycarbonate (PC) as matrix. For non-continuous fiber composites, Ghazzawi *et al.* pointed at the effect of fiber length by comparing fibers with different physical and thermal properties (glass, basalt and carbon) considering PC and polypropylene (PP) as charring [109] and non-charring [110] matrices, respectively.

Of special interest is the effect of the reinforcement orientation or, seen from a different perspective, fiber misalignment, on the thermostructural response of composites. Anjang *et al.* [111] studied the effect of fiber misalignment in sandwich configurations. They found that the maximum fiber misalignment depends on the time of survival when exposed to a radiant heat source and applied stress. In their study, a sandwich panel with glass/VE skins and balsa wood core was exposed was loaded in tension to different level of the tensile strength determined at room temperature (σ_{RT}). For instance, with the aid of their model, they determined maximum values for off-axis ply angle depending on the survival time (300, 600 and 900 s) when exposed to q of 35 kW m^{-2}, ranging from 12.5° to 9° at 10 % of σ_{RT} for a survival time of 300 and 900 s, respectively. These angle values decreased down to 1° at 60 % of σ_{RT} for a survival time of 300 s.

Eibl [112] compared the effect of fiber orientation by analyzing UD and quasi-isotropic (QI)

laminates using a non-woven carbon/epoxy system (Hexcel 8552/IM7). Specimens measuring 100 mm x 100 mm with different thickness (0.25–8.0 mm) were evaluated using a CC at several q values (15–80 kW m^{-2}). Specimens were instrumented with intra-ply Type K thermocouples at several positions to analyze the temperature evolution. Initial tests were carried out using TGA to study the behavior of the composite material system as well as the resin's constituents (epoxy and poly ether sulphone (PES) as toughener), all in air and inert (N_2) atmospheres. Among the differences between laminate configurations, it can be highlighted that QI specimens ignited faster than UD due to preferred delamination and higher soot, smoke and HRRs were observed on UD configurations, which became increasingly marked on thicker specimens. Fiber pitting was shown although not discussed. The author emphasized the importance of fiber orientation and lay-up in the design process.

Eibl and Swanson [113] analyzed the out-of-plane effect of the same material system by obtaining relatively thick samples (5 mm) obliquely machined from a cured quasi-isotropic block (120 mm thick) made with 960 plies of the carbon/epoxy prepreg. This analysis was relevant given the anisotropic properties of CFs. Their thermal conductivity in the longitudinal and radial directions usually differ by one-order-of-magnitude, being higher in the former due to CF skin arrangement. They found that the fiber orientation has a marked influence on the HRR, explained by angle-controlled heat distribution. With the help of an empirical model, they showed that the pyrolysis front at 90° is approximately four times faster than its counterpart at 0°.

Eibl [101] also analyzed the difference between two epoxy-based composites with different fiber architectures, i.e., CF unwoven roving (tape) and woven fabric, considering UD and QI laminates with the same thickness in the range of 1 mm to 8 mm. Considering only a toughened epoxy modified with fire retardants (M18-1 from Hexcel; see section "Effects of constituents; Matrix"), Eibl compared the migration of volatiles between woven- and tape-based specimens. Differences were observed between configurations although a clear trend could not be discerned. However, the fiber diameter reduction was found to be clearly in correlation with the panel thickness, suggesting that the latter plays a important role in the diffusion of oxidizing species. The author also reported the creation of respirable fiber fragments, bringing the hazards of burning CF-based composites back under the spotlight.

Carpier *et al.* [114] evaluated the evolution of tensile stiffness and strength of CF/PPS laminates with QI configuration and a woven architecture (T300 3K 5HS). They rapidly heated the test enclosure (50 °C min^{-1}) and held the temperature for 2 min prior to loading the specimens at 220, 270, 320 and 470 °C. These temperatures correspond to different stages of degradation experienced by the PPS matrix, and thus different failure modes were reported.

They also observed a creep-like behavior at high stress levels.

From these references, it can be inferred that the reinforcement architecture and orientation should be given careful attention when assessing the flammability of PMCs. However, fire resistance aspects remain unknown. Moreover, most of the literature is based on simulated fire conditions, i.e., radiant heat sources, and the only flames involved are those created upon ignition of the volatile gases created by the decomposing composite. Consequently, they fail to capture the full effect of highly reactive species found in open flames on the degradation of the reinforcing fibers.

Core Cores are a first-hand option to provide increased bending stiffness while keeping a low density. Foams can be found in aircraft interiors whereas honeycomb cores are widespread in other structural applications including radomes, acoustic liners and some critical components such as rudders, elevators and spoilers. NOMEX™-based (meta-aramid) honeycomb cores are extensively used in current aircraft applications due to its low flammability properties. These materials are typically saturated with phenolic resin, providing a fire retardant behaviour. Aluminum cores can also be used, being incombustible under the conditions commonly encountered in aircraft, although melting may take place under severe flame attack.

Besides the improvement of mechanical properties, the addition of a core into the composite structure entails a change on its fire behavior. Although different studies have been carried out to analyze the effect of adding cores of different materials, most of the efforts m have focused on the flammability properties, and less attention has been paid to the thermomechanical aspects. However, Anjang *et al.* performed a series of analyses on sandwich configurations to evaluate the effects of simultaneous tensile load & radiant heat effects [115] subjecting a panel with cross-ply woven glass/VE skins and balsa wood core to such thermomechanical loads. They proposed a thermomechanical model and confirmed that the failure mode was load-dependent, triggered by either the back or front skin due to the large temperature gradients created by the decomposing core. Considering $q = 25$, 35 and $50\,\mathrm{kW\,m^{-2}}$, failure was expedited at higher values. Later, they adapted their model to obtain residual properties [116], subjecting the same materials to tensile and compressive loads after static heat exposure to determine their post-fire mechanical properties. They subjected the panels to a larger range of q, i.e., 10, 25, 35, 50 and $75\,\mathrm{kW\,m^{-2}}$. Their predictions for the tensile case were in reasonable agreement with the experimental results. However, they reported large discrepancies for the compressive load cases due to small errors induced by the calculated char thickness which translated into larger errors in the post-fire buckling stress. It was not possible to properly include the stabilizing effect of the damaged core in the model. In a third step, they analyzed the effect of water absorption [117]. Besides the weakening

of the VE-based skins due to moisture diffusion and weakening of shear strength, the balsa wood core underwent hydrolysis, causing the sandwich panel to fail faster at high stress values, although longer exposures did not yield significant differences in its thermomechanical behavior considering a tensile load case.

Effect of mechanical loads

Fire properties are different for each loading condition. Due to the nature of laminated PMCs, there is a coupling behaviour between extensional and bending stiffness. Resin degradation and further decomposition induce an imbalance [96].

Compressive mode is the most sensitive load case to failure, for instance, due to thermal imbalance and subsequent buckling, whereas residual tensile strength is commonly observed even if the matrix is completely volatilized or charred, since the remaining reinforcement aligned to the load axis, i.e., at 0°, is capable of bearing the tensile load [118]. Efforts made to model composites under fire attack and mechanical loading have shown that time-to-failure of laminates in compression can be about one order of magnitude shorter than those in tensile tests [97].

Burns *et al.* [119] analyzed the compressive behavior of woven carbon/epoxy laminates with a crossply configuration. The epoxy system had a very low T_g, i.e., 65 °C. They subjected the thick (9 mm) and slender specimens (50 mm x 560 mm) to compressive loads at different levels, exposing a 100 mm-long section to a radiant heat source at different q values, i.e., 10, 25 and 50 kW m^{-2}. They highlighted the role of matrix and its softening in the laminate's failure via buckling and/or delamination. Low compressive stresses yielded large differences in TTF between q values, whereas at high compressive stresses, differences were minimal. Aided by a thermomechanical model, they pointed at the resin's T_g as a key factor in failure promptness, with larger effect at low q.

Elmughrabi *et al.* [120] used a CC and a a piston-based custom loading frame to evaluate the flammability and TTF of ∼11 mm glass/VE and glass/polyester laminates with crossply configurations comprising 24 plies. They used small specimens with a an unexposed section of 100 mm x 30 mm. They compared the behavior of specimens loaded in tension and compression at three different load levels in each case considering a q of 75 kW m^{-2}. They found that tensile loading promotes matrix cracking to a larger extent when compared to compressive loads, with peak HRR being proportional and inversely proportional at higher loads, respectively. Under tension, the TTF varied considerably, being shorter at higher loads. Conversely, the TTF under compression did not show significant differences, with shear buckling as the main failure mode.

Benelfellah *et al.* [121] studied the effect of coupled thermomechanical loading. Using a small-scale test rig comprising a CC and a four-point bending fixture, they subjected 300 mm x 50 mm CF/epoxy specimens with different orientations to reproduce different types of loads, i.e., fiber or matrix dominated. The specimens were quasi-flat, extracted from filament-wound tanks, subjected to a q of 35 kW m^{-2} for different periods ranging from 100 to 250 s. They compared the results obtained from loaded and unloaded conditions, finding a minimal difference on the residual strength, with no clear effect on the backside temperature.

These results suggest that the fire resistance of PMCs is relevant to cases where structures can withstand structural loads for extended times while exposed to aggressive open flames. Under compressive loads, this translates into heavily-insulated structures, whereas composite structures loaded in tension which, even after resin decomposition and subsequent char oxidation, can withstand tensile stresses provided that the reinforcement is inert or undergoes gradual oxidation.

Fire resistance assessment

The structural analysis of composite materials under fire conditions can be divided in two categories: post-fire integrity tests and *in situ* mechanical evaluation [96]. In this regard, the evaluation of materials under simultaneous thermomechanical loads has become a necessity to better capture the coupled thermomechanical phenomena for both monolithic and sandwich PMCs.

Only the literature where burners have been employed is reviewed here, since research works utilizing radiant heat sources do not capture some important aspects such as the complex chemistry of the flame or ablation phenomena due to heat and mass transfer. Gas burners can be used to simulate the desired temperature and q if their parameters are well controlled, i.e., exit geometry, Reynolds number (calculated from the jet speed), fuel/oxidizer ratio and the distance between the nozzle and the specimen [122]. The most valuable information comes from tests that can provide simultaneous fire and mechanical testing. Performing tests under more realistic conditions, for instance using kerosene-based burners and simulated aeration, provides a better understanding of the evolution of the material properties and structural integrity. However, their operation can be complex. Therefore, several groups have opted for performing tests with gas burners, which provide easier means for testing.

Intermediate- and large-scale tests Publicly-available information on full-scale tests is scarce. However, the data collected from these tests are extremely valuable since they consider the most accurate conditions in terms of length and flame scales as well as ventilation when

trying to recreate, for instance, a post-crash fire scenario.

Full-scale tests have been performed mainly by regulatory bodies. For instance, the FAA performed a series of full-scale tests [123] using an existing Boeing 707 fuselage measuring ∼6 m long as a reusable fuselage test rig to evaluate the burn-through resistance of thermal-acoustical insulation. The rig featured a ∼2.4 m x 3.6 m test section used for evaluating the aluminum skin, thermal-acoustical insulation, floor and sidewall panels, carpets and cargo liners. Although these tests were carried out before the advent of CFRP-based fuselage, most of the previous items have relied on polymes and/or PMCs, hence its relevance to this dissertation. Instead of a kerosene burner, they used a ∼3 m long pan with Jet-A fuel, allowing the fuselage to be subjected to a q of ∼158–187 $\mathrm{kW\,m^{-2}}$. They evaluated several materials including encapsulated fiberglass-based insulation wrapped with metallized polyvinyl fluoride (PVF) film, fiberglass liners, floor panels with sandwich configuration, wool/nylon carpet, Nextel™ fiber paper, polyimide (PI) foam, quartz fabric and mats. Most of them in multiple configurations. Besides identifying materials capable of withstanding burn-through and with low flammability properties, their findings highlighted the method of attachment as critical together with the composition of the material (typically a thermoplastic film) used for bagging/insulating the fibrous material.

One of the most extensive and publicly available test campaign to find alternative firewall configurations was performed by the United States Air Force - Wright Aeronautical Laboratories, Wright-Patterson AFB, OH [124]. Their research was mainly triggered by the questions that arose from propane *vs.* oil burner differences. The physical properties of material candidates were not available, thus a plethora of combinations were tested with a kerosene-based burner in accordance with SAE's ASP 1055. Considering both structural and parasitic materials systems, 39 out of 68 material configurations (4 $\mathrm{ft^2}$) were deemed fireproof; 11 of the passing materials were further considered as superior / worth of being considered as firewalls. The successful configurations are roughly divided in ceramic fabrics (with and without coatings), flexible ceramic felts, PI foams, PI and bismaleimide (BMI) panels with and without filled honeycombs, and CMCs. On the other hand, silicone-based rubbers, ceramic fabrics, phenolic panels, a PI foam and PEEK/graphite laminates were among the failing material systems.

None of the aforementioned test campaigns considered simultaneous flame attack and mechanical loads other than the the force exerted by the flame jet. However, as stated in the in the federal regulations and related guidelines for aircraft certification, loads must be simulated (see §2.1.2).

Small-scale tests In the context of airworthiness, fire safety and certification, the fire resistance evaluation of composite structures is usually carried out at an intermediate length scale with specimens reaching 610 mm x 610 mm given the variability associated with combustion phenomena and PMCs. This renders multi-material evaluation campaigns prohibitively expensive and thus resource-efficient approaches are needed. The vast majority of the modelling efforts have been compared and validated using radiant heat sources. Several research groups have relied on open flames, although the burn-through process is yet to be addressed. Therefore, tests are still needed and development costs are needed to be kept to a minimum.

From a fire resistance standpoint in an aircraft certification context, material evaluation shall be carried out using oil burners as described in §2.1.2. However, given the dimensions used in such certification tests, extensive material screening campaigns can be prohibitively expensive. Therefore, several research groups have endeavored to obtain meaningful evaluations while using smaller scale approaches.

Small-scale tests can help to avoid costly experiments associated with larger scales. Test approaches relying on radiant heat sources have been used in the development of models under controlled conditions whereas a flame source approach can provide a harsher and, therefore, conditions closer to those found in real aircraft scenarios. Simultaneous heat and load approaches have been implemented for testing of CMCs, where radiant heat sources have been used to induce thermal bending stresses [125] and to study tensile behaviour [126, 127], as well as a high velocity oxy Fuel (HVOF) propane burner for fatigue analysis [128].

Simplified evaluation methods with small scale specimens can provide a good insight of the material behavior under different thermal conditions and duration of tests. Other parameters such as time-to-ignition, HRR, ignition/flammability variables and pyrolysed depth can be used to evaluate and compare materials of different nature. Variables such as humidity and vibration levels can also be relevant.

It has been shown by different research groups that heat flux [116], temperature and mechanical loads [115] are key factors in the failure process. Tests have been carried out using radiant sources, environmental chambers, gas- and oil-based torches, each one having advantages and drawbacks. Since all PMCs components need to be certified using an open flame at the intermediate scale, a small-scale burner is highly recommended to include the effect of a turbulent flame [129].

Several groups have endeavored to conceive resource-efficient evaluation methods to assess the fire resistant of metallic and PMC-based structures. Such protocols have opted for small-scale tests given the possibility to evaluate more specimens with the same amount of material required for aircraft certification.

Bartlett and Stratford [130] built a small-scale fire resistance evaluation setup based on an oxyacetylene torch. Their test conditions and pass-fail criteria were defined based on AC20-135 [53] and AC20-107 [49]. Using aluminum samples, they demonstrated the benefits of small-scale tests with open flames to assess the specimens' integrity while keeping costs low. They did not report the use of composites nor simultaneous mechanical loads.

Johnston *et al.* [131] evaluated nine structural configurations using 1 ft^2 panels comprising glass fiber (GF) and CF reinforcements with epoxy, PI, BMI and phenolic matrices. Sandwich configurations were tested too, and in some cases, a ceramic fabric (Nextel™) was incorporated as additional fire barrier. Using a small propane torch (2.5 cm in diameter) that yielded a calibrated flame per AC20-135, a quantitative comparison was performed considering the backside temperatures. Compressive testing was chosen to evaluate post-fire residual strength.

Gibson *et al.* [132] developed a small-scale test method using a propane burner capable of reaching 1100 °C and operate in a range of 25–180 $kW\,m^{-2}$. They have implemented it in an experiment that can simultaneously characterize composite structures (laminates and pipes) under load. Later, Tranchard *et al.* [133] used a calibrated propane burner in compliance to ISO2685 and 14 CFR §25.856(b) (capable of up to 200 $kW\,m^{-2}$). They used titanium-alloy (Ti6Al4V) coupons to validate their method, followed by the analysis of CFRP coupons. Other alternative approaches such as an oxyacetylene torch can be used [53] to develop a low-cost firewall penetration test rig [130].

Cutter *et al.* [134] proposed an evaluation method using 240 mm x 240 mm specimens, a propane burner and a load module that exerted a load at the center of the panel to mimic a cellulosic fire due to the final application of the composites, i.e., naval. They evaluated several thick (∼10 mm) cross-ply laminates using an undisclosed GF/epoxy material system. They reported a 50 and 75 % loss of stiffness within the first 2 and 4 min.

Di Modica *et al.* [135] evaluated the behavior of 100 mm x 100 mm CFRP laminates with QI stack up using a propane burner yielding a flame with a q of 116 $kW\,m^{-2}$. Simultaneously, they applied compressive loads using a custom hydraulic load frame, using antibuckling aids. They determined the TTF of three laminates with different thickness (5.05, 10.2 and 15.3 mm) at different strains using the aforementioned nominal q. Additionally, they compared the effect of varying q by performing tests at 50 and 185 $kW\,m^{-2}$ considering a specific strain condition (600 $\mu\epsilon$). They found differences on TTF with respect to q only with thick specimens (15.3 mm). Considering a q value similar to aircraft certification tests, i.e., 116 $kW\,m^{-2}$, TTF had a positive and inverse correlation *vs.* thickness and strain values, respectively.

Grigoriou and Mouritz [136] compared Al 2024-T3 and QI carbon/epoxy laminates in tension

and pointed at the elevated residual tensile strength of composites panels when compared to creep/melting-controlled failure of aluminum ones.

Aspinall *et al.* [137] developed a thermomechanical evaluation method using a CC with a three-point bending fixture adapted for simultaneous evaluation. They exposed 250 mm x 30 mm CFbased specimens to four different q (10, 20, 30 and 40 kW m^{-2}). Using a pre-load of 2 kN, they correlated the TTF with the incident q.

Schartel *et al.* [138] developed a test rig using a propane burner to assess the thermomechanical behavior of sandwich panels (see §2.1.3) loaded in compression at different stress levels. Their approach allowed to assess the level of thermal protection imparted to sandwich structures by intumescent systems (coatings). They tested 150 mm x 150 mm panels with different CF architectures, intumescent coatings and thicknesses. Their results also allowed to identify failure modes.

All of the aforementioned studies have characterized either the post-fire (residual) or *in situ* thermomechanical properties of PMC at a small scale. This has been possible via radiant heat sources and open flames. However, none of them has addressed the burn-through phenomenon, which is critical in aircraft certification tests.

2.2 Aircraft design aspects

Aircraft design is an iterative process in which functionality can be achieved through different avenues [139, 140], and thus compromises are needed between the different stakeholders. The initial statement of the problem is encompassed by a list of goals, objectives and constraints, usually provided by the customer [140]. However, the nature of the initial requirements is typically fuzzy, with boundaries being drawn progressively and constantly redefined.

Designing fire-safe aircraft structures is a twofold endeavor. First, the selected materials should perform under normal circumstances with high specific properties, i.e., materials with high stiffness and/or strength, yet low density. Second, the structure should be able to fulfill fire certification requirements while keeping the aforementioned features.

Problems quickly arise when aiming to identify lightweight protective solutions in the most resource-efficient way, motivating a research effort on how the evaluation of these materials should be carried out. One of the main virtues of composite materials resides in the interaction of their constituents and the unique properties that can be obtained therefrom [141]. The same holds true in their behavior under fire attack. The different test conditions described in §2.1.3 need to be considered based on the final application of the PMC-based component. As in any other design domain, once a list of potential candidate material systems has been

identified, a system is needed to select the best solution considering multiple and conflicting criteria. Therefore, there is a need for an *ad hoc* material evaluation and selection framework.

Diverse approaches and standards exist aiming for a systematic design methodology. However, there is a lack of guidance for aircraft-fire safety. In fact, the prescriptive approach from the regulating authorities provides enough freedom to aircraft and engine manufacturers in the design of PMC-based structures, as long as they can be considered analogous to metallic alloys with well understood fire behavior [43, 53, 72, 74]. To be able to leverage this freedom to benefit from the advantages of complex PMC-based material systems, appropriate design methodologies are needed. *Ad hoc* systematic design selection approaches to fire-resistant solutions are therefore required.

This section reviews the design aspects that relate to the conception and evaluation of composite structures in a general fashion. *Design*, in the context of this work, involves the conceptual phase, material evaluation and the selection of the most suitable configurations.

2.2.1 Material selection

Material selection is crucial for various reasons. First, lighter materials provide an easier means for reducing fuel consumption when compared to the efforts of improving the performance of powerplants. Historically, the improvement of jet aircraft efficiency in commercial aviation has been 2 % per year owing to advances in propulsion and materials [142]. As part of the design cycle, the material selection process drives structure and tooling definition as well as associated manufacturing and procurement activities [143, 144]. In this regard, PMC-based design leads to a plethora of materials to choose from and the theoretically-endless combinations thereof [145].

The material selection process addresses the client's needs and the design functional requirements defined thereof. This requires to consider the operating conditions encountered by the component in question. In general, the requirements of aircraft engine components [7, 146] differ to those encountered anywhere else in the aicraft structure. As mentioned in §2.1.1, the certification process of composite-based structures requires extensive validation, relying on testing of intermediate-scale specimens. Moreover, the certification of a single material system can take several years [51, 147]. In practice, however, aircraft designers rely on a reduced amount of certified/proven material systems. In the context of this dissertation, some questions still arise: from those suitable materials, which ones are fire-safe from an aircraft certification standpoint? Which one provides the best benefit/cost ratio?

Performing tests for each potential design configuration could translate into a long and pro-

hibitively expensive process. Moreover, the wrong choice of materials can lead components to under performance in one or several aspects which in turn will have an economical impact. For this reason, a thorough selection process should take into account different criteria which are not related and, most of the time, in conflict. Moreover, problems can take place years after certification in spite of the countless efforts nature of this process. An example of these unforeseen issues is represented by the update of increasinly stringent environmental regulations [54].

Approaches

Different material selection approaches exist for early identification of material candidates. Ashby *et al.* [145] defined the selection strategies as transfer functions that translate the design requirements into a list of "optimal" materials and process, which in turn need to be validated. The proposed selection strategies can be summarized as follows:

Free Search: quantitative analysis based on measured attributes.

Questionnaire-based: expert-opinion dependent.

Analogy: based on past cases or previous/similar applications.

Free Search involves crisp inputs, thus leading to straightforward designs. A graphical way to narrow down the search is by using so-called Ashby Charts [145] which facilitate the identification of candidates through material indexes. Nonetheless, qualitative parameters such as flammability do not support this kind of indicators. *Questionnaire-based* requires considerable expertise from different sources, e.g., seasoned designers or knowledge databases. Lessons-learned could also be considered in this category [148–150]. Unfortunately, this approach is resource intensive, since it requires the gathering of large amounts of information. Finally, *Analogy* refers either to legacy programs or proven materials that have been used for the same purposes or, as the name suggests, analogous applications. A fire-related example could be TPSs, which are exposed to extremely high heat fluxes used in spacecraft/ballistic applications [151]. In some other cases, this strategy may benefit from *serendipitous* events which can lead to side applications. However, it seems reasonable to consider *serendipity* inefficient within innovation and/or research [152]. In some cases, seasoned designers would simply discard some options based on their experience.

Screening

There is a need to evaluate material systems in a systematic manner to assess their suitability for fire protection purposes. A large number of possible material combinations can turn firewall testing into a long and resource-consuming survey [124, 153]. Hence, it is desirable to have a high-throughput test campaign that can help to decrease the cost and number of runs [154]. Nonetheless, the evaluation of fire resistance in the context of aircraft certification needs special test conditions that do not support a high cadence.

Owing to standardized tests, required material databases can feed material databases of qualified materials readily available or new materials can be considered for further screening. Some of these tests are even valid for spacecraft applications where other atmospheric/gravity constraints are in place [155]. A good example of this type of databases is contained in NASA STD-6001 [156], which provides flammability ratings that can be used to assess material suitability in preliminary design phases.

For burn-through purposes, material screening can be costly and time consuming. Alternative fire tests can be conceived to lower associated costs, such as alternative yet severe fire sources or small-scale tests with closer-to-reality thermomechanical loads. For relevant test methods, see §2.1.3.

Qualitative evaluation in fire tests

Engineering and design criteria can be vague in early phases such as conceptual design, or due to the nature of a property which cannot be assessed using discrete values. Regarding material evaluation, subjective scores impose themselves when the attributes cannot be measured. It becomes evident that crisp and non-crisp values should be considered in the material evaluation process. Moreover, due to different types of uncertainty present in fire evaluations, fuzzy evaluations are considered useful in the fire safety domain [82].

Material properties may not be available at preliminary design stages. In this regard, fire-induced phenomena can be interpreted through several physical and mechanical properties, e.g., backside temperature evaluation or residual strength. However, some of the evaluation criteria described in §2.1.2 such as burn-through resistance or those considered in traditional material selection processes (e.g. wear resistance, manufacturing ease) are not crisp nor straight-forward, hence the need for additional tools. Thus, qualitative evaluations can be useful (and actually needed) since some aspects of the materials' performance cannot be expressed with crisp values.

Paraphrasing Lord Kelvin[8], if something cannot be measured, the knowledge extracted therefrom is insufficient. Accordingly, instead of crisp values, linguistic evaluations can be obtained from the manufacturer or by an easy-to-implement/small-scale proof of concept.

Kawabata and Niwa [158] presented a revolutionary evaluation system for fabrics where not only their tensile, bending, shearing, and compression properties were incorporated into the evaluation process, but they also considered their handling properties strictly based on "feeling", i.e., stiffness, smoothness, fullness & softness, and crispness, all evaluated using a numerical scale ranging from "10-The strongest", down to "1-The weakest" and "0-No feeling". Furthermore, these scores could be expected to be different for the same material depending on the final application. These scores were translated intro a *total hand value*, which would rate a candidate from "5-Excellent", down to "1-Poor" and "0-Not useful". The final evaluation was done by integrating both qualitative and quantitative scores.

Kuhn [159] pointed at the value of qualitative measurements as the preamble to quantitative and meaningful evaluations. Based on this premise, fire tests should yield clear and measurable information that can be used in the material selection process. In this regard, fuzzy logic is considered as a useful tool in fire-related research as it does handle nuances [160]. This topic is detailed in §2.2.4.

2.2.2 Decision-making

People need to make decisions on a constant basis, regardless of the context. The human brain can handle decision-making problems to a certain extent, although biased judgments and decisions are inevitable [161, 162]. In other words, gains and losses are seen judged differently, and the outcome of a decision-making problem is easily affected by the way that a problem is formulated. This may be harmless in a common day-to-day situation. However, in an aircraft design context, a loss can compromise airworthiness and, consequently, people's safety. Unaccounted risks are simply unacceptable. Among the multiple decisions in this field (strategic planning, aircraft selection for certain), aircraft designers need to select materials and processes, often considering conflicting criteria.

In the context of aircraft design, decisions also have to be made all the time. For instance, Kellari *et al.* [45] performed an analysis of existing aircraft architectures. For a theoretical initial design space of 28 decision categories with multiple options each, the number of potential architectures and concepts considered in their study rose to 2.5×10^{14}. This extreme example highlights the need for decision-making tools.

[8] "If you cannot measure, your knowledge is meager and unsatisfactory" [157].

For this purpose, multi-criteria decision making (MCDM) tools have become powerful and essential means towards informed and sound decisions. In a general fire-safety context, several approaches exist when a decision is to be made and crisp data are available, such as the Edinburgh Cross-Impact Analysis, Hierarchical Cross-Impact Analysis and analytical hierarchy process (AHP). Other approaches involve the input from experts, such as the Delphi process [163].

The decision-making becomes more complicated when the criteria are heterogeneous and sometimes mutually-conflicting, as it often happens in the aircraft design process. Therefore, robust tools that enable the decision-making process are needed. Most of the time, conflicting or qualitative criteria hinders the design and decision-making process, pointing at the need for robust and unbiased decision-making methods [21]. The sheer number of methods and articles devoted to material selection using MCDM techniques indicates the plurality of possible approaches. Consequently, choosing a material selection method, is a decision-making problem itself [164]. Jahan *et al.* [21] comprehensively surveyed methods for material screening and their subsequent selection. Their review points at fuzzy MCDM methods when multi-dimensional, qualitative and or non-crisp data is available. This holds true for attributes like corrosion and wear resistance, or, in the context of this dissertation, *fire resistance*. Certainly, *fire resistance* can be broken down into specific quantitative attributes.

In this regard, any MCDM method has advantages and drawbacks which are well documented. For instance, ranking reversibility can take place when considering an alternative with lower performance. Chatterjee and Chakraborty [165] compared four MCDM methods in the context of material selection for a gear design. Although they used only crisp values, they pointed at the fact that the outcome of the ranking process is highly dependent on the input data. The authors also stated that the selection of the MCDM methods might not be the main issue, but rather the right definition of criteria and identification of alternatives. Athawale *et al.* [166] compared several MCDM methods on 3 different case studies to assess their effectiveness. Their findings also pointed at the importance of criteria definition rather than the selection method. The latter can thus be selected based on other factors.

Although MCDM methods have been used and adapted in a plethora of domains, the steadily growing body of fire-related literature indicates high potential for their introduction. For instance, Akka *et al.* [167] proposed a decision-making methodology to select a protective coating against fire for steel. The methodology, intended to handle the input of several decision makers, was based on AHP and considered 22 criteria divided in 4 families, i.e., economoy, safety, environmental and societal. To process the large amount of evalutions and criteria, they also relied on the geometric mean method (GMM).

On the traditional fire safety side (e.g. building/civil infrastructure), Cadena *et al.* [82] surveyed some popular uncertainty analysis methods used as part of the decision-making process. They highlighted the fact that no single approach can tackle all challenges related to uncertainty as part of a risk analysis. In other words, there is no *ultimate* decision-making tool.

2.2.3 Axiomatic design

Concepts

Axiomatic Design (AD), proposed by Suh [168,169], is a framework that confers a systematic and scientific approach to the design activities. According to Suh, AD was formulated after analyzing multiple design practices and products, and looking at what is needed for the conception of a good design. The cornerstone of AD is its two Axioms: *independence* and *information*. On the one hand, the *independence* Axiom "Maintain the independence of the FRs" relates to the intertwining, or in AD terms, coupling of FRs determined by the DPs. In other words, it means that the functions of a design must be independent of each other. On the other hand, the *information* Axiom "Minimize the information content of the design" simply states that the best design is the one with the highest probability of fulfilling a FR (or FRs). AD defines four different domains and their respective attributes as shown in Fig. 2.9 and described as follows:

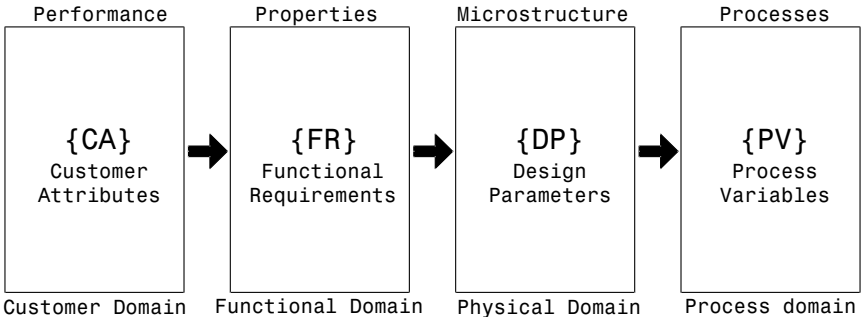

Figure 2.9 Axiomatic Design (AD) flowchart.

Customer Domain: customer attributes (CAs) are defined as the client's requirements.

Functional Domain: functional requirements (FRs) define the "what has to be achieved?".

Physical Domain: design parameters (DPs) define the "how it will be achieved?".

Process Domain: process variables (PVs) define the different tools to achieve the final product.

Each domain is related to at least another one as an input or output, and their definition is dictated by the previous domain. For instance, the FRs are the result of the requirements dictated by the customer, i.e., the CAs. In the case of FRs and DPs, both are input and output. Once that a level has been fully defined, a *zig-zagging* analysis is performed to ensure that each requirement or parameter is paired with its predecessor.

The idea of using AD instead of other design paradigms is that, by considering the functionality of the component in question and the required materials as well as the technology needed, other design approaches were also covered. For instance, by performing the mapping step between the FRs and DPs as well as between DPs and PV, the designer is forced to interact with other groups, which is characteristic of concurrent engineering.

Applications

AD can be used for any type of design. Ananthkrishnan [170] used AD to design a controller for a liquid ramjet engine. The approach was demonstrated by a decoupled design matrix to achieve performance, efficiency and safety defined as FRs.

Brown [171] suggested that a series of metrics (e.g. repeatability) should be established to evaluate the quality of the FRs to ensure that the CAs can be fulfilled adequately.

Cebi and Kahraman [172] merged AD and fuzzy sets into a tool that takes advantage of the benefits of AD as a systematic design methodology and the ability to define fuzzy design functionalities and criteria. The same authors subsequently demonstrated their methodology with a case study involving the design of a car indicator [173], determining the design parameters and their importance. They selected the best solution using the *information* axiom. More details about fuzzy sets are given in §2.2.4.

2.2.4 Fuzzy sets

The theory of fuzzy sets, formalized by Zadeh [174] in the 1960s, allows to deal with non-crisp definitions by using linguistic values. The concepts were shortly adapted and introduced into the field of decision-making by Bellman and Zadeh [175]. Therefore, in the context of this dissertation, fuzzy sets are relevant to the decision-making process owing to its capacity to deal with imprecise information towards making a decision, most commonly in the selection of an alternative. This can be done by ordering the global fuzzy score and thus selecting the

highest ranking, or by selecting the alternative closest to an ideal solution.

Basic concept

Fuzzy numbers are expressed by a membership function ($\mu(x)$). Fig. 2.10 shows the two $\mu(x)$ most commonly used: triangular or trapezoidal. In this example, the triangular $\mu(x)$ implies that the attribute has its full value or mean ($y = 1.0$) at $x = 3$, although it reaches 1.5 and 4.5 covering intermediate values to a smaller extent. A similar logic applies to the range contained in the trapezoidal $\mu(x)$. Further concepts will be given in Article #1 (§4). This section is limited to some applications found in the literature.

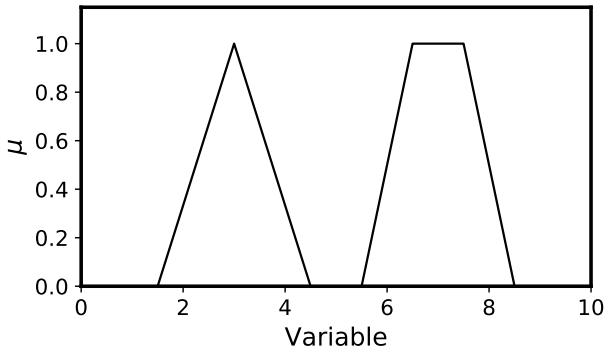

Figure 2.10 Basic fuzzy membership functions: triangular (left) and trapezoidal (right).

Applications

Different researchers have incorporated fuzzy sets in their general decision-making problems. Bellman and Zadeh [175] presented the bases of decision-making in a fuzzy environment by adapting fuzzy sets to a environment with fuzzy goals, constraints and, ultimately, decisions.

In the context of material selection, fuzzy MCDM has been considered a powerful tool since it can handle the vagueness of evaluation criteria such as material durability, corrosion resistance or, in the context of this dissertation, fire-resistance.

Aouam *et al.* [176] proposed a fuzzy multi-attribute decision making (MADM) method using an outranking intensity function, capable of considering both crisp and fuzzy attributes. Upon validation with a sensitivity analysis, the method was deemed lowly sensitive to the choice of parameters. However, they point at the fact that the selection of the fuzzy ranking method has a strong influence on the results.

Bruno *et al.* [177] addressed the problem of aircraft acquisition from an airline standpoint.

They proposed a hybrid model merging fuzzy sets and AHP to select an aircraft based on 8 criteria divided in four families: economical performance, technical performance, aircraft interior quality, environmental impact. They considered fuzzy sets given that some criteria such as seat comfort cannot be expressed in a specific number. They fuzzified the whole criteria set. The authors admitted that there is no "golden standard" for MCDM since each method entails its own advantages and drawbacks.

Carnahan *et al.* [178] explored the use of fuzzy ratings in MADM considering a material selection scenario. They used AHP to determine the level of importance of each criterion, and ordered the alternatives using Chen's "Max-Min" method [179].

Rao [180] developed a method that uses graph theory and matrices. If only qualitative data is available, fuzzy set theory is then applicable. Abdoli [181] used fuzzy logic in early design stages of complex engineering systems. They proposed a rule-based design framework that allows handling of qualitative criteria and uncertainty, demonstrated with case study focusing on the design of a warehouse with design requirements such as unloading, stacking, storing, picking shipping and considering future expansion and safety satisfaction as design goals.

Athanasopoulos *et al.* [182] presented a hybrid decision support system to be used in the selection process of a coating. Their model was based on fuzzy logic and a MCDM method, using Chen's "Max-Min set" [179] and Technique for Order of Preference by Similarity to Ideal Solution (TOPSIS) for ordering and ranking, respectively.

A fire-related application of AHP and fire safety was presented by Dodd and Donegan [183], who compared different techniques for relative importance assignment, highlighting the importance of fuzziness in fire safety.

2.3 CF fabrication and properties

After resin decomposition, pyrolysis and subsequent oxidation, the fire resistance of a structure is driven by the remaining reinforcement. Given the ubiquity of CFRP composites, it is important to understand the properties of CFs prior to reviewing their behavior under oxidative conditions. In this regard, the CF fabrication process drives the microstructure and, consequently, their physical, chemical and mechanical properties. These features influence their gasification behavior upon flame attack.

This section reviews the fabrication process of CFs, resulting microstructure, and tensile properties, which are relevant to the fire resistance of loaded composite structures.

2.3.1 Fabrication

Commercial CF fabrication methods rely on three types of precursors: polyacrylonitrile (PAN), pitch, and, to a lesser extent, rayon (cellulosic). Depending on the type of precursor and fabrication steps, CFs develop particular microstructures, hence the difference in mechanical (e.g., strength and stiffness) and physical properties (e.g. thermal conductivity, diameter, porosity) between types. Generally speaking, pitch-based CFs show higher modulus values when compared to PAN-based, while rayon-based CFs, although less and less used, deserves to be mentioned since they can be found in high temperature/ablative applications. PAN-based CFs account for most of the CF production ($\sim$96 %) [184], hence their widespread use in aerospace applications. Therefore, this dissertation focuses mainly on PAN-based CFs.

PAN fibers are initially manufactured via polymerization, followed by spinning and drawing. PAN fibers are then stabilized in oxidative atmosphere (e.g. air) at low temperatures (473 K $< T <$ 573 K) followed by high temperature carbonization (1273 K $< T <$ 1973 K) in an inert atmosphere. If higher moduli are sought, temperatures can reach up to 3000 K [34, 184].

Voids and structural defects may be traced back to the stabilization process where, depending on the nature of the PAN cyclization mechanism (radical or ionic for copolymers or homopolymers, respectively, although the latter are seldom used), chain scission due to uncontrolled or unwanted heating will have an effect on the final product [184]. Furthermore, the PAN fibers can be chemically modified to alter processing features such as stabilization time and to lower their activation energy. Some defects may be filled by metallic ions, yielding better mechanical properties. Other treatments increase the degree of crystallinity of PAN fibers, i.e., crystallite size and orientation [34].

Graphitization

The graphitization process consists in heat treatment at high temperatures. Part of the literature prior to the 1990s uses a CF classification consisting of three types, i.e., I, II and III which correspond to CFs processed at HTT ranges of $T \gtrsim 2000\,^{\circ}$C, 2000 °C $> T \gtrsim 1500\,^{\circ}$C, and $T \lesssim 1000\,^{\circ}$C, respectively. The first two correspond to current "high modulus" and "high strength" classifications, respectively, while the latter includes non-graphitized fibers and oxidized PAN fibers. Fig. 2.11 shows the overall process and a qualitative view of the level of crystallinity expected in carbon. Low processing temperatures yield amorphous carbons, with no apparent order, while high temperatures yield carbons with a better defined and ordered structure, closer to that of graphite.

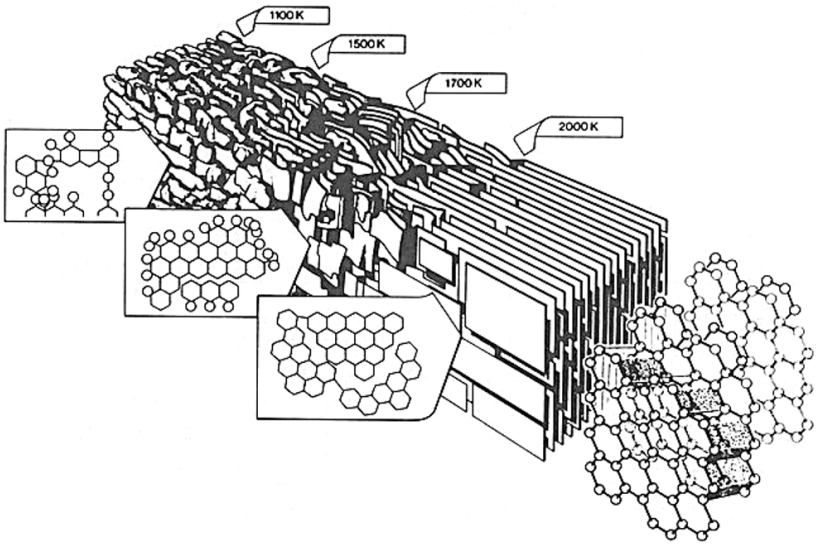

Figure 2.11 Marsh-Griffiths model of the HTT on carbon microstructure [185].

Additional treatments

After the graphitization process, CF may be treated with the aim of enhancing their adhesion properties, i.e., interfacial shear strength. Their surface can be modified by different means. Depending on the desired outcome, the functional groups' main function is to enhance chemical bonds whereas physical modification is indented to enhance mechanical interlocking [34, 184].

The surface treatment of CFs is a typical step within their fabrication process as part of the fiber/matrix adhesion improvement. Different treatment methods exist for surface modification, such as gaseous- and liquid-phase oxidation, whiskerization, pyrolytic carbon coating or polymer grafting. Additional approaches such as fiber sizing, which is an extended and popular technique, helps to protect fibers during textile processing [34] besides enhancing the fiber-matrix adhesion which in turn improves the mechanical properties of CFRPs (e.g. shear strength, related to the presence of functional groups [186]). Overall, all these methods modify the CF surface chemistry to some extent and some effects on the oxidation resistance / gasification process can be increased. However, some acid treatments may reduce the gasification rate of carbonaceous materials owing to Cl and P action [187].

2.3.2 Microstructure

The CF microstructure is dependent on the precursor used for their fabrication, although similarities are found between PAN-based CFs and their counterparts (pitch- and rayon-

based). In general terms, PAN-based CFs have a skin-core configuration comprised by a highly-ordered / *graphitic* outer section (skin or sheath) and a central amorphous/turbostratic structure. The following subsections describe the physical and chemical aspects of CFs from a microstructural standpoint.

Structural models

The crystal properties of basic structural units, namely interlayer spacing (d_{002}), lateral size (L_a) and stacking height (L_c), depend on the precursor's specific chemistry and processing conditions, i.e., stretching load, oxidation and carbonization temperature and time. This parameters will have an effect on the thermal and mechanical properties. For example, $lambda_L$ is related to the L_a [188], whereas the tensile modulus is driven by the degree of orientation and size of crystallites.

Barnet and Norr [189] proposed a CF core-sheath model after etching high modulus CFs in plasma, supported by their previous work [190]. Fig. 2.12a shows their model, where the core is composed of amorphous carbon while the sheath or skin has a more crystalline structure owing to the higher temperatures experienced during the graphitization process. Similarly, Bennett *et al.* [191] proposed the model shown in Fig. 2.12b, which describes the outer portions of the CF as aligned layers, whereas the core was conceptualized as randomly-oriented. Voids are the result of misaligned layering and crumpling.

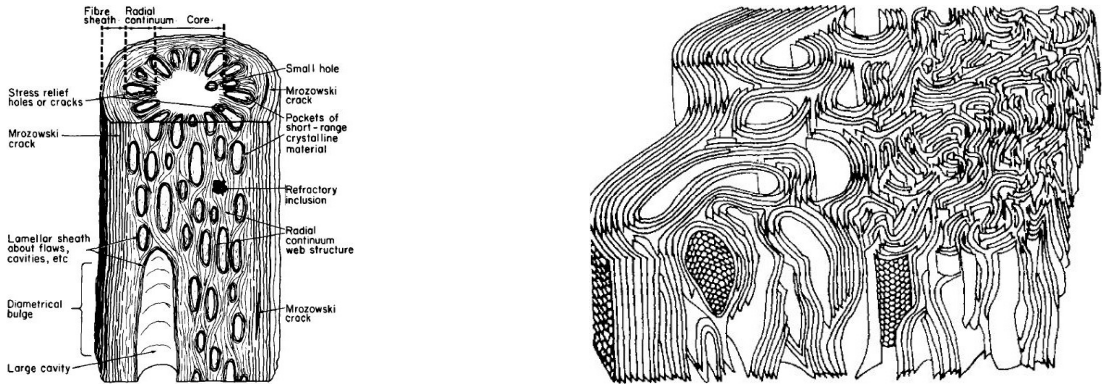

(a) (b)

Figure 2.12 (a) Skin-core model of high-modulus CFs proposed by Barnet and Norr (Reprinted from [189], with permission from Elsevier). (b) Schematic three-dimensional model of structure proposed by Bennett *et al.* (Reprinted from [191], with permission from Springer Nature).

According to Guigon *et al.* PAN-based CFs may be described with two typical structures,

depending on the level of crystallinity. For low and intermediate modulus fibres, their structure comprises a skin composed of small crystals with a turbostratic arrangement, somewhat aligned with the longitudinal axis, along with an amorphous carbon core [192]. For high modulus fibres, skin and inner crumpled sheets composed formed of larger crystal sheets [193].

Defects and heteroatoms

Defects found in the crystal structure of CFs influence their oxidative resistance. This section is limited to the description of possible defects found in the basic structural units (BSUs) and graphene layers. Their effects on the oxidative resistance of carbonaceous materials will be addressed in §2.4.2.

Fig. 2.13 shows different defects found in graphene-like materials at the nano-scale. Structural defects may lead to concave or convex surfaces, while topological ones may not affect considerably the C−C bonds nor the general geometry, although the graphene layering may be affected. Doping defects relate to sites occupied by heteroatoms, which may have catalytic or poisoning effects in an oxidative environment. Non-sp^2 hybridized carbon defects relate to missing C−C bonds, represented by zig-zag and *armchair* edges, vacancies, interstitials and adatoms. Meanwhile, folding affects the electronic state of the graphene layers.

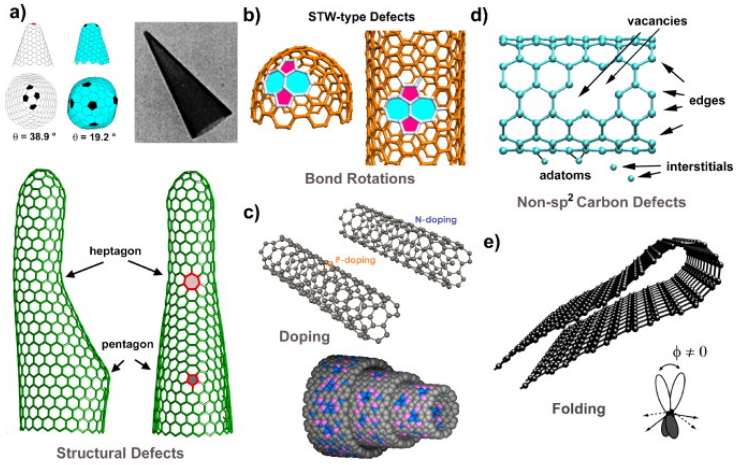

Figure 2.13 Schematic models representing different types of defects in graphene-like materials: (a) structural, (b) topological, (c) doping, (d) non-sp^2 hybridized carbon, and (e) folding-induced (Reprinted from [194], with permission from Elsevier).

Heteroatoms are relevant since they represent sites with preferential oxidation. Such is the case of impurities that may be more reactive to reactive species such as O_2, O, CO_2 and CO [195]. The main element to be considered is N, which has its origins in the PAN structure [184]. Boehm [196] suggested that the catalytic activity of carbon is affected by the presence

of nitrogen atoms in their structure. Guigon and Oberlin [197] highlighted the importance of N content in the CF crystal structure. On the one hand, they argued that high N contents between BSUs units help to increase the tensile strength. High levels of N can be found, for instance, in high strength CFs which are fabricated using relatively low HTTs. This is in line with the work of Yang *et al.* [198] who analyzed the effect of the amorphous content of PAN-based CFs by means of X-ray diffraction (XRD). The amorphous content has a major impact on the CF tensile strength, whereas the crystalline portion affects its stiffness, i.e., tensile modulus.

2.4 Carbon fiber oxidation

Carbon fibers (CFs) have excellent mechanical and physical properties over a wide temperature range, hence their ubiquity in modern aircraft where PMCs need to fulfill highly demanding structural functions (see §2.1.1). However, they are prone to damage at high temperatures in reactive environments and their continuous use under extreme heat is typically limited to inert conditions or where appropriate protective methods are available. In contrast, some design envelopes actually consider such reactivity a feature, with components being designed to overcome extreme heat and oxidative conditions for limited times while providing outstanding mechanical properties. Such is the case of C/C composites found in aircraft brakes [199, 200] and rocket nozzles [201]. In other cases, some CF-based materials are used in TPSs as ablatives [151].

CF oxidation is a topic that has received attention in several aerospace applications, namely in the long-term oxidation resistance of "high" temperature PMCs (e.g. BMI- or PI-based) [202], C/SiC high-temperature composites [203], thermal protection system (TPS) [151] and C/C rocket nozzles [201]. Other high-temperature applications from distant disciplines, such as nuclear engineering where graphite oxidation is a big safety concern in case of air ingress within a reactor, have helped to extend this understanding [204–207]. Additionally, the fundamental aspects of incomplete combustion, which translates into pollutant creation, has led to the investigation of carbon oxidation in the form of soot [208, 209].

2.4.1 Oxidation kinetics

Carbon is internally and externally gasified upon reaction with air or other O_2 sources in gas-phase reactive environments, e.g., flames [210, 211]. The main carbon oxidation reactions

are described by the surface reactions

$$\mathrm{C} + \mathrm{O_2} \longrightarrow \mathrm{CO_2} \tag{2.1}$$

$$2\,\mathrm{C} + \mathrm{O_2} \longrightarrow 2\,\mathrm{CO} \tag{2.2}$$

of which the latter predominates at high temperatures ($T > 1000\,\mathrm{K}$), with negligible contribution from the former. Regarding CO production, Eq. 2.2 starts at low temperatures ($T \approx 600\,\mathrm{K}$) and yields to the gas phase reaction

$$\mathrm{C} + \mathrm{CO_2} \longrightarrow 2\,\mathrm{CO} \tag{2.3}$$

at $T \approx 1600\,\mathrm{K}$. Moreover, the reaction

$$\mathrm{C} + \mathrm{H_2O} \longrightarrow \mathrm{CO} + \mathrm{H_2} \tag{2.4}$$

provides additional fuel which, besides the main $\mathrm{C}-\mathrm{O_2}$ reactions (Eqs. 2.1 & 2.2), CO can react with $\mathrm{O_2}$ as

$$2\,\mathrm{CO} + \mathrm{O_2} \longrightarrow 2\,\mathrm{CO_2} \tag{2.5}$$

promoting a loop with Eq. 2.4 in presence of $\mathrm{H_2O}$.

In presence of catalysts, the carbon oxidative process takes place in a different fashion. Such is the case when CO is considered. Two different avenues have been proposed to explain the CO-O interaction in present of a catalyst: the Langmuir-Hinshelwood and Eley-Rideal mechanisms [212]. The former relates to the chemisorption of the two reacting species on the catalyst surface before the reaction takes place, whereas the latter states that the chemisorbed species react directly with the one of the species in the gas phase. Baxter and Hu [212] showed that the former is the preferred oxidation mechanism.

Given the complexity of combustion-related processes, diverse pragmatic studies have been developed to describe the carbon oxidation phenomenon and its kinetics. Examples of these are graphite rods with an impinging oxidizing flow [213] or small carbon particle injection in flame reaction zones [214].

Carbon reaction regimes

As other carbonaceous materials [211, 215], CFs become highly reactive in the presence of $\mathrm{O_2}$ and other oxidative species as the temperature increases. Depending on several factors, oxi-

dation can take place in three different regimes [187, 215]. At temperatures below ∼375 °C, CFs are weakly reactive and the reaction rate is controlled by chemisorption of oxidative species at the surface. Investigations in this regime usually address long term stability of PMCs in harsh operating conditions [216–218]. At temperatures above ∼700 °C, the reaction rate is much higher than in the previous case, but less temperature-dependent when a stagnant gaseous atmosphere is assumed to surround the fibres. In this regime, the limiting factor is diffusion in the boundary layer adjacent to the surface and within pores in the solid. This situation is relevant for CC composites or the few CF-based CMCs where fibres can be exposed to oxidative species upon matrix damage [203].

Fig. 2.14 shows the effect of temperature on the gas-carbon reaction rate. At low temperatures (Zone I), the reactions are driven by the solid's reactivity, i.e.,chemisorption of reactants, and rearrangement of chemisorbed species to desorbable products, followed by desorption of the latter from the surface. In this regime, the measured activation energy (E_a) has the same value as the true E_a. Furthermore, at higher temperatures (Zone III), E_a has values close to zero, and the reaction is chiefly driven by the diffusion of oxidative species through the gaseous and relatively-stagnant layer that surrounds the carbonaceous particle [215]. Accordingly, Zone II is the transition zone between Zones I and III, with an in-pore diffusion controlled regime. Additionally, there is reactant chemisorption as in Zone I as well as transport of reactants towards active sites. E_a is approximately half of the value at Zone I [215].

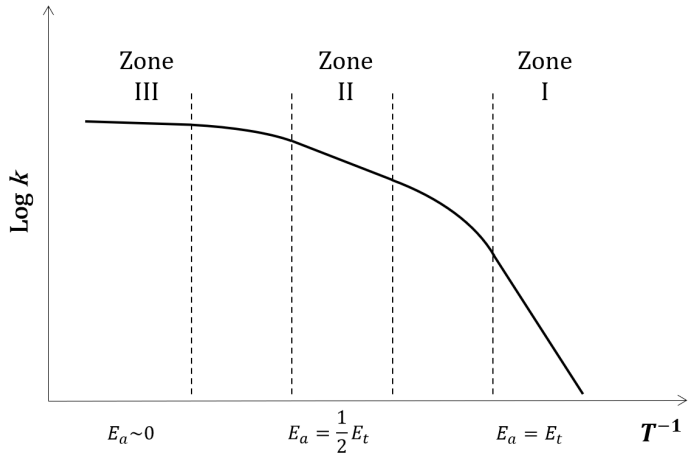

Figure 2.14 Carbon reaction regimes.

Fuertes *et al.* [219] modelled the gasification of CF. More specifically, they focused on the evolution of the CF's internal pore network taking into account different reaction regimes. In their model, they initially assumed the fibers to be formed of concentric cylindrical layers with

reactants uniformly distributed in between. They pointed at the importance of the Φ, since it describes the pore diffusional resistance. At low and high Φ values, oxidation takes place in the chemical and diffusion control regimes (Zones I and III, respectively).They described a non-uniform porosity distribution, with different pore growth rates existing between the fiber's center and its periphery. They also pointed at the fact that the internal porosity develops differently when compared to the fiber diameter. In practical terms, this means that fibers can be weakened due to higher internal porosity before observing a significant change in diameter.

Gee and Little [220] studied the oxidation of woven C/C composites made from rayon-based CFs and phenolic resin focusing on the diffusion of oxygen. They used high density isotropic graphite as benchmark. They coated the composites and graphite with SiC at different thicknesses, and applied a B_2O_3 in the form of paste. The oxidation kinetics analyses were carried out in a vertical tube furnace with air flowing at 6 mL/min from 500–1200 °C and most of the time at 20 °C min^{-1}. Their results confirmed the different oxidation regimes with different control mechanisms. At low temperatures, the oxidation rate is surface reaction-controlled, while at higher temperatures, in the chemical regime, the oxidation is limited by the desorption of the oxidation products off the surface, typically initiated at active sites. They observed extensive pitting on the graphite specimen, and concluded that the kinetics of carbon gasification are affected by impurities, concentration of active sites, degree of crystallinity, the pore network and the way the oxidizing gases diffuse towards the active sites.

In the fire hazard scenarios considered in the certification standards mentioned in §2.1.2, the temperature of the solid phase exposed to the pilot flame call fall in an intermediate range ($375\,^{\circ}\mathrm{C} \lesssim T \lesssim 700\,^{\circ}\mathrm{C}$) [221]. Here the situation is more complex as there is bulk fluid motion induced by the pilot flame and, as a result, the reaction rate is controlled by a combination of advection, diffusion and chemisorption. Consequently, assessing the reactivity of CFs in the context of fire resistance in this temperature range is best done using realistic flames.

Thermal characterization

For practical design purposes, standard tests are available for comparison of the CF oxidation behaviour at low temperatures. For instance, CFs can be evaluated in air-circulating ovens at 315 or 375 °C for 500 or 24 h, respectively, to determine their long-term thermal stability [222].

The oxidative behavior of CFs can be determined using traditional thermoanalytical techniques [203, 223] to obtain useful information regarding their kinetic parameters. TGA can help to reveal the CF behavior at higher temperatures and different oxidizer flow rates. Al-

though the temperatures considered in such techniques are far from the conditions found in a fire, the results may be useful for screening purposes.

Differences based on heat-up rate (HUR) and fiber type have been seldom discussed in the literature focusing on the CF oxidative behavior. In some cases, isothermal methods have been favoured over non-isothermal conditions [203, 223–225] mainly due to a major focus on long term stability. Additionally, such works have used established methods to obtain activation energies. In other cases, non-isothermal analyses were used as an alternative tool to obtain activation energies considering dynamic atmospheres. However, similar mass loss rates were reported, although yielding different oxidation onset temperatures with increasing HURs [226].

Gibbs *et al.* [217] studied the oxidative stability of several commercially-available CFs. They analyzed their thermal stability using an oven ($V = 28\,\mathrm{L}$; 1 h for full air re-circulation cycle) and a TGA apparatus. With the former, they aged the specimens in air in the 533–589 K range for hundreds of hours. The latter method was used to run tests at $20\,^{\circ}\mathrm{C\,min^{-1}}$ in air. They also endeavored to correlate the results from the aforementioned thermal analyses with the fibers' crystal parameters by means of XRD. They concluded that the TGA cannot be considered reliable for predicting thermal-oxidative stability at the temperatures studied. However, their results clearly revealed a direct relationship between the CF stability and the Na content, i.e., lower Na levels led to the higher CFs oxidative stability. The XRD results were found to be an unreliable indicator of the CFs' thermal stability. However, the crystal size is determined by the CF's HTT; high HTTs lead to larger/more ordered crystals and higher density. At the same time, impurity vaporization (such as Na) is promoted. Consequently, large crystal parameters correlate with lower impurities.

Asaro *et al.* compared blends of phenolic resin with carbon black and mesoporous SiO_2 particles, both at 5 and 20 % (wt.). They tested them under the attack of an oxyacetylene torch and reported a considerable improvement in the ablative behavior when compared to neat phenolic. Interestingly, they compared their results with data obtained from TGA, highlighting the fact that such technique does not give a full picture of materials in extremely reactive conditions such as a C_2H_2-O_2 flame.

Eckstein [218] analyzed the thermal oxidative stability of PAN-, pitch- (both isotropic and mesophase), and rayon-based CFs in air for 1000 h in the 230–375 K range. The contents of C, H and ash (in %) as well of impurities (Li, Na, K, Mg, Ca, Ba; in ppm) were determined by TGA and atomic absorption, respectively. E_a values varied between CFs, being attributed to the difference of precursor. The form of the carbon was identified as a key factor in the oxidation process. The results also suggest that there is no significant difference between CFs

as long as high C levels are present. For instance, similar C contents of pitch-based fibers can be achieved with PAN-based CFs by increasing the HTT. SEM observations did not show significant differences, supporting the idea that complementary methods should be used.

The apparent E_a values can be affected by several factors [203] with the selected evaluation method. The E_a values obtained with TGA usually correspond to low HURs and, thus, are only applicable to the low-temperature reaction zone, i.e., Zone I of the gas-carbon reaction scheme. Different values can be obtained from similar carbon types due to different temperature and pressure ranges, oxidizer type as well as evaluation method, i.e., isothermal or non-isothermal. Other aspects involve fiber size and packing, which in turn influence the diffusion of oxidative species within the sample. Contescu *et al.* [206] emphasized the fact that the data obtained by means of TGA are highly dependent on the test conditions. For instance, they showed that the transition between Zones I and II depends on the oxidizer flow since it affects the in-pore diffusion regime. Their tests considered the same type of high purity graphite and same heating ramp. They showed that, under the same heating and oxidizer flow conditions, various graphite materials yield different activation energy values. They concluded their work comparing their results with previous data obtained from similar exercises, revealing big discrepancies in reaction rates even for analytical grade graphite.

Reactivity

The oxidation process of carbonaceous materials is highly dependent on several factors, namely temperature, humidity, pressure, and oxidative species. From the carbonaceous material standpoint, the reactivity is driven by the microstructure which can also be described by several means such as crystallinity, porosity, impurities and internal surface.

Laine *et al.* [227] pioneered the concept of active surface area (ASA) and its importance on the oxidative behavior of carbonaceous materials, highlighting that this factor is more relevant than the total area. They highlighted the evolution of ASA as a result of the burn-off process.

Ehrburger *et al.* [228] analyzed the carbon reactivity considering the concept of active sites. They measured the total surface area (TSA) and ASA by means of Kr adsorption with the Brunauer-Emmett-Teller (BET) method and following the method of Laine *et al.* [227] of different carbonaceous materials: graphitized carbon black, oxidized PAN felts, pyrolytic carbon, and a char obtained from phenolic resin. Except for the first material, all of them where treated at low and high temperatures to analyze the effect of graphitization. Elemental analysis was performed, identifying Na and Fe in all CF felts and pyrolytic carbons, regardless of the heat treatment. Additionally, K, Ca, and Zn were found on the CF felts. They reported an increase of TSA for disordered carbon (e.g. felts) at low burn-off levels ($\lesssim 20\,\%$), followed

by stabilization. A similar behavior was observed on ASA. E_a values varied with respect to the degree of graphitization, with pyrolytic carbons and char yielding the highest and lowest values, respectively.

Hippo *et al.* [187] reviewed the factors that intervene in carbon gasification and possible approaches towards its inhibition. As shown in Table 2.1, these can be grouped in temperature (environment and sample), oxidizer (type and flow rate), carbon type (translating into pore size, distribution and crystal parameters), catalysts and inhibitors. They emphasized the role of active sites, which are present within graphite lattice structures, and the more-vulnerable *zig-zag* edges with respect to arm-chair structures.

Table 2.1 Factors involved in carbon gasification and related inhibition (adapted from [187]).

Main elements	Factor(s)
Environmental conditions	Temperature Pressure
Carbonaceous material	Temperature Active Surface Area Pores Crystal structure
Oxidizer	Type Flow rate
Catalyst	Type / state Concentration Cluster size Spill-over rate
Inhibitor	Type

As previously mentioned, the ASA is a key parameter in the oxidation process of carbonaceous materials [187,227,229,230], representing the amount of sites that readily react with oxidative species. Its value depends on the CF type and evolves upon fiber burn-off, which in turn yields different oxidative behavior.

Specific CF-related analyses have been also conducted to assess their oxidation behavior and allow a comparison based on the type of precursor. Oh *et al.* [231] reported different oxidation mechanisms between two standard modulus CFs, with a more pronounced core damage on fibers with higher tensile strength, i.e., higher amorphous content [198]. Ismail [230] provided a detailed account of the thermal behaviour of PAN-, pitch- and rayon-based CFs

based on isothermal heating. The role of pore creation and oxygen diffusion thereof . In a subsequent work, Ismail and Hurley [226] explored the non-isothermal oxidation of the same CF families and proposed temperature corresponding to the maximum oxidation rate (T_{max}) and temperature attained at 0.5 fractional burn-off ($T_{0.5}$) as reactivity indices that could be used to model CF oxidation without further details on the active surface, namely ASA or TSA.

Halbig *et al.* [203] studied the oxidation behaviour of C/SiC composites with no oxidation inhibitors. The oxidation of T300 (high strength, standard modulus) CFs within a cracked SiC matrix with a load being applied. Standalone fibers were analyzed via isothermal TGA at different temperatures. The oxidative behaviour of the C/SiC composite was analyzed under equilibrium and stressed conditions. They obtained E_a values in the three regimes, i.e.,118.3, 64.4 and 7.7 $\mathrm{kJ\,mol^{-1}}$, which are typical of high strength / standard modulus CFs.

Govorov *et al.* [232] analyzed the behavior of PAN-based CF, treating oxidized PAN fibres (PANEX 35 from Zoltek) in a vacuum furnace up to HTTs of 1500, 2000, 2400 and 2800 °C using a HUR of 10 $\mathrm{°C\,min^{-1}}$ and a dwell time of 1 h. Subsequently, the CFs were analyzed by means of TGA under air atmosphere with different HURs 5, 10 and 20 $\mathrm{°C\,min^{-1}}$ to obtain E_a values. Apparent E_a increased with HTT due to removal of impurities and crystal enlargement. The number of defects also reduced with increased HTT active sites where oxidative species can be chemisorbed were reduced. [232].

2.4.2 Influencing factors

Microstructure

As mentioned in §2.3.2, the CF microstructure is chiefly defined by the precursor and the subsequent fabrication steps. Consequently, CFs with different mechanical properties have portions where amorphous carbon and more-graphitic portions predominate to different extents. It is therefore important to understand the influence of microstructure on the CF oxidation process since CFs with different thermal treatments are expected to show distinct oxidative resistance.

From carbon nanotube (CNT) purification experiments, Ajayan *et al.* [233] showed that even with highly ordered carbonaceous structures, weight loss takes place at different temperatures. For example, fullerenes (C_{60}) decompose at lower temperatures than single (SWCNTs) and multi-walled carbon nanotubes (MWCNTs), mainly due to the pentagon arrangement needed in icospiral structures. Additionally, the CNTs' caps open first, confirming that non-hexagonal C arrangements and curvature-induced strain promote preferential oxidation.

Later Ebbesen *et al.* [234] complemented the aforementioned results, indicating that the burn-off intended for separation of CNTs from a blend with carbonaceous nanoparticles entailed a weight loss of 99 %, suggesting the high oxidative resistance of the former with respect to the latter.

From a chemical standpoint, the surface chemistry has an impact on the oxidation process as well in catalysis. Depending on the surface groups, selective oxidation reactions can take place as discussed by Figueiredo *et al.* [195]. These groups can be divided in N-based (e.g., pyrrole, pyridone, oxidized N, quaternary N, pyridine) and O-based (e.g., carboxyl, lactone, lactol, phenol, carbonyl, anhydride, ether, quinone, pyrone, chromene). Nonetheless, it is unclear which functional groups have a greater impact on CFs exposed to highly oxidative atmospheres.

Ismail [229] compared the surface characteristics and oxidative behavior of PAN- (T-300, standard modulus) and pitch-based (P-55) CFs before and after graphitization at 2973 K. Initial porosity assessment using BET measurements revealed a closed pore network. Upon graphitization, the diameter of PAN- and pitch-based CFs decreased and increased respectively. The former was attributed to the transformation of amorphous carbon into crystalline materials, while the latter, described as *puffing*, was attributed to the release of S which is characteristic of pitch-based CFs. Graphitization also lowered the concentration of Na and K in both cases. Upon treatment at 573 K in high purity O_2 at pressures ranging from 0.067–13.3 kPa for 500–3100 h, they found that the apparent ASA of the pitch-based CFs did not change significantly. However, the PAN-based had a different behavior, mainly explained by a larger amount of imperfections, suggesting that the removal of one active site may generate as many as three sites. It was also concluded that the method developed by Laine *et al.* yields unrealistic values of ASA when applied to CFs.

Subsequently, Ismail and Walker Jr. [235] analyzed the interaction of Saran[9] char with O_2 at a relatively low temperature range 77–222 °C using TGA and DSC. They also analyzed its oxidative behavior from 450–550 °C. Due to the nature of the precursor (vinylidene chloride and vinyl chloride), Cl was expected in the char. After pyrolysis, Cl traces were confirmed by means of NAA. Additionally, some metal impurities (Fe, B, Al, Ca, Si, Cu) were found by emission spectroscopy. They proposed two gasification avenues. On the one hand, direct impingement of O_2 onto vacant carbon sites followed by immediate gasification. On the other hand, O_2 diffusion from carbon sites with no C/O_2 interaction to sites prone to gasification. They also proposed the existence of super active sites at low temperatures, which get annealed at higher temperatures and that do not participate in subsequent gasification.

[9] Commercial name of a copolymer of vinylidene chloride and vinyl chloride.

These works highlight the importance of CF microstructure in their oxidation process. Thus, it is expected that CFs with different mechanical properties, i.e., different microstructure, will not behave in the same fashion when exposed to highly reactive environments, such as those found under open flame attack.

Impurities

Impurities can enhance or hinder the carbon gasification process [215], hence the importance of knowing their concentration in CFs. Besides having an effect on CF's mechanical properties [236] due to disruptions in the cyclic layered structure, impurities do influence the CF oxidative resistance. Such is the case of alkali and alkaline earth metals, whose catalytic effect has been confirmed under conditions different to those found in fire scenarios [202, 217, 218, 230].

Blyholder *et al.* [237] were some of the first to analyze the oxidation kinetics of carbonized filaments, suggesting that active sites and impurities were causing the somewhat large differences reported by other groups.

Amariglio and Duval [238] analyzed the catalytic gasification of high purity graphite, and found that Pb enhanced five orders of magnitude the oxidation of the base material, which meant 2000 times that of Na. They impregnated 1 g of ultra-high purity graphite with various impurities using a precise impregnation methodology. With most of the impurities ranging in the 70-130 ppm threshold, their results can be arbitrarily grouped in uncatalyzed (Be: 1x & B: 1x)) as well as small (Al: 3x, Ca: 4x, Mg: 6x, Sr: 8x), moderate (Ni: 32x, Cd: 90x, Ba: 100x), high (Na: 230x, Au: 240x, V: 340x, Cu: 500x, Ag: 1340x), and ultra-high (Cs: 64 000x, Mn:86 000x and Pb: 470 000x) catalytic reactions.

Iacocca and Duquette [239] studied the catalytic effect of Pt on the oxidation of CFs, being relevant since some thermoanalytical devices use Pt-based crucibles. Using a tube furnace, they compared the mass loss of PAN-based CFs extracted from 50K tows using Pt- and SiO_2-based crucibles exposed to dry air at 500, 550 and 600 °C for several hours. They obtained marked differences between containers at the two lowest temperatures, whereas mass loss rates were not possible to be determined at 600 °C. Using SEM, they reported extreme pitting, bifurcated fibers, and fibers with beads where oxidation apparently took place at lower speeds only on the CFs treated in the Pt crucible. Moreover, and surprisingly, the E_a obtained from the Pt- and SiO_2-based experiments yielded 301 and 177 $\mathrm{kJ\,mol^{-1}}$. Only the latter is in line with other values reported in the literature for CFs. The former is closer to values obtained from graphite specimens, making less sense given the higher reactivity observed in micrographs.

Scola and Laube [202] suggested that high Na concentrations are not the main factor for some fiber oxidation. Instead, they pointed at the O_2 and N_2 surface concentrations and crystal order. HM63 fibers show no N_2 concentrations. This can be translated into more stable fibers, showing no traces of their former N_2-rich PAN structure.

Whether impurities are intentionally added or a result of in-process contamination, they may work as oxidation catalysts. Most of the relevant literature on CF gasification and the effects of catalysts is either the result of efforts made on alleviating electrical and health hazards, or long term oxidation resistance for high-temperature CFRP composites. Their presence can have catalytic effects [215, 240] that are recognized to be more important than microstructure in the fibre oxidation phenomena [216, 218, 230]. Their origin can be traced back to the manufacturing of the fibre precursor itself and the final processing conditions. Subsequently, more impurities can be added by surface treatments that enhance fibre/matrix interaction [34]. In particular, alkali metals remaining from precursors or fibre treatments can have a spectacular effect on degradation rate [218, 230]. In most cases, oxidation is to be avoided [151, 200, 202, 203] but in certain scenarios these impurities are desirable to promote efficient fibre combustion, mitigating health and electrical hazards [11–13, 241].

In an effort to ensure full CF gasification to alleviate electrical hazards from potential aircraft crashed and subsequent fires, Hull *et al.* [13] analyzed the effect of different Ca and Li acetate surface treatments on the CF gasification while avoiding detrimental effects on the mechanical properties. Using a propane torch, they analyzed the fiber release after 450 s exposure of treated and untreated fiber-based composites (unknown composition). They found a two orders of magnitude reduction of fibers released on treated samples. Ganjei *et al.* [12] tested several resin additives and incorporated metal-based acetates (Pb, Pb/Li, $Pb(NO_3)_2$, $Bi(NO_3)_3$, V, Cs, Li, K, Na, Ba, Ca, Sr, Cu, $AgNO_3$, Co, Cr, Mn, Ce) in different carbon/epoxy samples. They found out that Pb was an extremely effective catalyst, potentially reducing the temperature at which thermal runaway starts on treated CFs. They did not find evidence on detrimental synergistic effects, i.e., different additives would have the effect of the most aggressive one by its own. However, they found that some of the epoxy formulations may hinder the catalytic effect of these additives, thus necessitating higher concentrations. In this regard, Bell [10] separately mentioned a hypothetical effect of burnt resin, suggesting that this could leave residues with catalytic effects, although this was not proven.

Other elements which are common in CF surface treatment have been identified as effective catalysts. For example, Gibbs *et al.* reported the long term stability at low temperature, i.e., 315 °C for 700 h, of CFs with different Na contents. Fibers with a 2000 to 10 000 ppm Na content exhibited a significant weight loss, and thus an oxidation mechanism was proposed

for fibers treated with Na_2SO_4.

However, other elements can stabilize the carbon structure and inhibit the catalytic oxidation process by reducing the amount of sites prone to oxygen attack. The intercalation of some elements may have a positive result towards the improvement of the oxidative resistance of carbonaceous materials. For instance, the presence of Si can have a stabilizing effect by forming silicates [242]. In a similar fashion, it has been reported that the presence of S hinders the catalyst effect of some alkaline earth metals (i.e.,Ca, Ba and Sr) [243]. Wang *et al.* [244] demonstrated that the addition of B improved the oxidative resistance of PAN-based CFs. This was demonstrated when the oxidation onset was shifted to ∼800 °C. Wu and Radovic also showed with C/C composites that the addition of B [245] or P [246] could inhibit the catalytic oxidation process by reducing the amount of vacant sites, i.e., active sites, or by poisoning the catalytic effect, e.g., with help of Cl. This poisoning effect is catalyst-dependent. For instance, the catalyst effect of Ca acetate was suppressed, whereas the K-based catalyst effect was slightly hindered. Other avenues such as fiber coating with B, can also prove to be effective. For example, Tang [247] reported and increase of 260 °C on the oxidation onset and doubling of the E_a.

It must be noted that the flame nature and metallic impurities remain under the spotlight owing to new hazards brought by Li-ion batteries. Their thermal instability can result in large-scale fires. Unsurprisingly, the FAA has limited their transport to personal devices in passenger aircraft, banning their presence in the cargo compartment of passenger aircraft. Their transportation at a larger scale is now only possible in cargo aircraft [61], hence its relevance in the design process of *fire resistant* cargo liners. The experience with battery-related fires in automotive applications [248] suggests new challenges in the fire resistance of fully-electric aircraft structures, which continue to rely extensively on CFRP composites.

2.4.3 Effect on mechanical properties

The damage-induced failure mechanisms have been studied in other types of fibers under different conditions, shedding some light on the possible damage in CFs and their bundles under tension. For instance, Evans *et al.* [249] and Caddock [250] studied the effect of corrosion on GF bundles exposed to HCl following a statistical approach, i.e., considering Weibull parameters. At short exposure times, they reported a slight decrease in tensile strength and modulus but less variability (higher shape parameter, i.e., m value), possibly explained due to flaw reduction owing the initial surface smoothing.

The study of CF strength and stiffness under fire attack has been limited to simulated conditions, i.e, relatively high temperature in non-inert atmospheres, where flames have not

been considered.

Yin *et al.* [251] used a muffle furnace to oxidize fibers in the range of 823–1133 K. Additionally, they assessed the weight loss via TGA. Subsequently, the crystal structure was evaluated with XRD and the resulting chemical composition by means of EDS. Similarly, Kim *et al.* [252] compared the oxidation behaviour of pitch-, PAN- and rayon-based fibers.

Alcañiz-Monge *et al.* [253] addressed the activation of pitch-based CFs and the effect that microporosity and its evolution had on the tensile strength. They activated the aforementioned fibers in CO_2 and H_2O vapour and assessed porosity by adsorption means. They observed different pore growth and fiber tensile strengths from each activating agent. That is, steam promoted a faster evolution of microporosity *vs.* CO_2. However, CO_2 generated more micropores while fiber diameter remained relatively unchanged.

Bertran *et al.* [225] oxidized HTA fibers under controlled conditions using a TGA apparatus. In their study, they analyzed the thermal stability in the 673–873 K range with and without moisture. They observed changes on surface roughness that entailed the enlargement of existing defects or the creation of new ones. Thus, a severe reduction of mechanical properties was observed even at low weight losses ($\lesssim 15\,\%$). Their findings are in line with the work of Feih and Mouritz [224].

At this point, it is important to mention the research of Feih and Mouritz [224]. It is arguably the most complete work to date addressing the evolution of CF oxidation under simulated fire conditions and the evolution of their tensile properties. They performed a series of tests based on high-temperature / quiescent conditions subjecting CFs to 600 °C using a furnace tube, seeking homogeneous/gradual burn-off. Single fibers tensile tests were subsequently performed, from which tensile strength and modulus were obtained. Owing to the homogeneous fiber diameter reduction observed in their tests, the well-known skin-core model was confirmed. Fig. 2.15a shows the evolution of the CF's Young's modulus with respect to its mass loss. The plot shows two different sections which correspond to the skin-dominated ($\lesssim 35\,\%$ mass loss) and core-dominated ($\gtrsim 35\,\%$ mass loss) portions. These results confirm the skin-core model previously described. This loss in Young's modulus is explained by the gradual loss of the stiffer skin and, once the more-graphitic portion has been fully oxidized, the more-compliant core dominates this behavior. From a statistical standpoint, Fig. 2.15b shows the change on the Weibull strength distributions when CFs were treated at 500 °C (top) and 650 °C (bottom) for 30 min and 1 h, respectively, in air and N_2. Regardless of the HTT and atmosphere, the Weibull strength decreased when compared to the unheated CFs tested at room temperature, hinting at the creation of flaws. To complement these results, Fig. 2.16a shows the evolution of the Weibull strength with respect to the HTT for

two different exposures, i.e., 30 min and 2 h. The plot shows that there is a considerable reduction of the Weibull strength taking place in a temperature window ranging from 400 to 600 °C. Differences in Weibull strength between exposure times can be observed within the aforementioned temperature window. However, it stabilizes in both cases at ∼58 % of the original Weibull strength. Finally, they calculated the average flaw size based on the Weibull strength values. Fig. 2.16b shows that below ∼450 °C, the critical flaw size remains stable, close to ∼30 nm. However, once past this temperature, the flaw size increased, reaching its maximum values at ∼600 °C and stabilizing afterwards. These results show that, in addition to the reduction of fiber diameter, the CF oxidation process entails the creation of new flaws or growth of existing ones. Consequently, these flaws increase the probability failure at lower stresses, translating into lower Weibull strength values.

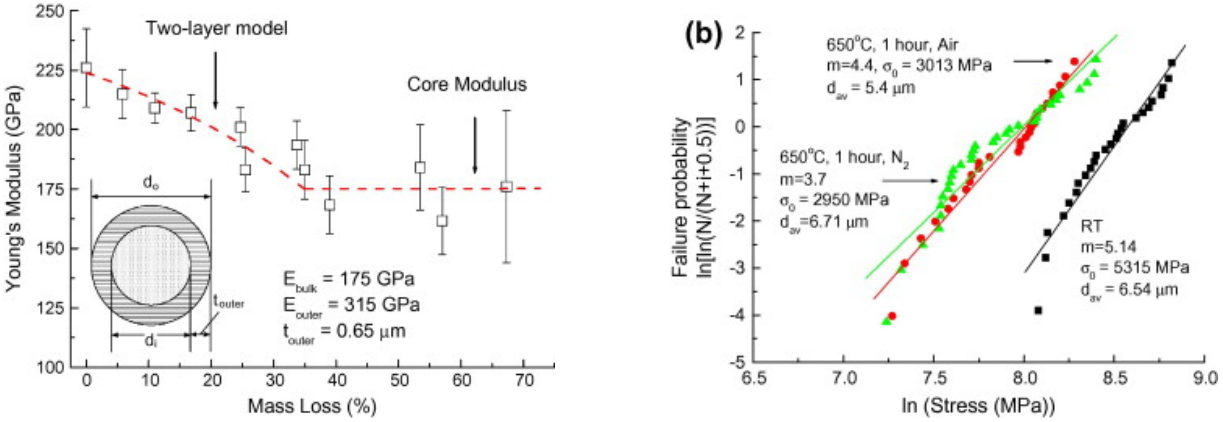

Figure 2.15 (a) Relationship between Young's modulus and mass loss of carbon fibre when heated in air, and (b) Weibull strength distribution plots for the original carbon fibre and the fibre following heat-treatment at (top) 500 °C and 30 min (partial strength loss) and (bottom) 650 °C for 1 h (steady-state strength loss) (Both reprinted from [224], with permission from Elsevier).

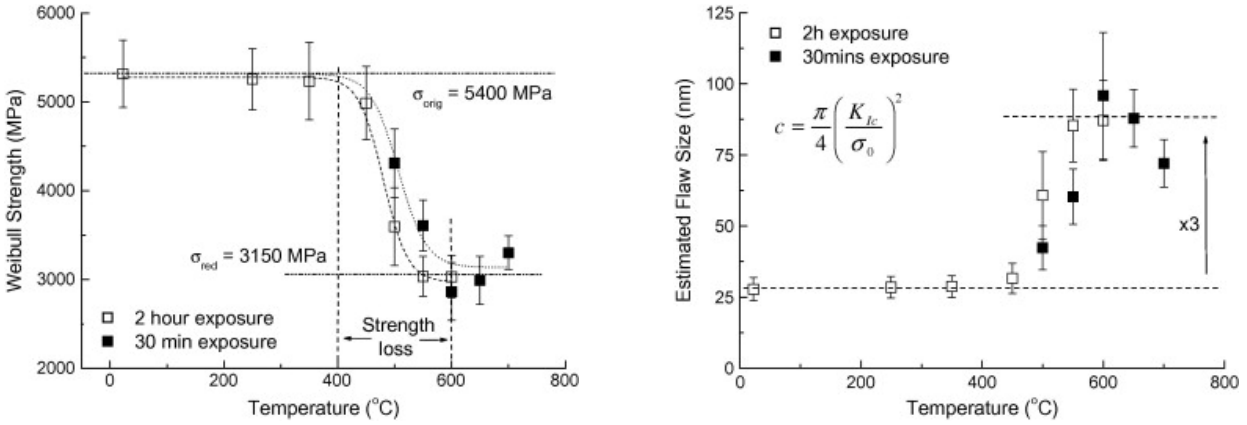

(a) (b)

Figure 2.16 (a) Effect of temperature on carbon fibre strength when heated in air, and (b) Estimated flaw size on fibre surface following heat-treatment in air at different temperatures (Both reprinted from [224], with permission from Elsevier).

Vautard *et al.* [254] oxidized CFs using chemical means and performed tensile tests on single fibers. They noticed a change on crystal dimensions (L_a) and reported a change on Weibull parameters of their tensile strength.

2.4.4 Fire-induced damage

This dissertation revolves around the oxidation-induced damage of CFs under true flame attack, for which relevant literature is quite scarce. However, some insight was gained in the late 1970s from a series of tests performed by the NASA and some of their contractors [10]. They reported a difference between tests performed with propane burner and those from large pool fires. Fiber size reduction was predominant on thinner samples than in thicker ones. Moreover, the effect of air circulation on smoldering composites was confirmed when these flows led to thinner fibers (less than 4 µm *vs.* usual 6–8 µm). Some of these tests explored the effect of fuel/oxidizer ratios using a custom setup [255] that used a radiant heat source as well as the injection of a gaseous fuel (natural gas) / air mix to better simulate real fire conditions. Individual CF plies extracted from already-burnt CFRP composites were subjected to lean and rich conditions. The lean configuration yielded a 100 % weight loss at half of the time of the latter, with a linear behaviour on both cases. Besides the effects of mechanical aggressiveness of lean combustion conditions on the mass loss weight was confirmed, combustion gases agitation, pulsated injection of inert gases, as well as simulated blasts (either with explosives or aggressive high speed bursts) were some of the conditions

that were studied. Part of these results point at the lower combustion resistance of standard modulus fibers, which are the most widespread.

Eibl [256] compared the mass loss and diameter evolution of standard (HTA40) and intermediate (IM7) modulus CFs in CC-based tests. Differences were reported as a function of q (20, 40, 60 and 80 $\mathrm{kW\,m^{-2}}$)/temperature (600, 650, 700 and 750 °C) and time (5, 10, 15 and 20 min), specimen weight (5, 25, 50, 100, 250 and 500 mg). The author also analyzed the HTA40 fibers as part of a carbon/epoxy laminate with TGA. The effect of different fire retardants ($Mg(OH)_2$, $Al(OH)_3$, zinc borate, and combinations thereof) on the fiber diameter reduction was also studied. It was found that zinc borate creates a glassy protective layer that prevents fiber diameter reduction. In general, IM7 fibers showed more marked differences than AS4 fibers. The reduction of CF diameter and weight was reported highlighting differences owing to heat flux, exposure time and initial fiber diameter. Pits were reported as "defects". No relevant pitting was observed on specimens that were immediately removed from the heating zone, but rather only on those left in the test area, allowing oxygen diffusion from the surroundings.

Detailed analyses of CF oxidation due to fire attack are still needed. However, carbon oxidation under true flame conditions has been assessed using other carbonaceous materials. For instance, it has been reported that soot oxidation is highly influenced by hydroxyl (OH) radicals in absence of O_2. Fenimore and Jones [208] studied the oxidation of soot obtained from ethylene/oxygen/argon flames, feeding a second burner. In absence of O_2, the oxidizing action was attributed to OH. This can be explained by the main oxidation mechanism of CO [257] given by:

$$\mathrm{OH + CO \longrightarrow CO_2 + H} \tag{2.6}$$

which will feedback with Eq. 2.3. In a second experiment, soot contained Mn at 1 % (weight). Catalysis was only observed on flames containing O_2, suggesting that OH radicals did not promote catalysis.

Bradley *et al.* [258] and Dixon-Lewis *et al.* [214] analyzed in two sequential works the oxidation of graphite particles (4 µm mean diameter) using a lean CH_4/air flat flame. They measured the burning rate of the particles and confirmed the influence of transient species, i.e., flame radicals (O, OH, H), in oxidation control.

Rybak *et al.* [259] assessed the oxidation of carbon black using ethylene (C_2H_4)/air flames at different equivalence ratios ($\phi = [0.83, 1.0, 1.2]$), flow rates and pressures, and pointed at the dependence of the gasification rate on the pressure in fuel-lean flames, whereas fuel-rich

flames did not show this dependence.

2.4.5 Pitting

Phenomenology

Pits are the result of preferential attack on the basal plane, defects and active sites [187, 229, 260, 261]. with different growth speeds depending on the type of edge (arm chair of zigzag), defect, whether it is mono- or multi-layer, and whether impurities are present.

Pits are not uncommon and have been reported upon etching, for example, using oxygen- [190] and air-based plasmas [262] as well as nitric acid [263]. Generally speaking, their genesis can be linked to material removal and subsequent exposure of pre-existing flaws, i.e., buried macropores. In other cases, pores has been attributed to low inter-platelet shear strength upon conventional CF electrolytic oxidation [264].

If impurities are present, channelling can take place instead, depending on the nature of the catalyst involved [265]. This mobility has been ascribed to the Tammann temperature (T_{Ta}) which corresponds to a T where there is a rapid shift in the rate of movement of ions or atoms [266]. It corresponds approximately to half of the melting point (T_m) of the metal in question [240]. Baker [265] described, on the one hand, that some elements adsorb oxygen dissociatively (e.g. Ti, V, Cr, Mo, W, Re, Cu and Zn). Such species tend to *spread* and oxides are formed. In some cases, these oxides may behave as catalysts. On the other hand, elements such Pd, Ag, Pt and Au adsorb oxygen in a non-dissociative fashion. In this case, there is no preferred carbon edge orientation to be oxidized. Interestingly, different forms of attack from the same elements are possible, for example the case of Ru, Rh and Ir.

Early graphite oxidation analyses [267] point at the effect of screw dislocations and single lattice vacancies as the origin of pitting in presence of O_2, even at very low impurity levels. These features were initially followed-up in natural graphite [267–270] and highly ordered pyrolytic graphite (HOPG) [261, 271, 272].

The nucleation and growth of oxidation-induced flaws in carbon materials has been studied in both amorphous carbon and graphitic substrates under controlled atmospheres. However, in the case of CFs and fire scenarios, these phenomena are rarely discussed in detail. To assess the pitting and channelling phenomena, direct observations have helped to provide a better understanding of the processes involved. This has been achieved with other carbonaceous materials by following up characteristic details *in situ* throughout the oxidation process at various length scales.

Only recently, detailed pitting analyses have gained attention. Fu *et al.* [273] simulated the

oxidation-induced pitting phenomena based on previous observations of oxidized CFs obtained from FiberForm, a fibrous system used in TPSs. They simulated the CF pitting phenomenon considering a q of 200 kW m^{-2} and varying the surface roughness. They considered physical parameters not found in commercially-available PAN-based fibers, e.g., diameter of 100 µm instead of typical 4–7 µm. However, they considered fiber fracture, predicting an ∼81 % of the fiber being oxidized ∼19 % being fractured and detached.

Detailed observations

Dedicated analyses are needed to understand the CF pitting process due to its serious implications on CFRP integrity the CF strength is driven by its flaws [274]. Strength is dramatically reduced by oxidation-induced flaws, even at early stages of flaw creation [224, 225]. Even in absence of pitting, the evolution of internal porosity due to the diffusion of oxidizing gases can affect the tensile strength owing to slow internal porosity evolution, as ascertained in CF activation studies [253, 275].

Some of the first observations of the pitting process were made by means of optical microscopy. Hugues and Thomas [267] analyzed natural graphite (Ticonderoga) with impurities mostly being B and Si, ranging from 30–180 ppm. After treating the specimens in O_2 in the 700–900 °C range, they observed different pit growth rates depending on the orientation of the basal plane. They did not report pitting when using CO_2 after 5 h treatment in the range of 800–900 °C. They observed a change on pit orientation by pretreating the graphite in H_2 at 1000 °C for 2 h. They described a preferred oxidation of *armchair* and *zig-zag* carbon atoms, and attributed the origin of pits mainly to screw dislocations and, to a minor extent, single lattice vacancies. They concluded that even minimal impurity contents promote pitting if defects are present.

Subsequently, pitting observations were possible thanks to gold-etch decoration. Evans *et al.* [276] analyzed the oxidation of natural graphite by O_2 at 1.33 Pa at different temperatures. At 1113 K they observed slower etching in monolayer pits with respect to multilayer ones. They attributed these differences to oxide formation and its effect on adjacent graphene layers.

Chu and Schmidt [271] studied the pitting process of HOPG under non-catalytic (O_2/Ar and H_2Ar, both at 15/85 %) and catalyzed etching conditions (2 nm vacuum-deposited layer of Pt) by means of *post hoc* scanning tunneling microscopy (STM) observations. They pointed at different geometries depending on reaction times: circular pits for longer exposure and hexagonal pits for shorter exposures, being typically larger and smaller, respectively. Additionally, the hexagonal pits were observed in multilayer pits. In the case of Pt-treated

specimens, they reported multilayer irregular chanelling due to impurity mobility. The phenomenon varied depending on the gas used for treatment, being somewhat aleatory under O_2 whereas with H_2 the channels seemed to follow well-defined crystallographic directions. In a subsequent study, Chu *et al.* [277] delved into the effect of catalysts on the gasification process complementing the STM observations with atomic force microscopy (AFM). They used natural graphite to analyze the catalytic reactions with Pt, V_2O_5 and K_2CO_3 under H_2, O_2 and CO_2 respectively. They also used HOPG for reactions with Pd and Rh under H_2 and NO. The results showed catalyst- and atmosphere-specific multilayer channelling given the mobility of all the aforementioned elements and compounds. Localized pitting was observed to a lesser extent. Their findings also revealed that the etching rates are linked to the size of the impurities.

Cho *et al.* [278] observed pitting after subjecting a CC composite to a fuel-lean oxyacetylene flame ($4:1$ O_2/C_2H_2 ratio). The composite was the result of phenolic resin impregnation of high strength PAN-based CFs (i.e., standard modulus). They ascribed structural defects to the failure process and described ablation as a *peeling off* process where severe thermal, chemical and mechanical conditions are present. Subsequently, Cho *et al.* analyzed intermediate modulus PAN-based CFs. This time, they also treated the fibers with different concentrations of H_3PO_4 (0.5, 1.0, 2.0 and 4.0 %). They analyzed the untreated and 0.5 %-coated fibers via TGA at 656, 770, 821 and 910 °C. They reported uneven diameter reduction of untreated CFs along severe pitting, whereas the P-based treatment helped to protect the fibers. Aided by EDS analyses, they suggested the diffusion of P and blockage of active sites as an explanation. Finally, Cho and Yoon [279] endeavored to link the previous results to the ablative behavior of C/C with matrices obtained with different methods. Using an argon/hydrogen flame ($4:1$ Ar/H_2 ratio), they surprisingly report little or less severe pitting, ascribing this effect to the absence of O_2. However, their results show the *peel off* and conical shapes on CFs, characteristic of hyperthermal conditions. They also point at specific ablative resistance to each type of carbonaceous matrix.

Hahn *et al.* [272] studied the etching process on HOPG by bombarding specimens with mass- and energy-selected Ar^+ (50–500 eV) in ultrahigh vacuum to tailor defect populations. Subsequently, they oxidized the specimens in an oven using dry air in the 450–650 °C range for different periods, and studied the surfaces by means of STM. They found a relationship between the ion impact energy and the relative population of mono- and double-layer pits, the latter being the product of higher energies. They did not observe vertical etching on undamaged graphite below 650 °C, and atributed multilayer pits solely to ion-generated defects. Under their conditions, the monolayer etching rate was determined to be 1.38 nm min^{-1}, while multilayer etching took place 2–3 times faster. They also reported generalized circular pit-

ting specially in multi-layer pits, seldom observing anisotropic patterns or channelling, which the authors attributed to possible contamination of the alumina container. After calculating the E_a from Arrhenius plots relating temperature and etch rate constant for single-, double- and triple layer pits, they suggested the importance of entropy in the etching process, since higher A values of the Arrhenius equation entails a higher collision rate of reactant. They also reported different O_2 adsorption mechanisms, pointing at Eley-Rideal mechanism as the preferred path, in contrast with the observations from Baxter and Hu [212].

In a subsequent work, Hahn [261] found out that temperature has an impact on the pitting direction in graphite. HOPG was oxidized in dry air between 550–650 °C and later analyzed using STM. Low temperatures yield a narrow pore size distribution solely initiated at point defects, whereas higher temperatures yield broader distributions, where oxidation is initiated from basal carbon atoms and point defects. Additionally, at low temperature, pits start at natural (point) defects. At high temperatures pits also behave "vertically", where several layers are etched closely. Moreover, Hahn also pointed at the dissociation of H_2O, CO_2 and O_2 at high temperatures, leading to highly reactive O species, which in turn create vacancies on the basal planes very efficiently. At high temperatures, there is a dynamic pit distribution due to continuous pit creation.

Dobrik *et al.* [280] showed a method for controlled etching of HOPG to obtain armchair edge formation regardless of the initial edge state, i.e., ziz-zag or armchair. They used a quartz tube, oxygen/inert gas mixtures (0–45 % of O_2) and a heating rate of $\sim$50 °C min^{-1}. They obtained average pit diameters using AFM and STM. They determined that the temperature had an exponential effect while the response with respect to exposure time and oxygen concentration showed a linear behavior. With their experimental conditions, they attributed monolayer pits to point defects whereas multilayer pits were predominant in presence of grain boundaries or dislocations where the graphene edges were more exposed.

Damage follow-up

Chang and Bard [281] determined the pit growth rate on HOPG specimens by means of STM. They measured the diameter of monolayer etch pits as a function of the reaction after treating the samples in air at 650 °C, obtaining 5.2 nm min^{-1}. Geometry wise, they found that pits smaller than 4 nm were irregular and those between 40 and 200 nm were usually hexagonal. Above the upper limit of this range, most of the geometries were circular. Subsequently, the same authors [282] studied the effect of different temperatures on the final diameter, showing an exponential behavior with increasing temperature. They found that pits formed above 700 °C were circular, independent of their size.

Morishita and Takarada developed a fixed-point observation technique that allowed sequential analysis of the same CNTs and subsequent observations using transmission electron microscopy (TEM) [283] and SEM [284]. Subsequently, the same approach was used by Shimada *et al.* [285] to follow up the gasification of MWCNTs. Such detailed pitting analyses were possible by means of *post hoc* observations. In some cases, pit growth rates have been determined, elucidating the oxidation kinetics of such carbonaceous materials under controlled conditions.

Live observations are limited to certain temperature and pressure conditions, hence the seeming difficulty to recreate combustion conditions. To address these limitations, *post hoc* analyses have provided the means to calculate reaction rates and gain insight into carbon oxidation. For instance, optical microscopy was initially used to assess microscale hexagonal pitting, spanning tens of microns on natural graphite surfaces [268]. Monolayer recession rates were also calculated on HOPG using STM after oxidation at different temperatures [271]. Later on, a fixed-point observation technique was developed to follow up specific pits and graphene layer peeling in carbon nanotubes using TEM [283, 285] and SEM [284].

Delehouzé *et al.* [286] analyzed the pitting process of HOPG using high temperature environmental scanning electron microscopy (ESEM) and AFM in dry O_2 at 140 Pa, determining pit growth rates as well as a transition temperature zone between hexagonal ($T < 1025\,\mathrm{K}$) and circular pits ($T > 1050\,\mathrm{K}$). They were also able to determine the growth rate of pits, showing a linear increase with respect of the inverse of temperature in a semi-log scale, i.e., an Arrhenius plot. They modelled the HOPG oxidation using the Kinetic Monte Carlo technique, of which results were in agreement with the experimental data.

Toth *et al.* [209] analyzed the *in situ* oxidation of soot and carbon black at 600 and 900 °C at 1 and 10 Pa by means of environmental transmission electron microscopy (ETEM). They confirmed different oxidation mechanisms that had been previously proposed as well. They confirmed three types of interacting surface oxidation, namely crystallite flaking, partial detachment of BSUs and formation of fullerenes.

Cochell *et al.* [287] followed the oxidation of CFs using a scanning transmission electron microscopy (STEM) with a closed environmental cell. They sectioned a single CF extracted from FiberForm, a material intended for TPSs. While heating from room temperature up to 1050 °C, they were able to observe the evolution of a pit *in situ* starting at 550 °C.

CHAPTER 3 RESEARCH OBJECTIVES AND COHERENCE OF ARTICLES

Upon review of the literature presented in §2, three main issues pertaining to the fire resistance of PMCs used in aircraft structures became apparent:

- There are no material selection tools nor design methodologies dedicated to fire-resistant aircraft structures. Moreover, general design approaches addressing the selection of materials and processes chiefly consider quantitative properties, while qualitative performance assessments need special treatment. In this regard, fire resistance is typically assessed with *Pass/Fail* evaluations, missing the opportunity to consider other data extracted from fire tests in the decision-making process.
- The failure of CF-based structures under true flame attack is not yet well understood. Several thermomechanical models mainly pay attention to the degradation of the matrix, but rarely consider the damage process of the reinforcement, which is relevant to PMCs under fire attack and simultaneously loaded in tension. Moreover, most previous studies targeting CF oxidation have been performed under controlled conditions, in atmospheres that do not consider the highly reactive atmosphere of an open flame as encountered in typical certification tests.
- The amount of research pertaining to the fire-induced damage of CFs is limited. This phenomenon at the heart of failure mechanisms for composite firewalls is typically assessed in an indirect fashion, i.e., through the residual strength or thermoanalytical results for PMC laminates, but seldom paying attention to the transient fiber morphology.

In light of the problems listed above, the general objective of this dissertation is to define a methodology for the development of fire-resistant PMCs in a resource-efficient fashion, while increasing the understanding of the fundamental processes involved. This in turn translates into two main challenges. The first is to find efficient and systematic means to conceive fire-resistant PMCs. This will be achieved through a design & evaluation methodology for PMCs considering small-scale tests. The second is to understand the failure processes of structural PMCs subjected to flame attack, linked to the CF degradation.

3.1 Specific research objectives

Responding to the aforementioned challenges, three specific objectives were defined:

1. Develop a resource-efficient design & evaluation methodology for fire-resistant PMCs using a small-scale testing approach.
2. Determine the effect of fire and mechanical loads on CF failure.
3. Identify the key intrinsic parameters of CFs involved in their damage process under flame attack.

3.2 Articles and coherence

The core results of this dissertation are divided in three parts, each one presented in the form of a journal article and addressing the specific objectives described in §3.1. The article-based format of the thesis requires that each chapter contain a literature review serving the article's objective. This entails the repetition of certain information already presented in §2, although synthesized differently. The author apologizes for the duplication of the content.

Article 1: A design and evaluation methodology for fire-resistant polymer matrix composites using small-scale tests

This article tackles the first specific objective stated in §3.1, and addresses the design of fire resistant PMCs from a practical perspective. It proposes a holistic design methodology involving the conceptual phase, screening, evaluation and ranking while incorporating several tools. First, AD is used as design paradigm to guide the creative process of design. Then, general guidelines are presented to identify potential candidates. The core of the article, the fire-resistance evaluation using a small-scale approach, is presented in a third step. Finally, the fuzzy sets and MCDM concepts are proposed for ranking. A case study considering an aircraft engine casing intended to work as a firewall is used to demonstrate and validate the whole process. The manuscript was submitted to the *International Journal of Mechanics and Materials in Design* (Springer, 2021 Impact Factor (IF): 3.561) on July 4, 2022. The author of this thesis conceived the core idea of the article, integrating the different design, evaluation and calculations tools into one method. He created the engineering drawings of the PMC laminates, coordinated their fabrication, performed the fire & load evaluations, curated the raw data, programmed of the python code for fuzzy-set calculations, analyzed the data, and redacted 90 % of the manuscript. T. Pelzmann designed and fabricated the small-scale setup

used to evaluate the fire resistance of PMC specimens, and reviewed the article. Professors É. Robert and L. Laberge Lebel supervised the project in its entirety, provided guidance, and helped to draft and review the article.

Article 2: Carbon fiber oxidation in combustion environments–Effect of flame chemistry and load on bundle failure

The second article presents one of the two original experimental methods developed by the author. It addresses the second specific objective from §3.1 by evaluating the effect of flame chemistry and tensile loads on CF bundles while being exposed to an open flame. The results are compared against data obtained from the same types of fibers using classical thermoanalytical means. An exploratory microscopic analysis is presented to show the type of damage caused by flame attack. The article has been published in the journal *Materials Today Communications* [288] (Elsevier, 2021 IF: 3.662). The author of this dissertation conceived the idea of exposing CF bundles to the flame using a set of pulleys and dead weights, designed the test fixtures, performed the TGA/DSC evaluations, the SEM observations, half of the fire & load test campaign, documented the process, analyzed the data and redacted 90 % of the manuscript. T. Pelzmann prepared the initial setup of the FFB including gas mixing and water cooling, and reviewed the manuscript. J. Zahlawi performed half of the fire & load tests. Professors L. Laberge Lebel and É. Robert supervised the project in its entirety, provided guidance, and helped to draft and review the article.

Article 3: Carbon fiber damage evolution under flame attack and the role of impurities

The last article covers the third specific objective from §3.1, providing a detailed account of the CF damage process due to direct flame attack and the role of impurities. It presents the results obtained after implementing the second novel technique, based on the findings of the second article. Damage features, namely pitting, channelling and amorphous erosion, are described and linked to the presence of structural defects and impurities. From an oxidation standpoint, concepts from coal, carbon black, soot and pure graphite are reviewed to complement the understanding of the oxidation process of CFs. This article has been published in the journal *Fire and Materials* [289] (Wiley, 2021 IF: 1.979). The author of this dissertation conceived the idea of detailed microscopic observations, designed the test fixtures, performed the fire tests, the sequential SEM/EDS observations, performed the data analysis, and redacted 90 % of the manuscript. T. Pelzmann prepared the basic setup of the FFB including gas mixing and water cooling, and reviewed the manuscript. D. R. Hall

proposed the use of NAA, performed such analyses, and reviewed the manuscript. C. Chilian coordinated and supervised the NAA experiments. Professors L. Laberge Lebel and É. Robert supervised the project in its entirety, provided guidance, and helped to draft and review the article.

CHAPTER 4 ARTICLE 1: A design and evaluation methodology for fire-resistant polymer matrix composites using small-scale tests

Submitted to *International Journal of Mechanics and Materials in Design* on July 4, 2022.

By
Pablo Chávez-Gómez, Tanja Pelzmann, Étienne Robert, Louis Laberge Lebel

ABSTRACT

Fire poses a serious threat to airworthiness and, in consequence, to passenger safety. Thus, the increasing use of PMCs in aircraft structures compels a thorough evaluation and selection of fire-resistant configurations. Intermediate-scale tests are typically needed for certification purposes, rendering extensive material screening campaigns prohibitively expensive. We propose here a methodology comprising the conceptual design, screening, small-scale evaluation and ranking of fire-resistant PMCs towards a resource-efficient selection process. Following a general design scheme, two tools are introduced to facilitate the overall exercise. First, AD is used for guidance in the conceptual design phase. Material screening strategies are subsequently discussed considering an aircraft fire safety context. Small-scale testing is then presented as a cost-effective alternative for material evaluation. The idealization of component and thermomechanical loads is required to simplify the analysis. Finally, the ranking of material candidates is performed using MCDM and fuzzy concepts to account for the imprecise/qualitative nature of design requirements and evaluation criteria previously defined with AD. A case study involving an aircraft engine casing is presented to illustrate and validate our methodology.

4.1 Introduction

Fire poses a serious threat to aircraft airworthiness and, in consequence, passenger safety [56, 62, 95]. In this regard, although polymer matrix composites (PMCs) are ubiquitous in modern aviation owing to their high specific properties, the flammable nature of most of their constituents is a major drawback [6]. Aircraft manufacturers rely heavily on them when designing primary and secondary structures, engine nacelles, cabin components and cargo liners. Paradoxically, in certain cases, some of these components need to act as firewalls.

In spite of this apparent contradiction, their use can be justified since some PMC material systems can prove to be fire-safe [99, 290–292]. One of the main advantages of PMCs here too lies in the ability to tailor their properties. Selecting configurations with improved fire resistance is thus of the utmost importance to safely exploit their potential.

From an aircraft fire safety standpoint, the behavior of PMCs can be roughly divided in two categories: flammability and fire resistance [6]. The former relates to the material's ability to burn under certain conditions and allow the flames to propagate, being relevant to a fire scenario in the main cabin. The latter, which is the main focus of this work, is the ability of a component to withstand the attack of an open flame and provide protection for a certain time by preventing its spread [67]. To demonstrate the fire resistance of PMC-based components, regulators such as the U.S. FAA and EASA typically mandate intermediate-scale tests for certification purposes. Principal design criteria depend on the application and whether in-flight or post-crash fire scenario is relevant. For instance, in the case of powerplant firewalls, aircraft and engine manufacturers rely on the FAA's AC20-135 [53, 293] or ISO 2685 [84]. These guidelines, in line with other requirements such as the U.S. Code of Federal Regulations [43], typically specify the use of 610 mm x 610 mm specimens, custom oil- or gas-based burners capable of yielding a $\sim$1100 °C flame with a q ranging from 105 to 116 kW m^{-2}, and the recreation of operating conditions, i.e., vibratory and aerodynamic loads. Including the manufacture of the specimen and the fire assessment, the cost of each test can exceed \$10K USD, rendering a multi-material evaluation campaign prohibitively expensive.

To avoid extensive and costly material screening, predictive modeling is quite attractive to analyze the fire behavior of PMCs [96, 97, 99, 115, 221, 294–300] before any laminate is physically tested. Thermal, chemical and mechanical models as well as combinations thereof allow to predict the fire behavior of PMCs and select configurations that fulfill FST as well as structural requirements. The vast majority of these models rely on experimental data obtained under controlled conditions, e.g., TGA and DSC. Given the complex phenomena involved in the combustion of PMCs, several assumptions are typically made to facilitate calculations. Some physical phenomena such as delaminations and the effect of fiber architecture are typically disregarded, yet models show good agreement with several parameters measured, namely TTI, T profiles, and post-fire stiffness/strength. However, the results obtained for a specific material system and thermomechanical condition cannot be extrapolated to other laminate configurations nor fire conditions [93]. When tensile load cases are considered, other phenomena such as fiber softening, combustion, or oxidation have been also ignored in most of the cases to avoid more complex models and ease the calculations. Nevertheless, these aspects have been analyzed under simulated fire conditions [223–225, 301], revealing that glass

and CF failure is highly dependent on temperature and mechanical loads. When true fire conditions are considered, more factors come into play. Furthermore, we have recently shown that the flame chemistry, a parameter often overlooked in fire tests, as well as the type of CF and their microstructure play a major role in their failure process [288, 289]. The complex interaction between PMCs and fire, as well as the synergistic effects of their constituents still present a challenge to predictive tools. Thus, several aspects of fire resistance still need to be addressed experimentally, making test campaigns unavoidable.

The conception of fire-resistant PMCs for aircraft use, as any other engineering structure, needs to be carried out in a systematic way [9] to ensure the timely identification of design variables and constraints as well as functional requirements. As part of the engineering design process, the material selection is extremely important since it drives several aspects such as the physical properties, shape and processing needed for the component in question [4, 139, 144]. Loosely-defined constraints and requirements dominate at early stages of engineering design, often accompanied by conflicting criteria. Moreover, functionality can be achieved in multiple ways and, usually, do not have well defined boundaries [140, 145], hence the compromises needed between the different stakeholders. To this end, there are several engineering design and manufacturing paradigms, with some of their main goals being improved quality, reliability, flexibility, agility, robustness, and adaptability [139, 302–304]. Ultimately, cost reduction entails improved design and manufacturing processes, being one of the major goals of any organization. In aviation, for instance, each original equipment manufacturer (OEM) has its own set of design practices as well as manufacturing methods and technologies that confer them certain strategic advantages [46, 47, 302, 304]. OEMs rely on experimented designers, subject matter experts from different domains working closely with one another, advanced modeling tools, in-house practices, databases and heuristics to conceive sound structures. However, despite this joint body of knowledge, experience has shown that some key factors may be overlooked in the design process, with flaws becoming apparent only years later. Based on 35 aviation accident reports, Kinnersley and Roelen [63] found that half of those events can be traced to flawed design assumptions. In a fire safety context, a relevant yet mournful example is given by the Swissair MD-11 that crashed near Peggy's cove, Nova Scotia, Canada back in 1998 [62]. Thermal/acoustic insulating materials were identified as the main cause of an uncontrolled fire. Some of these materials were certified on an individual basis in terms of flammability, yet the specific installation paved the way for thermal runaway. As previously mentioned, fire test results cannot be extrapolated. Even if materials are individually deemed safe, it is still essential to perform tests in conditions as close as possible to those found in aircraft operation. This highlights again the need for robust design practices and the importance of material selection as part of the

design process.

To select the best material system among several candidates, the designer faces a decision-making problem. In this regard, it is recognized that the decision-making process involved in common and daily activities is typically biased, i.e., person-dependent, and the outcome highly depends on the problem definition, even for the same situation [161, 162]. From an engineering design standpoint, the decision-making problems are only worsened since criteria are often numerous, mutually conflicting, vague and of dissimilar nature. The material selection process is consequently a significant challenge and thus the use of dedicated tools is imperative. To this end, multi-criteria decision making (MCDM) techniques provide the means to weigh criteria and rank the different options. MCDM methods have been profusely developed, with applications in virtually all disciplines, including material selection [21,305]. Since the decision-making process typically involves vague information, the concept of fuzziness has been addressed [175]. Consequently, a plethora of MCDM methods have been adjusted to incorporate fuzzy concepts and evaluations, hence the broad range of applicability for fuzzy MCDM [306]. However, each MCDM method has its own advantages and drawbacks. The selection of a MCDM method entails a decision-making process itself, which has been referred to as a *selection paradox* [164]. It has been suggested that a proper definition of criteria and narrowing the selection of alternatives from a larger pool of candidates is equally important [166].

Since the nature of the design process is iterative, a question then arises: How can fire-resistant PMCs be designed, assessed and selected in a resource-effective way? The conceptual design of fire-resistant PMCs requires thorough consideration of quantitative and qualitative criteria as well as constraints to avoid additional iterations, which have costly implications. The non-linear nature of composites, the complex fire-related phenomena and associated scaling effects [93] represent a big challenge to their fire evaluation and the material selection process since the test component must represent as accurately as possible the final configuration. Thus, a resource-effective design methodology is regarded as a highly desirable tool.

To overcome the major challenges encountered in the design of fire-resistant aircraft components, we propose a methodology for PMCs encompassing conceptual design, screening, evaluation, and final ranking. The conceptual design stage is carried out using Axiomatic Design (AD) [168] which provides a systematic approach to translate customer needs into functional requirements, design parameters and process variables. Given that some of the constraints and evaluation criteria defined by the different stakeholders can be vague in nature, the framework incorporates fuzzy sets [174] to handle qualitative criteria/evaluations.

Material & process screening is performed based on a methodology involving free search, questionnaire and expert input [145]. For the evaluation process, we present a small-scale testing approach which considers the operating conditions encountered in the final application. At the last stage, the ranking step makes use of an MCDM tool to discern the best design option. A case study focusing on an engine casing intended to work as a firewall is presented to illustrate the process and demonstrate its validity.

4.2 Proposed Methodology

Fig. 4.1 shows the four stages of the methodology, i.e., conceptual design, initial screening, material evaluation, and ranking. The main goal of the methodology is to overcome the lack of fire-related material properties, the inherent fuzziness of some design process steps, uncertainty of combustion phenomena, as well as the probabilistic nature of composites' structural integrity. It is intended to generate new empirical quantitative and, at the same time, to consider qualitative evaluations which are translated into inputs used in the ranking process.

The proposed sequence takes several concepts from a general material selection strategy presented by Ashby *et al.* [145], AD [168, 169] and fuzzy sets [174]. The latter are used in a simple way to expand the design and decision-making processes [175], handling different kinds of criteria and evaluations for final ranking [305, 307]. Each stage is described in detail further below.

4.2.1 Stage 1–Conceptual design

The first stage of the framework consists in the conceptual design of the structure with fire resistance requirements. To guide the conceptual process, we propose the use of AD [168,169] as a systematic design tool to guide the process of translating the customer needs into a final product. It promotes the maximization of functional independence and the selection of the concept with the highest probability of success, thus enabling a more robust design. A detailed account of AD, its axioms, corollaries and general design theorems can be found in [169, 308]. Below, we describe the main aspects needed to understand its implementation in the present methodology.

AD's process contains four domains as shown in Fig. 4.2, namely customer, functional, physical and process. Each domain is embodied by a characteristic vector containing a set of features, i.e., customer attributes (CAs), functional requirements (FRs), design parameters (DPs) and process variables (PVs). From a materials standpoint, the first step involves

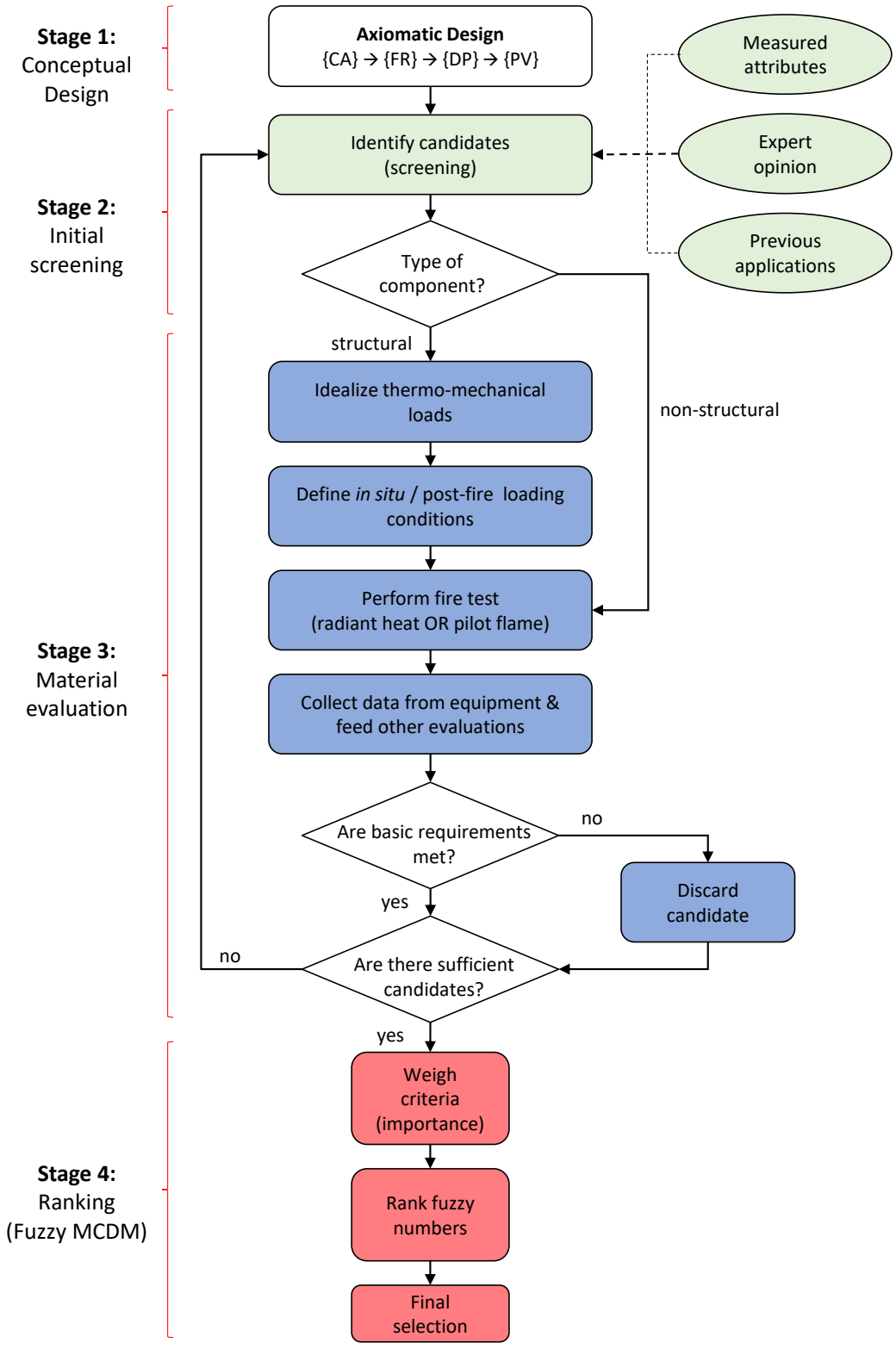

Figure 4.1 Flowchart of the proposed design methodology with four main stages: conceptual design, initial screening, material evaluation, and ranking.

translating the CAs which represent the needs of the customer in terms of desired performance, into a set of FRs. The FRs represent the required properties of the product usually represented in the type of an action. For instance, if the CA is "the product shall be impact resistant", a possible FR could be "to provide energy absorption means". Subsequently, a set of DPs will be defined based on the FRs previously defined. These DPs are the embodiment of the CAs, represented by the properties of the material or features of the microstructure. For the aforementioned energy absorption FR, toughness is an example of DP. Three cases are possible depending on the relative amount of FRs and DPs: ideal (if functional independence is ensured), coupled and redundant designs, where the quantity of DPs is equal, lower, and greater than FRs, respectively. Finally, the PVs should reflect the means to achieve the DPs, i.e., the tools, processes or fabrication steps required to achieve the final concept. Regarding the toughness case, a typical way to increase such property in thermoset resins is the addition of a thermoplastic constituent. This may modify the method required to cure the laminate as well as the temperature and pressure involved in this process.

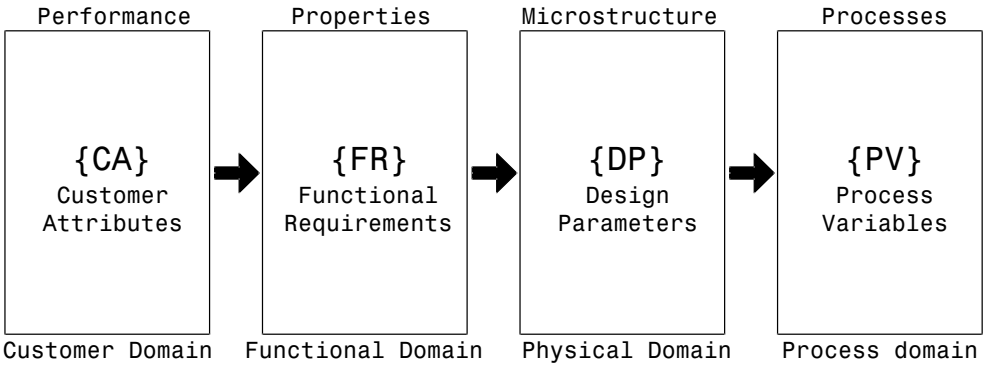

Figure 4.2 AD process showing the four different domains. Each arrow represents the mapping process between domains, sequentially dependent to its predecessor.

A mapping process is performed between each pair of sequential domains, with the goal of linking the "what" with the "how". This ensures the fulfillment of the predecessor, and is done by *zig-zagging* as shown in Fig. 4.3. In this example, the top FR is covered by a DP at the same level. Once it is addressed, the top FR may cover two secondary FRs, i.e., FR_1 and FR_2. If the latter has additional sublevels, the *zig-zagging* process is continued until each element (FR_{21} and FR_{22}) of the preceding domain is covered by its counterpart in the subsequent domain at the same level.

The relationship between FRs and DPs is given by

$$\{\mathrm{FR}\} = [A]\{\mathrm{DP}\} \tag{4.1}$$

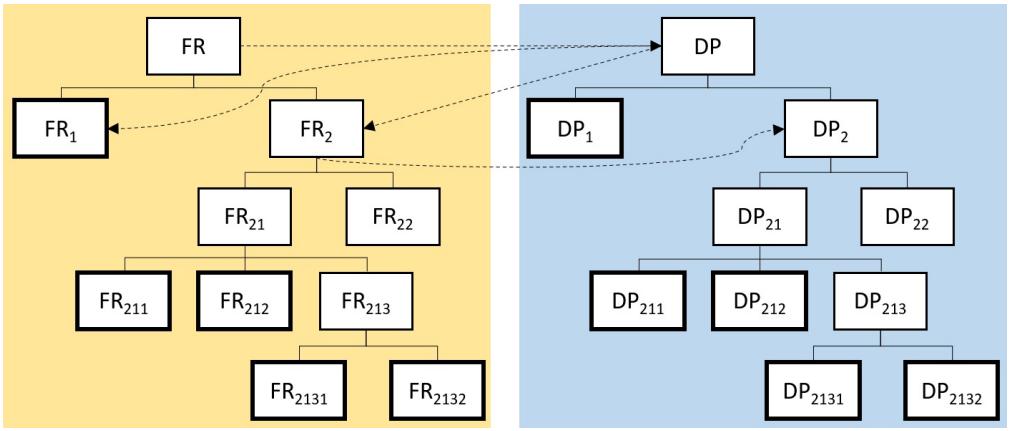

Figure 4.3 Mapping between domains by *zig-zagging*. Each FR is addressed by a DP at each level. Once a FR is covered by a DP, lower levels wills will be compared in a similar fashion.

and a similar expression is given for the relationship between DP and PVs by

$$\{\mathrm{DP}\} = [B]\{\mathrm{PV}\} \tag{4.2}$$

where $[A]$ and $[B]$ are the design matrices denoting the relationship between FRs and DPs as well as DPs and PVs, respectively. Three different families of design matrices are possible, depending on the degree of independence between the left and right sides of equations 4.1 and 4.2. Considering a square matrix, i.e., same quantity of FRs and DPs, a design matrix can be represented by

$$\begin{bmatrix} X & 0 & 0 \\ 0 & X & 0 \\ 0 & 0 & X \end{bmatrix} \quad \text{(4.3a)} \qquad \begin{bmatrix} X & 0 & 0 \\ X & X & 0 \\ X & X & X \end{bmatrix} \quad \text{or} \quad \begin{bmatrix} X & X & X \\ 0 & X & X \\ 0 & 0 & X \end{bmatrix} \quad \text{(4.3b)}$$

where the diagonal matrix 4.3a represents an *uncoupled design*, i.e., it fully abides by the *independence* axiom, and lower/upper triangular matrices in 4.3b represent a *decoupled design*. A third case, a *coupled design*, is represented by a matrix not fulfilling the previous criteria. In any case, X represents either a constant or a function of the right hand domain in the case of linear and non-linear designs, respectively.

The initial statement of the problem is encompassed by a list of goals, objectives and constraints, usually provided by the customer [140]. However, the design process in early stages can contain CAs, material properties or criteria that can be vague in nature. For instance, the customer can express the following needs: *"the TRL [309] of a material candidate should*

be high", or the *"cost should be as low as possible"*. In the context of this work, *"after fire testing, the component shall show the least signs of damage that may compromise other components"* seems to be a reasonable need, yet quite vague. None of the previous requirements is crisp and, therefore, the criteria definition or calculation of a score at a later stage may not be evident nor straight forward. To tackle this, AD can still be carried out in a fuzzy environment [172, 173] and enable the use of such criteria in the evaluation process. The basic concepts of fuzzy sets are given in §4.2.4 to address the ranking step. For now, the reader is reminded that vague criteria or subjective evaluations are indeed useful [57, 158], and will be used along quantitative evaluations for ranking purposes.

4.2.2 Stage 2–Initial screening

The second stage of the process involves the identification of candidates from the universe of available materials. In accordance with Stage 1 (§4.2.1), the candidate systems must cover the material properties and processing features represented by the DPs and PVs, respectively. Typical strategies can be classified in three categories: "Free Search", "Questionnaire-based" or by "Analogy" [145] as shown in Fig. 4.1. These strategies involve the consideration of measured and desired attributes (e.g. thermomechanical properties as well as cost and environmental considerations), expert opinion (e.g. input from subject matter experts) and previous applications (e.g. publicly available literature, lessons learned within an organization or legacy programs with proven technologies), respectively.

The first option, *Measured attributes*, is the least constrained of the three approaches since it involves a free search that is carried out considering quantitative attributes. It promotes innovation, although little to no guidance is available [145]. Potential candidates can be readily identified through open search from available information found in supplier datasheets, scientific articles, technical reports, material databases or handbooks [72,150,156,310]. Other approaches include the so-called Ashby charts [14, 145] or, if there is enough experimental data, material-specific charts for load-bearing components [311, 312].

The second approach involves the input from subject matter experts, to whom a *Survey/Questionnaire* can be handed [145]. In line with the present work, the designer is expected to be versed in the fire behavior of PMCs to identify the most promising options. This approach is also useful for a less-experienced designer since it involves the analysis of economic (cost), technical and environmental aspects, to name a few. Questions such as "Have all the relevant discrete material properties been obtained and understood?", "Will the design conditions change with time?", "Are there any chemical, toxicological, radiation or micro-organism effects that need to be considered?" are some examples [313]. This can be

considered as a more guided approach than *Measured Attributes*, since the series of questions can be used as a checklist.

The third approach is closely related to the second one, since it considers *Past Applications* with successful approaches [145]. Besides the input from experts, this information can be found in material databases developed within OEMs, internal documentation of material/structure suppliers, or lessons learned. Nonetheless, these sources are mainly proprietary and access is limited to in-house usage. If there is no such information available, other publicly available documents can provide useful information such as conference proceedings, journal articles or technical reports and lessons learned from certification authorities (e.g. [149] for aircraft/ fire-related information). Lastly, a patent landscape can be an additional source of inspiration for proven materials or configurations. It is recognized that patents are a source for innovation and that the technical information of a large body of patent literature is not found elsewhere [314], hence their importance.

4.2.3 Stage 3–Small-scale evaluation

The core idea of the evaluation stage is to miniaturize the specimen in order to reduce the material usage. Small-scale screening methods have proved to be particularly resource-efficient in other fire-related applications, e.g., low flammability polymers for cabin applications [291, 315, 316] or protection of metallic structures [317].

The third stage involves a series of steps to determine the type of small-scale evaluation that needs to be carried out. The purpose of this is twofold. First, it allows to test more specimens with the same amount of material dedicated to a certification test and, second, a reduced specimen size can be aligned with the dimensions specified in standardized mechanical tests, for instance, to evaluate the tensile [318] and compressive strength [319] of PMCs.

It is necessary to determine whether the component in question has to withstand mechanical loads while being under flame attack as shown in Fig. 4.1. On the one hand, if the answer is "no", the next step is to directly perform the fire evaluation (see "*non-structural*" arrow in Fig. 4.1). For instance, certain PMC-based cargo liners have to block the fire and heat typically produced by hazardous materials [56]. This case may be considered as non-structural in spite of the force exerted by the component's own weight. On the other hand, should the structure be mechanically loaded whilst enduring the flame attack, this needs to be considered in the small-scale test protocol. This is exemplified by some powerplant components with fire-blocking functions (in case of a fire fed by broken fuel or oil lines), while being mechanically loaded owing to aerodynamic and/or vibratory forces [7].

Depending on the load case, different standards for mechanical testing can be followed for guidance. For example, in case of a component loaded in tension, long and slender samples can be used [318]. In the case of components that must work in compression, specimens with fixtures featuring lateral guides can be employed [319], although long and slender specimens can be used should Euler buckling be a relevant failure case. Static evaluations of bare and protected laminates under simulated [114, 132, 320–327] and open flame conditions [129–131,133,138,327–336] followed by visual inspection and assessment of residual mechanical properties can provide meaningful results. However, simultaneous thermomechanical evaluations have also been performed under simulated [97,103,120,127,136,300,337,338] and under open flame attack [132, 134, 135, 339, 340], typically followed by post fire mechanical testing of surviving laminates. Compared to radiant heat sources, flame-based tests provide better insight on the structural integrity of bare and protected PMCs and thus are used in this methodology.

4.2.4 Stage 4–Ranking

The final stage of the methodology selection involves the weighing of the evaluation criteria, ranking of the alternatives and the final selection based on the latter, as shown in Fig. 4.1 at Stage 4. Since the conceptual design was carried out with both quantitative and qualitative criteria, the use of fuzzy sets is strongly suggested to allow the integration of both types of evaluations. Crisp values can be translated into fuzzy numbers to harmonize the type of data. In this case, a value of $\pm 10\,\%$ has been proposed [305] to consider some level of uncertainty, although the designer or decision-maker can adjust if deemed necessary.

Since the goal of this work is not to analyze the advantages and drawbacks of different fuzzy MCDM techniques, we propose the partial use of a method developed by Liao [305], which employs the ranking technique of integral value proposed by Liou and Wang [307]. Only the calculations from [305] are considered since the final candidates have been already identified in Stages 1 through 3 of our methodology (see §4.3.2 to §4.3.4).

At this point, it is important to delve into the concept of fuzzy numbers that will allow to translate the qualitative criteria into values that can be used for calculations and comparison. Fuzzy numbers can be represented by a membership function ($\mu_{\tilde{n}}(x)$), with Fig. 4.4a showing the two $\mu_{\tilde{n}}(x)$ most commonly used: triangular and trapezoidal. Accordingly, each $\mu_{\tilde{n}}(x)$ has the general form:

$$\mu_{\tilde{n}}(x) = \begin{cases} 0, & x \leq a \\ \frac{x-a}{b-a}, & a \leq x \leq b \\ 1, & b \leq x \leq c \\ \frac{c-x}{d-c}, & c \leq x \leq d \\ 0, & x > d \end{cases} \tag{4.4}$$

and can be represented by the fuzzy number $\tilde{n} = (a, b, c, d)$. Thus, on the one hand, the trapezoidal membership function ($\mu_{\sqcap}(x)$) of Fig. 4.4a can be represented by the fuzzy number $\tilde{n}_{\sqcap} = (0.55, 0.65, 0.75, 0.85)$. On the other hand, the triangular membership function ($\mu_{\wedge}(x)$) which can be considered as a simplified case of $\mu_{\sqcap}$ where b and c are the same, would be represented as $\tilde{n}_{\wedge} = (0.15, 0.3, 0.3, 0.45)$. In this example, the triangular μ implies that the attribute has its full value or mean ($y = 1.0$) at $x = 0.3$, although it extends down to 0.15 and up to 0.45 at a "lower intensity". Similarly, the trapezoidal μ covers the 0.65 to 0.75 range at full value, i.e., 1.0, while extending to 0.55 and 0.85 to a decreasing extent.

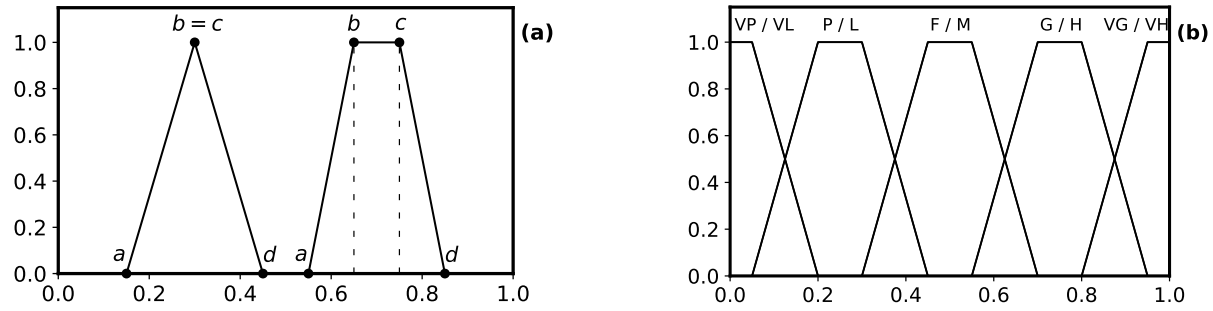

Figure 4.4 (a) Basic fuzzy membership functions: triangular (left) and trapezoidal (right). (b) Linguistic variables and their membership functions.

For the criteria whose score can only be expressed with a linguistic value, we propose the use of two scales with five divisions as shown in Table 4.1. On the one hand, for criteria that involve some sort of performance, the scale comprises *very poor* (VP), *poor* (P), *fair* (F), *good* (G), and *very good* (VG). On the other hand, if a level should be described, the linguistic values are *very low* (VL), *low* (L), *medium* (M), *high* (H), and *very high* (VH). Table 4.1 shows the fuzzy number ($\tilde{n}$) for each linguistic value, given by the quartet (a,b,c,d). Fig. 4.4b shows the graphical representation of both scales sharing the same set of $\tilde{n}$. Depending on the designer preferences and criteria, it is possible to use scales with more or less levels, and the values of $\tilde{n}$ can be adjusted as needed.

Table 4.1 Linguistic values for two scales of fuzzy ratings applicable to performance (VP, P, F, G, VG) and level (VL, L, M, H, VH) of a certain criterion.

Linguistic value		Fuzzy number ($\tilde{n}$)			
		a	b	c	d
VL	Very low	0	0	0.05	0.2
VP	Very poor				
L	Low	0.05	0.2	0.3	0.45
P	Poor				
M	Medium	0.3	0.45	0.55	0.7
F	Fair				
H	High	0.55	0.7	0.8	0.95
G	Good				
VH	Very high	0.8	0.95	1	1
VG	Very good				

To obtain the final ranking of candidates, Algorithm 1 present the calculation sequence consisting of three steps. First, in **procedure 1**, a *suitability index* ($\tilde{S}_{ij}$) is calculated for each criterion and candidate, indicated by i and j subscripts, respectively. $\tilde{S}_{ij}$ depends on whether the property needs to be maximized or minimized. Subsequently, in **procedure 2**, a *final suitability index* $\tilde{S}_i$ is calculated based on $\tilde{S}_{ij}$. Finally, the *integral value* [307] for each option, i.e., $I_T^{\alpha}(\tilde{S}_i)$, is calculated in **procedure 3** considering an index of optimism (α) [307] defined by the decision-maker. The degree of optimism expresses the decision-maker's preference for the left (α =0) or right (α =1) integral value of a fuzzy number. Thus, α =0.5 corresponds to a neutral choice. Finally, the candidate ranking is given by simply sorting them based on $I_T^{\alpha}(\tilde{S}_i)$. It is strongly recommended that the designer assesses the influence of the integral value in the final ranking as a function of α. The importance of comparing rankings as a function of α will be demonstrated in §4.3.5. For further details on the operations, the reader is referred to [305, 307].

The iterative nature of design and material selection [4, 139, 140] is not explicitly stated in Fig. 4.1 only for the sake of clarity. However, it is expected that some design features may become obvious only at later stages, thus the designer may need to go back to an earlier stage to adjust inputs or criteria and reconsider DPs and PVs, or even trigger discussions with the customer to readjust CAs and FRs. In other words, the process receives feedback from itself as in any design exercise in a self-refining loop.

Algorithm 1 Ranking of candidates with fuzzified data (adapted from [305]).

procedure 1. FUZZY SUITABILITY INDEX CALCULATION($\tilde{S}_{ij}$)
  for $i = 1$ to n_{cand} **do** ▷ n_{cand} = # of candidates
    for $j = 1$ to n_{crit} **do** ▷ n_{crit} = # of criteria
      if $\tilde{D}_{ij}$ has to be high **then**
        $\tilde{S}_{ij} = (\tilde{AP}_{ij} \ominus \tilde{D}_j) \oplus \tilde{D}_j$
        where:
        $\tilde{AP}_{ij} = nd_j \oplus (pa_{ij}, pb_{ij}, pc_{ij}, pd_{ij})$
        and:
        $nd_j = |\min(pa_{ij}) - dd_j|$
      else if $\tilde{D}_{ij}$ has to be low **then**
        $\tilde{S}_{ij} = (\tilde{D}_j \ominus \tilde{AP}_{ij}) \oplus \tilde{D}_j$
        where:
        $\tilde{AP}_{ij} = (pa_{ij}, pb_{ij}, pc_{ij}, pd_{ij}) \ominus nd_j$
        and:
        $nd_j = |da_j - \max(pd_{ij})|$
      end if
    end for
  end for
end procedure
procedure 2. FINAL SUITABILITY INDEX CALCULATION($\tilde{S}_i$)
  for $i = 1$ to n_{cand} **do**
    $\tilde{S}_i = 1/n \otimes [(\tilde{S}_{i1} \otimes \tilde{w}_1) \oplus (\tilde{S}_{i2} \otimes \tilde{w}_2) \oplus \cdots \oplus (\tilde{S}_{in_{crit}} \otimes \tilde{w}_{n_{crit}})]$
  end for
end procedure
procedure 3. RANKING: INTEGRAL VALUE CALCULATION($I_T^\alpha(\tilde{S}_i)$) ▷ $\alpha = [0, 1]$
  for $i = 1$ to n_{cand} **do**
    $I_T^\alpha(\tilde{S}_i) = \frac{1}{2}[\alpha(c + d) + (1 - \alpha)(a + b)]$
  end for
  rank candidates **per** $I_T^\alpha(\tilde{S})$ ▷ simple sorting algorithm not shown
end procedure

4.3 Case study: engine firewall

4.3.1 Problem statement

To demonstrate the methodology presented in §4.2, an aircraft firewall with structural requirements has been chosen, exemplified by an engine casing. The rationale for selecting this type of component is that, among the fire scenarios where fire resistance of PMCs is relevant, the certification tests of powerplant firewalls mandate the longest exposure ($t = 15\,\text{min}$). As described in §4.1, components need to withstand the attack of an open flame yielding a nominal temperature of 1100 °C and a heat flux density ranging from 105 to 116 kW m^{-2}. This case study was also intended to consider the use of integral and/or external protection, depending on the outcome of the conceptual design stage.

Fig. 4.5a shows the cross-section of a typical high by-pass turbofan engine. The hatched and red zones represent the areas where acoustically-treated casings are found. Such constructions typically have a sandwich configuration. In certain cases, these components need to fulfill fire-blocking functions. The outer skin, which will be directly attacked by the flame during a fire scenario, needs to act as a firewall. In case of an in-flight fire, the engine may need to keep running for several minutes, depending on the flight phase. For instance, during take-off, the engine has to keep running at full thrust in order to let the aircraft reach a certain altitude and ensure a safe landing. Only then, the engine would be turned off but the firewall shall keep its blocking functions in windmilling conditions [53]. The red portions would be affected by the air blown by the fan.

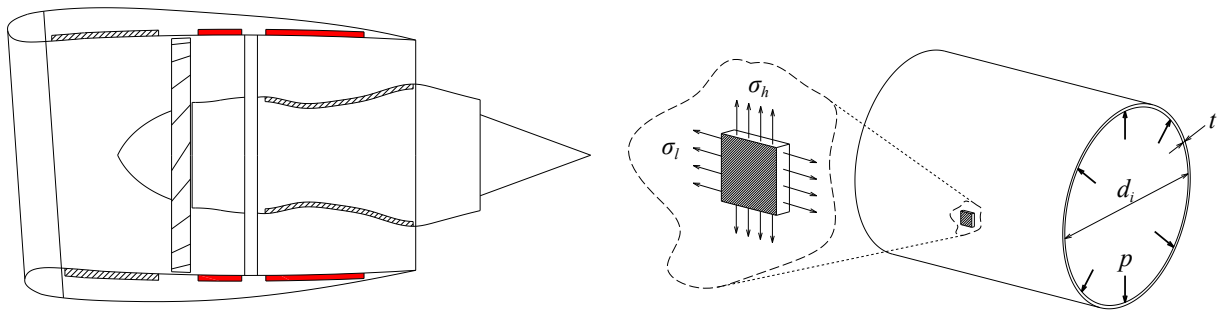

(a) (b)

Figure 4.5 (a) Turbofan cross-section showing the acoustically-treated panels with firewall functions. (b) Casing idealized as a cylindrical shell, showing longitudinal (σ_l) and hoop (σ_h) stresses caused by the pressurized flow it contains (modified from [334]).

Considering the aforementioned engine operating scenarios, the casing can be idealized as a cylindrical shell as shown in Fig. 4.5b. In the case of a thin-walled pressurized shell, the

internal flow can induce longitudinal (σ_l) and membrane/hoop (σ_h) stresses. Fig. 4.5 shows the detail of a discrete element, for which σ_h is given by

$$\sigma_h = \frac{P_i d_i}{2t} \tag{4.5}$$

where P_i is the pressure induced by the internal (tangential) flow, d_i is the internal diameter of the cylinder and t is the thickness of the shell. The value of σ_l, on the same direction as the internal flow, is half of σ_h. This assumption leads to consider tensile loads during the fire attack of the composite structure and will be considered at Stage 3 (§4.3.4).

4.3.2 Stage 1–Conceptual design

Table 4.2 shows the four domains of AD, containing the CAs, FRs, DPs, and PVs. To exemplify our methodology, we have synthesized the customer requirements into five major CAs which not only contain fire resistance requirements (CA_3) but also other aspects such as sound attenuation (CA_1), structural requirements in normal operating conditions (CA_2), a design capable of evolving as required (CA_4) and ease of manufacturing/repairing. These aspects will later guide the criteria selection as well as the functional independence of the structure.

After careful consideration, it was decided that the cost would not be explicitly stated in the CAs since it is coupled to virtually all aspects across domains, e.g., materials and processes. Some design features needed to be considered in the CAs to include requirements and constraints, exemplified by CA_1 which relates to noise reduction. This is typically achieved by a sandwich configuration with acoustic treatment. In consequence, it implicitly imposes design constraints that prevent the designer from meddling with the casing's acoustics.

The mapping between domains has been performed by *zig-zagging* as described in §4.2.1. This is exemplified by considering the different fire resistance-related FRs and DPs as described in §4.3.2. Afterwards, the definition of the design matrix for each pair of characteristic vectors has been carried out. This step is captured by the design equation

$$\begin{Bmatrix} \mathrm{FR}_{31} \\ \mathrm{FR}_{32} \\ \mathrm{FR}_{33} \end{Bmatrix} = \begin{bmatrix} X & ? & ? \\ ? & X & ? \\ ? & ? & X \end{bmatrix} \begin{Bmatrix} \mathrm{DP}_{31} \\ \mathrm{DP}_{32} \\ \mathrm{DP}_{33} \end{Bmatrix} \tag{4.6}$$

where $\{\mathrm{FR}_{31}\ \mathrm{FR}_{32}\ \mathrm{FR}_{33}\}^T$ and $\{\mathrm{DP}_{31}\ \mathrm{DP}_{32}\ \mathrm{DP}_{33}\}^T$ are the characteristic vectors related to fire resistance. The design matrix $[A]$ is represented by a diagonal matrix, denoting an uncoupled design, in compliance with the *independence* axiom.

The question marks replace the traditional "0" to demonstrate the effect of considering two different configurations on the functional independence. The burn-through requirement FR_{31} is driven by an oxidation-resistant reinforcement (DP_{31}), while a volatile gas barrier (DP_{32}) and a thermal insulator (DP_{33}) may not contribute when selecting external protection. However, should an integral solution comprising a fully-structural material system, the reinforcement would serve as the volatile barrier and the thermal insulator once the resin and the char it produces are fully pyrolyzed and oxidized, respectively. This is the case of a bare laminate, and the design matrix linking the three aforementioned FRs and DPs would denote a coupled design.

4.3.3 Stage 2–Initial screening

The first step of screening involved exploring material selection charts, i.e. Ashby type, using an educational license of a commercial software [341]. We customized charts exploring several relevant properties, for instance, maximum service temperature, tensile and compressive strength and modulus, thermal conductivity and specific heat capacity, as well as several combinations thereof. Flammability wise, it is possible to find qualitative information, e.g., evaluations such as highly flammable, slow-burning, self extinguishing and non flammable. Such information can be found in other databases (e.g. [342]). Unfortunately, information regarding fire resistance is virtually non existent. However, useful insights have been obtained by analyzing strength and density *vs.* maximum temperature charts.

Part of the searching step consisted in referring to patents for the reasons given in §4.2.2. A non-exhaustive patent review [343–362] revealed several common traits. Sandwich configurations, laminates with high char yield polymers and adhesives, high-temperature resistant fabrics and mats (ceramic-based) as well as blocking inter-layers are among the solutions found in this type of references.

Structural materials

Based on the discussion presented in §4.2.2 regarding the different factors controlling the thermomechanical behavior of PMCs, four alternative laminate configurations were proposed and are shown shown in Table 4.3. To streamline the certification process, only aerospace-grade material systems were considered. Laminate CF1 is made with an out-of-autoclave carbon/epoxy prepreg. Configuration CF2 uses the same material system and has the same stack-up as CF1, but a GF fabric has been cured in a second step using a different epoxy-based prepreg. CF3 was fabricated using a different carbon/epoxy prepreg intended for autoclave curing while considering the same amount of plies. The reinforcement however incorporates

Table 4.2 Definition of the engine casing across the four domains of AD.

CAs		FRs		DPs		PVs	
$CA_1 =$	The casing helps to reduce noise.	$FR_1 =$	Reduce fan-induced noise.	$DP_1 =$	Sound-attenuating geometry (Helmholz resonator concept).	$PV_1 =$	Bonding of honeycomb core and facesheets.
$CA_2 =$	The structure must be strong, stiff and withstand vibration.	$FR_2 =$	Withstand multidirectional stresses & vibration.	$DP_2 =$	Strong & stiff structure.	$PV_2 =$	Consolidation method.
$CA_3 =$	The component must work as a firewall in case of in-flight fire.	$FR_3 =$	Work as a firewall in case of in-flight fire.	$DP_3 =$	Fire-resistant material system.	$PV_3 =$	Integration method.
• $CA_{31} =$	Burn-through is not permitted.	• $FR_{31} =$	Prevent burn-through.	• $DP_{31} =$	Oxidation-resistant reinforcement.	• $PV_{31} =$	Consolidation of the protective material system.
• $CA_{32} =$	The component's backside must not ignite.	• $FR_{32} =$	Prevent backside ignition..	• $DP_{32} =$	Volatile gas barrier.	• $PV_{32} =$	Weaving and lay-up.
• $CA_{33} =$	The structure needs to retain its structural integrity as much as possible.	• $FR_{33} =$	Retain sound thermomechanical conditions, i.e., $T \lesssim T_g$..	• $DP_{33} =$	Thermal insulator.	• $PV_{33} =$	Insulation layering.
$CA_4 =$	The configuration should be flexible and replaceable in case of damage or design evolution.	$FR_4 =$	Provide means for easy replacement (in case of damage).	$DP_4 =$	Detachable protection.	$PV_4 =$	Mechanical attachment.
$CA_5 =$	The selected materials need to endure maintenance and in-service conditions.	$FR_5 =$	Resist environmental attack.	$DP_5 =$	Water & aircraft-fluids resistant material.	$PV_5 =$	Enveloping with liquid-resistant material.

6K CF tows instead of 3K, hence an increased nominal ply thickness *vs.* CF1. The main rationale behind considering this material was to explore a different weave/fiber count architecture and ensuring minimal void content owing to the autoclave fabrication process. Finally, CF4 was considered to analyze the effect of changing the matrix from a thermoset to a high performance thermoplastic, i.e., PEEK. Besides its well-known mechanical properties, PEEK is also known for its excellent FST properties and high char yield.

Table 4.3 Evaluation data of structural candidates. The linguistic definitions and values are defined in Table 4.1 and Fig. 4.4b, respectively. The ↑ and ↓ arrows indicate that the value should be as high or low as possible, respectively.

		Priority:	VH	H	H	L	M
		Target:	≥ G	< 50 %	≤ M	≥ F	VH
ID	Material Candidate		Post-fire specimen integrity ↑	Weight increase [%] ↓	Cost ↓	Ease of manufacturing ↑	TRL ↑
CF1	C/epoxy 5 plies (HTS40 PW 3K)		–	–	–	–	–
CF2	C/epoxy 5 plies (HTS40 PW 3K) + 1 GF ply (7781)		VP	32.4	M	VG	VH
CF3	C/epoxy 5 plies (HTA40 2x2 Twill 6K)		F	59.4	H	VG	VH
CF4	C/PEEK 6 plies (HTA40 5HS 3K)		VG	77.2	VH	F	H

Parasitic protection

Several sources focusing on burn-through and fire resistance imparted by non-structural materials were consulted following the strategies described in §4.2.2: material brochures, scientific literature [322, 363–365], conference proceedings [330], publicly available technical reports [124] and patents. In the end, some of the materials contained in a report [124] were selected as follows. This reference presents an evaluation campaign intended to identify lightweight aircraft engine firewall configurations. It contains the results of 68 aerospace grade and experimental material systems from approved aircraft material suppliers. A kerosene burner intended for firewall evaluation was used to evaluate a 610 mm x 610 mm panel of each configuration. The report highlights 39 material systems that withstood the flame attack for 900 s. From this pool of candidates, only 11 were deemed satisfactory by the author of the report [124] in terms of burn-through and backside temperature, staying below ∼371 °C which represents the limit to avoid a hazardous situation with JP-8 fuel. Besides the backside temperature and the weight saving with respect to a stainless steel plate as baseline, the report mostly contains subjective evaluations (water and fluids resistance, damage tolerance, and ease of maintenance) which we translated into linguistic terms based on the scales contained in Table 4.1 and Fig. 4.4b. Since 4 structural materials have been already defined at §4.3.3, we restricted the number of parasitic protection material candidates to 7

for our purposes, which are shown in Table 4.4. Moreover, to consider two additional criteria, i.e., cost and TRL, Table 4.4 contains the linguistic evaluations assigned to them based on comments found in the report and our experience.

Table 4.4 Evaluation data for parasitic protection candidates (adapted from [124]; Cost and TRL were added for this exercise). The linguistic definitions and values are defined in Table 4.1 and Fig. 4.4b, respectively. The ↑ and ↓ arrows indicate that the value should be as high or low as possible, respectively.

		Priority:	H	VH	H	M	M	M	L	L
		Target:	≤ 195 °C	≥ 50 %	≤ M	≥ H	≥ G	≥ G	≥ F	≥ F
ID	Material candidate		Max. backside temp. [°C] ↓	Weight saving [%] ↑	Cost ↓	TRL ↑	Water resistance ↑	Resistance to aircraft fluids ↑	Damage tolerance ↑	Ease of installation/ repair ↑
P1	Alumina fabric/silica mat quilt		200	60.0	H	H	G	P	G	G
P2	Woven alumina fabric		315	72.0	M	H	G	P	G	G
P3	Alumina/silica/glass quilt		140	57.6	H	H	G	F	G	G
P4	Flexible ceramic mat with quartz fabric edges		210	21.2	H	H	G	G	P	G
P5	Ceramic mat wrapped by a dimpled S/S foil		250	37.2	M	VH	VG	VG	G	F
P6	Ceramic blanket wrapped by a dimpled S/S foil		240	32.0	M	VH	VG	VG	G	F
P7	Aluminum sheet with polysiloxane coating		185	17.6	L	M	VG	F	F	F

4.3.4 Stage 3–Small-scale evaluation: structural materials

Fig. 4.6 provides an overview of the test rig developed for thermomechanical evaluation. Figs. 4.6a and 4.6b show the schematic side and front views, respectively, indicating the main components of the small-scale test rig. Figs. 4.6a and 4.6b depict a tensile load case, although the procedure can be adapted to test conditions where compressive loads are relevant. The setup in installed on a servohydraulic UTM (Model 810, MTS) with a load capacity of 25 kN.

Item 1 is a propane torch (standard burner no. 1270, Bullfinch) capable of yielding a flame with T and q representative of an aircraft fire-resistance test. The flame used in this method is obtained with a mixture of propane (consumer grade HD-5, PNE) diluted with CO_2 (10 % by volume) supplied at 9 SLPM[1] by two mass flow controllers (HFC202, Teledyne Hastings). The flow reacts with the surrounding air, yielding a slightly fuel-lean flame ($\phi < 1.0$). To avoid overheating and stabilize the flame, the torch is water-cooled using a cooling bath (EX-111, Neslab). Water is kept at room temperature and flows through an external copper tube welded to the torch in a similar fashion to [133]. A detailed account of the flame, gas mixing and calibration procedure is provided in [129]. The same burner model has been used by other research groups [133, 138, 366] and comparison with the literature is thus possible. Moreover, the use of a propane torch is justified by its simplicity and ease of use

[1]Standard liters per minute.

when compared to kerosene-based burners, although the results obtained with propane-based flames are known to differ considerably from those using kerosene burners [53, 86] and the underlying phenomena are yet to be completely understood. However, we have recently demonstrated [129] that the modification of simple flame parameters while keeping the q and T nominally identical in tests at the same length scale can provide similar results to those of a kerosene flame in terms of post-fire residual strength. Therefore, the present methodology is considered capable of providing meaningful results for fire resistance evaluation.

Item 2 is a 25 mm x 305 mm CFRP test specimen, in compliance with [318]. The specimen is located 185 mm away from the burner. The backside temperature is tracked using a springloaded TC (Item 3) type K (SMP-HT-K-6, Omega), ensuring proper contact with the specimen's surface and providing a more reliable means for temperature sensing than freefloating TCs due to reduced convective losses [334]. Alternatively, the backside temperature can be tracked by means of infrared thermography provided that the dynamic nature of emissivity is considered [367]. The specimen is attached to a stainless steel extension (Item 4) by a pin (Item 5) on each extremity. The extensions are clamped to the UTM. To avoid flame wrapping (the flame diameter is indicated by the dashed circle), a pair of alumina-silica ceramic walls (Item 6) (UNIFORM A, Zircar) is placed flush to the specimen's front side. Should the specimen have a protective layer, the walls' position can be adapted. Finally, the test volume is protected by a custom aluminum enclosure ($V \approx 87\,\mathrm{L}$) (Item 7) of to avoid damaging the universal tester. The enclosure has optical access ports and openings to allow burner installation and backside temperature sensing. The enclosure is also connected to an air extraction system (two intakes with a maximum flow of $\sim$65 and $\sim$73 $\mathrm{L\,s^{-1}}$) adjusted to avoid disturbance of the open flame. The purpose of air circulation was threefold: removal of toxic fumes and particulates, prevention of excessive heating within the enclosure, and avoidance of a semi-quiescent atmosphere which may be less representative of an air-bathed aircraft component. Fig. 4.6c shows a picture of the test enclosure and burner fixed to the UTM, while the arrow indicates the position from which the picture shown in 4.6d was taken.

Test conditions

Considering standard tensile evaluation [318], 25 mm x 305 mm specimens of the CFRP configurations described in §4.3.3 were waterjet-cut from larger panels. Coupons dedicated for fire & load tests were drilled on both extremities for pinning to the extensions connected to the UTM grips. The four configurations were evaluated in a virgin state as well as after 300 and 900 s of flame attack. To analyze the temporal evolution of ultimate tensile strength (UTS), specimens were exposed to the open flame for shorter periods, i.e., 15 and

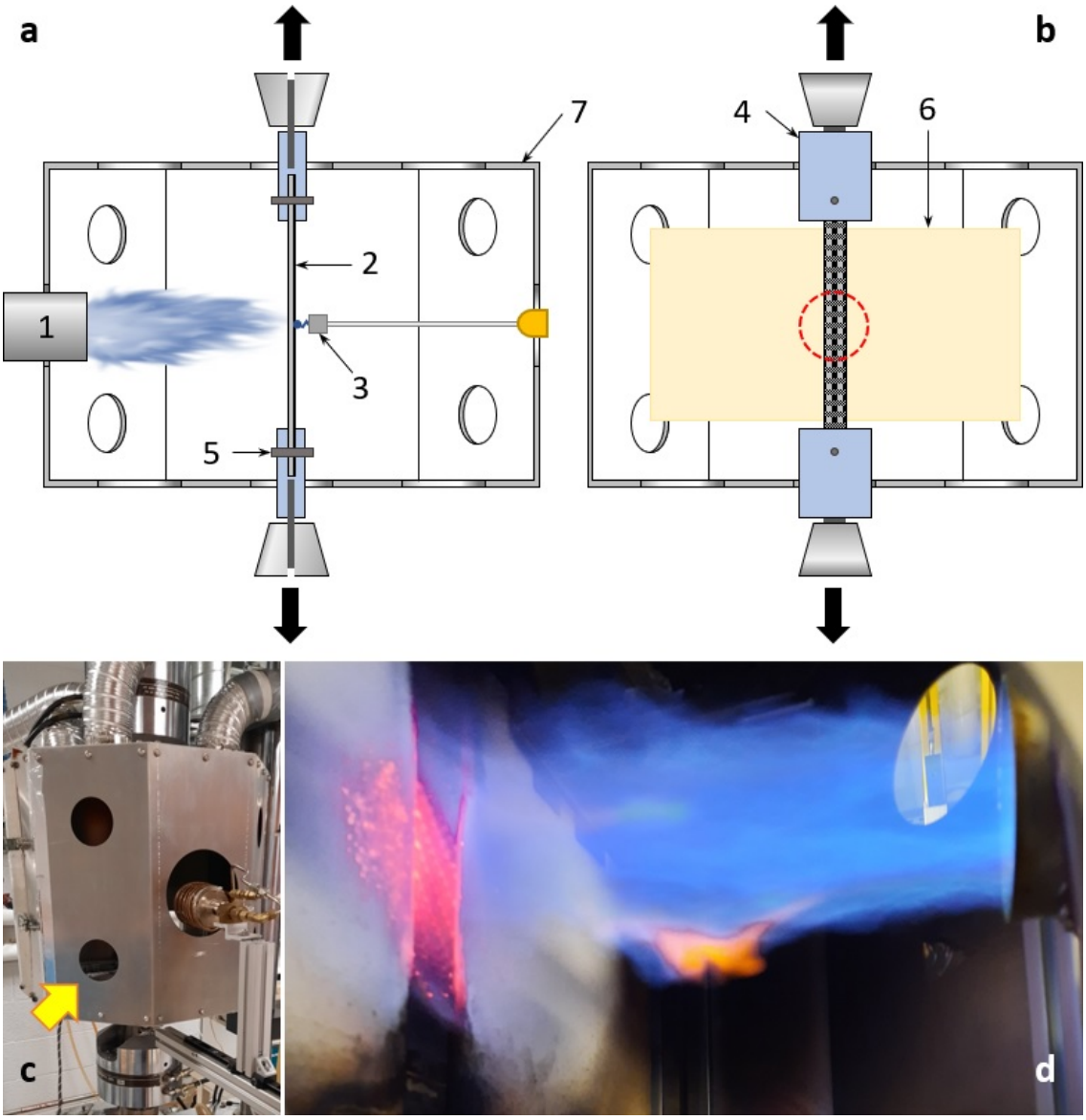

Figure 4.6 Simultaneous fire and load testing setup using a propane-based flame and a UTM. (a) and (b) are schematic side and front views of the test rig, respectively, showing the main items: 1-propane burner; 2-CFRP specimen; 3-springloaded TC; 4-stainless steel extension; 5-pin; 6-ceramic wall; 7-aluminum enclosure. (c) Picture of the test enclosure with access ports, the ventilation tubes and the grips of the universal testing machine. The arrow indicates the position from which figure (d) was taken. (d) Picture of specimen under flame attack and tensile load, with ceramic sidewalls to prevent the flame wrapping.

45 s, and immediately quenched using a stream of CO_2. Due to specimen availability, CF4 was tested after 90 s instead of 15 and 45 s. At least five specimens per configuration and burnt condition were tested to obtain mean values and CIs.

For each fire & load test, a hoop stress was simulated by applying a tensile load for the first 300 s corresponding to the duration where the rig is pressurized in ISO 2685 [84]. The loads correspond to 4.2, 5.0, 3.5 and 2.2 % of the UTS value of configurations CF1, CF2, CF3 and CF4, respectively. The load was brought back to zero after 300 s to end the simulated hoop stress induced by the fan flow at full-thrust (see §4.3.1), and the clamps were held in place until the end of test for specimens tested until 900 s. In case of burn-through, tests were immediately halted. In all cases, specimens were removed only after cooling down.

The mechanical evaluation of virgin and burnt/quenched samples was carried out in a second UTM (same model) to avoid the modification of the setup, i.e., specimens were clamped directly with the hydraulic grip wedges. Both burnt and virgin specimens were tested under quasi-static tensile loading until failure in line with ASTM D3039 [318]. Specimens were not tabbed since this practice is only recommended for UD/non-woven-reinforced specimens. Specimens were loaded under tension using a crosshead speed of $2\,\mathrm{mm\,min^{-1}}$. The failure load was used to determine the UTS considering the original sample's cross-section area. This in turn yielded an UTS_{eq} value for burnt configurations.

Temperature evolution and specimen integrity

Fig. 4.7 shows the evolution of backside temperature for different laminates configurations. The mean temperature is indicated by the lines and the shaded areas indicate the 95 % CI. The load realease (LR) and burn-through (BT) labels indicate the two major events during the tests. From this plot, two characteristic behaviors can be distinguished.

The first behavior is depicted by CF1 in Fig. 4.7, showing the fastest backside heating while reaching and exceeding 600 °C in the first 60 s. Then, the profile shows some variation in the t = [60,300] s range, most likely due to flame fluctuations, the decrease in heat flux upon heating of the specimen, and char depletion between plies as well as within CF tows. This in turn promotes the creation of voids working as insulating pockets, and thus changing the heat conduction and convection process. Upon reaching the LR point, a small yet abrupt temperature decrease of ∼20 °C can be distinguished. This is explained by the relaxation of the plies and the "spring out" effect of the woven architecture of the fabrics due to their crimp. This effect increases the size of internal pockets, enhancing the insulating effect on the rearmost ply (backside ply). Fig. 4.8 shows a typical CF1 specimen (leftmost) after a 300 s exposure. The specimen shows full resin and char depletion, with minimal damage

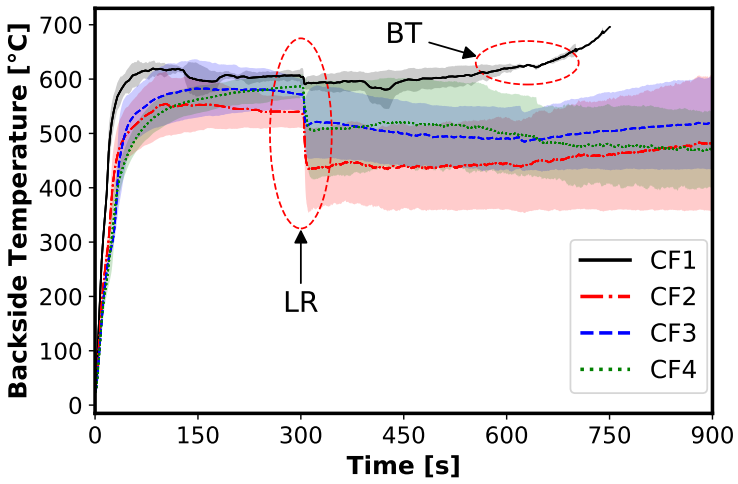

Figure 4.7 Backside temperature readings of the different CF/epoxy (configurations CF1, CF2, CF3) and CF/PEEK (configuration CF4)

on the remaining plies. The particular problem of BT described in §4.3.1 becomes evident when, at $t \approx 500\,\text{s}$, a temperature "runaway" effect is seen due to the damage undergone by the front plies. This phenomenon takes place sequentially due to CFs oxidation with different effects: diameter reduction [224], internal gasification leading to pore growth [253], thus creating internal and surface flaws, i.e., pits [289, 368]. Subsequent fiber breakage is enhanced by flame disturbance [288] due to its turbulent nature. The tests had to be halted at $t \approx 700\,\text{s}$ due to flames reaching the springloaded TC probe. A typical specimen at this stage is shown in Fig. 4.8 (second leftmost specimen).

The second typical behavior observed in Fig. 4.7 is represented by laminates CF2 to CF4. Although some differences existed between CF3 and CF4 configurations in terms of matrix system and CF's woven architecture, their temperature profiles are similar due to having the same nominal thickness. The temperature profiles of CF2 to CF4 during the first $\sim$100 s are similar, with rapid heating and within the experimental uncertainty indicated by the shaded zones. In contrast with CF1, the backside temperature of CF2 to CF4 specimens did not exceed 600 °C, mainly explained by the thermal blocking provided by the increased thickness or the additional GF ply. Moreover, the effect of LR and subsequent swelling due to fabric crimp heavily influences the mean temperature profile, and reductions of approximately 100, 50 and 75 °C can be observed for CF2, CF3 and CF4, respectively. Once past the LR marker, these configurations withstood the flame attack and did not show BT signs, as indicated by the temperature profiles continuing until the end of the test ($t = 900\,\text{s}$). However, different damage levels were identified from visual inspection and sometimes correlated with

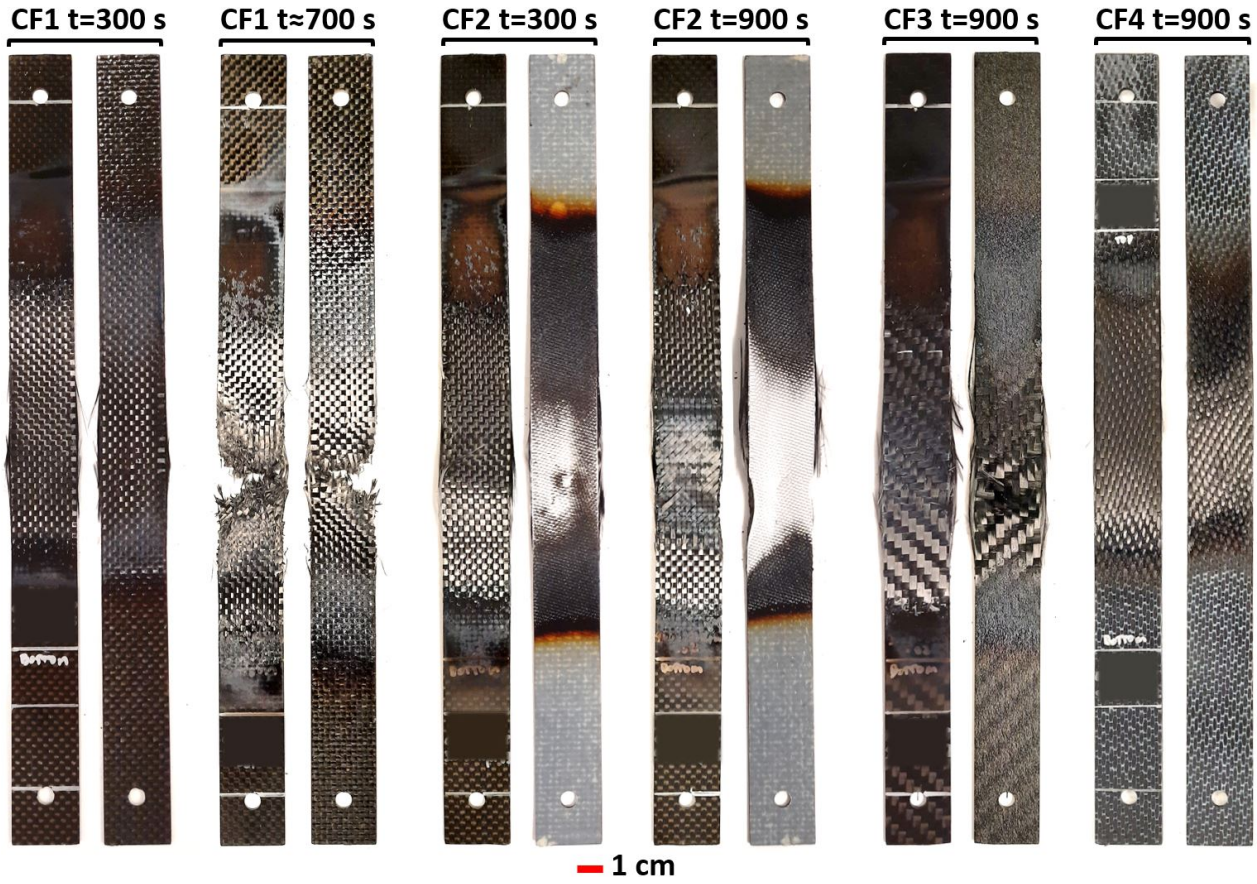

Figure 4.8 Typical post-fire images of configurations CF1, CF2, CF3 and CF4. Each pair corresponds to the front (left) and back (right) views of each specimen. A constant tensile load was applied during the first 300 s. CF1 at $t \approx 700$ s shows burn-through, which translated into flame penetration.

the backside temperature profile.

Fig. 4.8 shows a CF2 specimen after 300 s (third from left to right) with almost full char depletion on both sides within the flame impingement zone. CF tows look barely affected while the GF ply on the backside still has some char within tows. CF2 shows the lowest backside temperature profile in the $t = [300,600]$ s range owing to the additional GF ply, although the temperature started increasing steadily past the 600 s threshold, as shown in Fig. 4.7. This is most likely explained by heavy CF damage, in a similar fashion to CF1. The temperature increase at $t \gtrsim 600$ s coincides with the BT of CF1. A typical CF2 specimen after a full 900 s test is shown in Fig. 4.8 (third rightmost specimen). The front side shows a heavily damaged set of CF plies, with some $\pm 45°$ tows from intermediate plies being visible. The backside shows the GF ply with no major damage signs, although some shrinkage can be observed on both sides.

CF3 specimens yielded a higher temperature profile with respect to CF2, as seen in Fig. 4.7, although an improved BT behavior was also observed after a full 900 s as shown in Fig. 4.8 (second rightmost specimen). In the latter, some fiber damage can be observed on both faces, although no intermediate layers are exposed. This suggests an improved fire resistance by the different fabric architecture (6K, Twill 2x2) instead of the smaller tows of CF1 (3K, plaine weave). This is in line with the work of Zhang *et al.* [369] who reported the effect of fabric architecture and fiber count on the thermal insulation of CF fabrics.

Finally, CF4 was the slowest configuration to reach its maximum temperature, which took place at LR as shown in Fig. 4.7. This behavior may be explained by the increased thermal stability of PEEK and its higher char yield. Moreover, the CF4 laminate shown in Fig. 4.8 (rightmost specimen) represents the least damaged configuration after 900 s of flame attack. In general, the char resulting from the PEEK pyrolysis tended to be more robust than that of both epoxy systems (CF1/CF2/CF3). Virtually no fiber damage was observed although most of the char was already oxidized by the end of the test, i.e., at $t = 900$ s.

Since the temperature profiles shown in Fig. 4.7 do not show any practical difference between them, i.e., profiles share uncertainty regions, either meaningful scores nor conclusions can be drawn. Nonetheless, a visual evaluation comes in handy despite its subjective and fuzzy nature, providing a very valuable means for the final ranking of candidates. Thus, the post-fire integrity of the specimens was visually evaluated. Based on the aforementioned descriptions and considering the linguistic evaluation scale from Table 4.1 and Fig. 4.4b, the scores *very poor* (VP), *fair* (F) and *very good* (VG) were assigned to CF2, CF3 and CF4, respectively, as shown in Table 4.3.

Tensile strength evolution

Fig. 4.9 shows the evolution of the mean residual UTS_{eq} for CF1 to CF4 configurations, normalized to the virgin UTS of configuration CF1, with error bars indicating the 95 % CI. The UTS_{eq} is calculated considering the original specimen's cross sectional area. Fig 4.9a shows the evolution of UTS for CF1 as a function of flame exposure duration. After only 15 s of flame attack, it can be seen that the laminate has lost almost half of its strength (residual UTS_{eq} = 56 %). Subsequently, ∼80 % is lost after 45 s with a residual UTS_{eq} of only 22 %. At this point, almost the entirety of the matrix has been pyrolyzed and charred and thus the residual strength is governed by the fibers, with virtually no contribution from the degraded matrix. After 300 s, the residual strength slightly decreased further compared to the specimens burnt for only 45 s, leaving only a residual UTS_{eq} of 15.4 %. Since all of the specimens started to show burn-through signs around 700 s, tests were halted and UTS_{eq} values were not obtained for an exposure of 900 s.

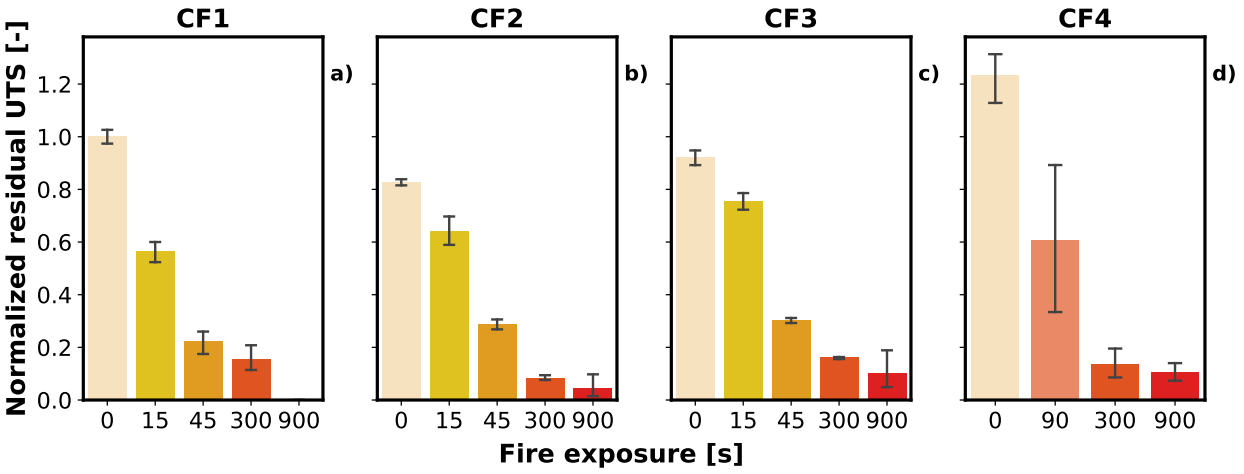

Figure 4.9 Evolution of residual equivalent UTS_{eq} with respect to the test duration. Samples were quenched upon flame removal and tested under tension until failure after cooling down. The error bars indicate the 95 % CI.

Slightly different behaviors were observed on CF2 and CF3 laminates, although the drop of UTS_{eq} after 15 and 45 s was less pronounced than for CF1. Fig. 4.9b shows the evolution of CF2 which yielded a lower virgin UTS value, from to the increased thickness due to the GF ply. However, after 15 and 45 s exposures, the UTS_{eq} had a lower drop staying at 77 and 35 % of its original value, respectively. After 300 s, only 10 % of the original UTS was retained. However, given that the specimen did not show complete burn-through owing to the protection of the GF ply, it was possible to evaluate specimens after upon completion of the 900 s test, yielding only 5.5 % of the original strength. Regarding CF3, a similar

behavior was observed as for CF2 specimens, which had a normalized UTS closer to that of CF1. After 15 and 45 s, the residual UTS_{eq} dropped to 82 and 33 %. Higher residual UTS_{eq} values were observed after 300 and 900 s, retaining 17 and 12 % of the original UTS. In both cases, the less-severe drop in UTS_{eq} after 15 and 45 s can be explained by a slightly thicker configuration, presumably providing additional protection to the rearmost plies, where the matrix takes longer to be degraded and loose its load-distribution properties. Furthermore, the higher UTS_{eq} values observed on CF3 specimens after 300 and 900 s may be explained by a larger fiber count per tow, i.e., 6K *vs.* CF2's 3K, despite having a lower ply count.

Finally, CF4 had a normalized UTS which exceeded that of CF1 by 23 %, enhanced by the PEEK matrix. A significant difference when compared to the rest of the structural configurations is that, even after a 90 s exposure, the UTS_{eq} only dropped to 49 % of its original value. This may be attributed to the higher thermal stability of PEEK and improved protection of the back layers of the laminate. Nonetheless, after 300 and 900 s, CF4 yielded very similar UTS_{eq} values to those from CF2, i.e., only 11 and 6 % of its original UTS.

4.3.5 Stage 4–Ranking

The final step involved the ranking of both structural and parasitic protection candidates following the steps shown in Algorithm 1. Before showing the final ranking of the candidates for each category, a graphical representation for each criterion is in order, showing the membership functions of the candidates and the target. By doing so, the reader will have a better understanding of the final ranking and adjust criteria and/or their importance as needed.

The calculations shown in Algorithm 1 were straightforward once the criteria and their importance as well as the individual scores were defined. However, the decision-maker's degree of "optimism" embodied by α was expected to influence the final ranking. To analyze its effect, **procedure 3** of Algorithm 1 was performed for eleven values, i.e., $\alpha = \{0, 0.1, \ldots, 0.9, 1.0\}$. The final order is presented as a function of α.

Structural materials

Fig. 4.10 shows the membership functions of the structural candidates' evaluations along the target, highlighted for each criterion. CF1 was discarded and thus not shown since it did not meet the burn-through requirement. Fig. 4.10a shows the scores for *Post-fire evaluation*, indicating that CF4 fulfills the "G or higher" criterion as indicated in Table 4.3, while CF3's "F" score partially meets this requirement. CF2 scored "VP" since it was heavily damaged and it barely withstood the test, showing no overlap with the target. These results contrast

with the *Weight increase* and *Cost* criteria, shown in Figs. 4.10b and 4.10c, respectively. On the one hand, CF2 completely fulfills the requirements of the target while CF3 complies only to some extent. On the other hand, CF4 does not meet the target scenario in either case. Regarding the *Ease of manufacturing*, the three candidates fall within the target range. CF4, being a PEEK-based material system, poses a challenge in terms of processing owing to the geometry of the engine casing, hence its lower score. Nonetheless, it covers the target. Finally, the CF2 and CF3 completely fulfill the *TRL* criterion since they are thermoset prepregs capable of achieving complex geometries, whereas CF4 may need further technological development.

The final rankings of structural materials are shown in Fig. 4.12a. It can be seen that for the lowest values of α, i.e., $\{0, 0.1, 0.2\}$, CF2 is the best option among the three materials, followed by CF3 and CF4. The order only changes once α assumes the value of 0.3, when CF3 and CF4 climb shift upwards and CF3 is now the lowest ranked option. However, this situation changes when $\alpha \geq 0.4$. Owing to the reduced number of candidates as well as the clear differences between their scores and the target for each criterion, it is possible to explain these rankings based on the visual representation of Fig. 4.10.

Parasitic materials

Fig. 4.11 shows the membership functions of the different parasitic material alternatives for the different criteria. The ideal solution is indicated by the highlighted areas.

The three criteria with the highest priority are first discussed. Regarding the *Max. Backside Temp.* criterion shown in Fig. 4.11a, whose priority is "H", it can be seen that only P3 and P7 fully meet this criterion. P1 and P4 partially meet the target, both exceeding the maximum value although P1 to a lesser extent. Candidates P2, P5 and P6 completely fail to meet this requirement. Considering the criterion with the highest priority, i.e., *Weight saving*, Fig. 4.11b shows that P1, P2 and P3 fully meet the target, while the rest of the candidates fail to meet this requirement. *Cost* wise, with a priority of "H", P7 is the cheapest candidate shown in Fig. 4.11c, while P2, P5 and P6 are mid-range options, yet all of them are within the target envelope. P1, P3 and P4 are more expensive and partially meet this criterion.

Now, considering the criteria with medium priority, P1 through P4 have the highest score in *TRL* followed by P5 and P6, as seen in Fig. 4.11d. The six candidates cover the target, whereas P7 merely reaches the lower portion of the target. In terms of *Water resistance*, Fig. 4.11e indicates that all the candidates meet the target, although to different extents, i.e., P5 through P7 have the best performance while P1 through P4 have a slightly lower performance.

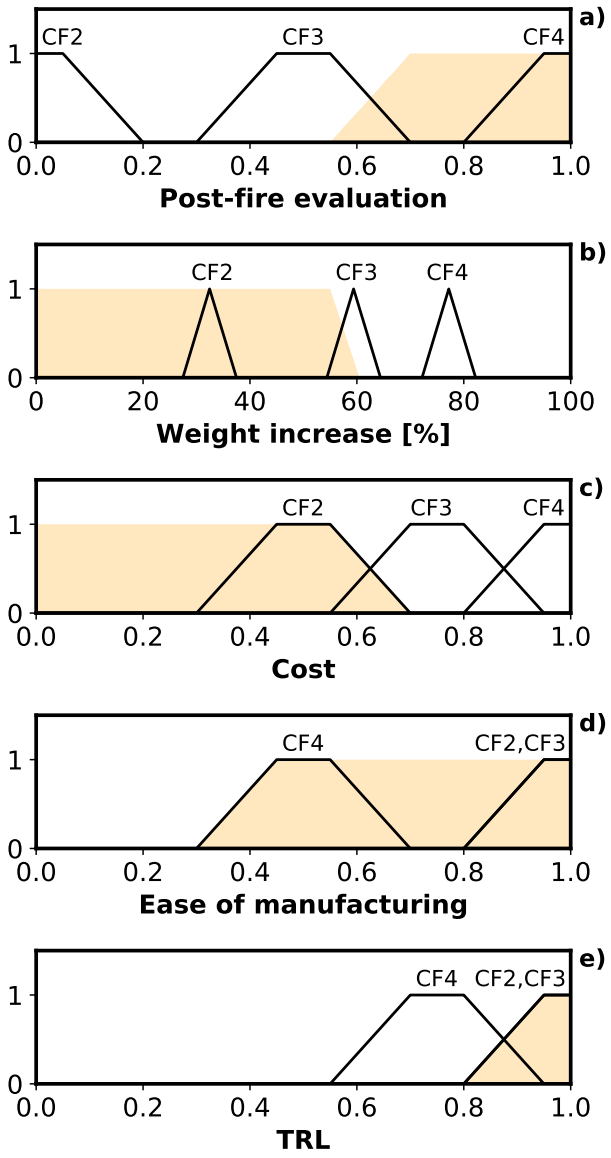

Figure 4.10 Membership functions of the structural candidates (indicated as CF2 to CF4) and target for each criterion (highlighted area), in accordance with values from Table 4.3.

The final criterion of this category, *Resistance to aircraft fluids*, shows in Fig. 4.11f that the two lightest solutions have the lowest scores, i.e., P1 and P2 have a "P" evaluation. P3 and P7 scored "F" and reach the lower portion of the target. P4, P5 and P6 fulfill the requirement of the target, being the last two with the best performance.

The two last criteria shown in Figs. 4.11g and 4.11h are *Damage Tolerance* and *Ease of installation/repair*, respectively. Both have a low priority ("L") as indicated in Table 4.4. On the one hand, P4 has the lowest damage tolerance, although it partially covers the target as seen in Fig. 4.11g. The rest of the candidates meet the target although P7 has a lower score ("F) than P1 to P3, P5 and P6 with a "G" note. Finally, Fig. 4.11h shows that all candidates meet the requirement of ease of installation/repair. P5, P6, P7 have an "F" note, while P1 through P4 are seemingly easier to work with.

The effect of varying α was assessed in a similar way to the structural candidates as described in §4.3.5. Fig. 4.12b shows that the best performance is shared by three candidates, depending on the value of α. P2, P3 and P5 outranked the rest of the candidates when α was set to $\{0.9, 1.0\}$, $\{0.5, 0.6, 0.7, 0.8\}$ and $\{0, 0.1, 0.2, 0.3, 0.4, 0.5\}$, respectively. P3 and P5 were consistently ranked within the first three places regardless of α, while P5 rank improved with higher α values. Since P5 and P3 have the most consistent results, it is suggested that further analyses consider these two options, although P2 also deserves attention.

On a final note, it is worth mentioning that certain candidates fell short while meeting the target requirements of the criteria with the highest priority. For instance, P1, which is highly ranked in *Weight saving* and partially meets the *Max. Backside Temp.*, is consistently found in the low-to-middle ranks as shown in Fig. 4.12b. This apparent contradiction is observed for in highly-ranked candidates such as P5, which did not meet altogether the aforementioned criteria. However, it fully meets the rest of the requirements, and thus it outranks P1 even when $\alpha = 1.0$. This example not only highlights the usefulness of MCDM tools for the ranking step and the effect on the final selection, but also suggests that the result may need to be compared against other MCDM methods. As previously mentioned, each MCDM tool has its own advantages and drawbacks. In the end, the designer/decision-maker needs to bear in mind that criteria, weights and scores may need to be revised in subsequent iterations to obtain unambiguous results. Based on the final steps of the material selection methodology presented by Liao [305], we relied on the integral value method proposed by Liou and Wang [307] to perform the ranking of candidates with the aid of an index of optimism (α), which relates to the preference of the decision maker for lower or higher portions of a fuzzy score. If only one combination of structural and parasitic material systems were to be chosen, it is recommended to proceed with CF4 and P3, given that these candidates have

the best ranking when $\alpha = 0.5$ is considered.

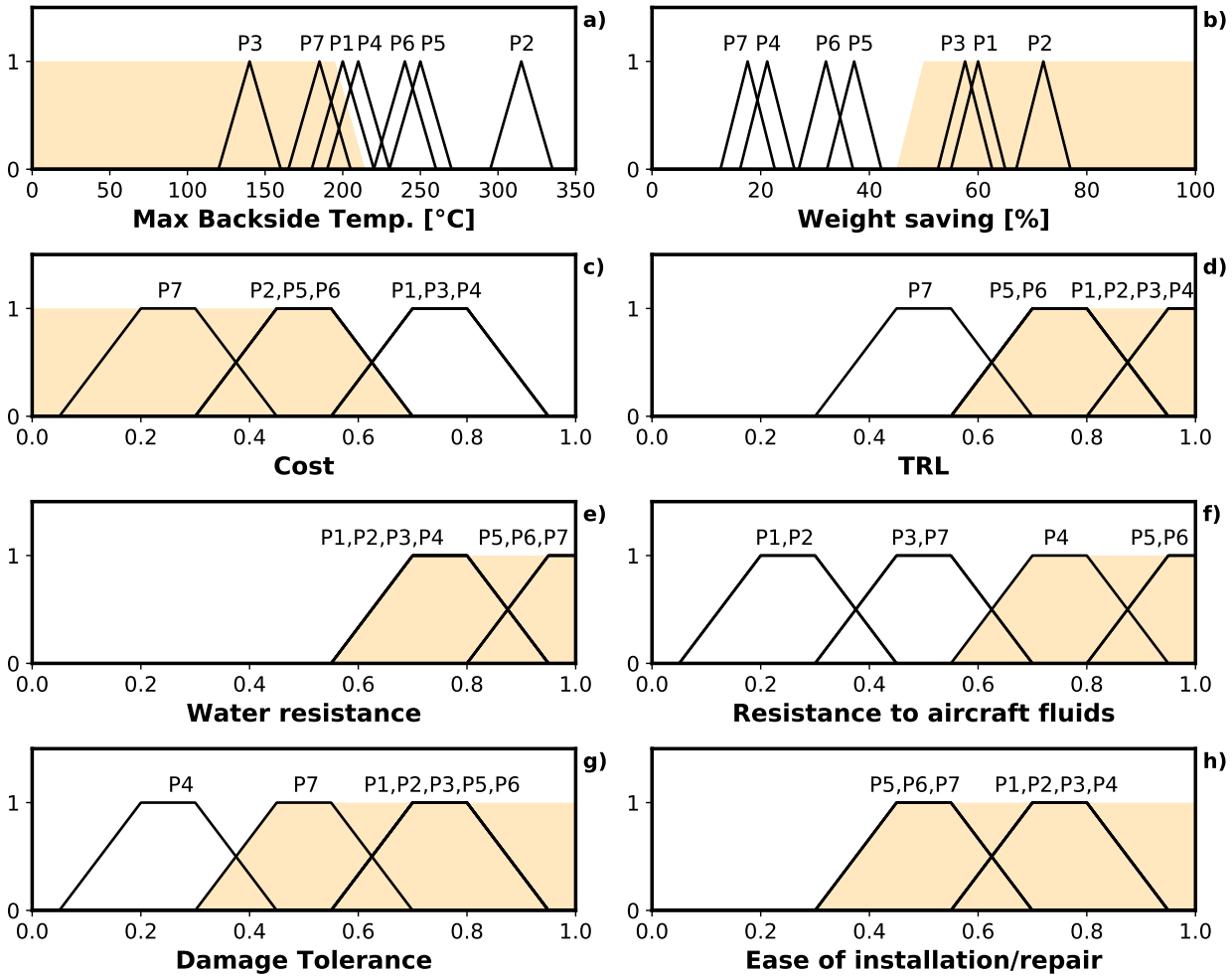

Figure 4.11 Membership functions of the parasitic protection candidates (indicated by P1 to P7) and target for each criterion (highlighted area), in accordance with values from Table 4.4.

4.4 Conclusions

This work focused on the fire resistance of PMC-based structures intended for aircraft applications. We proposed a four-stage design & evaluation methodology aimed towards fire-resistant aircraft structures. A sequence was presented comprising the conceptual design, initial material screening, small-scale evaluation and ranking phases. As a first stage, we proposed the use of AD to guide the conceptual design phase. By following this approach in Stage 1, it is possible to identify design features, material properties and processing routes systematically. Subsequently, standard design practices were introduced in Stage 2 to identify

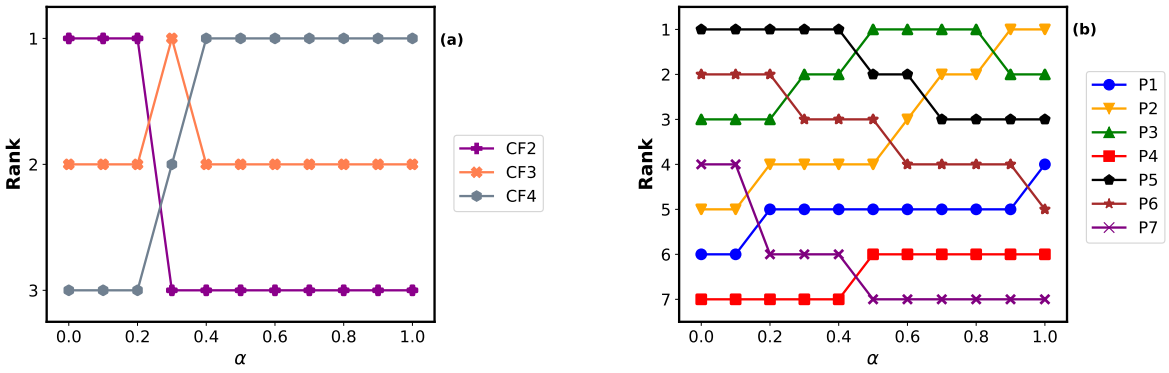

Figure 4.12 Final ranking of structural (a) and parasitic (b) as a function of α=[0,1].

materials that potentially meet the requirements previously defined. At Stage 3, we proposed a small-scale fire evaluation evaluation approach using a propane burner and a UTM. Given the complexity of phenomena involved in the combustion of PMCs, this approach does not purport to replace intermediate-scale fire tests for aircraft certification (e.g. [53] or [84]), but it is rather intended as a tool for advanced screening of PMCs to discern configurations capable of withstanding fire attack while enduring mechanical loads. As a final step, we incorporated concepts of fuzzy sets and MCDM in order to rank the material candidates.

To demonstrate our methodology, we presented a case study focusing on an aircraft engine casing. At Stage 1, AD helped to determine, for instance, that the thermal protection had to be decoupled from the structure if some functional aspects of the final structure were to be kept independent. Based on the design aspects defined during conceptual design, we considered two families of material systems during initial material screening at Stage 2: structural and parasitic protective materials. Standalone structural materials were evaluated at Stage 3 to determine their fire resistance when no protection is available. We showed that burn-through can take place at a small scale using a propane burner relying on a modified fuel mixture with respect to test conditions found in the literature. Thus, it was possible to have meaningful material evaluations considering aggressive oxidative conditions with simultaneous mechanical loads, which have been typically achieved only with radiant heat sources or richer mixtures. Finally, in Stage 4, the use of fuzzy sets allowed to consider both quantitative and qualitative scores, while the use of a MCDM method capable of handling fuzzy numbers allowed the ranking of candidates considering dissimilar criteria, weights and evaluation scales. It was shown that, with the ranking method selected, the decision maker's preference (α) has an impact of the final material selection. The variation of α between 0

and 1 manifested itself in different rankings, becoming more pronounced when the number of candidates increased from $n = 3$ to $n = 7$ in the case of structural and parasitic protection candidates, respectively. For a neutral approach, the ranking of structural and parasitic material systems can be determined by setting α at 0.5. These results highlight one of the many challenges faced by designers in the ranking and decision-making process. In this work, only one MCDM method was used. Further research is needed to compare the outcome between different methods.

Overall, we expect that this work will be useful to aircraft designers in the endeavor of conceiving fire-resistant PMC. The four-stage design & evaluation tool is expected to be versatile, with potential use in other aircraft fire safety applications. Future research on the impact of the four stages is needed. The effect of design coupling, criteria, weights, and other MCDM tools certainly deserve attention to further improve the methodology.

Acknowledgments

The authors want to acknowledge the financial support from the Natural Sciences and Engineering Research Council of Canada (NSERC/CRSNG) grant no. CRDPJ 478687-15, and the partners from CRIAQ ENV-708 project. Pablo Chávez-Gómez is extremely grateful to the National Science and Technology Council of Mexico (CONACYT) for his doctoral scholarship.

CHAPTER 5 ARTICLE 2: Carbon fiber oxidation in combustion environments–Effect of flame chemistry and load on bundle failure

Published in *Materials Today Communications*, vol. 31, pp. 103560, June 2022 [288].

By
Pablo Chávez-Gómez, Tanja Pelzmann, Joanna Zahlawi, Louis Laberge Lebel, Étienne Robert

ABSTRACT

CF-based composites are susceptible to fire attack. In this work, we assess the effect of flame chemistry and load on the oxidation-induced failure of three polyacrylonitrile-based CFs with different tensile modulus. Traditional thermal analyses initially showed the influence of microstructure and heating rate on the oxidative behavior. Two different flame-based tests were implemented to address the CF behavior under true fire conditions. Filaments were inserted into a premixed methane/air flame. Subsequent scanning electron microscopy revealed prompt and heterogeneous fiber pitting even after short exposures ($t \approx 0.5\,\mathrm{s}$). The flame stoichiometry, characterized by the fuel/oxidizer ratio (ϕ), was varied to assess its effect on the CF bundle failure considering TTF as an indicator of fire resistance. The trends are similar for the three CF types. The stoichiometric flame ($\phi = 1.0$) yielded the least aggressive conditions despite being the hottest. Slightly faster bundle failures were caused by the fuel-rich configuration ($\phi = 1.2$), suggesting a contribution from OH radicals. Higher tensile loads tended to reduce this difference. The enhanced aggressiveness of the fuel-lean condition ($\phi = 0.7$), i.e., oxygen-rich flame, was confirmed by a TTF at least 50% shorter than its stoichiometric counterpart. Moreover, we found a striking one order-of-magnitude difference in TTF between the high and standard/intermediate modulus CF bundles, regardless of ϕ. The results highlight the critical importance of flame chemistry and fiber microstructure in the fire resistance of CF-based structures.

5.1 Introduction

Carbon fibre reinforced polymer (CFRP) composites are increasingly used in the transportation sector (e.g. aerospace, automotive, naval, rail) owing to their high specific properties.

Their backbone, carbon fibers (CFs), help to fulfill structural requirements with lower weight penalties when compared to metallic configurations [34]. However, fire hazards can push these components out of their operational limits, with electrification bringing new challenges [248].

To demonstrate fire resistance, standardized tests are mandated by regulatory agencies. This testing often involves exposing composites to an external flame, with conditions typically characterized by T and q. For instance, aircraft structures are evaluated following either the ISO 2685 standard [84] or FAA's certification guidelines [53], with testing conditions on the order of $T \approx 1100\,^{\circ}\mathrm{C}$ and $q \approx 116\,\mathrm{kW\,m^{-2}}$. In practice, these T and q values can be achieved using different fuels and flame chemistries [293]. As a result, different fire resistance assessments can be obtained with the same thermal conditions [370,371]. A critical parameter often overlooked is flame stoichiometry, which defines oxygen and radical concentration in the hot combustion products impacting the sample tested.

Besides the oxidizing atmosphere, CF reactivity is influenced by intrinsic parameters such as microstructure and impurity levels, which are dependent on the precursor used as well as on the processing conditions. Three different precursors are commercially available for CF fabrication, namely polyacrylonitrile (PAN), mesophase pitch and viscose rayon. PAN-based CFs dominate the market ($\sim 96\%$ [184]) and, therefore, their microstructure is most relevant for the present discussion. Upon oxidative stabilization and carbonization, PAN-based CFs acquire a very characteristic microstructure, which can be described by a skin-core model [189]. This implies that a highly-ordered carbon sheath surrounds an amorphous core, with the graphitic/amorphous carbon ratio depending on the processing conditions. In this regard, stretching and heat treatment temperature (HTT) drive the microstructure definition, and consequently the mechanical properties [34, 184]. The graphitization process, i.e., higher HTTs than carbonization, leads to fibers with fewer impurities and high graphitic order, hence higher modulus and fewer defects. This in turn translates into less potential attack sites for oxidation [230] when exposed to reactive atmospheres.

To address the fire resistance of CFs, the effect of mechanical loading at high temperatures needs to be considered as well. This has chiefly been addressed under inert atmospheres [372–375]. When fiber oxidation and tensile load are considered simultaneously, tests have been limited to air-filled ovens with CFs under monotonic loading [376]. In other cases, the mechanical properties have been assessed post-hoc on cooled samples [223–225,251]. Potential synergistic effects between mechanical loads, active sites and impurities therefore require an investigation under conditions representative of a fire hazard [368]. In the few studies where pilot flames are used, the effect of CFs microstructure is not considered [214, 258, 259].

In this work, we assess the oxidative behavior of polyacrylonitrile (PAN)-based CFs under

controlled atmosphere and true fire conditions. Fibers with varying modulus are used to gain insight into the the effect of microstructure on oxidation under load and flame attack. The virgin CFs were first characterized through traditional thermal analyses under controlled atmosphere. Fiber bundles were then exposed to open flame attack under tensile loads using an original method. The results and discussion focus on the influence of the fuel/oxidizer ratio (ϕ) and fiber properties.

5.2 Experimental

5.2.1 Materials

Three commercial CFs with different properties have been selected: AS4, IM7 and HM63, which correspond to standard, intermediate, and high modulus CFs, respectively. Their characteristics (density (ρ), tensile strength (σ) and modulus (E), thermal conductivity (λ), electrical resistance (R), specific heat (C_P) and diameter) are presented in Table 5.1. To minimize differences between samples that could originate from diverse fabrication sources, all fibers are PAN-based and were sourced from the same supplier (Hextow®, Hexcel). The nominal cross-sectional area was intended to be as similar as possible for all samples, hence the different filament counts between AS4 (6K) and IM7/HM63 (12K) fiber bundles.

Table 5.1 Physical properties of selected PAN-based CFs.

Fiber	Filament count	Density ρ ($\mathrm{g\,cm^{-3}}$)	Tensile strength σ (MPa)	Tensile Modulus E (GPa)	Thermal Conductivity[1] λ ($\mathrm{W\,m^{-1}\,K^{-1}}$)	Elec. Resistance[1] R ($\Omega\,\mathrm{m}$)	Spec. Heat[1] C_p ($\mathrm{J\,g^{-1}\,K^{-1}}$)	Diameter (µm)
AS4 [377][2]	6K	1.79	4447	231	6.83	1.7×10^{-5}	1.129	7.1
IM7 [378][2]	12K	1.78	5688	276	5.40	1.5×10^{-5}	0.878	5.2
HM63 [379][3]	12K	1.83[1]	4826	435	55.0	0.9×10^{-5}	0.878	4.9

[1] Tow/bundle-based values.
[2] Unsized.
[3] GP-sized.

5.2.2 Thermal and morphology characterization

Thermogravimetric analysis (TGA) and differential scanning calorimetry (DSC) runs were performed using a simultaneous thermal analysis (STA) instrument (TGA/DSC 1, Mettler Toledo) to obtain information on fiber reactivity. Fiber bundles were cut to a length of 3 mm and 10 mg samples were loaded into 70 µL alumina crucibles. A dynamic oxidizing atmosphere was simulated using a $60\,\mathrm{mL\,min^{-1}}$ filtered air flow. Samples were stabilized at 303 K and then heated up to 1273 K at four different constant heat-up rates (HURs), i.e., 5, 10, 20 and $25\,\mathrm{K\,min^{-1}}$.

A high resolution field emission microscope (JSM7600F, JEOL) was used for SEM observa-

tions of burnt fibers (§5.2.3). Acceleration voltage and current were set at 6 kV and 226.4 µA, respectively.

5.2.3 Flame-based experiments

A flat flame burner (FFB) (standard model, Holthuis & Associates) with a stainless steel body and a water-cooled burner bronze plate (OD 73.5 mm, shroud included) was selected to carry out our tests. Three different equivalence ratios (ϕ), i.e., mixtures with different fuel/oxidizer ratios [210], were selected to assess the effect of species concentrations. Fuel-lean (ϕ=0.7), stoichiometric (ϕ=1.0) and fuel-rich (ϕ=1.2) flames were replicated from the work of Weigand *et al.* [380] (flames No. 1, 3 and 5, respectively). The adiabatic (T_{ad}) and non-adiabatic (T_{CARS}) temperatures as well as mole fraction (X) for major species (O_2, N_2, H_2O, CO_2, CO, and H_2) are given in Table 5.2. Theoretically, the three flames would differ in adiabatic temperature by several hundred K. However, due to the heat losses experienced in real conditions, they all fall in the 1706–1790 K range. The fiber surface temperature is expected to be significantly lower than the flame temperature due to radiative and conductive losses. Furthermore, the temperature distribution within the bundle will also be non uniform, from the anisotropy of heat conduction in the fibers and from superficial nature of radiation losses. Consequently only the flame temperature can be used here to characterize the conditions experienced by the fibers. There are minor differences between the reference conditions of [380] and our experiments: water cooling was done with a lower flow rate and slightly higher temperature ($4\,\mathrm{L\,min^{-1}}$ at $\sim 21\,^{\circ}\mathrm{C}$ *vs.* $1\,\mathrm{L\,s^{-1}}$ at $16\,^{\circ}\mathrm{C}$), and the oxidizer (compressed air) was replaced by a dry mixture of N_2 (79%) and O_2 (21%) to reduce oxidation enhancement caused by additional H_2O from untreated air. High purity CH_4 (99%), O_2 (99.6%) and N_2 (99.998%) (Linde) were used. The gas flows were controlled individually using flow controllers (HFC-202, Teledyne Hastings Instruments) and a custom-made computer interface (LabVIEW, National Instruments), with a 2% accuracy. The true gas flow rates were measured for each gas and flow rate ($n \geq 340$ per condition), yielding CH_4 = 1.315 (SD=0.026) and 1.123 (SD=0.026) SLPM for rich/stoichiometric and lean conditions, respectively, whereas Air = 10.477 (SD=0.172), 12.483 (SD=0.219) and 15.035 (SD=0.629) SLPM for rich, stoichiometric and lean conditions, respectively. The fuel/oxidizer mixing was carried out using a T-connector and circulated through a flashback arrestor (RF53N, WITT-Gasetechnik) prior to injecting it into the burner. Finally, in all tests, some fibers were blown away from the flame cone upon breakage. Thus, an air extraction system was positioned above the test cell to avoid fiber spread, ensuring no visible flame disturbances.

Table 5.2 Flame details at atmospheric pressure. These values correspond to a height of 15 mm above the burner outlet, i.e., within flame cone (data from [380]).

Flame No.	Gas Flow [SLPM]		ϕ	T_{ad} [K]	T_{CARS} [K]	X_{O_2}	X_{N_2}	X_{H_2O}	X_{CO_2}	X_{CO}	X_{H_2}
	CH_4	Air									
1	1.1	15.0	0.70	1838	1706	0.0577	0.7349	0.1367	0.0684	0.0000	0.0000
3	1.31	12.4	1.00	2226	1790	0.0005	0.7144	0.1894	0.0942	0.0008	0.0004
5	1.31	10.4	1.20	2137	1723	0.0000	0.6764	0.1844	0.0673	0.0406	0.0313

Unloaded fibers

A few unloaded fibers were extracted from each spool and inserted into the flame cone at the selected height (15 mm) using a rod/servomotor system (QUICKSHAFT® LM1247-100-01, Faulhaber). A residence time of ∼0.5 s was selected to assess the extent of damage. These burnt fibers were subsequently analyzed by SEM (§5.2.2).

Loaded fiber bundles

Fig. 5.1 shows the arrangement used to expose tensile-loaded fiber bundles to the aforementioned flame conditions. Fiber bundles were subjected to a constant load using four dead weights, resulting in different tensile loads (3.35, 17.56, 75.22 and 128.07 N). At least ten tests were considered for each combination of fiber type, fuel/oxidizer ratio and tensile load. Two single-grove pulleys with internal bearing (#3213T52, McMaster-Carr) were installed 635 mm apart (center-to-center) (L) to yield a distance of 15 mm (d) from the FFB outlet to the fiber bundle. The vertical distance from the pulleys' center to the grips on the fixed and free-floating end were set at 200 and 300 mm, respectively.

5.3 Results & Discussion

5.3.1 Thermal behavior

Fig. 5.2 shows the outcome of simultaneous TGA and DSC runs, performed at different HURs for each fiber type. The two upper rows show the mass loss evolution (Figs. 5.2a-c) and normalized mass loss rate (Figs. 5.2d-e) obtained from TGA, respectively. The lower row (Figs. 5.2g-i) corresponds to the heat flow obtained via DSC. In general, higher HURs entailed higher oxidation onset temperatures and heat release over larger temperature ranges. However, some HURs yielded similar onset thresholds, depending on the fiber type. Two different trends can be observed. The first trend involves AS4 (Figs. 5.2a & d) and HM63 (Figs. 5.2c & f) fibers, which show two oxidation onset temperature thresholds each, i.e.,

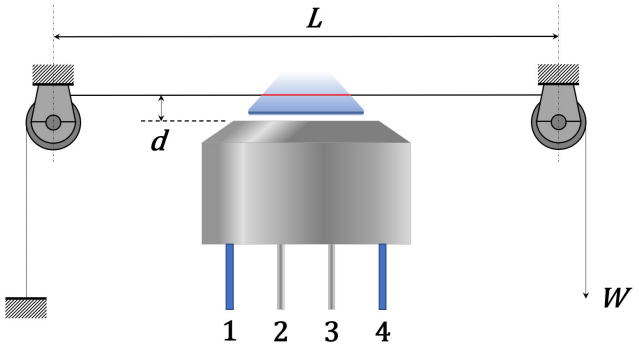

Figure 5.1 Simultaneous tensile loading and flame attack test setup: cooling water inlet (1) and outlet (4), fuel mixture (2), and shroud flow (3). L, d and W indicate distance between pulley center lines, height of the CF bundle with respect to the burner surface, and the dead weight, respectively.

the temperature ranges at which weight starts to decrease [381]. When heated at 5, 10 and 20 K min^{-1}, AS4 and HM63 fibers started losing mass at ∼850 K and ∼900 K, respectively. However, when heated at 25 K min^{-1}, the thresholds increased by ∼50 K. The second trend involves only IM7 fibers (Figs. 5.2b and e), which show three oxidation onset temperature thresholds at ∼780 K for 5 K min^{-1}, ∼850 K for 10 and 20 K min^{-1} and ∼900 K for 25 K min^{-1}. In all cases, fibers sharing the same onset temperature threshold show an additional trend: higher HURs caused lower maximum mass loss rates and substantially higher heat flows. For example, AS4 fibers heated at 5, 10 and 20 K min^{-1} started getting oxidized at ∼850 K. However, with increasing HUR, lower mass loss rates through a wider range of temperatures and higher heat release were observed, as indicated in Figs. 5.2d and 5.2g, respectively. These differences may be attributed to the competition between surface regression and the low thermal diffusion in the CF's radial direction.

The physical properties contained in Table 5.1 shed light on seemingly unexpected behaviors. For instance, higher tensile modulus values are indicative of higher crystallinity and hence less defects, suggesting an increased oxidative resistance. This is true when comparing HM63 fibers to their counterparts, although the same assumption may be misleading between IM7 and AS4. Based on their tensile modulus, the oxidation of the former was expected to take place at higher temperatures with respect to latter. However, IM7 fibers started oxidizing at slightly lower temperatures as seen in Figs. 5.2a and 5.2b. Again, the aforementioned assumption only holds if made on the basis of modulus alone. Now, considering other physical properties, Table 5.1 shows a smaller diameter than AS4 fibers' by 1.9 µm. A similar difference in oxidative behavior was reported when comparing IM7 and HTA40 (standard modulus, analogous to AS4) fibers [256], pointing at fiber diameter as a factor in the fiber oxidation

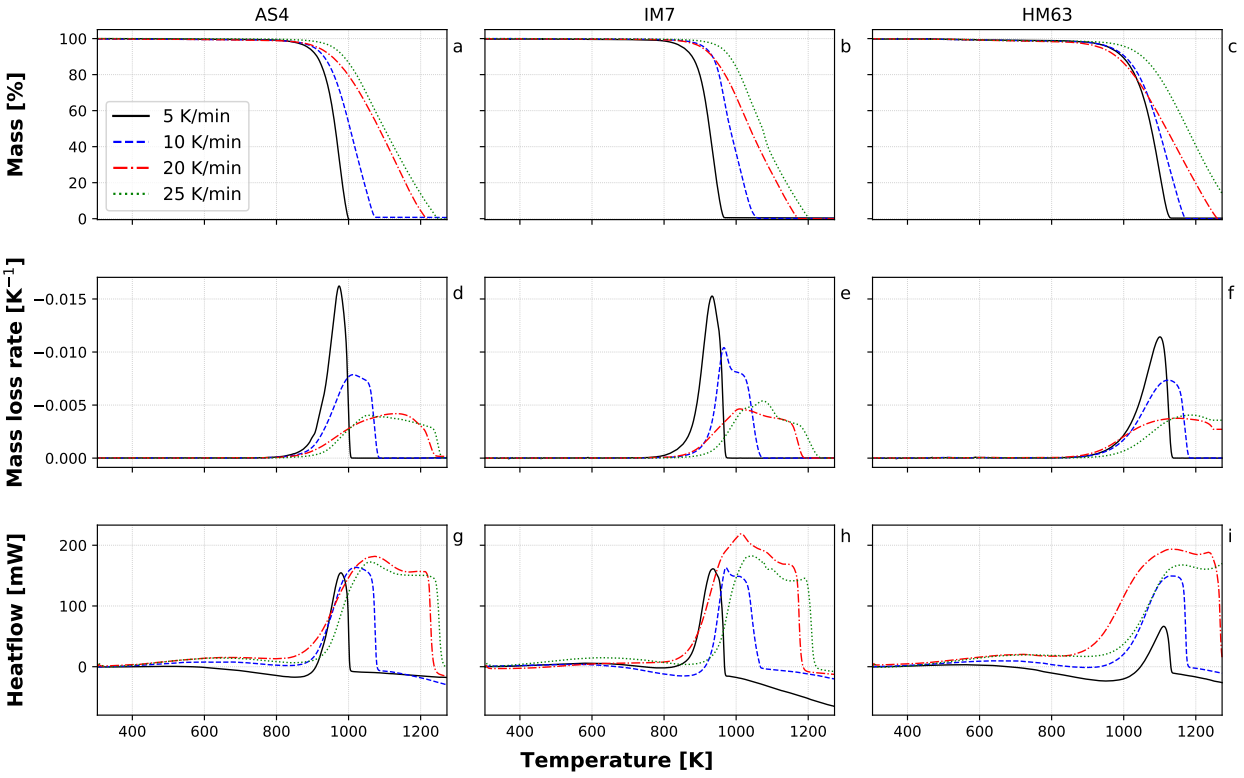

Figure 5.2 Non-isothermal TGA (top & middle) & DSC (bottom) curves for the three fiber types at different HURs. DSC positive heat values correspond to exothermic reactions.

rate. However, Jiang *et al.* [382] compared the oxidative behavior of graphite powders with different average particle size, and arrived to the same conclusion as other researchers that the oxidation is driven by the availability of active sites [227, 230]. As seen in Table 5.1, IM7 fibers have a higher tensile strength *vs.* HM63 and AS4, i.e., 17% and 27%, respectively. Since the amorphous phase drives the tensile strength in carbon fibers [198], this suggests a higher amorphous carbon content, and thus more active sites. Additionally, IM7 fibers may have lost additional N atoms due to desorption during intermediate HTT without reaching larger crystallite size as high modulus fibers. This in turn involves more active sites [274] and higher ASA values [230, 383], hence the onset of oxidation at lower temperatures.

Closer inspection of DSC results, i.e., Figs. 5.2g to 5.2i, reveals that higher HURs increase exothermicity and the complexity of the reaction scheme (the number of reactions). A common subtle endothermic trend can be seen for the three fibers at low temperatures and HURs, preceding the onset of highly-exothermic oxidation reactions and rapid weight loss. For the lowest HUR, i.e., $5\,\mathrm{K\,min^{-1}}$, a single peak can be observed on both mass loss rate (Figs. 5.2d-f) and heat flow (Figs. 5.2g-i) plots, which can be attributed to a single reaction. However, at higher HURs, multiple and competing reactions can take place [384]. This is also reflected in several peaks of mass loss, as observed in 5.2d to 5.2f. As previously mentioned, this behavior can be influenced by the fiber crystallinity and available active sites as well as the impurity concentration levels [230]. From Figs. 5.2f and 5.2i, it can be seen that HM63 fibers show the lowest mass loss rate as well as lower exothermic peaks, respectively. This behavior may be explained by higher graphitic order and less impurity-induced catalytic effects.

5.3.2 Morphology of burnt fibers

Fig. 5.3 shows the micrographs of AS4 (a), IM7 (b) and HM63 (c) CFs after insertion into the stoichiometric flame cone ($\phi = 1.0$) for $\sim$0.5 s. The three CF types show similar localized damage features, i.e., pits. Pitting can be traced back to structural defects and/or impurities [385]. The other two flames, i.e., fuel-lean ($\phi = 0.7$) and rich ($\phi = 1.2$), showed similar heterogeneous damage with no clear differences when compared to those obtained from the stoichiometric condition; they are therefore not shown. Fig. 5.3a shows two fibers, with the lower one featuring a central pit cluster with a $\sim$2.5 µm diameter, while medium-size individual pits ($\sim$0.7 µm) are found on both extremities. Multiple smaller ($\lesssim$0.3 µm) and apparently shallower pits are found along the fiber surface. The upper fiber shows less pronounced pitting signs. Similar damage mechanisms were observed on IM7 fibers, as shown in Fig. 5.3b. The central fiber shows a shallow large pit ($\sim$2 µm in diameter). To its left, three smaller oval pits (between $\sim$0.9 and $\sim$1.23 µm) with various depths that

started coalescing indicate different oxidation rate within this region. The rest of the fiber appears to be smooth, with scattered smaller pits (ranging from ∼0.3 to ∼0.6 µm in length. The fibers in the background appear to have less signs of pitting. Fig. 5.3c shows additional features in the central damaged area, with some bubble-shaped residues. The origins of these residues is unknown, although it is reasonable to attribute their origin to a combination of structural defect and impurities. From these micrographs, it can be deduced that pitting is a heterogenous process, with no apparent order or preference. It takes place upon exposure to the oxidizing species, even after a minimal exposure $t < 1\,\mathrm{s}$. Feih and Mouritz [224] showed that the strength of PAN-based CFs subjected to oxidative conditions is reduced by ∼40% as the critical flaw size increases from ∼25 nm in the virgin state, to ∼85 nm after exposures to 600 °C of 30 to 120 minutes. Thus, with larger defects such as the pits observed in Figs. 5.3a-c, a significant reduction on the fibers' load-bearing capabilities can be expected.

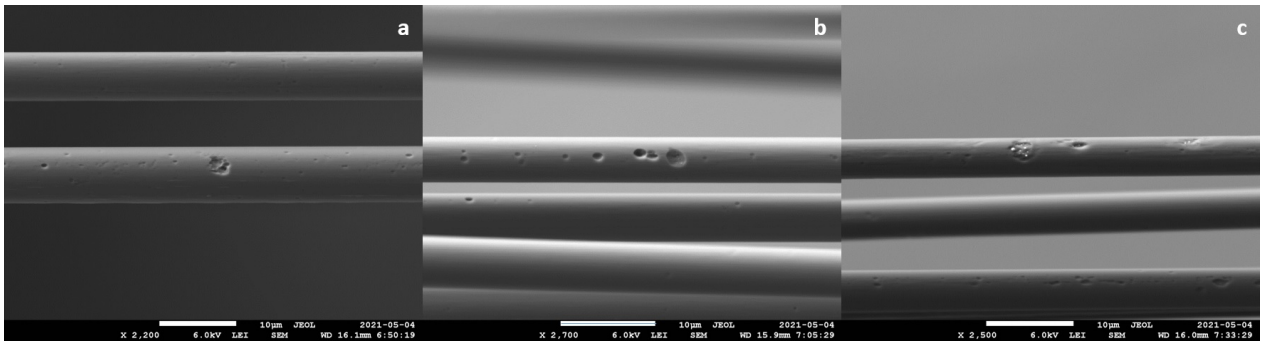

Figure 5.3 SEM micrographs of burnt AS4 (a), IM7 (b) and HM63 (c) fibers. Fibers were extracted from a bundle and inserted into the stoichiometric flame cone ($\phi = 1.0$) for $t \approx 0.5\,\mathrm{s}$.

5.3.3 Loaded fiber bundles under flame attack

Failure modes

Fig. 5.4 shows two load-independent fiber bundle failure mechanisms. First, the sequence comprising Figs. 5.4a1-a5 depicts the evolution of an IM7 bundle exposed to a stoichiometric flame, i.e., ϕ=1.0. As seen in Fig. 5.4a5, bundle failure was mainly observed at the flame cone periphery, with reduced fiber breakage in the middle section. This effect created notches on both sides of the bundle which coincided with the visible boundaries of the flame cone. This mechanism was observed on fibers exposed to stoichiometric and fuel-rich flames, where O_2 is virtually absent within the burnt gases region. Thus, the notching effect was initially attributed to O_2 diffusion from the surrounding atmosphere since no inert gas shroud was

used for flame shielding. However, the OH radicals present in the flame plume are known to be active oxidizers for carbonaceous materials in the absence of O_2 [208]. In this regard, premixed stoichiometric or rich CH_4/air flames similar to those used here were shown to yield high OH concentrations in the flame cone's periphery, with lower levels observed towards the center [386]. This spatial distribution of OH radicals would explain the preferential fiber breakage near the flame cone boundaries rather than the central part of the incandescent zone. This behavior is revisited in §5.3.3 where fiber failure promptness is addressed.

The second typical failure mode is shown in Fig. 5.4b, where discrete broken elements are visible. Fiber failure at random positions can be seen throughout the incandescent portion, without preferential damage location. All fiber bundles exposed to fuel-lean flames exhibited this behavior. In contrast to localized damage from oxygen-starved flames, fiber breakage at random locations was attributed to a uniform O_2 distribution within the flame cone. In both cases, fiber packing plays an important role in limiting the diffusion of oxidative species.

A typical orange glow was observed when AS4 and IM7 bundles were exposed to stoichiometric and fuel-rich flames. As shown in the sequence comprised by Figs. 5.4a1 through 5.4a5, the intensity of this incandescent effect increased towards the end of each test. Under the same flame conditions, HM63 fibers failed in a similar way, although the glowing effect was seldom observed or only faintly visible to the naked eye under low light conditions. Two different explanations were initially proposed for this phenomenon. First, it was assumed that these flames were sooty in nature. Sooty flames are typical of fuel-rich conditions, from the incomplete combustion of hydrocarbons [210]. Based on the observations made by Toth *et al.* [209] where fullerenes were created as part of the soot oxidation process, the radiative glow was assumed to be caused by similar unburnt carbon structures coming from the amorphous core of AS4 and IM7. Both fiber types contain a higher level of disordered carbon compared to their high modulus counterpart HM63. Thus, icospiral nucleation process [387] could be favoured. Such carbon-based structures have been observed in experiments where carbon was used as fuel and the C/O ratios were propitious [388]. A second complementary explanation was suggested considering small fiber fragments. These in turn were assumed to be the result of fiber breakage caused by oxidation-induced percolative fragmentation [219,389]. However, neither of these hypotheses explained the absent luminescence in HM63-based tests. Considering traditional sodium-based fiber surface treatments [34], a third and simpler avenue involved the presence of excited Na species, which typically produce a chemiluminescent effect with a yellow-orange flame front. Conversely, none of the fibers yielded this glowing effect when exposed to fuel-lean flames, suggesting complete sodium oxidation in addition to its catalytic effect .

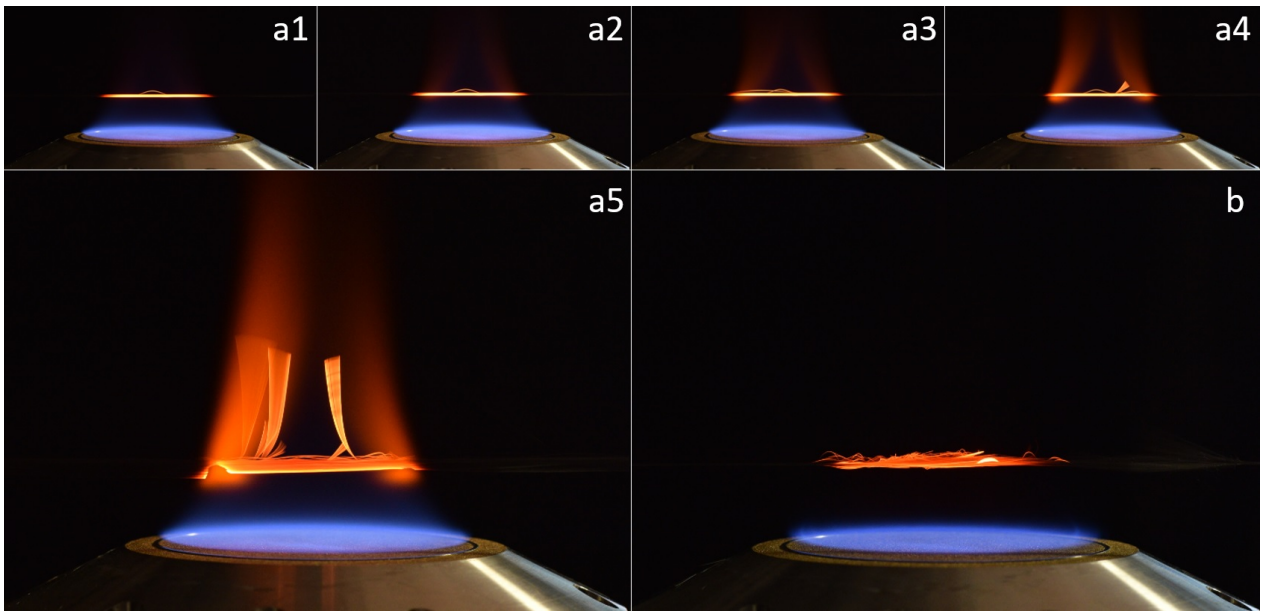

Figure 5.4 (a1-a5): Evolution of an IM7 bundle under tensile load, being attacked by a stoichiometric flame (ϕ=1.0). Fiber bundle failure is mainly localized at the boundary of the burnt-gases cone. (b): HM63 fiber bundle exposed to a fuel-lean flame (ϕ=0.7). Fiber failure took place randomly within the burnt gases cone.

Time-to-failure

Fig. 5.5 shows the evolution of the time-to-failure (TTF) (in s) for each fiber type and flame condition with respect to the initial tensile stress ratio σ/σ_{TDS} (%). The TTF is defined as the time taken by the fiber bundle to yield completely. The initial tensile stress ratio is defined as the ratio of the stress exerted by the dead weight on the whole bundle to the reported fiber strength. Its value is given only for reference since it considers an ideal loading case. The implications of this assumption are discussed further below. Average values for each load and flame configuration are shown with error bars indicating a 95% confidence interval (CI). Regression lines were obtained from all values for each flame condition, again with 95% CIs indicated by shaded areas. The horizontal axes are the same in the three plots, whereas the vertical axes do not show the same scale for clarity. AS4 and IM7 share the same timescale, whereas HM63 results are shown with a timescale one order of magnitude higher, with maximum TTF values in the order of ∼650, 400 and 6800 s for AS4, IM7 and HM63, respectively.

The relative flame aggressiveness was determined by the fiber bundle failure promptness. Each flame yielded a characteristic failure trend. In all cases, an increase of tensile load entailed a reduction of TTF. From the fit lines shown in Fig. 5.5, it can be seen that the

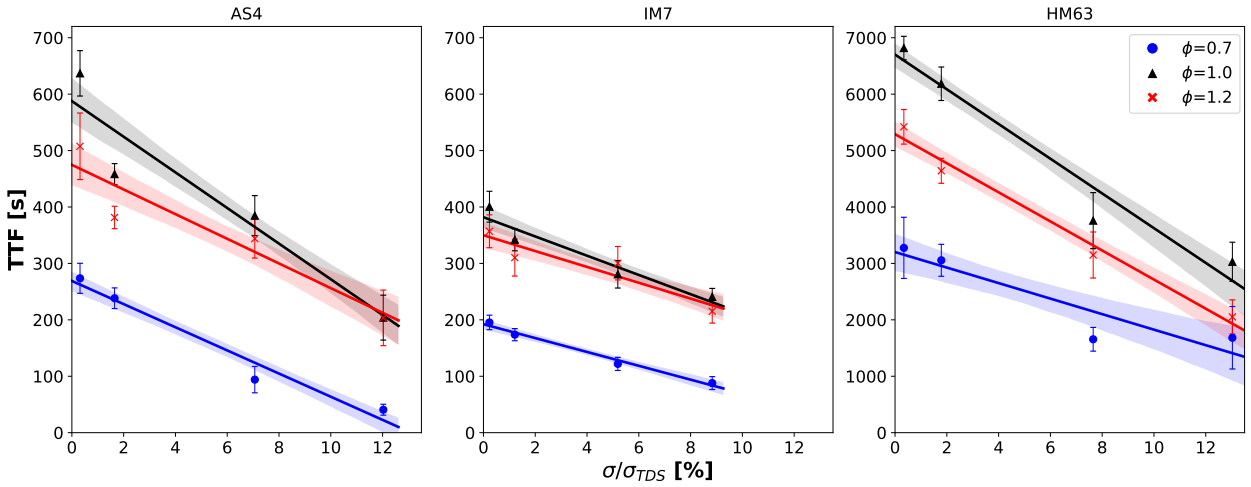

Figure 5.5 Time-to-failure (TTF) *vs.* initial applied stress ratio (σ/σ_{TDS}), considering the stress exerted by the dead weight divided by fiber strength (reported by manufacturer). Each point indicates the average ($n = 10$) for each combination of fiber type, fuel/oxidizer ratio and tensile load. Error bars show the 95% CI of each individual flame & stress ratio condition. The shaded areas of the regression lines show the 95% CI considering all values for each flame type.

stoichiometric flame ($\phi = 1.0$) yielded the longest TTF values in all cases. Thus, it can be considered as the least aggressive condition, despite the fact that it is the hottest flame. In second place, the fuel-rich flame ($\phi = 1.2$) shortened the TTF even in absence of O_2 in the burnt gases. Considering the averaged TTF values obtained at low stress levels, i.e., $\sigma/\sigma_{TDS} \lesssim 2\%$, the fuel-rich condition enhanced fiber oxidation, yielding $\sim 21\%$, $\sim 10\%$ and $\sim 23\%$ lower TTF values for AS4, IM7 and HM63, respectively. This accelerated failure becomes less significant as the load is increased, suggesting reduced influence from the flame chemistry at high mechanical loading conditions.

Notably, the fuel-lean flame ($\phi = 0.7$) reduces the TTF of all fiber types by at least $\sim 50\%$ when compared to the stoichiometric condition. Such marked difference between fuel-lean flames and its two counterparts are in agreement with previous weight loss tests performed on carbon fiber fabrics exposed to C_3H_8 open flames at $T = 1145\,\mathrm{K}$ with rich and lean conditions [10]. HM63 shows remarkable TTF values, which are one order of magnitude higher than those of AS4 and IM7. This behavior could be explained by higher crystalline order specific to high modulus fibers as discussed in §5.3.1. A more developed crystal structure in HM63 fibers is also translated into an increased thermal conductivity, which is one order-of-magnitude higher than in standard and intermediate modulus fibers. This in turn may contribute to lowering the fibers' temperature and, therefore, impact the reaction rate. Based on the

temperature of the reference flames, the extent of this cooling effect is however unknown. This effect was not investigated further here given that the oxidation is expected to be in the diffusion-controlled regime, where the reaction rate is less affected by the temperature. Since the bundle temperature is known to be significantly lower than the reference flame in question, its true temperature needs to be precisely measured in further studies to corroborate this hypothesis. Moreover, HM63 fibers may have lower impurity concentrations, as suggested by other thermal oxidative stability tests [216,218] where oxidation timescales have spanned over several orders-of-magnitude depending on fiber microstructure and varying impurity levels due to precursor nature and fabrication conditions.

To explain the faster failure induced by the fuel-rich flame with respect to the stoichiometric condition, let us consider the role of permanent and intermediate flame species. In absence of O_2, OH radicals are expected to have a dominating effect on carbon oxidation. However, the burnt gases region of fuel-rich CH_4/air flames has slightly lower OH concentrations compared to its stoichiometric counterpart [208, 257]. Therefore, other species must also contribute towards enhanced gasification. Based on the flame properties shown in Table 5.2, the CO_2 level decreases while CO and H_2 concentrations increase in fuel-rich flames *vs.* the stoichiometric condition. Consequently, additional surface- and gas-phase reactions are plausible. Panerai *et al.* [390] did not observe any contribution from CO impingement alone in CF oxidation. Nonetheless, considering the temperatures involved in this study, as CO reacts with O_2 in the upstream part of the reaction zone, CO_2 is formed and can enhance the $C + CO_2 \longrightarrow 2\,CO$ surface reaction [210]. Moreover, the higher H_2 level in the fuel-rich flame can lead to reactions with O_2 and H_2O, hinting again at the role of intermediate species, i.e., OH created within the hydrogen-oxygen system [210]. This explanation is in line with the notch failure mode discussed in §5.3.3.

Stable species such as O_2 and CO_2 preferentially attack different reactive sites in the crystalline structure. These sites are more easily found on the crystallite edges than on the basal plane, yet it is expected that high modulus fibers (HM63) will have less defects based on their higher treatment (carbonization) temperature. All experiments were conducted within the region of the flame reaction zone where radical recombination occurs. It is therefore expected that radicals affect the oxidation process, especially the OH radical which is known to play a role in soot oxidation [208].

5.4 Conclusions

This work addressed the CF bundle failure under flame attack, focusing on the effect of flame chemistry and tensile load. Traditional thermal analyses, i.e., TGA/DSC, and two fire-based

tests revealed the oxidative behavior under flame exposure of three PAN-based CFs with different microstructure. The TGA/DSC results showed that, for a given oxidizer flow, the oxidation onset temperature and reactions highly depend on the fiber microstructure and heating rate. Moreover, the fire-based tests relying on flat premixed methane/air flames provided a set of results that the thermoanalytical techniques cannot yield due to the nature of their controlled atmosphere. The first method revealed that localized damage, i.e., pitting, takes place promptly and heterogenously on the fiber surface upon exposure to flame reactive species. Even after short exposures ($t \approx 0.5\,\mathrm{s}$), nano- and micron-sized pits were observed on the fibers, regardless of the fiber microstructure. The second flame-based test showed that flame chemistry and mechanical loads closely correlate with fiber failure. On the basis of TTF values, stoichiometric flames yielded the least severe conditions despite being the hottest. Fuel-rich flames accelerated bundle failure, which was ascribed to the increased presence of OH radicals. This effect was more evident in high modulus fibers. Higher tensile loads seem to reduce this difference. Further studies need to address the effect of different CO/CO_2 levels and true bundle temperature on the failure process. Fuel-lean flames were found to be extremely aggressive, shortening the TTF of CF bundles by at least $\sim 50\%$ *vs.* the stoichiometric condition. Moreover, we found a striking one order-of-magnitude difference in TTF between the high modulus and the other two types of CF. This could not have been inferred from TGA/DSC results nor from fiber physical properties. It is therefore essential to perform fire resistance tests under conditions as close as possible to those encountered in fire hazards expected in the final application. Future studies also need to address the effect of impurities which, alongside microstructure, could be defining factors in structural soundness of CF-based structures.

Acknowledgments

The authors want to acknowledge the financial support from the Natural Sciences and Engineering Research Council of Canada (NSERC/CRSNG) grant no. RGPIN-06410-2016 (NSERC Discovery). Pablo Chávez-Gómez is extremely grateful to the National Science and Technology Council of Mexico (CONACYT) for his doctoral scholarship. The authors also thank Dr. Martin Luckabauer for his valuable feedback, as well as Max Thouin and Eddie Rubey from Hexcel Corp. for supplying some of the samples used in the study.

CHAPTER 6 ARTICLE 3: Carbon fiber damage evolution under flame attack and the role of impurities

Published in *Fire and Materials* on June 29, 2022 [289].

By
Pablo Chávez-Gómez, Tanja Pelzmann, Darren R. Hall, Cornelian Chilian, Louis Laberge Lebel, Étienne Robert

ABSTRACT

CFs are prone to extensive oxidation under fire attack, for instance, in an aircraft fire scenario. This work addresses the damage mechanisms observed on PAN-based CFs with different microstructure exposed to open flames. A fixed-point technique was developed to follow up individual CFs by means of time-controlled insertion into premixed methane/air flames, followed by SEM and EDS analyses. Besides diameter reduction, three localized damage mechanisms were discerned in presence of impurities, which were quantified by NAA. Severe pitting was ascribed to catalytic oxidation mainly caused by alkali and alkaline earth metals. After an initial period where catalytic reactions between impurities and the carbon surface dominate, the flame stoichiometry governed the CF gasification process, with lean flames being much more aggressive than rich ones. A second mechanism, channelling, was caused by mobile metallic impurities. Some impurities showed an opposite effect, lowering reactivity and thus preventing further catalysis. Amorphous damage with a skin-peeling effect is believed to be the result of localized impurities at high concentrations and microstructural variations. Hindrance or synergistic effects between impurities are discussed. Finally, apparent axial pit growth rates were determined and compared with other carbonaceous materials, revealing a strong influence of impurities and the flame reactive atmosphere on CF oxidation.

6.1 Introduction

In-flight or post-crash aircraft fires pose a threat to passenger safety, either from a smoke and toxicity standpoint, or repercussions on the vehicle structural integrity [56]. This translates into challenging design constraints for modern aircraft, since they extensively rely on inherently-flammable CFRP composites [6]. The intricate thermal, physical and chemical

processes involved in CFRP combustion [221, 384] make the fate of CFs exposed to fire difficult to predict. Moreover, desirable outcomes are sometimes conflicting. On one hand, full gasification might be sought [12, 13] to avoid the release of CF fragments from burning composites, resulting in health and electrical hazards [11, 391, 392]. On the other hand, oxidative resistance is required to prevent burn-through if the component is structural or serves as a firewall [56]. However, the conditions under which this resistance is assessed varies, with samples typically exposed to the atmospheres created by non-premixed or partially premixed turbulent flames.

CFs readily gasify at high temperatures when exposed to reactive or oxidizing environments. Like any other carbonaceous material [215], the fiber reactivity is mainly driven by its ASA [187, 230], which is defined by structural order and available functional groups [195]. CF oxidation takes place through preferential etching starting at defects (e.g. vacancies, Stone-Wales type, interstitials, adatoms [194]) and crystal edges (armchair & zigzag) [187, 229, 260, 261, 272]. Such features mainly arise during the fiber manufacturing process [34, 184]. The heterogeneous CF microstructure involving turbostratic and amorphous regions [34, 190, 192, 193, 393] results in intricate oxidation processes [394]. Moreover, fibers from the same precursor, e.g. PAN, have different structures depending on the HTT. High strength/low modulus CFs show a core-sheath structure with small crystallites in the skin zone and regions of amorphous carbon in the core [192], while high modulus CFs have a less disordered structure [193] as aresult of higher HTT.

Fiber gasification is influenced by several factors, namely the composition of the atmosphere, temperature and pressure [195, 203, 230, 232, 252, 288]. For instance, with molecular oxygen (O_2), oxidation takes place by O_2 chemisorption and subsequent carbon monoxide and dioxide (CO/CO_2) desorption. Other mechanisms can come into play in the absence of O_2, such as the Boudouard reaction in the presence of CO_2 [215]. These mechanisms enlarge pores, create more active sites and new defects thus increasing the ASA, enhancing the oxidation process and degrading the CF mechanical properties [223–225, 254, 395], with analogous processes observed with other carbonaceous materials [396]. These phenomena can be accelerated by the presence of impurities in the carbon structure, which act locally or with a certain mobility [240, 265, 266, 397]. As with other carbonaceous materials, alkali and alkaline earth metals, along with their carbonate and acetate compounds, are known to catalyze the CF oxidation process [12, 13, 202, 216–218, 230]. Other elements can mitigate catalytic effects, for instance boron doping results in active site blockage and crystallite size increase [245, 398], while some halogens, sulphur (S) and phosphorus (P) can poison impurities with catalytic effects [243, 246].

CF gasification invariably leads to diameter reduction [224, 251] and internal porosity may develop in a process analogous to carbon activation, i.e., controlled pore and ASA enlargement [219,275]. However, locally accelerated oxidation may take place in the presence of impurities and large structural defects. This process, known as pitting, has been reported on CFs under liquid or gaseous oxidative conditions, such as electrolyte [264] and acid treatments [263, 399], TGA [203, 225, 230, 400–402], plasma etching [190, 399], as well as using tube furnaces [225, 239], flow tube reactors [390, 403], air-filled ovens [223, 230], environmental electron microscopes [287] and other heated processing systems [395]. Under open flame attack, exacerbated pitting was observed on CF bundles after exposures of a few minutes to CH_4-based flames [368]. Pitting has also been observed on C/C composites after exposure to oxyacetylene flames [278] as well as on burnt CFRP composites. In flammability tests where samples are exposed to a radiative heat source, matrix decomposition and flaming combustion can expose CFs to the reactive atmosphere [256]. Samples have also been directly exposed to fuel pool fires to simulate post-crash flame conditions and investigate health hazards from CF fragments released following oxidation-induced diameter reduction, pitting, and fibrillation [10,11]. However, the vast majority of the aforementioned studies were performed in environments that do not represent the conditions encountered in aircraft fire scenarios where continuous open flame attack is a threat. This is the case of post-crash conditions involving CFRP-based fuselage skins or in-flight fires involving, for instance, powerplant firewalls or cargo liners. For certification purposes, standardized intermediate-scale tests [53, 72, 84] are necessary to determine, among other attributes, the burn-through resistance of the aforementioned structures. In such standardized tests, temperature, heat flux and fuel type are controlled, although little attention is given to flame chemistry. However, a previous work [288] showed that, in addition to the mechanical loads, CF failure is highly influenced by the flame stoichiometry. Thus, it is necessary to revisit the fire-induced carbon fiber damage processes.

Studies involving CF exposure to controlled flame conditions are limited, specifically with regards to the characterization of the reactive atmosphere and the systematic investigations of CF pitting. However, results obtained with other carbonaceous materials [240] can shed light on this phenomenon. For instance, pitting and impurity-induced channelling have been widely studied in graphite model materials, such as natural graphite [267,268,397] and HOPG [260, 261, 270–272, 280–282, 286, 404, 405], as well as in CNTs [285] and graphene [406]). The effect of the gaseous atmosphere composition on pitting has been assessed for air [260, 261, 272], pure oxygen (O_2) and mixtures [260, 267, 268, 271, 280, 404], hydrogen H_2 [271, 407], and in presence of transient or atomic species (e.g. oxygen $O(^3P)$ [270, 405, 408], nitrogen (N) and hydrogen (H) [409]), revealing characteristic behaviors influenced by each material

and testing condition. In these studies, *in situ* or *post hoc* observations have allowed the determination of pit growth rates. Numerical models dedicated to CF pitting are being developed based on pit growth rates found in highly oxidative environments, for instance, in simulated atmospheric re-entry conditions [273]. Again, fire-induced oxidation and the role played by microstructure or impurities in pitting have not been investigated, and direct comparison between materials is not yet possible. This demonstrates the need for dedicated CF pitting analyses, especially in aggressive and fire-representative environments.

In view of these challenges, we investigated the fire-induced damage mechanisms of PAN-based CFs, focusing on surface pitting and its growth rate. Other effects such as channelling, porosity development and amorphous erosion were also addressed. Considering three commercial CFs, we closely followed up these features after successive CF insertions into premixed laminar methane (CH_4)/air flames. Using a scanning electron microscopy (SEM)-based fixed-point technique, apparent pit growth rates were determined for standard and intermediate modulus CFs. NAA and energy dispersive X-ray spectroscopy (EDS) were used to quantify and localize the presence of impurities. The pit growth values measured were then directly compared with values available in the literature for controlled conditions, i.e., atmosphere and graphite models.

6.2 Experimental

6.2.1 Materials

Three commercial PAN-based CFs (Hextow®, Hexcel) with different properties have been selected: AS4 [377], IM7 [378] and HM63 [379], which correspond to standard, intermediate, and high modulus, respectively. The fiber bundles were taken from the same spools used in a previous work [288], enabling direct comparison with other flame exposure results.

6.2.2 Fiber characterization

Qualitative morphology analyses were carried out via scanning electron microscopy (SEM) on both virgin and burnt CFs using a high resolution field emission microscope (JSM7600F, JEOL). Acceleration voltage and current were set at 6 kV and 226.4 µA, respectively. Impurities on the surface of fibers, along with O, N and C levels, were assessed with a built-in energy dispersive X-ray spectroscopy (EDS) detector (X-Max^N, Oxford Instruments) using an energy range of 10 keV. Measurements of fiber features were performed using the Fiji/ImageJ software [410].

The presence of potential oxidation catalysts was quantified through neutron activation analysis (NAA) using a Safe LOW-POwer Kritical Experiment (SLOWPOKE-2) nuclear reactor located at Polytechnique Montréal [411]. The specific details related to this method are described in detail elsewhere [412]. Two different samples for each type of CF bundle were cut to a length of 2.6 m and irradiated using a neutron flux of $5 \times 10^{11}\,\mathrm{cm^{-2}\,s^{-1}}$. One CF sample was dedicated to short-lived radioisotopes, irradiated for 10 min and counted upon a 6 min decay. The second sample was intended for medium- and long-lived radioisotopes, irradiated for 135 min, and a count was performed after 4- and 10-day decays, respectively.

6.2.3 Controlled insertion

A fixed-point method was conceived, inspired by the *post-hoc* observations of oven-based CNTs oxidation by Morishita *et al.* [283–285]. This allowed SEM/EDS analyses to be carried out with the same sample holder used to burn the CFs. A FFB (standard model, Holthuis & Associates) comprising a stainless steel body and a water-cooled bronze plate was used to obtain premixed fuel-lean, stoechiometric and rich CH_4/air flames, respectively with fuel-to-oxidizer equivalence ratios $\phi = \{0.7, 1.0, 1.2\}$ and $T \approx 1706$, 1790 and 1723 K. The flame properties, i.e., temperature and species concentrations, details on the FFB configuration and gas measurements are described elsewhere [288, 380]. Although flames found in real or simulated aircraft fires are typically turbulent and non-premixed, the use of this burner allowed to control the flame stoichiometry with minimal influence of other factors such as flame speed and turbulence, reducing fiber breakage and thus enabling the close follow-up of individual damage features. Fig. 6.1 shows the custom horseshoe-shaped aluminum 6061 sample holder designed to hold fiber samples during flame exposure and subsequent SEM observations. Its inner contour was defined by the FFB's bronze outlet (OD = 73.5 mm, plus 1.75 mm clearance). The external contour allows self-aligned installation in the SEM sample holder (SM-71090, JEOL). The horseshoe was fixed using 8 mm double-sided conductive carbon tape (No. 5028581, Fisher Scientific). To guide the fibers, AISI 304 stainless steel (SS) tubes (OD = 1.2 mm, ID = 1.0 mm, Unimed) were cut to a length of 40 mm and bonded onto the horseshoe using an ethyl cyanoacrylate glue (Super Glue Gel Control®, LePage) and carbon-taped to ensure electrical conductivity. Four pairs of tubes were installed 8.5 mm from each other. The outermost pair of tubes was not used, and only served as visual reference. For fiber installation, a small CF bundle was extracted from the spool and guided through a pair of aligned steel tubes with a Chromel wire, as shown in Fig. 6.1c, using a needle threading-like technique. The bundles were fixed with the same carbon tape, followed by sequential cutting and removal from the central opening to decrease the amount of fibers that would be exposed to the flame.

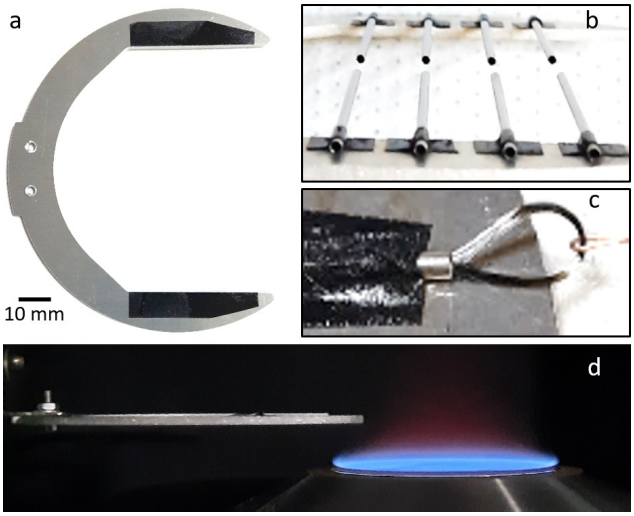

Figure 6.1 Top view of sample holder with carbon tape (a), stainless steel tubes (b), CF bundle threading method (c), and side view (d) of the insertion method into the flame.

Fibers were intermittently exposed to the flame 15 mm above the burner's porous surface. To maximize the accuracy of exposure time and height as well as to minimize the displacement time, the fibers were translated in and out the flame using a brushless DC-servomotor and a 100 mm stroke rod (QUICKSHAFT® LM1247-100-01, Faulhaber). The motion controller (MCLM 3006, Faulhaber) was set to yield the actuator's maximum speed, i.e., $\sim 3\,\mathrm{m\,s^{-1}}$. The insertion time and the speed were verified using a high speed camera (FASTCAM Mini AX200, Photron) recording at 10,000 fps. Based on the sample holder tip position, the travel time (from start to stop) was estimated at $\sim$100 ms. The reported flame exposure values correspond to static residence time only.

6.3 Results & Discussion

6.3.1 Virgin fibers

Morphology

Fig. 6.2 shows SEM images of the three different virgin fibers. Homogeneous surfaces with no bumps nor pits and constant diameters are prevalent. However, some features such as light striations running lengthwise can be seen on the unsized fibers (AS4 and IM7). Additional sub-micron features are observed on some of the AS4 and HM63 fibers. In both cases, they seem to be either particles fused with the fiber or foreign grain-like items, in the case of HM63 fibers. Moreover, some oval-shape bulges can be observed on the surface of some AS4 fibers.

Several points were scanned along ∼25 µm of the fiber surface with EDS and no significant elementary differences were observed when compared to smoother portions. This suggests the presence of buried impurities or surface defects with uniform chemical composition. EDS measurements and elemental analysis are discussed below in §6.3.1 and §6.3.1, respectively.

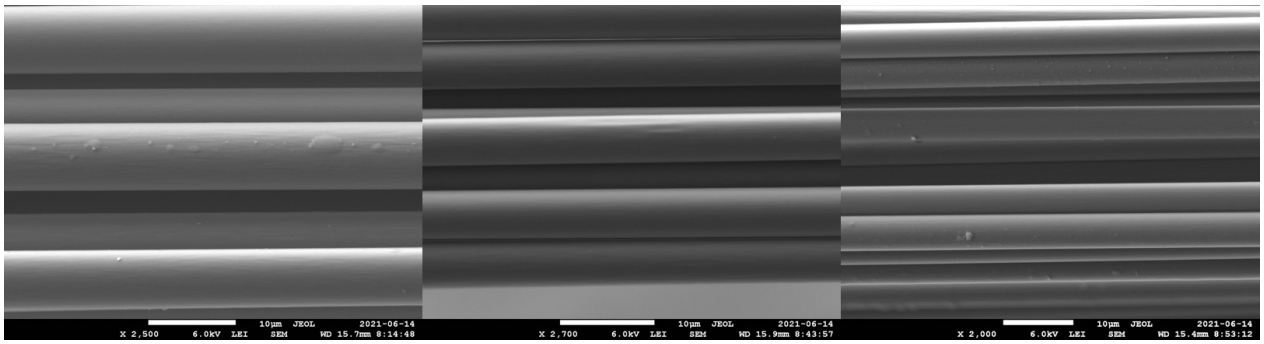

Figure 6.2 SEM images of virgin AS4, IM7 and HM63 fibers (left, center & right, respectively) as extracted from the fiber spool.

Surface composition

Fig. 6.3 shows the EDS spectrum for each virgin fiber surface in a semi-log plot. The y-axis has been transformed to allow the identification of weak signals caused by minuscule impurities. Otherwise, in a linear scale, they are typically indiscernible in comparison with the dominating signatures of C, N and O. The main peak describing the carbon content at 0.277 keV is self-evident. With respect to heteroatoms, i.e., O and N, two different situations are observed. The first involves AS4 (Fig. 6.3a) and IM7 (Fig. 6.3b) fibers, where O and N peaks are second and third in prominence at 0.525 and 0.392 keV, respectively. Their presence is expected in PAN-based CFs, since N atoms can be traced back to the precursor chains, whereas O atoms are attributed to the stabilization step. Several surface functional groups are possible in the presence of N and O atoms [195] within the basal planes or bound to the graphene layers' edges, providing sites with increased oxidative potential [196]. Moreover, sodium (Na) and silicon (Si) impurities can be discerned from smaller peaks at 1.041 and 1.739 keV, respectively. The presence of Na already suggests catalyzed oxidation upon exposure to flames, whereas Si is not expected to react adversely with the fiber structure and actually has a deactivating effect on alkali and alkaline earth impurities [242]. Their concentration levels are discussed in detail at §6.3.1. HM63 fibers show a contrasting composition in Fig. 6.3c, since the N, Na and Si peaks are absent, as opposed to AS4 or IM7 fibers. This might be explained by the higher HTTs that high modulus PAN-based CFs undergo at

the graphitization step, which helps to volatilize impurities and remove N atoms from the original PAN structure.

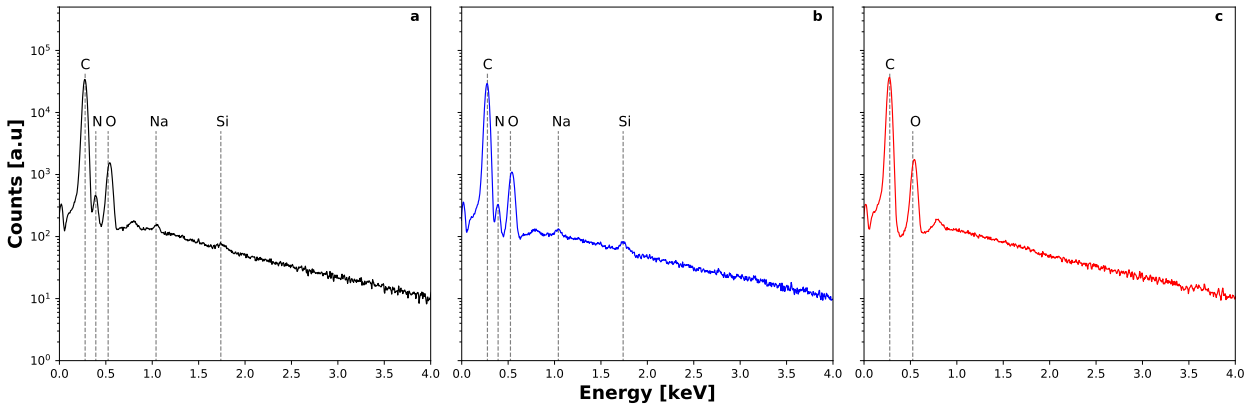

Figure 6.3 EDS spectra of virgin AS4, IM7 and HM63 fibers (from left to right). All confirmed peaks correspond to the K_α values. The plots are shown in an unconventional semi-log scale for clarity of peaks above ~1.0 keV.

Impurity analysis

Fig. 6.4 shows the concentration of impurity elements (in ppm) detected via NAA for the three fiber types. Only elements with well defined gamma-ray peaks are shown, namely Na, calcium (Ca), aluminum (Al), chlorine (Cl), magnesium (Mg), iodine (I), bromine (Br), manganese (Mn) and antimony (Sb). The detection limits were not the same for all elements in all fibers, with certain species detected in only one or two fibers. Such is the case for AS4 and IM7 fibers, which yielded a quantifiable mercury Hg content. Conversely, HM63 yielded titanium (Ti), vanadium (V), and copper (Cu) atoms. The latter is noteworthy since some particles were visualized by SEM and confirmed by EDS to contain Cu. This is further discussed in §6.3.2. The full NAA data can be found in the supplementary material (see Annex A).

First, we address impurities that have a known catalytic effect. As an alkali metal, Na is recognized as a very effective carbon oxidation promoter [12,216–218,230,238]. In our tests, it was found to be the most abundant impurity in AS4 and IM7 fibers at 1024±41 and 1079±43 ppm, respectively. In contrast, HM63 yielded a much lower concentration, 11.9±0.5 ppm. In addition to a higher crystallinity, such reduction by two orders of magnitude is believed to be a critical factor in HM63's increased oxidative resistance, as shown in tests under flame and mechanical load [288]. The root causes of such marked differences in Na concentration can be traced back to the processing steps of PAN-based CFs, where the precursor can be

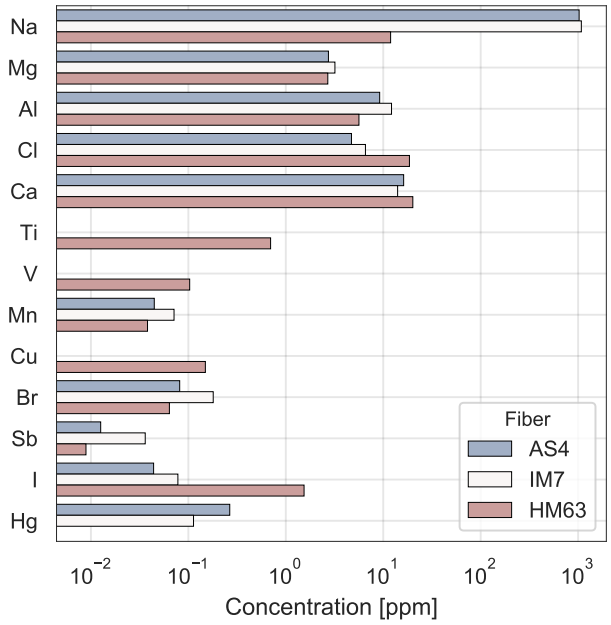

Figure 6.4 Impurity concentrations obtained via NAA from standard (AS4), intermediate (IM7) and high modulus (HM63) fibers. Only fully confirmed elements are shown.

dissolved using sodium thiocyanate (NaSCN) in the polymerization step [184]. Subsequently, it remains within the carbon structure through the oxidative stabilization and carbonization steps. Further graphitization helps to vaporize internal impurities [216, 236], hence the lower Na concentration in HM63 fibers. Additional Na-based impurities may come from anodic oxidation which aim at improving fiber/matrix adhesion. This can be achieved with diverse electrolytes, namely sodium chloride (NaCl) and sodium hypochlorite (NaOCl) [34]. These in turn can also explain the presence of Cl, which is discussed below. Overall, Na levels are in good agreement with those found in the literature for PAN-based CFs [202,216,218,230]. The presence of other alkalis could not be precisely determined. With regard to the confirmed alkaline earth metals, i.e., Ca and Mg, both elements are known to be effective catalysts. Different catalytic effects have been reported with related acetates and carbonates [12]. Their concentration levels are very similar in the three fiber types. Ca concentrations were found at 16.2±2.2, 14.1±2.6. and 20.1±1.3 ppm, whereas Mg yielded 2.74±0.75, 3.19±0.74 and 2.70±0.24 ppm for AS4, IM7 and HM63, respectively. Their effect is expected to be more pronounced in standard (AS4) and intermediate (IM7) CFs. These fibers have a higher amorphous carbon content and a more pronounced turbostratic structure than their high modulus (HM63) counterpart [288], hence increased reactivity due to a higher number of active sites.

Conversely, some impurities may not have a catalytic effect and instead support catalyst deactivation, commonly referred to as poisoning. This has been observed with some halogens, e.g. Cl [187], which can be chemisorbed on active sites and prevent further C-O_2 reactions [215]. The origin of Cl-based species can be traced back to the electrolyte used for anodic oxidation, closely related to Na as mentioned earlier. In our case, HM63 yielded a higher Cl concentration of 18.6±0.8 ppm *vs.* 4.72±0.34 and 6.57±0.42 ppm for AS4 and IM7, respectively. A possible explanation for this difference is that high modulus fibers need higher treatment currents [34], which may enhance Cl adsorption. The presence of two more halogens was confirmed in the three fibers, with Br & I concentrations of 0.0815±0.0166 & 0.0440±0.0056, 0.180±0.019 & 0.0781±0.0072 and 0.064±0.005 & 1.54±0.06 ppm for AS4, IM7 and HM63 fibers, respectively.

Other species were confirmed at very low levels. Mn & Sb impurities were detected in the three fibers, i.e., AS4, IM7 and HM63 (0.0447±0.0029 & 0.0126±0.0019, 0.0713±0.0200 & 0.0361±0.0023 and 0.0381±0.0040 & 0.0089±0.00088 ppm, respectively). Other elements where only confirmed in either HM63 (Ti at 0.698±0.107 ppm, V at 0.103±0.004 ppm and Cu at 0.150±0.039 ppm) or AS4 & IM7 fibers (Hg at 0.266±0.055 and 0.113±0.057 ppm, respectively). From these elements, Ti and V have been reported to accelerate CF combustion [413], following a similar approach as in other works aiming at preventing fiber fragment release [11–13]. From this last group of impurities, the only element that was visually confirmed was Cu. Micron-sized Cu-based particles were observed via SEM and their characteristic effects are discussed in §6.3.2. We cannot explain the origin of Cu, Hg and Sb impurities detected due to the proprietary nature of CF manufacturing process. Nonetheless, further analyses could focus on the synergistic effects that the aforementioned impurities may have [240].

Overall, it is possible that the one-order-of-magnitude difference in TTF reported between AS4/IM7 and HM63 in our previous analysis [288] may be the result of the latter's lower impurity levels in addition to higher crystallinity and less functional sites (as suggested by the reported modulus and thermal conductivity values [379]). However, since the nature of impurities and their compounds is not precisely known, this hypothesis needs to be tested in future studies.

6.3.2 Burnt fibers – controlled insertion

Damage morphology

Fig. 6.5 shows three different CF pit group arrangements representative of our SEM observations following insertion into flames. These damage morphologies have an oval shape and are typically created by the attack of defects on the basal planes and edge sites of graphite [260, 269, 270]. In our tests, pits were attributed to the presence of buried defects as well as highly reactive species and impurities such as alkali and alkaline earth metals. These impurities can adsorb O_2 dissociatively and readily create oxides, showing strong interaction with the graphene defects and layer edges, usually spreading and having an edge-recession effect [240, 265]. Fig. 6.5a shows the results of several pits that coalesced and, due to their proximity, yielded a larger pit. The residues appearing white in SEM images correspond to Ca-based compounds that initially promoted catalyzed gasification and but then react with Al, and Si to form stable compounds with weak catalytic activity, as confirmed by EDS. In-depth discussion pertaining to the chemical analysis of burnt fibers is presented in §6.3.2. The second type of pit arrangement is shown in Fig. 6.5b as a pit chain which extends on both sides of the field of view. It seems reasonable to attribute this highly-aligned pit formation to the precursor spinning phase. Finally, Fig. 6.5c shows a cluster of randomly-placed pits which, as opposed to the aforementioned chain arrangement, could be attributed to post-carbonization surface treatment. In this case, impurities may have remained at random locations on the surface upon electrolyte drying.

A second damage mechanism is channelling, as depicted in Fig. 6.6a, which shows a channel created by a copper-based macroparticle (confirmed by EDS). Channels are the result of mobile metallic impurities, which adsorb oxygen in a non-dissociative manner. These in turn react with the carbon surface without creating stable oxides [240, 265, 414] and usually gasify the carbon surface laterally, a pattern commonly described in other carbonaceous materials as worm-like. The trailing path seen in Fig. 6.6a shows the high mobility of these impurities, promoting fiber gasification without getting fully oxidized nor deactivated and thus generating extended superficial erosion. In our tests, these mobile impurities likely reach and exceed the T_{Ta} [240, 266], which is typically described as half of the metal or metal compound's T_m. The T_{Ta} has been interpreted as the temperature where the impurities appear to merge with the carbonaceous surface in a "sintering-like" manner [240] without melting, thus ensuring active contact and promoting carbon desorption, bulk diffusion towards the oxidant and final gasification. The contaminant particles detected are therefore likely active catalyzers as the flame temperatures encountered are well above the T_{Ta} of relevant impurities such as Cu-based oxides CuO and Cu_2O ($T_{Ta} \approx 799$ and 752 K, respectively) or Ca-based carbonate

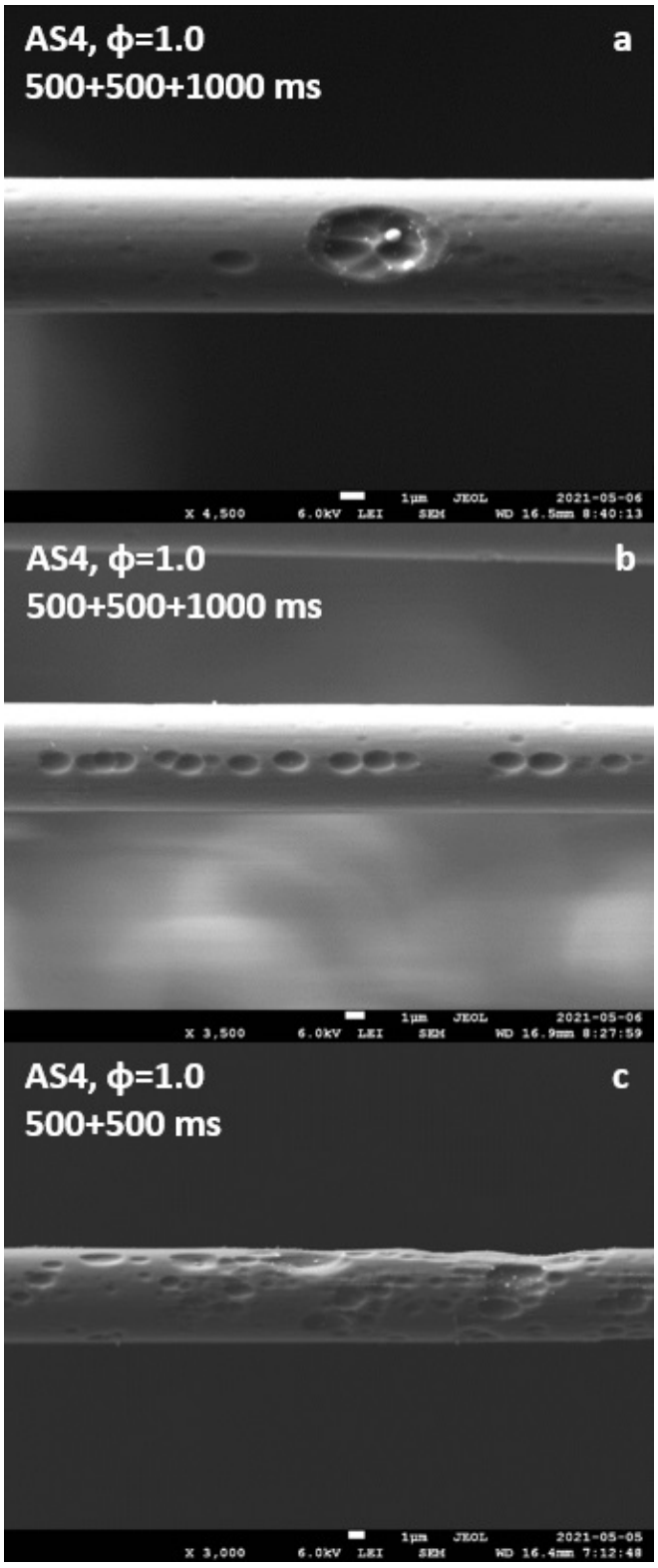

Figure 6.5 Different types of pits observed on AS4 fibers after exposure to stoechiometric flames ($\phi = 1.0$): a) localized damage, b) chain of individual pits and c) random arrangement.

($CaCO_3$) ($T_{Ta} \approx 549$ or 806 K) and highly-reactive oxide (CaO) ($T_{Ta} \approx 1422$ K) [200,414,415].

The third type of damage observed upon flame attack is amorphous etching. Figs. 6.6b and 6.6c show HM63 fibers with localized thinning, yielding an hourglass-like shape. This effect is most likely induced by the Cu-based impurities next to the damaged areas, as confirmed by EDS. Iacocca and Duquette [239] previously analyzed the catalyzed oxidation of high modulus PAN-based CFs in presence of platinum (Pt) in their sample holder. They reported distinct damage mechanisms, namely beaded fiber portions due to uneven thinning as well as fiber splitting, both attributed to changes in fiber morphology. Based on their results and the proximity of Cu-based impurities, we attribute this localized thinning to either microstructural changes within the fiber, concentrated impurities, or a combination thereof. Regarding the origin of such Cu-based impurities, their size and the associated low Cu levels confirmed via NAA do not allow the determination of a clear origin. The same rationale applies to Ti and V impurities confirmed in HM63 fibers (§6.3.1), although not discernible upon combined SEM/EDS analyses. Given that HM63 was the only sized fiber, it is possible that these elements were part of the sizing compound.

Fig. 6.7 shows an HM63 fiber heavily damaged with several residues throughout the affected area, depicting the outcome of catalytic oxidation and poisoning. Amorphous damage spanning ~ 20 µm can be observed where large portions of fiber skin, core or both were etched yielding an heterogeneous central portion, resulting in a similar "hourglass" effect as in Figs. 6.6b and 6.6c. The red rectangle indicates a region probed with EDS and its spectrum is shown in Fig. 6.9c, confirming the presence of Ca, Mg, Si, Al and P species. This damage pattern is most likely caused by the concentrated presence of impurities that results in initial violent localized reaction, followed by deactivation and conversion to more stable and less catalytically active species. The residues visible as white specks in Fig. 6.7 are therefore a mixture of P-based compounds, which are known for inhibiting catalytic reactions [246], Ca- & Mg-based carbonates and/or oxides, well known carbon catalysts [240], along with more stable species such as aluminosilicates. The EDS spectra of the largest flake, provided as supplementary material, and of the residues observed on the AS4 fiber, shown in Fig. 6.9a, show similar elemental signatures and support this hypothesis.

If no external force is exerted, fiber rupture can be caused by small mechanical loads induced by the flame itself, fiber diameter reduction or pore/pit growth and subsequent coalescence. Fig. 6.8a shows an IM7 fiber which failed after only 500 ms of stoichiometric flame exposure due to collaborative pit growth. Despite the quiescent nature of the flame, the flow exerted a small yet sufficient force to bend the fiber, causing fracture. Much slower and more homogeneous diameter reduction was also observed for the same fiber, as shown in Fig. 6.8b,

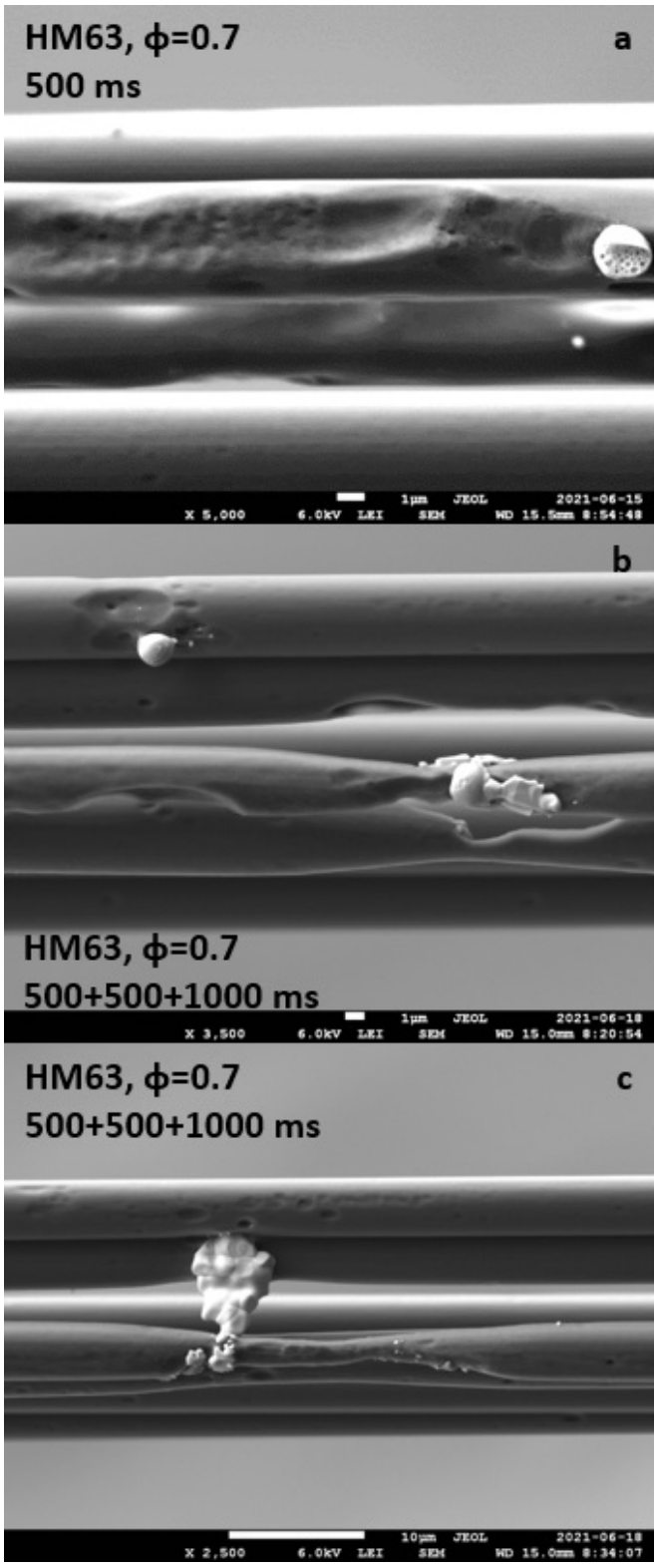

Figure 6.6 HM63 fibers with mobile Cu-based impurities causing channelling (a) and amorphous erosion (b and c).

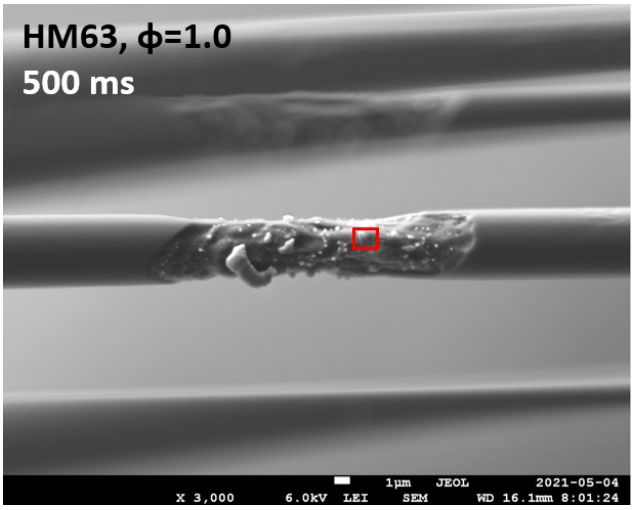

Figure 6.7 HM63 fiber after 500 ms of $\phi = 1.0$ flame exposure. See EDS spectrum in Fig. 6.9c.

despite being exposed for a longer period (2000 ms) to a fuel-lean flame ($\phi = 0.7$) with a more aggressive oxidizing atmosphere. The EDS spectrum of this slowly degrading fiber location reveals less abundant impurities, without the presence of Ca, as shown in Fig. 6.9b, clearly demonstrating the dominating role of a limited number of catalytically active species in the fiber failure mechanisms. Fig. 6.8c shows an HM63 fiber with heterogeneous damage caused by pitting, channelling and amorphous erosion after 8000 ms of accumulated exposure.

Surface & pit chemical analysis

Fig. 6.9 shows the EDS spectra representative of the three fibers types after flame exposure. Again, the y-axis has been transformed to allow the identification of weak signals caused by minuscule impurities. Otherwise, in a linear scale, they are typically indiscernible in comparison with the dominating signatures of C, N and O. Fig.6.12c shows a small red rectangle enclosing a round white particle, with the corresponding EDS spectrum shown in Fig. 6.9a. It can be observed that HM63 fibers do not show a N peak. This confirms that the higher HTT needed for high modulus fibers also help to completely remove the N atoms from the original PAN structure. The residues observed in large pits yielded well-defined Si and Ca peaks, along with small contributions from Na, Mg and Al atoms. IM7 fibers are an exception here, as no impurities residues appearing as white particles in SEM images could be observed and EDS spectra lacked Ca, Al and Mg peaks. The relative particle immobility suggests that, upon pit creation, the aforementioned alkali and alkaline earth metals reacted with Si and Al species forming stable aluminosilicates from otherwise reactive elements [242].

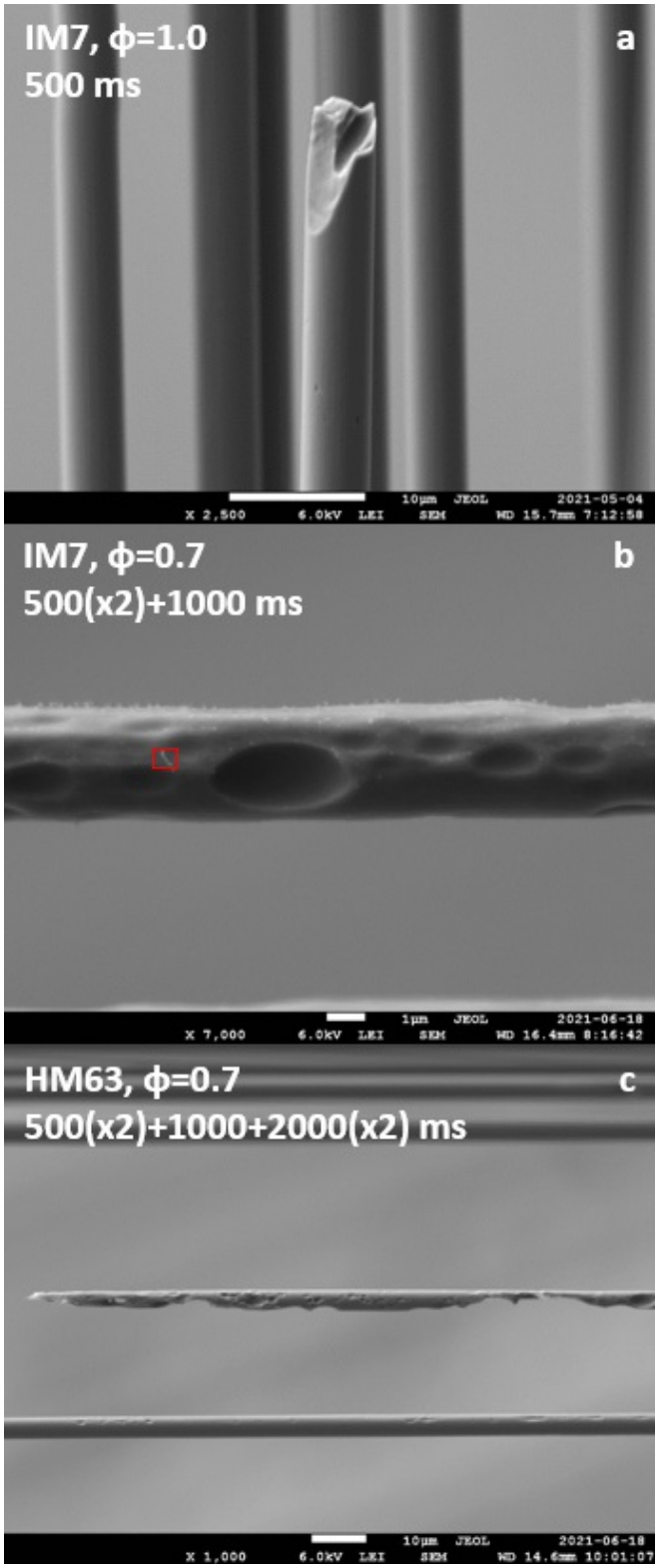

Figure 6.8 Different damage types: (a) competing pits with no appreciable fiber diameter reduction. (b) Fairly homogeneous pitting and diameter reduction (the EDS spectrum of the red rectangle is shown in Fig. 6.9b). (c) Heavy heterogeneous damage after long exposure.

Although it has been suggested that "inert" oxides (e.g. TiO_2 or Al_2O_3) may mechanically erode graphite layers in other oxidative conditions [282], here we attribute the genesis of pits to Ca- and, to some extent, Na- and Mg-based species. Upon reaction with Al and Si atoms, more stable species were likely created thus preventing further catalytic gasification.

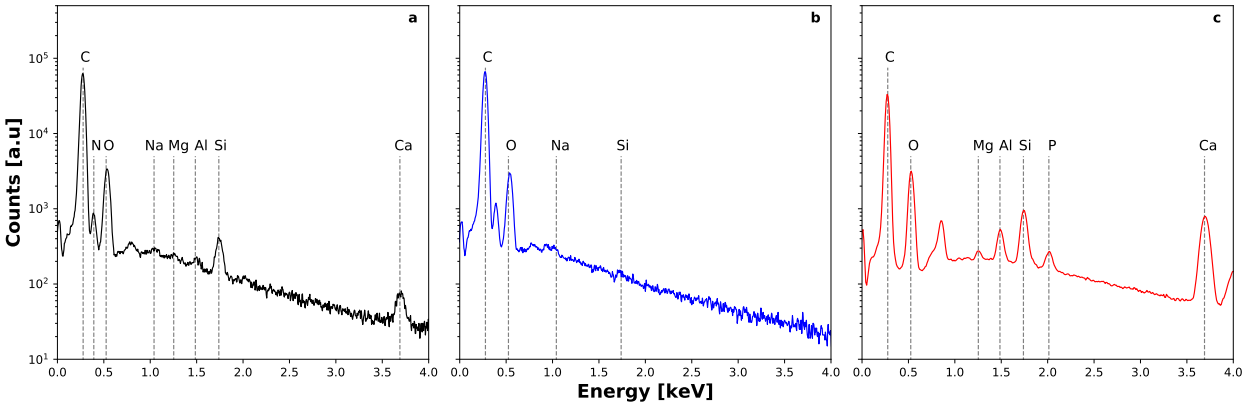

Figure 6.9 Examples of EDS spectra from burnt fibers: a) AS4 (Fig. 6.12c), b) IM7 (Fig. 6.8b) and c) HM63 (Fig. 6.7) fiber surfaces. All confirmed peaks correspond to the K_α values. The plots are shown in an unconventional semi-log scale for clarity of peaks above ~1.0 keV.

Damage evolution

The sequential flame insertion approach implemented, followed by repeated fixed-point SEM analysis, allowed the observation of damage evolution resulting from controlled flame exposure. Fig. 6.10 shows the genesis of a pit and subsequent channelling effect of mobile impurities, indicated by the solid line oval. The right side of Fig. 6.10a shows a small region with amorphous damage, with a large pit on the right, created after a 500 ms flame exposure. After an additionnal 500 ms insertion, a new small pit appears on the lower right side of the existing pit, as shown in Fig. 6.10b. This is the starting point of the channel, and can be attributed to an impurity that remained buried and did not react in the first flame exposure. Finally, Fig. 6.10c shows the resulting angled channel after a total of 2000 ms in the flame atmosphere.

Most other features on the same fiber did not grow as fast as the channel, confirming that most catalyst particles were quickly deactivated or removed following initial flame exposure. Amorphous erosion in form of skin peeling was observed in a few locations, as indicated by an arrow in 6.10a, but did not appear to evolved following subsequent flame insertions. Defective carbon structure combined with interleaved impurities could have promoted this exfoliation [400, 416]. However, a tunnel created by a mobile impurity going completely

through a fiber is indicated in 6.10a and 6.10b by the dashed-line oval.

Fig. 6.11 shows the rapid porosity evolution within an extremely large pit created on the surface of an AS4 fiber during the first half second of exposure to the flame. The pit is most likely due to a mixture of Ca-, Na- and/or Mg-based species which reacted with Al and/or Si, as suggested by EDS analyses of similar residues (e.g. Figs. 6.7 and 6.12c), as discussed in §§6.3.2 and 6.3.2. The pit's long axis dimension exceeds the fiber diameter itself, with an apparent pit growth rate ($\sim$14 800 nm s^{-1}) that largely exceeds the average pit growth rates observed under the same conditions. After the second insertion, the pit did not show a noticeable change of dimensions. Moreover, its periphery shows heterogeneous damage with several dents and half pits with apparent growth rates in the 400–1000 nm s^{-1} range. On the other hand, the smaller pit located on the upper left side yields a moderate and more constant growth rate of $\sim$115 nm s^{-1}. This reveals a very large variability in growth rates for extremely large pits, whereas the growth rate of submicron surface pits appears more homogeneous. Although it was possible to identify certain elements at selected damaged locations via EDS, their effect on pit growth rates cannot be determined since different compounds from the same metallic impurity can promote catalysis to different extents, as well synergistic or poisoning effects in the presence of two or more catalysts [240]. Knowledge of the original location of impurities as well as of the nature of their compounds is therefore needed.

To evaluate the effect of flame chemistry on pit evolution, the three fibers were sequentially inserted into the three types of flame. Unfortunately, it was only possible to follow up the same pits or channels on two out of the three fibers, i.e., AS4 and IM7. The pit growth rates reported here for these two fiber types were also obtained in different flame conditions, fuel-lean ($\phi = 0.7$) for AS4 and stoichiometric ($\phi = 1.0$) for IM7. Figs. 6.12a-c show the evolution of a cluster that appeared upon the first 500 ms insertion on the surface of an AS4 fiber, with coalescence of individual pits upon subsequent insertions. Fig. 6.12d shows IM7 fibers with pits created during the first exposure to stoichiometric flames. These pits did not change significantly in size following sequential insertion as shown in Figs. 6.12e-f.

To gain insight into the role played by flame chemistry and fiber microstructure, the apparent pit growth rates were calculated for all exposure intervals. The results are reported in Fig. 6.13a for random pits found on AS4 ($n = 18$, from Figs.6.12a-c) and IM7 fibers ($n = 13$, from Figs.6.12d-f). Pits were only measured lengthwise to avoid parallax errors induced in widths due to fiber curvature. Most of these pits tend to grow faster lengthwise, following crystallite orientation, which in turn is a function of CFs HTT [417]. When fibers did not break nor were hidden by other fibers due to flame-induced rearrangement, the same pits

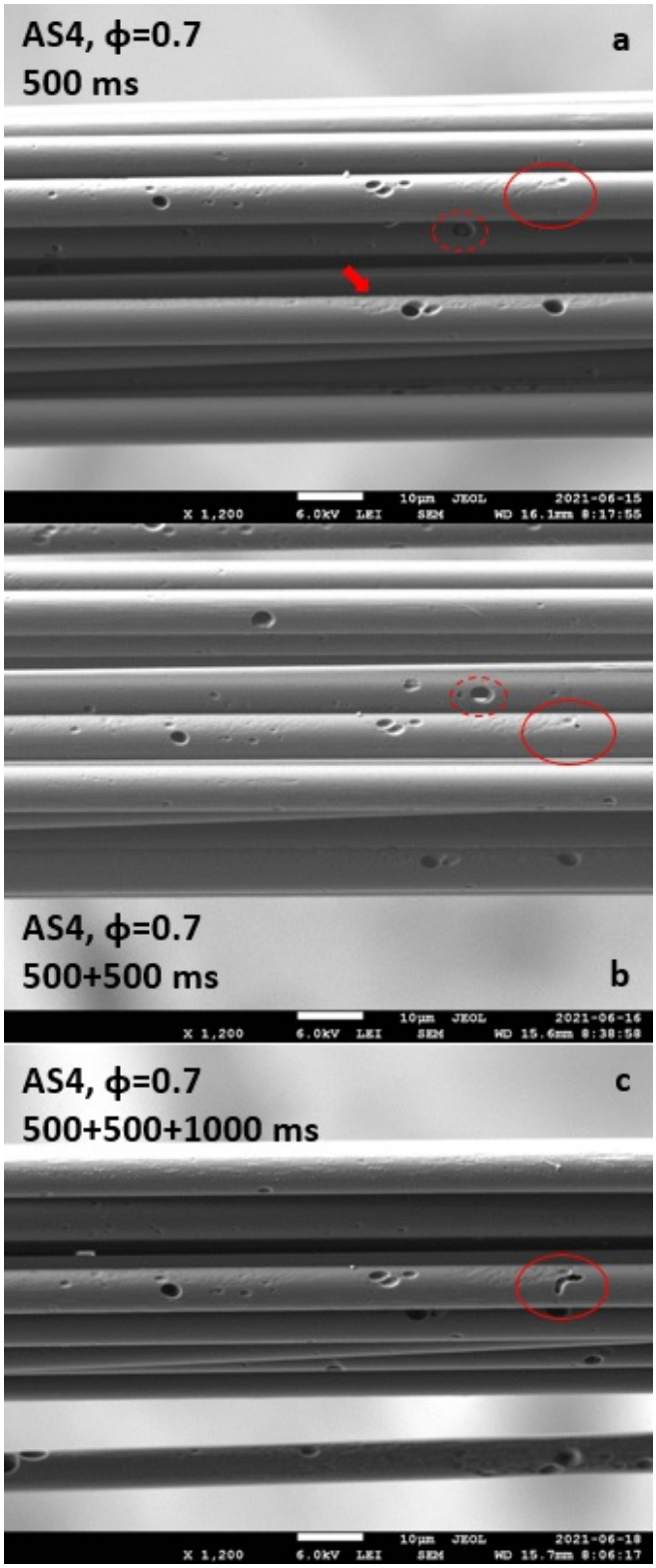

Figure 6.10 Sequential exposure of AS4 fibers (ϕ=0.7), showing the evolution of a channel caused by a mobile impurity (solid-line oval): absent pit (a), pit genesis (b) and transition into a fully developed channel (c).

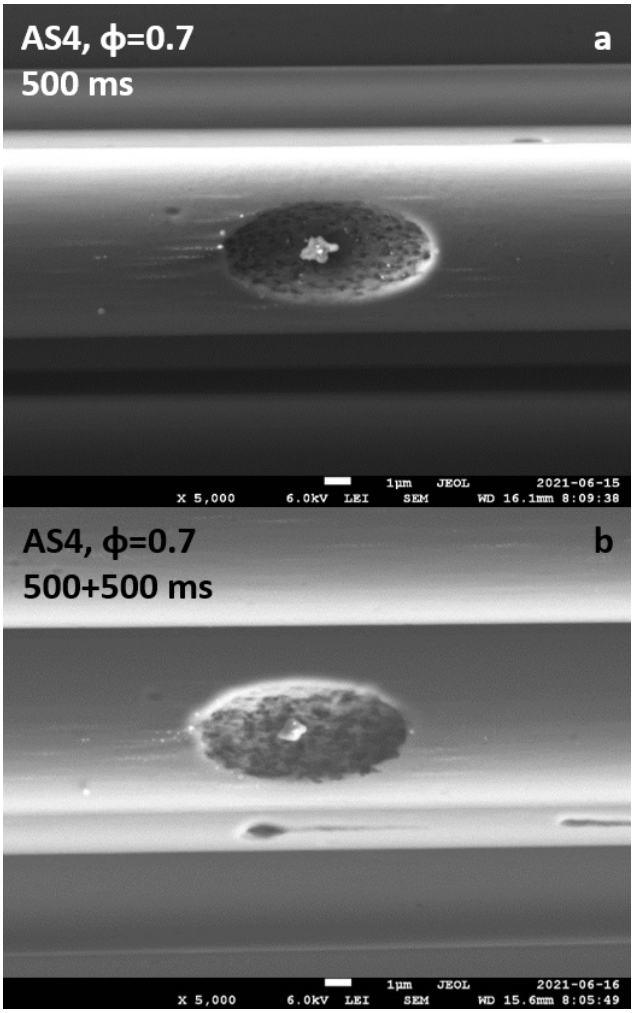

Figure 6.11 Pit and internal porosity evolution of an AS4 fiber upon sequential flame exposure (ϕ=0.7).

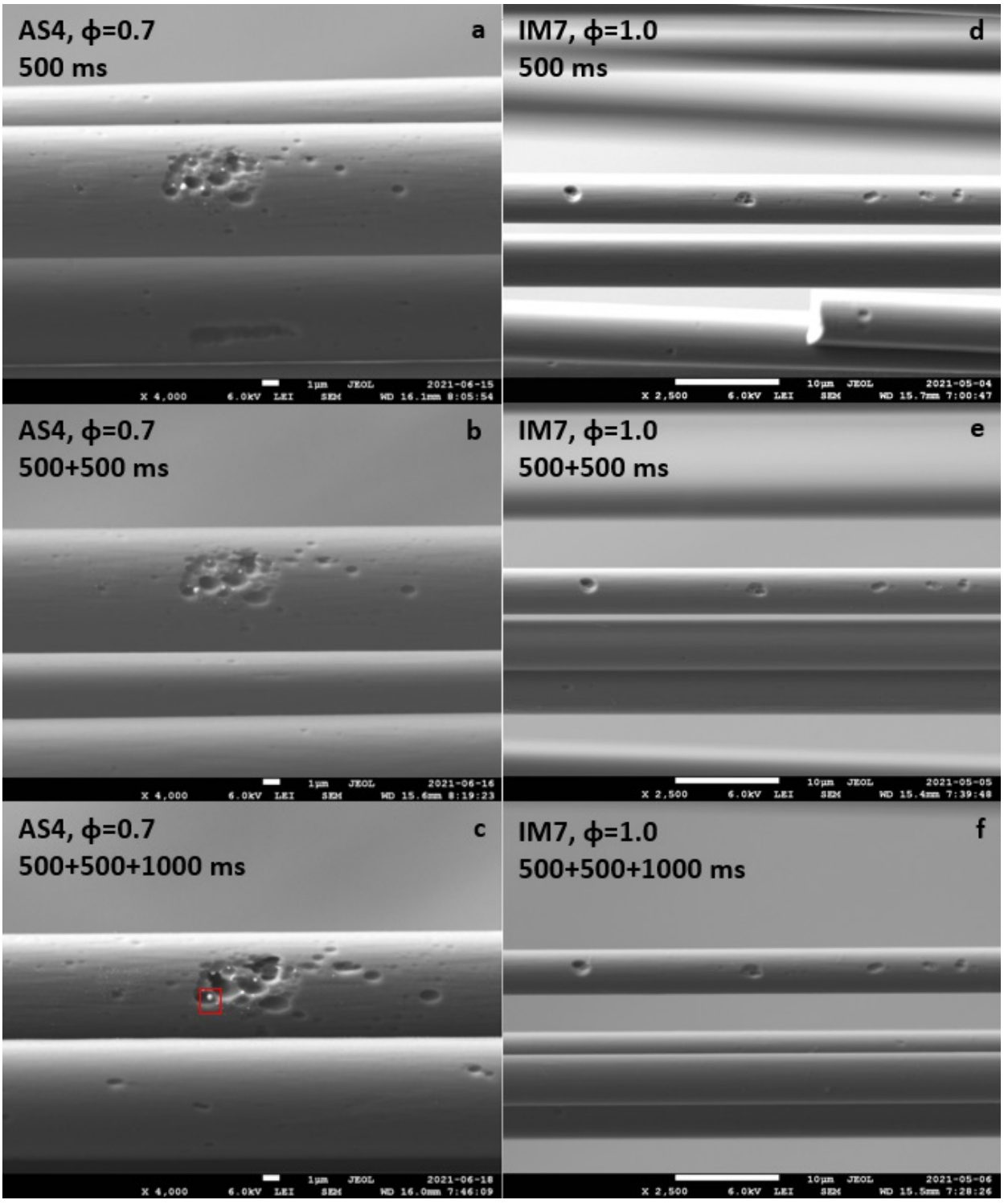

Figure 6.12 Pit evolution of AS4 (a-c) and IM7 (d-f) fibers after sequential exposure to lean ($\phi = 0.7$) and stoichiometric ($\phi = 1.0$) CH_4/air flames, respectively. Rectangle at (c) shows the probed area of the EDS spectrum shown in Fig. 6.9a.

were measured after successive insertions. For each step, a mean apparent growth rate and its 95% CI were calculated considering all pits. During the first 500 ms insertion, rapid pit nucleation took place in both fuel-lean and stoichiometric flames, yielding 1189±326 and 1637±563 $\mathrm{nm\,s^{-1}}$ for AS4 and IM7 fibers, respectively. Upon a second 500 ms insertion, the growth rates decreased by an order-of-magnitude, indicating a major reduction of impurity-induced catalytic effects in these specific areas. It is possible that some impurities remained active, although to a lesser extent. Henceforth, in absence of catalysts, pit growth would have been driven by the oxidative species present in the flame atmosphere, as well as by the amount and nature of active sites presented by the fiber microstructure. Both flames yielded an apparent pit growth rate of 196 ± 57 and 129 ± 48 $\mathrm{nm\,s^{-1}}$ for AS4 and IM7 fibers, respectively. The third and final insertion lasted for 1000 ms, clearly revealing the immediate effect of flame chemistry. The axial pit growth rate of 294 ± 78 $\mathrm{nm\,s^{-1}}$ measured for AS4 fibers is much larger than the 111 ± 40 $\mathrm{nm\,s^{-1}}$ of IM7 fibers. This difference is in contrast to the TGA/DSC data discussed in our previous work [288], which indicates a higher reactivity of IM7 fibers *vs.* AS4 in air. After the third insertion, the pit growth in IM7 fibers remains esentially unchanged, suggesting a stable attack by the stoichiometric flame. However, the fiber (AS4) exposed to the lean flame atmosphere, where significantly more O_2 is present, shows an increase in growth rate.

Unfortunately, it was not possible to follow-up these trends over long durations due to fiber breakage. Moreover, although the high modulus fibers (HM63) showed similar damage mechanisms to those observed on AS4 and IM7 fibers, pit growth rates are not shown in Fig. 6.13a since it was not possible to follow up any oxidation-induced features throughout after each sequence.

Considering our test conditions and the definition of macroporosity, i.e., $\gtrsim$ 50 nm [418], it seems reasonable to assume enhanced CF reactivity in presence of macropores in such reactive environment. In the case of CFs with well-defined core-sheath structure, i.e. standard (AS4) and intermediate (IM7) modulus fibers, large pits will reveal a larger portion of the amorphous core, increasing the fiber reactivity owing to the inner imperfect structure. In other words, surface pitting contributes toward more-developed internal pore networks, which in turn can translate into accelerated fiber failure even under ideal low external forces due to percolative fragmentation [219, 389]. Other factors may come at play affecting fiber failure, for instance the flow regime, e.g. Knudsen and transition flow, as well as the Thiele modulus, as pointed out by other researchers [390, 403]. More research is needed to evaluate the evolution of the internal pore network and ASA and their effect on the gasification rate, i.e. oxidation kinetics. These analyses could be aided by adsorption or small-angle scattering techniques.

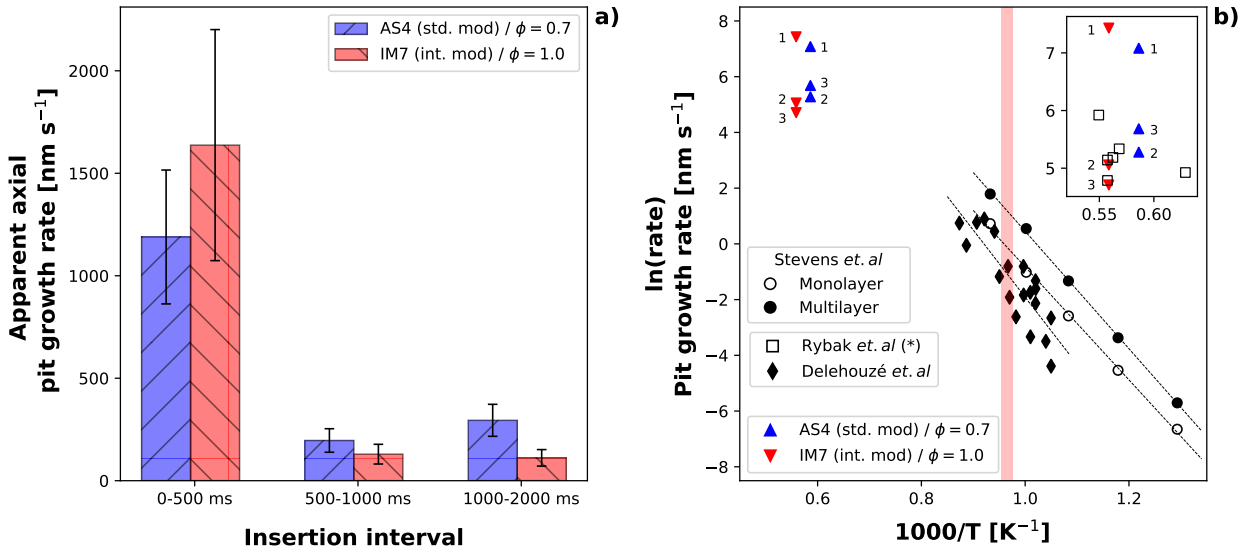

Figure 6.13 (a) Apparent axial pit growth rate *vs.* insertion interval. The means (AS4, $n = 18$; IM7 $n = 13$) were obtained from randomly-chosen pits shown in Fig. 6.12. Error bars indicate the 95% CI. (b) Arrhenius plot comparing the pit growth rates from a), i.e. AS4 (▲) and IM7 (▼) *vs.* data from Stevens *et al.* (●,○) [404] (unknown O_2 partial pressure; unrestricted air flow at room pressure using a tube furnace) and Delehouzé *et al.* (♦) [286] (pure O_2 at 140 Pa using a HT-SEM). The vertical strip indicates the hexagonal-circular pit transition zone from [286]. Markers 1, 2, 3 correspond to the 0–500 ms, 500–1000 ms, and 1000–2000 ms insertion intervals, respectively. The inset compares the values from (a) *vs.* carbon black diameter reduction rate in ethylene flames from Rybak *et al.* (□) [259] (ethylene/air flame at 100 kPa using a custom burner setup).

Pit shape & growth rate comparison

An Arrhenius plot is presented to put the values discussed in §6.3.2 into perspective. Fig. 6.13b contains the pit growth rates of AS4 (▲) and IM7 (▼) fibers from Fig. 6.13a marked as 1, 2 and 3, which correspond to the apparent rates obtained from the 0–500, 500–1000, and 1000–2000 ms insertion intervals, respectively. For comparison purposes, other pit diameter growth rates are shown, i.e., values from Stevens *et al.* (●,○) [404] and Delehouzé *et al.* (♦) [286]. Both reference data sets were obtained from HOPG surfaces at similar length scales (from hundreds of nm up to a few microns), after O_2 attack under different experimental conditions: unrestricted air flow at room pressure using a tube furnace with unknown O_2 partial pressure [404], and pure O_2 at 140 Pa using a HT-SEM [286]. A vertical red strip indicates the hexagonal-circular pit transition zone (∼1025–1050 K) also reported by Delehouzé *et al.* [286]. Under pure O_2 and low pressure (140 Pa) conditions, they found that hexagonal pits were formed below this temperature threshold, while round features were favoured at higher temperatures. Two characteristic trends can be identified upon examination of Fig. 6.13b and comparison between different datasets, namely temperature-driven pit geometry and apparent growth rate.

Regarding pit geometry, our oxidation tests were carried at a position that ensures flame temperatures at least ∼650 K above the transition threshold [286], hence hexagonal pitting was not expected. It is extremely unlikely that hexagonal pits form on the CF surface. Only round pitting has been reported in other CF-based works, regardless of the etching conditions [10,11,190,203,223,225,230,239,256,263,264,278,287,368,390,395,399–403], either as well-defined individual features, pit clustering and subsequent coalescence, or seemingly amorphous. This is explained by the heterogeneity of PAN-based CFs structure, highly disordered compared to graphite models, e.g. HOPG or natural graphite. Moreover, it has been suggested that oxidative etching of CF surfaces results in the removal of full crystallites [264] which have a size on the order of a few nanometers for the CFs studies here [288]. Highly oxidizing environments also do not yield hexagonal pitting since highly-energetic species such as radicals or atomic species are able to attack the graphitic structure regardless of the type of site, i.e. edge site or on the basal plane. For instance, Nicholson *et al.* [270] showed that round pitting was formed on HOPG surfaces under attack of highly reactive species ($O(^3P)/O_2$ mixture) even at rather mild temperatures (∼298–423 K).

Values obtained for AS4 and IM7 fibers range from hundreds to thousands of nm s^{-1}, whereas the reference etch rates from [286,404] remain below ∼10 nm s^{-1}. As pointed out by Blyholder *et al.* [237] and Stevens *et al.* [404], direct comparison between homogeneous surface oxidation and pit growth rates is a challenge owing to different test conditions, even when similar

materials are considered owing to the different processing conditions of different carbonaceous materials. Since none of the reference works considered fire conditions, a flame-based benchmark was defined. Diameter change rates of carbon black oxidized in ethylene flame reported by Rybak *et al.* (□) [259] are shown in the inset for direct comparison with our pit growth rates. Both datasets are in the same range ($\sim$100–400 nm s^{-1}) except for the values obtained after initial exposure due to catalytic effects (marked as 1). Despite the challenge of comparing the reactivity of dissimilar carbonaceous materials under different oxidizing conditions, the similarity between our data and carbon black oxidation in flames is encouraging. Pit growth rates have not previously been reported for CFs surfaces under highly-reactive conditions, let alone from direct exposure to flame conditions. We consider that the values reported here are a good starting point for the validation of damage models intended for CF-based materials in combustion environments representative of fire hazards.

6.4 Conclusions

The oxidative behavior of CFs under open flame attack was studied using an original technique consisting in time-controlled insertion of three different types of unloaded CFs into flames and *post hoc* fixed point observations. This enabled sequential damage assessment and precise follow-up on fire-induced damages. Localized pitting and homogeneous fiber diameter reduction were both observed, with our investigation focusing on the former. Analytical methods were implemented to precisely identify and quantify impurities (NAA, SEM, and EDS), before and after flame exposure. Pitting was driven by the presence of metallic impurities, namely alkali and alkaline earth metals, that catalyzed the oxidation process. Some impurities remain active for several seconds and had a channelling effect owing to their mobility (e.g. Cu-based). Other were found to be quickly deactivated or removed following the first flame exposure, such as Na, Mg and Ca. Intense pit nucleation and growth were observed for all fiber types during the first 500 ms of flame exposure, with apparent diameter growth rates of 1189$\pm$326 and 1637$\pm$563 nm s^{-1} for AS4 and IM7 fibers, respectively. After this initial period, the CF degradation rate drops by an order of magnitude and appears to be controlled by flame chemistry rather than the presence of impurities, with fuel-lean flames resulting in slightly faster pit growth rates from their increased O_2 content. The pit growth rates were compared with the literature which considers different experimental conditions. Extrapolation from such works is not possible given the difference in materials, temperatures and the concentration of oxygen or other reactive species, e.g., radicals. However, our results are coherent with these literature data, since they are in the same order of magnitude reported in other flame-based works.

Although impurities were assessed quantitatively by NAA, it was not possible to determine the effect of specific elements on pit growth rates. Impurities were qualitatively identified via EDS at certain damaged locations, but the nature of their original compounds remains unknown, i.e., whether metals were found as carbonates, acetates, oxides, etc. Precise knowledge of the spatial location of impurities and of the nature of their compounds is needed in future studies aiming to model their effect on the thermomechanical behavior of CFs.

Our results highlight that flame chemistry, microstructure, and impurities are all key parameters in CF oxidation, with the former often overlooked in the assessment of CF fire properties. On a more practical side, we expect that this works helps to improve the fire safety of CF-based structures, since current models often assume homogeneous diameter reduction. Moreover, fire resistance regulations tend to disregard the importance of the flame stoichiometry, considering it an outcome of flame calibration focusing on temperature and heat flux. Using a simple gaseous fuel (CH_4), we have demonstrated that the composition of the reactive atmosphere needs to be given careful consideration in standardized fire tests, but also in other highly reactive conditions where carbon gasification is of interest.

Acknowledgments

The authors want to acknowledge the financial support from the Natural Sciences and Engineering Research Council of Canada (NSERC/CRSNG) grant no. RGPIN-06410-2016 (NSERC Discovery). Pablo Chávez-Gómez is extremely grateful to the National Science and Technology Council of Mexico (CONACYT) for his doctoral scholarship. The authors also thank Dr. Martin Luckabauer for his valuable feedback, as well as Max Thouin and Eddie Rubey from Hexcel Corp. for supplying some of the samples used in the study.

CHAPTER 7 GENERAL DISCUSSION

7.1 Design and evaluation of fire-resistant PMCs

The first article (§4) addressed the design an evaluation of PMCs with fire-resistant features, intended to be used in aircraft structures. The subject is covered from a practical engineering standpoint, to assist in the conceptual design of firewalls. The main focus of the article is the evaluation of PMCs used in aircraft firewalls through a proposed resource-efficient tool. Given the high costs associated with the evaluation and certification of these structures, a small-scale test evaluation method is presented. An experimental methodology exposing coupons simultaneously to fire & load was introduced, from which scores can be assigned and conclusions drawn based on temperature profiles and strength evaluations.

Since the results of the fire & load evaluation process are only a piece in the design puzzle, several tools were integrated into a single methodology involving conceptual design, material screening and evaluation, and final ranking. The aforementioned steps are increasingly being investigated as part of the general design process of composite structures. In fact, the work is guided by design methodologies and mathematical approaches proposed by experts in the field. The main contribution of this article is merging these concepts into one methodology intended for a streamlined material selection process. First, Suh's AD [168] was introduced to guide the design process. It provides a scientific design approach while ensuring functionality and independence of the product in question. Other experts agree with the use of axioms towards robust mechanical design and decision-making activities [419–421]. Second, Ashby's works [1, 14, 141, 145] in material science, design and selection were taken into account to define the strategies for initial screening. Third, an MCDM method had to be considered to overcome some challenges in the decision-making process faced during the selection process of a material, for instance, preference bias, subjectivity, and often-conflicting criteria. A tool capable of integrating both crisp and vague requirements as well as processing quantitative/qualitative scores was essential to ensure the success of the method. Fourth and last, to handle all the imprecise information entailed by any design activity, fuzzy sets [174, 175] were incorporated to help in most of the aforementioned steps due to their proven utility in decision making and design, especially AD in the context of this work.

The main novelty of the work is the integration of small-scale thermomechanical tests with AD, fuzzy sets, and MCDM into one methodology to design fire-resistant PMCs. This made possible the selection of two material systems among several candidates, each from different categories: structural and parasitic. Quantitative and qualitative criteria with different im-

portance were considered. The combination of both material systems is expected to provide the best performance and the highest probability of withstanding an intermediate-scale fire resistance test. The expected impact of this article will be seen in test campaigns with a larger number of candidates while considering test conditions closer to those found in real applications, easier evaluation process, and lower development costs.

7.2 CF oxidation under flame attack

The oxidative behavior of CFs under flame attack was analyzed in the second (§5) and third (§6) articles, addressing two separate yet complementary phenomena: the effect of flame chemistry and tensile loads on the damage mechanisms involved. The motivation behind the decision to address these topics mainly lies in the scarcity of dedicated studies considering conditions relevant to an aircraft fire. Almost the entirety of the works found in the literature addresses the CF oxidation phenomenon under controlled conditions which do not represent those encountered in combustive environments. To evaluate the effect of flame reactive species, two original small-scale methods were developed using a FFB to produce CH_4/air unstretched premixed flames.

The second article (§5) presented the first of these methods, where the effect of flame chemistry and tensile load on the oxidative behaviour of PAN-based CFs under flame attack were revealed. Three types of CF bundles with different microstructure were loaded at different stress levels and exposed to flames with different fuel/oxidizer ratios, i.e., $\phi = \{0.7, 1.0, 1.2\}$. The TTF was chosen as the main indicator for these tests. Two remarkable differences were found among fiber types and flames. First, stoichiometric flames ($\phi = 1.0$) were the least aggressive, despite slightly hotter than the other two. Fuel-lean flames ($\phi = 0.7$) demonstrated their aggressiveness by shortening the TTF in all cases at least by 50 % *vs* its stoichiometric counterpart. This is explained by the excess of O_2 in the flame zone attacking the CF's active sites. The fuel-rich flames ($\phi = 1.2$) yielded only slightly shorter TTF values with respect to the stoichiometric flame. These differences became less pronounced as stresses increased. The second striking difference was observed between CF types, where the high modulus CF yielded TTF values one order of magnitude larger that standard and intermediate modulus fibers, pointing at the microstructure as one of the key factors in the fire resistance of CF-based structures loaded in tension. These results were compared against profiles obtained via TGA/DSC, showing no direct correlation. None of the flame- and CF type-induced differences could have been predicted by using traditional thermoanalytical techniques since they rely on controlled atmospheres, hence the absence of highly reactive species such as OH radicals. However, some insights into the oxidation kinetics were obtained.

The main novelty of this article is the assessment of loaded CF bundles under true flame attack using an original small-scale test protocol. The results clearly show that flame chemistry has an impact on the TTF, regardless of the type of CF. In other words, not all flames show the same aggressiveness towards CFs. At higher load levels, these differences become less pronounced. It was also found that the type of CF has an impact of the TTF. CFs with higher level of graphitization withstood the flame attack for larger periods when compared to their standard and intermediate modulus counterparts. The overall impact of these findings is twofold. On the one hand, the flame chemistry, often overlooked in fire resistance tests, is expected to gain importance and be considered by certification authorities. On the other hand, this information can be used by aircraft designers to selectively use CFs with higher oxidative resistance where burn-through resistance is needed.

The second approach, presented in the third article (§6), allowed the precise monitoring of damage features via time-controlled sequential fibre insertion into flames with subsequent SEM analyses. Preferential attack of active sites by flame reactive species caused severe pitting. Pit appearance had been scarcely reported in oxidative behavior at temperatures typically found in fire scenarios, i.e., $300 \lesssim T \lesssim 1000\,^{\circ}\mathrm{C}$. However, when reported, pitting has been attributed to opening/widening of pre-existing flaws [225] or due to different level of structural order between the amorphous core and the turbostratic skin [383, 422]. The measurement of pit growth rates was possible by sequential flame attack, considering 0–500 ms, 500–1000 ms, and 1000–2000 ms flame exposure intervals, followed by the identification of the same pits. The calculated rates, which were in line with the oxidation rates of other carbonaceous materials in flame-based experiments [259], indicated that pit inception took place during the first insertion, with diametrical growth rates in the range of $\sim$1200–1600 $\mathrm{nm\,s^{-1}}$. Subsequent insertions yielded pit growth grates in the range of $\sim$130–290 $\mathrm{nm\,s^{-1}}$, suggesting the depletion of impurities that initially promoted the pitting process. The results also implied that subsequent oxidation was driven by the flame reactive species. The catalytic, stabilizing and poisoning effects were discussed on the basis of the results from NAA and SEM/EDS analyses. EDS analyses provided valuable insight into the CF surface composition. The selected EDS parameters limited the chemical analysis to the fibres' surface and small probing area. NAA provided the necessary means to analyze impurities throughout the bulk. Oxidation was catalyzed by some impurities such as alkali and alkaline earth metals. Sodium was found to be the most abundant impurity in standard and intermediate modulus CFs, whereas calcium dominated in the high modulus type. Channelling was caused by mobile impurities, of which Cu-based particles were confirmed. Other elements such as Al and Si were found to counteract this effect, preventing further catalytic oxidation by creating stable oxides. Other elements such as Cl and P, which are known as inhibitors, were

also identified. The results from the third article complement the findings on the CF failure promptness, confirming that the aforementioned damage features exert an influence in the fire-induced fibre failure process. In addition to their known high crystalline order, the low impurity levels is definitely a factor involved in the higher TTF values previously reported. However it is difficult to discern the contribution of each factor.

The novelty of this work resides in the detailed monitoring of fire-induced damages on CFs and the identification of impurities involved therein. The author of this dissertation is proud of the craftsmanship developed in the process. It was demonstrated that impurities have different effects on the CF oxidation process. There are elements together with their compounds that work as catalysts, promoting severe damage in form of pitting, channelling and amorphous erosion. Conversely, other elements create stable compounds or poison the catalyzed oxidative process. Sequential measurements of pits revealed that the oxidation rate during the first insertion into the flame depended on the availability of impurities. Subsequently, these rates decreased by one order-of-magnitude, mainly depending on the CF type and the flame chemistry. With the insights presented herein, it is expected that researchers will start considering the oxidation rates determined after true flame attack in their thermomechanical models, instead of values obtained under controlled conditions which can be several orders of magnitude lower than in the former case. Moreover, aircraft designers will be able to incorporate CFs with lower impurity levels where burn-through resistance is required.

7.3 General impact

The general impact of this work is manifold. First, from a practical aircraft certification standpoint, the results will trigger meaningful discussions between regulating agencies, aircraft & engine OEMs, fire laboratories and customers (e.g. airlines). Temperature and heat flux are the main considerations in related fire resistance tests, yet most of the time the flame chemistry is ignored. It is clear that not all flames yield the same aggressiveness towards PMC-based firewalls, entailing different risks. The safety of passengers will undoubtedly be improved, and the economical benefit of ensuring the integrity of cargo could be appealing to the involved parties. Second, it is expected that the results presented regarding the behavior of the different types of CF will influence the selection process not only due to their mechanical properties, but also owing to the ability to withstand flame attack. Third, the modelling efforts to predict the thermomechanical behavior of CF-based PMCs need not only to consider the type of CF, but to address the aggressiveness of an open flame. In other words, models could be created and validated using data from flame-based experiments instead of data from traditional thermoanalytical techniques. Finally, based on the fact that

alkali and alkaline earth metals have deleterious effects on the oxidation resistance of CFs, more research on the fire resistance of PMCs exposed to electrolyte-based flames will be increasingly necessary. This will be increasingly relevant with aircraft electrification and the rise of urban air mobility. A ripple effect is also expected, raising awareness in other fire safety communities such as civil, rail, naval and automotive, where CFRP structures are increasingly used.

CHAPTER 8 CONCLUSION AND RECOMMENDATIONS

This dissertation has addressed the fire resistance of PMCs intended for aircraft applications. The general objective was to provide the methods and knowledge necessary to enable the development of fire-resistant PMCs in a resource-efficient fashion, through small-scale testing. Two main challenges were identified in this endeavor. First, the development of a systematic design & evaluation approach was needed to aid in the conceptual process of fire-resistant PMC relying on small-scale evaluations. Second, given the ubiquity of CFRP-based structures in modern aircraft, it was necessary to understand the damage process of CF under oxidative conditions.

Based on the aforementioned challenges, three specific objectives were defined. The first objective involved the development of a resource-efficient design & evaluation methodology for fire-resistant PMCs based on small-scale tests. The second objective required to delve into the effect of fire and mechanical loads on CF failure. Finally, the third objective aimed to identify the key intrinsic parameters of CFs involved in their damage process under flame attack. These objectives have been successfully achieved and the outcome has been presented in the form of three peer-reviewed articles. Moreover, the general objective was achieved after evaluating the fire resistance of CFs and their composites at a small scale, increasing the knowledge in the field in a systematic and resource-efficient fashion, while considering true fire conditions.

8.1 Conclusions

8.1.1 Design and small-scale evaluation of PMCs

A design & evaluation methodology based on small-scale testing was presented to address the first specific objective of this dissertation. The proposed methodology is a holistic approach that fused several design, engineering and mathematical tools into one system, i.e., it integrated AD, material screening guidelines, an original small-scale fire & load evaluation approach, fuzzy sets and a MCDM method.

A case study successfully demonstrated the advantages of this resource-efficient methodology. At the conceptual design stage, the AD mapping process between domains allowed to identify design features that ensured functional independence of a fire-resistant aircraft engine casing. The screening process of material candidates, based on proven design practices, was described in detail. Subsequently, fire & load evaluation of several CF-based laminate

configurations successfully showed the capabilities of using a propane burner to determine the burn-through resistance as well as temperature and strength evolution. Simultaneous fire attack and mechanical loading at a small-scale allowed to mimic the conditions prescribed in aircraft certification regulations. This undoubtedly translates into a resource-efficient experimental campaign, allowing to consider either more material candidates or a higher number of test repetitions to decrease the uncertainty associated with the combustion of PMCs. Finally, the use of fuzzy sets and a MCDM tool capable of handling non-crisp criteria ans scores of dissimilar nature proved to be and adequate solution towards ranking and selection of the best material system.

The conception of PMCs-based aircraft structures endowed with fire resistance is a challenging task. Consequently, the are several expected benefits from this methodology. In first place, heterogenous criteria include those concerning environmental impact and the life cycle analysis (LCA) of PMCs [339], such as recyclability or compliance with international regulations [54], can be considered in the calculations despite their qualitative nature. Second, it is expected that OEMs, aircraft and engine designers as well as material suppliers will benefit from resource-efficient evaluation campaigns, where smaller specimens are needed and more material candidates could be tested within the budget typically allocated to a single certification test. This will lead to resource-efficient selection of material systems with the highest chance of success that will be further evaluated at the intermediate-scale.

8.1.2 CF oxidation under flame attack

The second and third specific objectives of this dissertation were covered in two articles that are intimately connected. Both covered original experimental methods relying on PAN-based CFs with different microstructure and a FFB producing premixed methane/air flames.

First, the effect of fire and mechanical loads on CF failure was determined considering TTF as measure. Three types of CF with different microstructure were analyzed, using fiber bundles to ease their handling and evaluation. It was demonstrated that different flame chemistries yielded markedly different results, regardless of the fiber type. Stoichiometric flames were the least aggressive despite being marginally the hottest. Fuel-rich flames were more aggressive, slightly shortening the fiber bundle life. Fuel-lean flames had a major impact on the fire resistance of the bundles, shortening the TTF by $\sim$50 % when compared to the stoichiometric case. Standard and intermediate modulus CFs showed similar results, with TTF values ranging in the hundreds of seconds. A striking difference was found when comparing those results with those obtained with the high modulus type fibers which has a more graphitic structure. Comparatively higher TTF values were found, in the thousands

of seconds, i.e., one order of magnitude above its counterparts. In addition to these results, the effect of mechanical loads was determined using the same flame conditions. As expected, the tensile loads expedited the failure of the fiber bundles. The aforementioned differences in TTF due to flame chemistry held at higher loads, although less markedly.

Once the flame/CF type differences were identified, the key intrinsic properties of CFs involved in their damage process under flame attack were brought into the spotlight. This led to analyses performed at an even smaller dimension, i.e., microscale, successfully covering the third specific objective. The presence of impurities was assessed by two different methods: EDS and NAA. The high modulus fiber yielded lower impurity levels when compared to its standard and intermediate modulus counterparts. Flame-induced CF damage mechanisms were clearly identified. The follow-up of damage features such as pitting and channelling was successfully achieved. It was concluded that pit nucleation takes place immediately upon insertion into flames, enhanced by the presence of impurities. Once the catalyzing impurities have fully reacted with the carbonaceous structure or with their poisoning counterparts, the pit growth is driven by the CF microstructure and the flame chemistry. These new insights complement the existing models and assumptions about CF-oxidation, which have been proposed under controlled atmospheres, i.e., without considering true flame attack.

Some aspects that have been generally neglected when assessing the combustion of CFRP composites were finally tackled. Microstructure, impurities and flame conditions play crucial roles in CF oxidation. Therefore, all aspects must be considered simultaneously to identify critical phenomena at play in CFRP fire resistance testing. Since the CF strength is governed by its flaws, further discussions are expected to be triggered on the topic and their incorporation in structural models towards accurate failure prediction.

8.2 Limitations and recommendations for future research

- **Increase the number of thermomechanical loading cases**: The small-scale evaluation presented in Article #1 was only demonstrated with the tensile load case. Further studies could benefit from incorporating rigid guides for tests under compressive load. Vibration and air cooling should also be incorporated to better represent the conditions found in real engine applications.

- **Determine the impact of selecting different conceptual design and MCDM tools**: The implementation of fuzzy sets demonstrated that vague/non-crisp requirements, criteria and scores can be successfully incorporated into the material selection process. However, there are several ways to handle these values, from the conceptual

design phase, to the ranking step. Future studies need to assess the impact of choosing different design paradigms and MCDM methods for ranking using fuzzy sets in the context of aircraft design and fire-resistance of PMCs.

- **Investigate the impact of OH and CO_2 on CF failure**: The effect of both OH and CO_2 concentrations in the flame atmosphere was limited to a qualitative discussion in light of the reference flame conditions [380]. Direct measurements of the flames used therein would have been desirable to support the discussion. The instrumentation required for advanced diagnostics, for instance Raman or fluorescence spectroscopy, significantly increase the complexity of the experimental campaign. However, precise quantification of permanent and transient species is strongly recommended for future work.

- **Clarify the O_2 diffusion statement**: Fuel-lean flames led to uniform fiber failure within the flame cone, whereas stoichiometric and fuel-rich flames favoured breakage at the cone periphery. The possibility of increased fiber attack owing to the presence of OH was considered. However, with both stoichiometric and fuel-rich flames, the failure mode did not change significantly. This is the reason behind the statement about the possible effect of O_2 diffusing from the surroundings in §5.3.3. An inert gas shroud could be used in future studies to remove this ambiguity. However, when addressing a material resistance to fire, the air diffusing from the surroundings to the flame cone is also representative of a real fire scenario.

- **Obtain detailed information on the CF active surface**: The ASA of carbonaceous materials dictates their reactivity. ASA measurements can be carried out using porosimetry or adsorption techniques (e.g. BET theory). These results could be complemented by small angle scattering. Some technical challenges can be outlined. Fiber failure was observed to be sequential, i.e., individual filaments did not fail in the same way nor at the same time. Some of them were expelled from the flame cone whereas surving fibers (those remaining attached to the bundle) could be oxidized to different extents depending on their position within the tow, i.e. outermost or central portions. Further studies focusing on surface area would need to reduce this variability by performing studies on isolated fibers.

- **Perform dedicated studies on CF oxidation kinetics**: Kinetic analyses are typically carried out under controlled atmospheres (e.g. TGA or tube furnace). TGA was considered in this dissertation. Accordingly, the alumina-based container used in such experiments had to be loaded with hundreds or thousands of short fibers to ease

handling and avoid blowing them away. Analyses focusing on oxidation kinetics considering combustion conditions such as those obtained with the FFB would need to consider individual fibers. It is possible that the failed fibers that remain attached to the bundle provide an protective effect to those fibers within the bundle and thus this effect needs to be isolated.

- **Perform a more detailed quantitative assessment of impurities and their effect on fiber damage**: It is virtually impossible to determine precisely where the impurities come from. This is specially true for commercially-available CFs whose processing parameters are of proprietary nature. However, the identification of potential sources are of the utmost importance if carbon fibres are to be developed with higher oxidative resistance. Considering the concentrations obtained by NAA from one-meter bundles, on the order of parts-per-million or less, this task was deemed unrealistic, at least with commercially-available fibers. Moreover, the methods considered for elementary analysis in this work, i.e., NAA and EDS, allowed to identify individual elements, but not their compounds. These are expected to have different effects, for instance, in case that a metal is found in its carbonate, acetate or oxide form. Additionally, the precise level of synergy/poisoning cannot be assessed unless impurities are spatially controlled. Therefore, the rate of oxidation cannot be directly linked to specific compounds and thus the discussions were limited to a qualitative description of their effects. Future research considering the location and/or controlled concentrations of impurities is desirable. This would enable further modelling of the damage process and its impact on mechanical properties.

- **Investigate the effect of CF crystallinity**: The knowledge of the CFs' crystal parameters could help to draw better conclusions regarding the oxidation modes and kinetics, as well as linking these data with the fire-resistance. Only the properties provided by the manufacturer were considered, and conclusions were drawn therefrom. Future work can benefit from crystallographic analysess to determine the amount of graphitic and amorphous carbon found in each CF type as well as the pore network to determine their effect in the fire-induced damage and failure process.

- **Incorporate oil-based burners and jet fuel**: The flame-based tests presented in this dissertation were obtained using gas-based burners relying on low molecular weight hydrocarbons, i.e., CH_4 and C_3H_8. The effect of kerosene's complex chemistry on the CF oxidation process is yet to be addressed. Future fire resistance studies can focus on the effect of different representative aircraft fuels, e.g., AVGAS and Jet A1.

REFERENCES

[1] M. Ashby and K. Johnson, "The art of materials selection," *Materials Today*, vol. 6, no. 12, pp. 24–35, 2003.

[2] O. Dessens *et al.*, "Aviation and climate change," *Transport Policy*, vol. 34, pp. 14–20, 2014.

[3] A. J. Timmis *et al.*, "Environmental impact assessment of aviation emission reduction through the implementation of composite materials," *The International Journal of Life Cycle Assessment*, vol. 20, no. 2, pp. 233–243, 2015.

[4] A. P. Mouritz, "Materials selection for aerospace," in *Introduction to aerospace materials*. Woodhead Publishing Limited, 2012, ch. 25, pp. 569–600.

[5] A. A. Baker and M. L. Scott, Eds., *Composite Materials for Aircraft Structures*, 3rd ed. American Institute of Aeronautics and Astronautics, 2016.

[6] A. P. Mouritz and A. G. Gibson, Eds., *Fire Properties of Polymer Composite Materials*. Springer Science & Business Media, 2006, vol. 143.

[7] R. A. Naik, "Durability of Composites in Aircraft Engine Applications," in *Long-Term Durability of Polymeric Matrix Composites*, K. Pochiraju, G. P. Tandon, and G. A. Schoeppner, Eds. Springer, 2012, ch. 15, pp. 597–624.

[8] J. Hamp and S. Caulfeild, "Fireproof Testing of Pressurized Acoustic Organic Composite Sandwich Structures," in *Proceedings of 62nd CASI Aeronautics Conference and AGM, May 19-21, Montreal, Canada*, 2015.

[9] S. Neveling *et al.*, "Analysis of Fire-Protected Load-Carrying Aircraft Structures for Electric Powertrains," in *Deutscher Luft- und Raumfahrtkongress 2020, September 1–3, Online*, 2020.

[10] V. L. Bell, "Release of carbon fibers from burning composites," in *Assessment of Carbon Fiber Electrical Effects*. National Aeronautics and Space Administration, December 1979, pp. 29–57, NASA Conference Publication 2119.

[11] B. Sussholz, "Evaluation of Micron Size Carbon Fibers Released from Burning Graphite Composites," National Aeronautics and Space Administration, Tech. Rep., April 1980, NASA-CR-159217.

[12] J. Ganjei *et al.*, "Catalyzed combustion of carbon fibers from carbon fiber-resin composites," Naval Research Laboratory, Washington D.C., Tech. Rep., 1981, NRL Memorandum Report 4486.

[13] G. Hull *et al.*, "Gasification of Carbon Fiber Composites for the Alleviation of Electrical Hazards," *Industrial & Engineering Chemistry Product Research and Development*, vol. 20, no. 3, pp. 552–555, 1981.

[14] M. F. Ashby, "Criteria for selecting the components of composites," *Acta Metallurgica et Materialia*, vol. 41, no. 5, pp. 1313–1335, 1993.

[15] A. P. Mouritz *et al.*, "Review of advanced composite structures for naval ships and submarines," *Composite Structures*, vol. 53, no. 1, pp. 21–42, 2001.

[16] G. Savage, "Formula 1 Composites Engineering," *Engineering Failure Analysis*, vol. 17, no. 1, pp. 92–115, 2010.

[17] S. Phillips and L. Lessard, "Application of natural fiber composites to musical instrument top plates," *Journal of Composite Materials*, vol. 46, no. 2, pp. 145–154, 2012.

[18] B. Rutan, C. Hiel, and B. Goldsworthy, "Design with Composite Materials: From Complete Chaos to Clear Concepts - Part I," *SAMPE Journal*, vol. 32, no. 5, pp. 18–23, 1996.

[19] B. Goldsworthy, B. Rutan, and C. Hiel, "Design with Composite Materials: From Complete Chaos to Clear Concepts - Part III," *SAMPE Journal*, vol. 33, no. 1, pp. 17–25, 1997.

[20] M. F. Ashby, "Introduction," in *Materials Selection in Mechanical Design*, 4th ed. Butterworth-Heinemann, 2011, ch. 1, pp. 1–13.

[21] A. Jahan *et al.*, "Material screening and choosing methods–A review," *Materials & Design*, vol. 31, no. 2, pp. 696–705, 2010.

[22] U.S. federal government, Multi-agency initiative, "MGI Infographic," [Online; accessed April 10, 2022]. [Online]. Available: https://www.mgi.gov/content/mgi-infographic

[23] D. Beason, "Aircraft Started with the Wright Materials," *MRS Bulletin*, vol. 20, no. 5, pp. 67–67, 1995.

[24] D. Crespy, M. Bozonnet, and M. Meier, "100 Years of Bakelite, the Material of a 1000 Uses," *Angewandte Chemie International Edition*, vol. 47, no. 18, pp. 3322–3328, 2008.

[25] N. A. de Bruyne, "Joint Design for Primary Structures," *Journal of Applied Polymer Science*, vol. 6, no. 20, pp. 122–129, 1962.

[26] D. H. Middleton, "The first fifty years of composite materials in aircraft construction," *The Aeronautical Journal*, vol. 96, no. 953, pp. 96–104, 1992.

[27] P. McMullen, "Fibre/resin composites for aircraft primary structures: a short history, 1936-1984," *Composites*, vol. 15, no. 3, pp. 222–230, 1984.

[28] J. Bishopp, "Aerospace: A Pioneer in Structural Adhesive Bonding," in *Handbook of Adhesives and Sealants: Basic Concepts and High Tech Bonding*, P. Cognard, Ed. Elsevier, 2005, vol. 1, ch. 5, pp. 215–347.

[29] B. C. Hoskin, "Introduction," in *Lectures on Composite Materials for Aircraft Structures*, B. C. Hoskin and A. A. Baker, Eds., Defence Science and Technology Organisation Aeronautical Research Laboratories, Melbourne, Victoria. Department of Defence Support, 1982, pp. 1–12, ARL-STRUC-REPORT-394/ARL-MAT-REPORT-114.

[30] R. A. Pride, "Carbon Fibers and Composites," in *Carbon Fiber Risk Analysis–An industry/government briefing held at Langley Research Center, Hampton, VA, October 31–November 1, 1978*. National Aeronautics and Space Administration, 1979.

[31] Unknown, "Composite Materials in the Airbus," *Aircraft Engineering and Aerospace Technology*, vol. 61, no. 12, pp. 20–29, 1989.

[32] W. G. Roeseler, B. Sarh, and M. U. Kismarton, "Composite Structures: The First 100 Years," in *16th International Conference on Composite Materials (ICCM 16), Kyoto, Japan, July 3-8*. International Committee on Composite Materials, 2007.

[33] J. S. Tomblin *et al.*, "Teardown Evaluation of a Decommissioned Boeing 737-200 Carbon Fiber-Reinforced Plastic Composite Right-Hand Horizontal Stabilizer," Federal Aviation Administration, Tech. Rep., December 2013, DOT/FAA/AR-12/1.

[34] P. Morgan, *Carbon fibers and their composites*. CRC press, 2005.

[35] J. Rouchon, "Certification of large airplane composite structures, recent progress and new trends in compliance philosophy," in *17th Congress of the International Council of the Aeronautical Sciences (ICAS 1990 Proceedings), Stockholm Sweden, September 9–14*, vol. 2. International Council of the Aeronautical Sciences, 1990, pp. 1439–1447.

[36] "Composite Materials in Aerospace Design," ser. Soviet Advanced Composites Technology Series *(J. N. Fridlyander and I. H. Marshall, Series Editors)*, G. I. Zagainov and G. E. Lozino-Lozinski, Eds. Springer Science+Business Media Dordrecht, 1996, vol. 6.

[37] A. P. Mouritz, *Introduction to aerospace materials*. Woodhead Publishing Limited, 2012.

[38] J. M. S. Keen, "The Use of Composite Materials in Aero Engines," in *National Aeronautic Meeting and 3rd International Simulation and Training Conference*. SAE International, 1967.

[39] G. Marsh, "Composites get in deep with new-generation engine," *Reinforced plastics*, vol. 50, no. 11, pp. 26–29, 2006.

[40] G. Marsh, "Aero engines lose weight thanks to composites," *Reinforced Plastics*, vol. 56, no. 6, pp. 32–35, 2012.

[41] J. M. Lee, "Rolls-Royce is Bankrupt; Blames Lockheed Project," *The New York Times*, p. 1, February 1971.

[42] R. Lindsey, "Lockheed to halt output of Tristar," *The New York Times*, p. 1, December 1981.

[43] "14 CFR Chapter I Subchapter C Part 25–Airworthiness Standards: Transport Category Airplanes," [Online; accessed April 26, 2022]. [Online]. Available: https://www.ecfr.gov/current/title-14/chapter-I/subchapter-C/part-25

[44] "14 CFR Chapter I Subchapter C Part 33–Airworthiness Standards: Aircraft Engines," [Online; accessed April 27, 2022]. [Online]. Available: https://www.ecfr.gov/current/title-14/chapter-I/subchapter-C/part-33

[45] D. Kellari, E. F. Crawley, and B. G. Cameron, "Architectural Decisions in Commercial Aircraft from the DC-3 to the 787," *Journal of Aircraft*, vol. 55, no. 2, pp. 792–804, 2018.

[46] A. S. J. van Heerden, M. D. Guenov, and A. Molina-Cristóbal, "Evolvability and design reuse in civil jet transport aircraft," *Progress in Aerospace Sciences*, vol. 108, pp. 121–155, 2019.

[47] R. Slayton and G. Spinardi, "Radical innovation in scaling up: Boeing's Dreamliner and the challenge of socio-technical transitions," *Technovation*, vol. 47, pp. 47–58, 2016.

[48] M. Mohaghegh, "Evolution of structures design philosophy and criteria," *Journal of Aircraft*, vol. 42, no. 4, pp. 814–831, 2005.

[49] Federal Aviation Administration, "Composite Aircraft Structure," Advisory Circular AC 20-107B ch. 1.

[50] Society of Automotive Engineers, National Institute for Aviation Research (U.S.), "Composite Materials Handbook–Volume 3. Polymer Matrix Composites–Materials Usage, Design, and Analysis." SAE International on behalf of CMH-17, a division of Wichita State University, 2012, ch. 7, pp. 7–1–7–26, CMH-17-3G.

[51] P. Feraboli, "Composite Materials Strength Determination Within the Current Certification Methodology for Aircraft Structures," *Journal of Aircraft*, vol. 46, no. 4, pp. 1365–1374, 2009.

[52] C. E. Harris, J. H. Starnes Jr., and M. J. Shuart, "Design and Manufacturing of Aerospace Composite Structures, State-of-the-Art Assessment," *Journal of Aircraft*, vol. 39, no. 4, pp. 545–560, 2002.

[53] Federal Aviation Administration, "Powerplant Installation and Propulsion System Component Fire Protection Test Methods, Standards and Criteria with change 1," Advisory Circular AC 20-135 ch. 1.

[54] European Chemicals Agency, An agency of the European Union, "Understanding REACH," [Online; accessed April 25, 2022]. [Online]. Available: https://echa.europa.eu/regulations/reach/understanding-reach

[55] G. Spinardi, "Fire safety regulation: Prescription, performance, and professionalism," *Fire Safety Journal*, vol. 80, pp. 83–88, 2016.

[56] C. Sarkos, "Improvements in Aircraft Fire Safety Derived From FAA Research Over the Last Decade," Federal Aviation Administration, Tech. Rep., May 2011, DOT/FAA/AR-TN11/8.

[57] R. Friedman, "Fire Safety in Spacecraft," *Fire and Materials*, vol. 20, no. 5, pp. 235–243, 1996.

[58] R. A. Denne, "Aircraft and the Fire Problem," *The Aeronautical Journal*, vol. 36, no. 257, pp. 433–443, 1932.

[59] W. G. Glendinning and J. W. Drinkwater, "The Prevention of Fire in Aircraft," *The Aeronautical Journal*, vol. 51, no. 439, pp. 616–650, 1947.

[60] H. L. Hansberry, "Aircraft Fire Protection Developments by the Federal Aviation Administration (1940-1970)," in *Proceedings of the ASME 1970 International Gas Turbine Conference and Products Show, Brussels, Belgium, May 24–28*. The American Society of Mechanical Engineers, 1970.

[61] Royal Aeronautical Society, *Smoke, Fire and Fumes in Transport Aircaft. Past History, Current Risks and Recommended Mitigations. Part 1: Reference*, 5th ed., October 2018.

[62] Transportation Safety Board of Canada, "Aviation Investigation Report, In-Flight Fire Leading to Collision with Water, Swissair Transport Limited McDonnell Douglas MD-11 HB-IWF Peggy's Cove, Nova Scotia 5 nm SW, 2 September 1998," Government of Canada, Tech. Rep., March 2003, Report Number A98H0003.

[63] S. Kinnersley and A. Roelen, "The contribution of design to accidents," *Safety Science*, vol. 45, no. 1-2, pp. 31–60, 2007.

[64] C. Soutis, "Fibre reinforced composites in aircraft construction," *Progress in Aerospace Sciences*, vol. 41, no. 2, pp. 143–151, 2005.

[65] J. G. Quintiere, R. N. Walters, and Crowley, "Flammability Properties of Aircraft Carbon-Fiber Structural Composite," Federal Aviation Administration, Tech. Rep., 2007, DOT/FAA/AR-07/57.

[66] Air Accidents Investigation Branch, "Report on the serious incident to Boeing B787-8, ET-AOP London Heathrow Airport 12 July 2013," Department for Transport, UK, Tech. Rep., August 2015, Aircraft Accident Report 2/2015 (EW/C2013/07/01).

[67] ASTM International, "Standard Terminology of Fire Standards," 2022, E176-21a.

[68] "14 CFR Chapter I Subchapter A Part 1 §1.1 General definitions," [Online; accessed April 26, 2022]. [Online]. Available: https://www.ecfr.gov/current/title-14/chapter-I/subchapter-A/part-1

[69] E. J. Fogle *et al.*, "Compression load failure of aluminum plates due to fire," *Engineering Structures*, vol. 34, pp. 155–162, 2012.

[70] Transportation Safety Board of Canada, "Aviation Investigation Report, Runway Overrun and Fire, Air France Airbus A340-313 F-GLZQ, Toronto/Lester B. Pearson International Airport, Ontario, 02 August 2005," Government of Canada, Tech. Rep., October 2007, Report Number A05H0002.

[71] Federal Aviation Administration, "Installation of Thermal/Acoustic Insulation for Burnthrough Protection," Advisory Circular AC 25.856-2A.

[72] Federal Aviation Administration, "Aircraft Materials Fire Test Handbook," [Online; accessed April 18, 2022]. [Online]. Available: https://www.fire.tc.faa.gov/Handbook

[73] National Transportation Safety Board, "United Airlines Flight 328 Boeing 777 Engine Incident," [Online; accessed April 25, 2022]. [Online]. Available: https://www.ntsb.gov/investigations/Pages/DCA21FA085.aspx

[74] Federal Aviation Administration, "Engine Fire Protection § 33.17," Advisory Circular AC 33.17-1A.

[75] "14 CFR Chapter I Subchapter C Part 25–Appendix F to Part 25," [Online; accessed April 26, 2022]. [Online]. Available: https://www.ecfr.gov/current/title-14/part-25/appendix-Appendix%20F%20to%20Part%2025

[76] V. Babrauskas and R. D. Peacock, "Heat Release Rate: The Single Most Important Variable in Fire Hazard," *Fire Safety Journal*, vol. 18, no. 3, pp. 255–272, 1992.

[77] H. Jiang *et al.*, "The pyrolysis mechanism of phenol formaldehyde resin," *Polymer Degradation and Stability*, vol. 97, 2012.

[78] K. Chetehouna *et al.*, "Release and flammability evaluation of pyrolysis gases from carbon-based composite materials undergoing fire conditions," *Journal of Analytical and applied Pyrolysis*, vol. 134, pp. 136–142, 2018.

[79] H. Sturm *et al.*, "SEM/EDX: Advanced investigation of structured fire residues and residue formation," *Polymer Testing*, vol. 31, no. 5, pp. 606–619, 2012.

[80] B. Schartel, M. Bartholmai, and U. Knoll, "Some comments on the use of cone calorimeter data," *Polymer Degradation and Stability*, vol. 88, no. 3, pp. 540–547, 2005.

[81] B. Schartel and T. R. Hull, "Development of fire-retarded materials—Interpretation of cone calorimeter data," *Fire and Materials*, vol. 31, no. 5, pp. 327–354, 2007.

[82] J. E. Cadena *et al.*, "Uncertainty-based decision-making in fire safety: Analyzing the alternatives," *Journal of Loss Prevention in the Process Industries*, vol. 68, p. 104288, 2020.

[83] R. Abu Talib, Abd *et al.*, "Detailed Investigation of Heat Flux Measurements Made in a Standard Propane-Air Fire-Certification Burner Compared to Levels Derived From

a Low-Temperature Analog Burner," *Journal of Engineering for Gas Turbines and Power*, vol. 127, no. 2, pp. 249–256, 2005.

[84] International Organization for Standardization, "Aircraft–Environmental test procedure for airborne equipment–Resistance to fire in designated fire zones," December 1998, ISO 2685:1998(E).

[85] L. Boulet *et al.*, "Modeling of conjugate heat transfer in a kerosene/air spray flame used for aeronautical fire resistance tests," *Flow, Turbulence and Combustion*, vol. 101, no. 2, pp. 579–602, 2018.

[86] S. Le Neve, "AC 20-135 / ISO 2685. Fire tests on components used in fire zones. Comparison of gas burner to oil burner." in *International Aircraft Materials Fire Test Working Group Meeting, Atlantic City, NJ, USA, October 21–22*, 2008.

[87] ASTM International, "Standard Test Method for Heat and Visible Smoke Release Rates for Materials and Products Using an Oxygen Consumption Calorimeter," 2022, E1354-22.

[88] International Organization for Standardization, "Reaction-to-fire tests–Heat release, smoke production and mass loss rate–Part 1: Heat release rate (cone calorimeter method) and smoke production rate (dynamic measurement)," December 1998, ISO 5660-1:2015.

[89] J. G. Quintiere, "The effects of angular orientation on flame spread over thin materials," *Fire Safety Journal*, vol. 36, no. 3, pp. 291–312, 2001.

[90] R. Filipczak, S. Crowley, and R. E. Lyon, "Heat release rate measurements of thin samples in the OSU apparatus and the cone calorimeter," *Fire Safety Journal*, vol. 40, no. 7, pp. 628–645, 2005.

[91] National Institute of Standards and Technology, "Cone Calorimeter," [Online; accessed June 14, 2022]. [Online]. Available: https://www.nist.gov/laboratories/tools-instruments/cone-calorimeter

[92] V. Babrauskas, "Designing Products for Fire Performance: The State of the Art of Test Methods and Fire Models," *Fire Safety Journal*, vol. 24, no. 3, pp. 299–312, 1995.

[93] J. G. Quintiere, "Scaling Applications in Fire Research," *Fire Safety Journal*, vol. 15, no. 1, pp. 3–29, 1989.

[94] A. L. Brown, "The Decomposition Behavior of Thermoset Carbon Fiber Epoxy Composites in the Fire Environment," in *Proceedings of Combustion Institute Joint US Sections May 19-22*, 2013.

[95] R. E. Lyon, "Fire-Resistant Materials: Research Overview," Federal Aviation Administration, Tech. Rep., December 1997, DOT/FAA/AR-97/99.

[96] A. P. Mouritz *et al.*, "Review of fire structural modelling of polymer composites," *Composites Part A: Applied Science and Manufacturing*, vol. 40, pp. 1800–1814, 2009.

[97] S. Feih *et al.*, "Modelling the tension and compression strengths of polymer laminates in fire," *Composites Science and Technology*, vol. 67, pp. 551–564, 2007.

[98] Z. Yu and A. Zhou, "Fiber Reinforced Polymer Composite Structures in Fire: Modelling and Validation," *Mechanics of Advanced Materials and Structures*, vol. 20, no. 5, pp. 361–372, 2013.

[99] R. E. Lyon *et al.*, "Material properties and fire test results," *Fire and Materials*, vol. 38, no. 2, pp. 264–278, 2014.

[100] R. E. Lyon and N. Safronava, "A Probabilistic Analysis of Pass/Fail Fire Tests," Federal Aviation Administration, Tech. Rep., October 2013, DOT/FAA/TC-12/13.

[101] S. Eibl, "Influence of unwoven roving and woven fabric carbon fiber reinforcements on reaction-to-fire properties of polymer matrix composites," *Fire and Materials*, vol. 44, no. 4, pp. 557–572, 2020.

[102] D. Q. Dao *et al.*, "Thermal degradation of epoxy resin/carbon fiber composites: Influence of carbon fiber fraction on the fire reaction properties and on the gaseous species release," *Fire and Materials*, vol. 40, no. 1, pp. 27–47, 2016.

[103] Y. Carpier *et al.*, "Study of thermomechanical coupling in carbon fibers woven-ply reinforced thermoplastic laminates: Tensile behavior under radiant heat flux," *Polymer Composites*, vol. 41, no. 9, pp. 3552–3563, 2020.

[104] S. Bourbigot and X. Flambard, "Heat Resistance and Flammability of High Performance Fibres: A Review," *Fire and Materials*, vol. 26, no. 4-5, pp. 155–168, 2002.

[105] T. Bhat *et al.*, "Fire structural resistance of basalt fibre composite," *Composites Part A: Applied Science and Manufacturing*, vol. 71, pp. 107–115, 2015.

[106] T. Bhat *et al.*, "Tensile properties of plant fibre-polymer composites in fire," *Fire and Materials*, vol. 41, no. 8, pp. 1040–1050, 2017.

[107] J. R. Brown and Z. Mathys, "Reinforcement and matrix effects on the combustion properties of glass reinforced polymer composites," *Composites Part A: Applied Science and Manufacturing*, vol. 28, no. 7, pp. 675–681, 1997.

[108] Y. M. Ghazzawi, A. F. Osorio, and M. T. Heitzmann, "Fire performance of continuous glass fibre reinforced polycarbonate composites: The effect of fibre architecture on the fire properties of polycarbonate composites," *Journal of Composite Materials*, vol. 53, no. 12, pp. 1705–1715, 2019.

[109] Y. M. Ghazzawi, A. F. Osorio, and M. T. Heitzmann, "The effect of fibre length and fibre type on the fire performance of thermoplastic composites: The behaviour of polycarbonate as an example of a charring matrix," *Construction and Building Materials*, vol. 234, p. 117889, 2020.

[110] Y. Ghazzawi *et al.*, "The effect of fibre length and matrix modification on the fire performance of thermoplastic composites: The behaviour of PP as an example of non-charring matrix," *Journal of Thermoplastic Composite Materials*, 2020.

[111] A. Anjang, A. P. Mouritz, and S. Feih, "Influence of fibre orientation on the tensile performance of sandwich composites in fire," *Composites Part A: Applied Science and Manufacturing*, vol. 100, pp. 342–351, 2017.

[112] S. Eibl, "Influence of carbon fibre orientation on reaction-to-fire properties of polymer matrix composites," *Fire and Materials*, vol. 36, no. 4, pp. 309–324, 2012.

[113] S. Eibl and D. Swanson, "Influence of out-of-plane fiber orientation on reaction-to-fire properties of carbon fiber reinforced polymer matrix composites," *Fire and Materials*, vol. 42, no. 2, pp. 234–243, 2018.

[114] Y. Carpier *et al.*, "About the tensile mechanical behaviour of carbon fibers fabrics reinforced thermoplastic composites under very high temperature conditions," *Composites Part B: Engineering*, vol. 181, p. 107586, 2020.

[115] A. Anjang *et al.*, "Tension modelling and testing of sandwich composites in fire," *Composite Structures*, vol. 113, pp. 437–445, 2014.

[116] A. Anjang *et al.*, "Post-fire mechanical properties of sandwich composite structures," *Composite Structures*, vol. 132, pp. 1019–1028, 2015.

[117] A. Anjang *et al.*, "Deterioration of the fire structural resistance of sandwich composite under tension due to water absorption," *Composites Part A: Applied Science and Manufacturing*, vol. 87, pp. 263–270, 2016.

[118] A. G. Gibson *et al.*, "Laminate Theory Analysis of Composites under Load in Fire," *Journal of Composite Materials*, vol. 40, no. 7, pp. 639–658, 2006.

[119] L. A. Burns, S. Feih, and A. P. Mouritz, "Compression failure of carbon fiber-epoxy laminates in fire," *Journal of Aircraft*, vol. 47, no. 2, pp. 528–533, 2010.

[120] A. E. Elmughrabi, M. Robinson, and A. G. Gibson, "Effect of stress on the fire reaction properties of polymer composite laminates," *Polymer Degradation and Stability*, vol. 93, pp. 1877–1883, 2008.

[121] A. Benelfellah *et al.*, "Effect of a coupled thermomechanical loading on the residual mechanical strength and on the surface temperature of wound carbon/epoxy composite," *Journal of Composite Materials*, vol. 51, no. 22, pp. 3137–3147, 2017.

[122] V. Hindasageri, R. P. Vedula, and S. V. Prabhu, "Heat transfer distribution for impinging methane–air premixed flame jets," *Applied Thermal Engineering*, vol. 73, no. 1, pp. 461–473, 2014.

[123] T. R. Marker, "Full-Scale Test Evaluation of Aircraft Fuel Fire Burnthrough Resistance Improvements," Federal Aviation Administration, Tech. Rep., January 1999, dOT/FAA/AR-98/52.

[124] J. J. Moyer, "Investigation of Experimental Lightweight Firewall Materials for A/C Engine Bay Applications," AFWAL/AFSC – Wright-Patterson AFB, OH, Tech. Rep., April 1985, AFWAL-TR-84-2082.

[125] L. Lebel, S. Turenne, and R. Boukhili, "An Experimental Apparatus and Procedure for the Simulation of Thermal Stresses in Gas Turbine Combustion Chamber Panels Made of Ceramic Matrix Composites," *Journal of Engineering for Gas Turbines and Power*, vol. 139, no. 9, 2017.

[126] J. Mills-Brown *et al.*, "The development of a high temperature tensile testing rig for composite laminates," *Composites Part A: Applied Science and Manufacturing*, vol. 52, pp. 99–105, 2013.

[127] J. Mills-Brown *et al.*, "Thermal and tensile properties of polysialate composites," *Ceramics International*, vol. 39, no. 8, pp. 8917–8924, 2013.

[128] T. T. Kim *et al.*, "Simultaneous Fatigue and Combustion Exposure of a SiC/SiC Ceramic Matrix Composite," *Journal of Composite Materials*, vol. 44, no. 25, pp. 2991–3016, 2010.

[129] T. Pelzmann *et al.*, "Effect of flame chemistry on the thermal degradatin of carbon fibre epoxy composites," 2022, Submitted for review.

[130] J. Bartlett and C. Stratford, "Fire Resistance Certification of Aircraft Composite Materials," *Practical Failure Analysis*, vol. 1, no. 6, pp. 37–43, 2001.

[131] A. Johnston *et al.*, "Evaluation of Fire Resistance of Composite Materials for Aircraft Structural Applications," in *12th International Conference on Composite Materials (ICCM 12), Paris, France, July 7–9.* International Committee on Composite Materials, 1999.

[132] A. G. Gibson *et al.*, "The Integrity of Polymer Composites During and After Fire," *Journal of Composite Materials*, vol. 38, no. 15, pp. 1283–1307, 2004.

[133] P. Tranchard *et al.*, "Fire behaviour of carbon fibre epoxy composite for aircraft: Novel test bench and experimental study," *Journal of Fire Sciences*, vol. 33, no. 3, pp. 247–266, 2015.

[134] P. A. Cutter *et al.*, "A New Small Scale Fire Resistance Test Method for Composite Materials," in *17th International Conference on Composite Materials (ICCM 17), Edinburgh, Scotland, July 27-31.* International Committee on Composite Materials, 2009.

[135] P. Di Modica, G. Kotsikos, and A. G. Gibson, "Fire Behaviour of Carbon Fibre Composites Under Load," in *16th European Conference on Composite Materials (ECCM16), Seville, Spain, June 22–26*, 2014.

[136] K. Grigoriou and A. P. Mouritz, "Comparative assessment of the fire structural performance of carbon-epoxy composite and aluminium alloy used in aerospace structures," *Materials and Design*, vol. 108, pp. 699–706, 2016.

[137] T. J. Aspinall *et al.*, "The Thermomechanical Behaviour of Carbon Fibre Reinforced Polymer Exposed to Fire Conditions," in *Defence and Security Doctoral Symposium (DSDS20), Cranfield University, 10 Nov*, 2020.

[138] B. Schartel *et al.*, "Assessing the structural integrity of carbon-fibre sandwich panels in fire: Bench-scale approach," *Composites Part B: Engineering*, vol. 164, pp. 82–89, 2019.

[139] M. F. Ashby, "The Design Process," in *Materials Selection in Mechanical Design*, 4th ed. Butterworth-Heinemann, 2011, ch. 2, pp. 15–29.

[140] M. H. Sadraey, "Systems Engineering Approach," in *Aircraft Design: A Systems Engineering Approach*. John Wiley & Sons, 2013, ch. 2, pp. 19–48.

[141] M. Ashby, "Designing architectured materials," *Scripta Materialia*, vol. 68, no. 1, pp. 4–7, 2013.

[142] A. H. Epstein, "Aircraft engines' needs from combustion science and engineering," *Combustion and Flame*, vol. 159, no. 5, pp. 1791–1792, 2012.

[143] M. H. Caldwell, "Material selection for the new-technology commercial transport–The designer's dilemma," in *Aircraft Design, Systems and Technology Meeting, Fort Worth, TX, 17–19 October*, 1983, Paper 2477.

[144] R. R. Boyer *et al.*, "Materials considerations for aerospace applications," *MRS Bulletin*, vol. 40, no. 12, pp. 1055–1066, 2015.

[145] M. F. Ashby *et al.*, "Selection strategies for materials and processes," *Materials & Design*, vol. 25, no. 1, pp. 51–67, 2004.

[146] G. Sjöberg, "Aircraft Engine Structure Materials," 2008, [Online; accessed June 4, 2022]. [Online]. Available: https://www.sto.nato.int/publications/STO%20Educational%20Notes/RTO-EN-AVT-207/EN-AVT-207-13.pdf

[147] A. G. Miller, D. T. Lovell, and J. C. Seferis, "The evolution of an aerospace material: Influence of design, manufacturing and in-service performance," *Composite Structures*, vol. 27, no. 1-2, pp. 193–206, 1994.

[148] C. E. Harris, J. H. Starnes Jr., and M. J. Shuart, "Advances Durability and Damage Tolerance Design and Analysis Methods for Composite Structures - Lessons Learned from NASA Technology Development Programs," National Aeronautics and Space Administration, Tech. Rep., 2003, NASA/TM-2003-212420.

[149] Federal Aviation Administration, "Lessons Learned from Civil Aviation Accidents," Accessed on June 24$^{\text{th}}$, 2020. [Online]. Available: https://lessonslearned.faa.gov/index.cfm

[150] "Lesson Info 735 - Material Selection Practices," 1999, [Online; accessed April 10, 2022]. [Online]. Available: https://llis.nasa.gov/lesson/735

[151] M. Natali, J. M. Kenny, and L. Torre, "Science and Technology of polymeric ablative materials for thermal protection systems and propulsion devices: A review," *Progress in Materials Science*, vol. 84, pp. 192–275, 2016.

[152] O. Yaqub, "Serendipity: Towards a taxonomy and a theory," *Research Policy*, vol. 47, no. 1, pp. 169–179, 2018.

[153] F. Takahashi *et al.*, "Thermal response characteristics of fire blanket materials," *Fire and Materials*, vol. 38, no. 6, pp. 609–638, 2014.

[154] M. Jimenez, S. Duquesne, and S. Bourbigot, "High-throughput fire testing for intumescent coatings," *Industrial & Engineering Chemistry Research*, vol. 45, no. 22, pp. 7475–7481, 2006.

[155] R. Friedman, B. Jackson, and S. Olson, "Testing and Selection of Fire-Resistant Materials for Spacecraft Use," National Aeronautics and Space Administration, Tech. Rep., 2000, NASA/TM-2000-209773.

[156] National Aeronautics and Space Administration, "Flammability, Offgassing, and Compatiblity Requirements and Test Procedures," National Aeronautics and Space Administration, Tech. Rep., 2011, NASA-STD-6001B Change 2.

[157] W. T. B. Kelvin, *Popular lectures and addresses*. Macmillan and Company, 1891, vol. 1.

[158] S. Kawabata and M. Niwa, "Fabric Performance in Clothing and Clothing Manufacture," *Journal of the Textile Institute*, vol. 80, no. 1, pp. 19–50, 1989.

[159] T. S. Kuhn, "The function of measurement in modern physical science," *Isis*, vol. 52, no. 2, pp. 161–193, 1961.

[160] J. M. Watts, "Fuzzy fire safety," *Fire Technology*, vol. 31, no. 3, pp. 193–194, 1995.

[161] A. Tversky and D. Kahneman, "Judgment under Uncertainty: Heuristics and Biases: Biases in judgments reveal some heuristics of thinking under uncertainty," *Science*, vol. 185, no. 4157, pp. 1124–1131, 1974.

[162] D. Kahneman and A. Tversky, "Choices, Values and Frames," *American Psychologist*, vol. 39, no. 4, pp. 341–350, 1984.

[163] H. A. Donegan, "Decision Analysis," in *SFPE Handbook of Fire Protection Engineering*. Springer, 2016, ch. 77, pp. 3048–3072.

[164] E. Triantaphyllou and S. H. Mann, "An examination of the effectiveness of multi-dimensional decision-making methods: A decision-making paradox," *Decision Support Systems*, vol. 5, no. 3, pp. 303–312, 1989.

[165] P. Chatterjee and S. Chakraborty, "Material selection using preferential ranking methods," *Materials and Design*, vol. 35, pp. 384–393, 2012.

[166] V. M. Athawale and S. Chakraborty, "Material selection using multi-criteria decision-making methods: a comparative study," *Proceedings of the Institution of Mechanical Engineers, Part L: Journal of Materials: Design and Applications*, vol. 226, no. 4, pp. 266–285, 2012.

[167] O. Akaa *et al.*, "A group-AHP decision analysis for the selection of applied fire protection to steel structures," *Fire Safety Journal*, vol. 86, pp. 95–105, 2016.

[168] N. P. Suh, "Axiomatic Design of Mechanical Systems," *Journal of Mechanical Design*, vol. 117, no. B, 1995.

[169] N. P. Suh, *Axiomatic design: advances and applications*. Oxford University Press, 2001.

[170] N. Ananthkrishnan, "Conceptual Design of an Aerospace Vehicle Controller Using Axiomatic Theory," *Journal of Aircraft*, vol. 47, no. 6, pp. 2149–2151, 2010.

[171] C. A. Brown and R. Henley, "Metrics for developing functional requirements and selecting design parameters in axiomatic design," *Procedia CIRP*, vol. 53, pp. 113–118, 2016.

[172] S. Cebi and C. Kahraman, "Extension of axiomatic design principles under fuzzy environment," *Expert Systems with Applications*, vol. 37, no. 3, pp. 2682–2689, 2010.

[173] S. Cebi and C. Kahraman, "Indicator design for passenger car using fuzzy axiomatic design principles," *Expert Systems with Applications*, vol. 37, no. 9, pp. 6470–6481, 2010.

[174] L. A. Zadeh, "Fuzzy Sets," *Information and Control*, vol. 8, pp. 338–353, 1965.

[175] R. E. Bellman and L. A. Zadeh, "Decision-making in a fuzzy environment," *Management Science*, vol. 17, no. 4, pp. B–141–B–164, 1970.

[176] T. Aouam, S. I. Chang, and E. S. Lee, "Fuzzy MADM: An outranking method," *European Journal of Operational Research*, vol. 145, no. 2, pp. 317–328, 2003.

[177] G. Bruno, E. Esposito, and A. Genovese, "A model for aircraft evaluation to support strategic decisions," *Expert Systems with Applications*, vol. 42, no. 13, pp. 5580–5590, 2015.

[178] J. V. Carnahan, D. L. Thurston, and T. Liu, "Fuzzing Ratings for Multiattribute Design Decision-Making," *Journal of Engineering Materials and Technology*, vol. 120, no. 2, 1994.

[179] S.-H. Chen, "Ranking fuzzy numbers with maximizing set and minimizing set," *Fuzzy Sets and Systems*, vol. 17, no. 2, pp. 113–129, 1985.

[180] R. V. Rao, "A material selection model using graph theory and matrix approach," *Materials Science and Engineering: A*, vol. 431, no. 1-2, pp. 248–255, 2006.

[181] S. Abdoli, "Application of fuzzy-logic for design assessment of complex engineering systems in the early design stages," *Journal of Engineering Design*, vol. 33, no. 3, pp. 234–258, 2022.

[182] G. Athanasopoulos, C. Romeva Riba, and C. Athanasopoulou, "A decision support system for coating selection based on fuzzy logic and multi-criteria decision making," *Expert Systems with Applications*, vol. 36, no. 8, pp. 10 848–10 853, 2009.

[183] F. J. Dodd and H. A. Donegan, "Prioritisation methodologies in fire safety evaluation," *Fire Technology*, vol. 30, no. 2, pp. 232–249, 1994.

[184] B. A. Newcomb, "Processing, structure, and properties of carbon fibers," *Composites Part A: Applied Science and Manufacturing*, vol. 91, pp. 262–282, 2016.

[185] H. Marsh and J. A. Griffiths, "A high resolution electron microscopy study of graphitization of graphitizable carbon," in *International Symposium on Carbon. Carbon Society of Japan. Annual meeting. 9*, 1982, pp. 81–83.

[186] K. Morita *et al.*, "Characterization of commercially available PAN (polyacrylonitrile)-based carbon fibers," *Pure and Applied Chemistry*, vol. 58, no. 3, pp. 455–468, 1986.

[187] E. J. Hippo, N. Murdie, and A. Hyjazie, "The role of active sites in the inhibition of gas-carbon reactions," *Carbon*, vol. 27, no. 5, pp. 689–695, 1989.

[188] L. Qiu *et al.*, "The effect of grain size on the lattice thermal conductivity of an individual polyacrylonitrile-based carbon fiber," *Carbon*, vol. 51, pp. 265–273, 2013.

[189] F. R. Barnet and M. K. Norr, "A three-dimensional structural model for a high modulus pan-based carbon fibre," *Composites*, vol. 7, no. 2, pp. 93–99, 1976.

[190] F. R. Barnet and M. K. Norr, "Carbon fiber etching in an oxygen plasma," *Carbon*, vol. 11, no. 4, pp. 281–288, 1973.

[191] S. C. Bennett, D. J. Johnson, and W. Johnson, "Strength-structure relationships in PAN-based carbon fibres," *Journal of Materials Science*, vol. 18, no. 11, pp. 3337–3347, 1983.

[192] M. Guigon, A. Oberlin, and G. Desarmot, "Microtexture and Structure of Some High Tensile Strength, PAN-Base Carbon Fibres," *Fibre Science and Technology*, vol. 20, no. 1, pp. 55–72, 1984.

[193] M. Guigon, A. Oberlin, and G. Desarmot, "Microtexture and Structure of Some High-modulus, PAN-Base Carbon Fibres," *Fibre Science and Technology*, vol. 20, no. 3, pp. 177–198, 1984.

[194] M. Terrones *et al.*, "Graphene and graphite nanoribbons: Morphology, properties, synthesis, defects and applications," *Nano Today*, vol. 5, no. 4, pp. 351–372, 2010.

[195] J. L. Figueiredo and M. F. R. Pereira, "The role of surface chemistry in catalysis with carbons," *Catalysis Today*, vol. 150, no. 1-2, pp. 2–7, 2010.

[196] H. P. Boehm, "Free radicals and graphite," *Carbon*, vol. 50, no. 9, pp. 3154–3157, 2012.

[197] M. Guigon and A. Oberlin, "Heat-treatment of High Tensile Strength PAN-based Carbon Fibres: Microtexture, Structure and Mechanical Properties," *Composites Science and Technology*, vol. 27, no. 1, pp. 1–23, 1986.

[198] F. Yang *et al.*, "Effect of amorphous carbon on the tensile behavior of polyacrylonitrile (PAN)-based carbon fibers," *Journal of Materials Science*, vol. 54, no. 11, pp. 8800–8813, 2019.

[199] R. Gadow and M. Jiménez, "Carbon fiber-reinforced carbon composites for aircraft brakes," *American Ceramic Society Bulletin*, vol. 98, no. 6, pp. 28–34, 2019.

[200] M. Bevilacqua, A. Babutskyi, and A. Chrysanthou, "A review of the catalytic oxidation of carbon–carbon composite aircraft brakes," *Carbon*, vol. 95, pp. 861–869, 2015.

[201] G. L. Vignoles, Y. Aspa, and M. Quintard, "Modelling of carbon–carbon composite ablation in rocket nozzles," *Composites Science and Technology*, vol. 70, no. 9, pp. 1303–1311, 2010.

[202] D. A. Scola and B. L. Laube, "A Comparison of the Thermo-Oxidative Stability of Commercial Graphite Fibers for Composite Applications," in *SAE Transactions*. SAE International, 1988, Technical Paper 880111.

[203] M. C. Halbig *et al.*, "Oxidation Kinetics and Stress Effects for the Oxidation of Continuous Carbon Fibers within a Microcracked C/SiC Ceramic Matrix Composite," *Journal of the American Ceramic Society*, vol. 91, no. 2, pp. 519–526, 2008.

[204] X. Luo, J.-C. Robin, and S. Yu, "Effect of temperature on graphite oxidation behavior," *Nuclear Engineering and Design*, vol. 227, no. 3, pp. 273–280, 2004.

[205] M. Balden *et al.*, "Oxidative erosion of graphite in air between 600 and 1000 K," *Journal of Nuclear Materials*, vol. 341, no. 1, pp. 31–44, 2005.

[206] C. I. Contescu *et al.*, "Practical aspects for characterizing air oxidation of graphite," *Journal of Nuclear Materials*, vol. 381, no. 1-2, pp. 15–24, 2008.

[207] J. J. Kane *et al.*, "Understanding the reaction of nuclear graphite with molecular oxygen: Kinetics, transport, and structural evolution," *Journal of Nuclear Materials*, vol. 493, pp. 343–367, 2017.

[208] C. P. Fenimore and G. W. Jones, "Oxidation of soot by hydroxyl radicals," *The Journal of Physical Chemistry*, vol. 71, no. 3, pp. 593–597, 1967.

[209] P. Toth *et al.*, "Real-time, in situ, atomic scale observation of soot oxidation," *Carbon*, vol. 145, pp. 149–160, 2019.

[210] C. K. Law, *Combustion Physics*. Cambridge university press, 2006.

[211] K. Annamalai and W. Ryan, "Interactive processes in gasification and combustion—-II. Isolated carbon, coal and porous char particles," *Progress in Energy and Combustion Science*, vol. 19, no. 5, pp. 383–446, 1993.

[212] R. J. Baxter and P. Hu, "Insight into why the Langmuir–Hinshelwood mechanism is generally preferred," *Journal of Chemical Physics*, vol. 116, no. 11, pp. 4379–4381, 2002.

[213] H. Chelliah *et al.*, "Modeling of Graphite Oxidation in a Stagnation-Point Flow Field Using Detailed Homogeneous and Semiglobal Heterogeneous Mechanisms with Comparisons to Experiments," *Combustion and Flame*, vol. 104, no. 4, pp. 469–480, 1996.

[214] G. Dixon-Lewis, D. Bradley, and S. El-Din Habik, "Oxidation Rates of Carbon Particles in Methane-Air Flames," *Combustion and Flame*, vol. 86, no. 1-2, pp. 12–20, 1991.

[215] F. Walker Jr, P. L.and Rusinko Jr. and L. Austin, "Gas Reactions of Carbon," in *Advances in Catalysis*, D. Eley, P. Selwood, and P. B. Weisz, Eds. Academic Press, 1959, vol. XI, pp. 133–221.

[216] P. McMahon, "Oxidative Resistance of Carbon Fibers and their Composites," in *Advanced Composite Materials—Environmental Effects*, J. Vinson, Ed. ASTM International, 1978.

[217] H. H. Gibbs, R. C. Wendt, and F. C. Wilson, "Carbon fiber structure and stability studies," *Polymer Engineering and Science*, vol. 19, no. 5, pp. 342–349, 1979.

[218] B. H. Eckstein, "The oxidation of carbon fibres in air between 230° and 375° C," *Fibre Science and Technology*, vol. 14, no. 2, pp. 139–156, 1981.

[219] A. B. Fuertes, G. Marban, and J. Muñiz, "Modelling the gasification of carbon fibres," *Carbon*, vol. 34, no. 2, pp. 223–230, 1996.

[220] S. M. Gee and J. A. Little, "Oxidation behaviour and protection of carbon/carbon composites," *Journal of Materials Science*, vol. 26, no. 4, pp. 1093–1100, 1991.

[221] J. Langot *et al.*, "Multi-physics modeling of the ignition of polymer matrix composites (PMCs) exposed to fire," *Fire Safety Journal*, vol. 122, p. 103312, June 2021.

[222] ASTM International, "Standard Test Method for Thermal Oxidative Resistance of Carbon Fibers," 2015, D4102-82(2015).

[223] Y. Tong *et al.*, "Oxidation kinetics of polyacrylonitrile-based carbon fibers in air and the effect on their tensile properties," *Corrosion Science*, vol. 53, no. 8, pp. 2484–2488, 2011.

[224] S. Feih and A. P. Mouritz, "Tensile properties of carbon fibres and carbon fibre-polymer composites in fire," *Composites Part A: Applied Science and Manufacturing*, vol. 43, no. 5, pp. 765–772, 2012.

[225] X. Bertran *et al.*, "Oxidation Behavior of PAN-based Carbon Fibers and the Effect on Mechanical Properties," *Oxidation of Metals*, vol. 80, no. 3, pp. 299–309, 2013.

[226] I. M. K. Ismail and W. C. Hurley, "Modelling carbon fibers oxidation in air at constant heating rates," *Carbon*, vol. 30, no. 3, pp. 419–427, 1992.

[227] N. R. Laine, F. J. Vastola, and P. L. Walker Jr., "The importance of active surface area in the carbon-oxygen reaction," *The Journal of Physical Chemistry*, vol. 67, no. 10, pp. 2030–2034, 1963.

[228] P. Ehrburger, F. Louys, and J. Lahaye, "The concept of active sites applied to the study of carbon reactivity," *Carbon*, vol. 27, no. 3, pp. 389–393, 1989.

[229] I. M. K. Ismail, "Structure and active surface area of carbon fibers," *Carbon*, vol. 25, no. 5, pp. 653–662, 1987.

[230] I. M. K. Ismail, "On the reactivity, structure, and porosity of carbon fibers and fabrics," *Carbon*, vol. 29, no. 6, pp. 777–792, 1991.

[231] S.-M. Oh *et al.*, "Microstructural changes of polyacrylonitrile-based carbon fibers (T300 and T700) due to isothermal oxidation (1): focusing on morphological changes using scanning electron microscopy," *Carbon letters*, vol. 18, pp. 18–23, 2016.

[232] A. V. Govorov *et al.*, "Study of Different Types of Carbon Fiber Oxidation Kinetics," *Refractories and Industrial Ceramics*, vol. 56, no. 6, pp. 605–609, 2016.

[233] P. M. Ajayan *et al.*, "Opening carbon nanotubes with oxygen and implications for filling," *Nature*, vol. 362, no. 6420, pp. 522–525, 1993.

[234] T. W. Ebbesen *et al.*, "Purification of nanotubes," *Nature*, vol. 367, no. 6463, pp. 519–519, 1994.

[235] I. M. K. Ismail and P. L. Walker Jr., "Detection of low temperature carbon gasification using DSC and TGA," *Carbon*, vol. 27, no. 4, pp. 549–559, 1989.

[236] M. L. Lieberman and G. T. Noles, "Impurity effects in carbon fibres," *Journal of Materials Science*, vol. 7, no. 6, pp. 654–662, 1972.

[237] G. Blyholder, J. S. Binford Jr., and H. Eyring, "A kinetic theory for the oxidation of carbonized filaments," *The Journal of Physical Chemistry*, vol. 62, no. 3, pp. 263–267, 1958.

[238] H. Amariglio and X. Duval, "Étude de la combustion catalytique du graphite," *Carbon*, vol. 4, no. 3, pp. 323–332, 1966.

[239] R. G. Iacocca and D. J. Duquette, "The catalytic effect of platinum on the oxidation of carbon fibres," *Journal of Materials Science*, vol. 28, no. 4, pp. 1113–1119, 1993.

[240] L. Sousa Lobo and S. A. C. Carabineiro, "Kinetics and mechanism of catalytic carbon gasification," *Fuel*, vol. 183, pp. 457–469, 2016.

[241] M. T. Wright *et al.*, "Composite Materials in Aircraft Mishaps Involving Fire: A Literature Review," Naval Air Warfare Center Weapons Division, China Lake, CA, Tech. Rep., June 2003, NAWCWD TP 8552.

[242] R. A. Arnold and J. M. Hill, "Catalysts for gasification: a review," *Sustainable Energy & Fuels*, vol. 3, no. 3, pp. 656–672, 2019.

[243] K. Otto, L. Bartosiewicz, and M. Shelef, "Catalytic steam gasification of graphite: effects of calcium, strontium, and barium with and without sulfur," *Carbon*, vol. 17, no. 4, pp. 351–357, 1979.

[244] H. Wang *et al.*, "Microstructural evolution and oxidation resistance of polyacrylonitrile-based carbon fibers doped with boron by the decomposition of B_4C," *Carbon*, vol. 56, pp. 296–308, 2013.

[245] X. Wu and L. R. Radovic, "Inhibition of catalytic oxidation of carbon/carbon composites by boron-doping," *Carbon*, vol. 43, no. 8, pp. 1768–1777, 2005.

[246] X. Wu and L. R. Radovic, "Inhibition of catalytic oxidation of carbon/carbon composites by phosphorus," *Carbon*, vol. 44, no. 1, pp. 141–151, 2006.

[247] L.-G. Tang, "Influence of boron treatment on oxidation of carbon fiber in air," *Journal of Applied Polymer Science*, vol. 59, no. 6, pp. 915–921, 1996.

[248] P. Sun *et al.*, "A Review of Battery Fires in Electric Vehicles," *Fire Technology*, pp. 1–50, 2020.

[249] K. E. Evans, B. D. Caddock, and K. L. Ainsworth, "Statistical changes during the corrosion of glass fibre bundles," *Journal of Materials Science*, vol. 23, no. 8, pp. 2926–2930, 1988.

[250] B. D. Caddock, K. E. Evans, and D. Hull, "Stress-corrosion failure envelopes for E-glass fibre bundles," *Journal of Materials Science*, vol. 25, no. 5, pp. 2498–2502, 1990.

[251] Y. Yin *et al.*, "The oxidation behaviour of carbon fibres," *Journal of Materials Science*, vol. 29, no. 8, pp. 2250–2254, 1994.

[252] D.-H. Kim *et al.*, "Analysis of the Microstructure and Oxidation Behavior of Some Commercial Carbon Fibers," *Journal of the Korean Chemical Society*, vol. 55, no. 5, pp. 819–823, 2011.

[253] J. Alcañiz Monge *et al.*, "Effect of the activating gas on tensile strength and pore structure of pitch-based carbon fibres," *Carbon*, vol. 32, no. 7, pp. 1277–1283, 1994.

[254] F. Vautard *et al.*, "Influence of surface defects on the tensile strength of carbon fibers," *Applied Surface Science*, vol. 322, pp. 185–193, 2014.

[255] J. G. Alexander, "Development of a Fire Test Facility for Graphite Fiber-Reinforced Composites," National Aeronautics and Space Administration, Tech. Rep., June 1980, NASA-CR-159193.

[256] S. Eibl, "Potential for the formation of respirable fibers in carbon fiber reinforced plastic materials after combustion," *Fire and Materials*, vol. 41, no. 7, pp. 808–816, 2017.

[257] J. H. Bechtel and R. E. Teets, "Hydroxyl and its concentration profile in methane-air flames," *Applied Optics*, vol. 18, no. 24, pp. 4138–4144, 1979.

[258] D. Bradley *et al.*, "The Oxidation of Graphite Powder in Flame Reaction Zones," in *Twentieth Symposium (International) on Combustion / The Combustion Institute*, vol. 20, no. 1. Elsevier, 1985, pp. 931–940.

[259] W. Rybak, P. Chambrion, and J. Lahaye, "Oxidation of carbon black particles in a premixed flame under pressure," *Carbon*, vol. 33, no. 3, pp. 259–264, 1995.

[260] S. M. Lee *et al.*, "Defect-Induced Oxidation of Graphite," *Physical Review Letters*, vol. 82, no. 1, pp. 217–220, 1999.

[261] J. R. Hahn, "Kinetic study of graphite oxidation along two lattice directions," *Carbon*, vol. 43, no. 7, pp. 1506–1511, 2005.

[262] L. Hao *et al.*, "Study of structure–mechanical heterogeneity of polyacrylonitrile-based carbon fiber monofilament by plasma etching-assisted radius profiling," *Carbon*, vol. 114, pp. 317–323, 2017.

[263] C. U. Pittman Jr. *et al.*, "Chemical modification of carbon fiber surfaces by nitric acid oxidation followed by reaction with tetraethylenepentamine," *Carbon*, vol. 35, no. 3, pp. 317–331, 1997.

[264] P. Marshall and J. Price, "Topography of carbon fibre surfaces," *Composites*, vol. 22, no. 5, pp. 388–393, 1991.

[265] R. T. K. Baker, "Factors controlling the mode by which a catalyst operates in the graphite-oxygen reaction," *Carbon*, vol. 24, no. 6, pp. 715–717, 1986.

[266] R. T. K. Baker, "The Relationship between Particle Motion on a Graphite Surface and Tammann Temperature," *Journal of Catalysis*, vol. 78, no. 2, pp. 473–476, 1982.

[267] E. G. Hughes and J. M. Thomas, "Topography of oxidized graphite crystals," *Nature*, vol. 193, no. 4818, pp. 838–840, 1962.

[268] J. M. Thomas and E. E. G. Hughes, "Localized oxidation rates on graphite surfaces by optical microscopy," *Carbon*, vol. 1, no. 2, pp. 209–214, 1964.

[269] D. E. Rosner and H. D. Allendorf, "Comparative Studies of the Attack of Pyrolytic and Isotropic Graphite by Atomic and Molecular Oxygen at High Temperatures," *AIAA Journal*, vol. 6, no. 4, pp. 650–654, 1968.

[270] K. T. Nicholson, T. K. Minton, and S. J. Sibener, "Spatially Anisotropic Etching of Graphite by Hyperthermal Atomic Oxygen," *The Journal of Physical Chemistry B*, vol. 109, no. 17, pp. 8476–8480, 2005.

[271] X. Chu and L. D. Schmidt, "Gasification of graphite studied by scanning tunneling microscopy," *Carbon*, vol. 29, no. 8, pp. 1251–1255, 1991.

[272] J. R. Hahn *et al.*, "Mechanistic Study of Defect-Induced Oxidation of Graphite," *The Journal of Physical Chemistry B*, vol. 103, no. 45, pp. 9944–9951, 1999.

[273] R. Fu, S. Schmitt, and A. Martin, "Thermo-Chemical-Structural Modeling of Carbon Fiber Pitting and Failure Mechanism," in *AIAA SciTech Forum, San Diego, CA & Virtual, January 3–7*. American Institute of Aeronautics and Astronautics, 2022.

[274] D. Loidl *et al.*, "Skin-core structure and bimodal Weibull distribution of the strength of carbon fibers," *Carbon*, vol. 45, no. 14, pp. 2801–2805, 2007.

[275] T.-H. Ko *et al.*, "The effects of activation by carbon dioxide on the mechanical properties and structure of PAN-based activated carbon fibers," *Carbon*, vol. 30, no. 4, pp. 647–655, 1992.

[276] E. L. Evans, R. J. M. Griffiths, and J. M. Thomas, "Kinetics of Single-Layer Graphite Oxidation: Evaluation by Electron Microscopy," *Science*, vol. 171, no. 3967, pp. 174–175, 1971.

[277] X. Chu *et al.*, "Catalyzed Carbon Gasification Studied by Scanning Tunneling Microscopy and Atomic Force Microscopy," *Journal of Catalysis*, vol. 140, no. 2, pp. 543–556, 1993.

[278] D. Cho, J. Y. Lee, and B. I. Yoon, "Microscopic observations of the ablation behaviours of carbon fibre/phenolic composites," *Journal of Materials Science Letters*, vol. 12, no. 24, pp. 1894–1896, 1993.

[279] D. Cho and B. I. Yoon, "Microstructural interpretation of the effect of various matrices on the ablation properties of carbon-fiber-reinforced composites," *Composites Science and Technology*, vol. 61, no. 2, pp. 271–280, 2001.

[280] G. Dobrik, L. Tapasztó, and L. P. Biró, "Selective etching of armchair edges in graphite," *Carbon*, vol. 56, pp. 332–338, 2013.

[281] H. Chang and A. J. Bard, "Formation of Monolayer Pits of Controlled Nanometer Size on Highly Oriented Pyrolytic Graphite by Gasification Reactions as Studied by Scanning Tunneling Microscopy," *Journal of the American Chemical Society*, vol. 112, no. 11, pp. 4598–4599, 1990.

[282] H. Chang and A. J. Bard, "Scanning Tunneling Microscopy Studies of Carbon-Oxygen Reactions on Highly Oriented Pyrolytic Graphite," *Journal of the American Chemical Society*, vol. 113, no. 15, pp. 5588–5596, 1991.

[283] K. Morishita and T. Takarada, "Gasification behavior of carbon nanotubes," *Carbon*, vol. 35, no. 7, pp. 977–981, 1997.

[284] K. Morishita and T. Takarada, "Scanning electron microscope observation of the purification behaviour of carbon nanotubes," *Journal of Materials Science*, vol. 34, no. 6, pp. 1169–1174, 1999.

[285] T. Shimada *et al.*, "Points of onset of gasification in a multi-walled carbon nanotube having an imperfect structure," *Carbon*, vol. 42, no. 8-9, pp. 1635–1639, 2004.

[286] A. Delehouzé *et al.*, "Temperature induced transition from hexagonal to circular pits in graphite oxidation by O_2," *Applied Physics Letters*, vol. 99, no. 4, p. 044102, 2011.

[287] T. J. Cochell *et al.*, "Nanoscale oxidation behavior of carbon fibers revealed with in situ gas cell STEM," *Scripta Materialia*, vol. 199, p. 113820, 2021.

[288] P. Chávez-Gómez *et al.*, "Carbon fiber oxidation in combustion environments–Effect of flame chemistry and load on bundle failure," *Materials Today Communications*, vol. 31, p. 103560, 2022.

[289] P. Chávez-Gómez *et al.*, "Carbon fiber damage evolution under flame attack and the role of impurities," *Fire and Materials*, 2022.

[290] J. . Parker *et al.*, "Fire dynamics of modern aircraft from a materials point of view," *Journal of Fire and Flammability*, vol. 6, no. 4, pp. 534–553, 1975.

[291] C. P. Sarkos, S. J. C., and N. E. B., "Laboratory Fire Testing of Cabin Materials Used in Commercial Aircraft," *Journal of Aircraft*, vol. 16, no. 2, 78–89.

[292] H. Zhang, "Fire-safe polymers and polymer composites," Federal Aviation Administration, Tech. Rep., 2004, DOT/FAA/AR-04/11.

[293] Y.-H. Kao *et al.*, "Experimental study of the burner for FAA fire test: NexGen burner," *Fire and Materials*, vol. 41, no. 7, pp. 898–907, 2017.

[294] A. P. Mouritz, "Simple models for determining the mechanical properties of burnt FRP composites," *Materials Science and Engineering: A*, vol. 359, no. 1-2, pp. 237–246, 2003.

[295] J. M. Davies, Y. C. Wang, and P. M. H. Wong, "Polymer composites in fire," *Composites Part A: Applied Science and Manufacturing*, vol. 37, no. 8, pp. 1131–1141, 2006.

[296] S. Feih *et al.*, "Modeling compressive skin failure of sandwich composites in fire," *Journal of Sandwich Structures & Materials*, vol. 10, no. 3, pp. 217–245, 2008.

[297] A. P. Mouritz *et al.*, "Thermal–mechanical modelling of laminates with fire protection coating," *Composites Part B: Engineering*, vol. 48, pp. 68–78, 2013.

[298] E. Kandare *et al.*, "Thermo-mechanical Responses of Fiber-reinforced Epoxy Composites Exposed to High Temperature Environments. Part I: Experimental Data Acquisition," *Journal of Composite Materials*, vol. 44, no. 26, pp. 3093–3114, 2010.

[299] E. Kandare *et al.*, "Fiber-reinforced epoxy composites exposed to high temperature environments. part ii: modeling mechanical property degradation," *Journal of composite materials*, vol. 45, no. 14, pp. 1511–1521, 2011.

[300] D. Swanson and J. Wolfrum, "Time to failure modeling of carbon fiber reinforced polymer composites subject to simultaneous tension and one-sided heat flux," *Journal of Composite Materials*, vol. 52, no. 18, pp. 2503–2514, 2018.

[301] S. Feih *et al.*, "Strength degradation of glass fibers at high temperatures," *Journal of Materials Science*, vol. 44, no. 2, pp. 392–400, 2009.

[302] T. Pardessus, "Concurrent engineering development and practices for aircraft design at Airbus," in *Proceedings of the 24th International Congress of Aeronautical Sciences, Yokohama, Japan, 29 August - 3 September*, 2004.

[303] E. Fricke and A. P. Schulz, "Design for changeability (DfC): Principles to enable changes in systems throughout their entire lifecycle," *Systems Engineering*, vol. 8, no. 4, pp. 342–359, 2005.

[304] G. Reinman *et al.*, "Design for variation," *Quality Engineering*, vol. 24, no. 2, pp. 317–345, 2012.

[305] T. W. Liao, "A Fuzzy Multicriteria Decision-Making Method for Material Selection," *Journal of Manufacturing Systems*, vol. 15, no. 1, pp. 1–12, 1996.

[306] C. Kahraman, "Multi-criteria decision making methods and fuzzy sets," in *Fuzzy Multi-Criteria Decision Making*, C. Kahraman, Ed. Springer, 2008, pp. 1–18.

[307] T.-S. Liou and M.-J. J. Wang, "Ranking fuzzy numbers with integral value," *Fuzzy Sets and Systems*, vol. 50, no. 3, pp. 247–255, 1992.

[308] N. P. Suh, *The Principles of Design*. Oxford University Press, 1990.

[309] T. R. Marker, "Technology Readiness Levels," Tech. Rep., April 1995, white Paper.

[310] R. E. Lyon and M. L. Janssens, "Polymer Flammability," Federal Aviation Administration, Tech. Rep., May 2005, DOT/FAA/AR-05/14.

[311] P. Gu and R. J. Asaro, "Designing polymer matrix composite panels for structural integrity in fire," *Composite Structures*, vol. 84, no. 4, pp. 300–309, 2008.

[312] P. Gu and R. J. Asaro, "Designing sandwich polymer matrix composite panels for structural integrity in fire," *Composite Structures*, vol. 88, no. 3, pp. 461–467, 2009.

[313] K. L. Edwards, "Selecting materials for optimum use in engineering components," *Materials & design*, vol. 26, no. 5, pp. 469–473, 2005.

[314] Trippe, Anthony, "Guidelines for Preparing Patent Landscape Reports," 2015, Guidelines prepared for the World Intellectual Property Organization (WIPO) [Online; accessed May, 8, 2022]. [Online]. Available: https://www.wipo.int/edocs/pubdocs/en/wipo_pub_946.pdf

[315] U. Sorathia and C. Beck, "Fire-screening results of polymers and composites," in *Improved Fire- and Smoke-Resistant Materials for Commercial Aircraft Interiors*, 1995.

[316] U. Sorathia *et al.*, "Screening Tests for Fire Safety of Composites for Marine Applications," *Fire and Materials*, vol. 25, no. 6, pp. 215–222, 2001.

[317] M. Jimenez, S. Duquesne, and S. Bourbigot, "Characterization of the performance of an intumescent fire protective coating," *Surface and Coatings Technology*, vol. 201, no. 3-4, pp. 979–987, 2006.

[318] ASTM International, "Standard Test Method for Tensile Properties of Polymer Matrix Composite Materials," 2017, D3039/D3039M-17.

[319] ASTM International, "Standard Test Method for Compressive Residual Strength Properties of Damaged Polymer Matrix Composite Plates," 2017, D7137/D71737M-17.

[320] A. G. Gibson *et al.*, "Modelling residual mechanical properties of polymer composites after fire," *Plastics, Rubber and Composites*, vol. 32, no. 2, pp. 81–90, 2003.

[321] H. Luinge *et al.*, "Burn-Through Aspects of Fuselage Structures: Sandwich versus Monolithic Design with Aluminium or Composite Materials," in *SAMPE Europe Technical Conference and "Table Top" Exhibition. Toulouse, France.* Society for the Advancement of Material and Process Engineering, 2006.

[322] G. G. Ren, P. J. Hogg, and D. H. Woolstencroft, "Development of low cost ceramic moulding composites as fire barriers," *Advances in Applied Ceramics*, vol. 108, no. 5, pp. 319–324, 2009.

[323] B. Vieille, C. Lefebvre, and A. Coppalle, "Post fire behavior of carbon fibers Polyphenylene Sulfide-and epoxy-based laminates for aeronautical applications: A comparative study," *Materials and Design*, vol. 63, pp. 56–68, 2014.

[324] P. Vollaro *et al.*, "Intumescent Coatings for Protection of Composites for Aircraft Application," in *16th European Conference on Composite Materials (ECCM16), Seville, Spain, June 22–26*, 2014.

[325] B. Vieille *et al.*, "Correlation between post fire behavior and microstructure degradation of aeronautical polymer composites," *Materials and Design*, vol. 74, pp. 76–85, 2015.

[326] P. Parlevliet and M. Geistbeck, "Investigations into lightweight solutions for epoxy composite fire property improvement," *Plastics, Rubber and Composites*, vol. 44, no. 3, pp. 104–110, 2015.

[327] N. Grange *et al.*, "Fire resistance of carbon-based composite materials under both ideal and realistic normative configurations," *Applied Thermal Engineering*, vol. 159, p. 113834, 2019.

[328] T. C. Chu, S. C. Yen, and J. Ramalingan, "Assessment of Fire Damage on Composite Materials from Surface Features," in *9th International Conference on Composite Materials (ICCM 9), Madrid, Spain, July 12-16*. International Committee on Composite Materials, 1993.

[329] H. L. McManus, "Prediction of Fire Damage to Composite Airfract Structures," in *9th International Conference on Composite Materials (ICCM 9), Madrid, Spain, July 12–16*. International Committee on Composite Materials, 1993.

[330] D. T. Misciagna and D. J. Landi, "Integrated Ceramic Composite Firewall," in *Aerospace Technology Conference and Exposition*. SAE International, 2005.

[331] I. Roese-Koerner *et al.*, "Fire protected carbon fibre reinforced plastics for structural aircraft components," in *20th International Conference on Composite Materials, Copenhagen Denmark, July 19–24*, 2015.

[332] P. Golewski and T. Sadowski, "A novel application of alumina fiber mats as TBC protection for CFRP/epoxy laminates–Laboratory tests and numerical modeling," *Journal of the European Ceramic Society*, vol. 38, no. 8, pp. 2920–2927, 2018.

[333] E. Schuhler *et al.*, "Behaviour of aeronautical polymer composite to flame: A comparative study of thermoset- and thermoplastic-based laminate," *Polymer Degradation and Stability*, vol. 152, pp. 105–115, 2018.

[334] P. Chávez Gómez *et al.*, "Evaluation of the fire resistance of protected carbon/epoxy laminates in small-scale experiments," in *AIAA SciTech 2019 Forum, San Diego, CA, January 7–11*. American Institute of Aeronautics and Astronautics, 2019.

[335] E. Schuhler *et al.*, "Fire behaviour of composite materials using kerosene burner tests at small-scales," *Fire Safety Journal*, vol. 121, p. 103290, 2021.

[336] B. Vieille *et al.*, "Kerosene flame behaviour of C/PEKK composite laminates: Influence of exposure time and laminates lay-up on residual mechanical properties," *Composites Part B: Engineering*, vol. 222, p. 109046, 2021.

[337] P. G. B. Seggewiß, "Methods to evaluate the fire resistance of carbon fiber reinforced plastics," in *Proceedings of the 60th SAMPE symposium & technical exhibition, Long Beach, CA*, 2004.

[338] K. Grigoriou and A. P. Mouritz, "Influence of ply stacking pattern on the structural properties of quasi-isotropic carbon-epoxy laminates in fire," *Composites Part A: Applied Science and Manufacturing*, vol. 99, pp. 113–120, 2017.

[339] S. Timme *et al.*, "Fire stability of carbon fiber reinforced polymer shells on the intermediate-scale," *Composite Structures*, vol. 178, pp. 320–329, 2017.

[340] W. Tabaka *et al.*, "Bench-scale fire stability testing – Assessment of protective systems on carbon fibre reinforced polymer composites," *Polymer Testing*, vol. 102, p. 107340, 2021.

[341] Granta Design Limited, "Granta ces 2012 edupack," version 11.9.9.

[342] N. Aeronautics and S. Administration, "MAPTIS - Materials And Processes Technical Information System," 2020, [Online; accessed November 16, 2020]. [Online]. Available: https://maptis.nasa.gov/Home

[343] A. L. Bauer and M. E. Rogalski, "Methods and apparatus to increase fire resistance and fracture toughness of a composite structure," Jul. 2020, U.S. Patent no. 10,710,348 B2.

[344] F. D. Blair and G. E. Green, "Fire resistant composite panel," Jan. 2003, U.S. Patent no. 6,511,730 B1.

[345] D. A. Buchacher, "Composite member with integrated thermal protection," Jan. 1989, U.S. Patent no. 4,801,496.

[346] M. R. Buckingham, F. D. Blair, and C. J. E. Harrington, "Composite panel with fire resistant face sheets," Jan. 2006, U.S. Patent no. 6,992,027 B1.

[347] N. R. Byrd and J. K. Donahoe, "Fire barrier compositions and composites," Mar. 1981, U.S. Patent no. 4,255,483.

[348] W. T. Chee, D. McLaren, and K. E. Therrien, "Composite material structure with integral fire protection," Aug. 1988, U.S. Patent no. 4,767,656.

[349] P. D. Christou, "Fibrous reinforcement suitable as fireproofing agent," May 2006, U.S. Patent no. 7,045,203 B2.

[350] R. M. Fay *et al.*, "Burn through resistant systems for transportation, especially aircraft," May 2003, U.S. Patent no. 6,565,040 B2.

[351] B. M. Fell and P. R. Ciriscioli, "Heat insulating blanket," Jun. 1985, U.S. Patent no. 4,522,673.

[352] M. L. Fellman, "Composite firewall structure," Jan. 2003, U.S. Patent no. 6,503,596 B1.

[353] F. J. Gorges, "Light-weight, fire-retardant structural panel," Dic. 1985, U.S. Patent no. 4,557,961.

[354] R. Heitkamp, "High temperature 2000 degrees-f burn-through resistant composite sandwich panel," Oct. 1995, U.S. Patent no. 5,460,864.

[355] D. López Fernández and M. A. García Patino, "Fireproof polymer matrix composite structure," November 2020, European Patent no. 3 248 774 B1.

[356] J. E. Meaney, J. K. Switzer, and R. L. Till, "Lightweight fire protection arrangement for aircraft gas turbine jet engine and method," Nov. 1999, U.S. Patent no. 5,976,997.

[357] D. T. Misciagna, D. J. Landi, and P. G. Persaud, "Monolithic composite firewall," Mar. 2005, U.S. Patent no. 6,863,980 B2.

[358] R. Mueller *et al.*, "Aircraft fuselage having burnthrough resistant components," Jan. 2018, U.S. Patent no. 9,878,770 B2.

[359] J. J. Sang *et al.*, "Multifunctional surfacing material with burn-through resistance," Aug 2021, U.S. Patent no. 11,108,220 B2.

[360] W. Schafer and G. Schaut, "Flame penetration blocker for fuselages," Jan. 1997, U.S. Patent no. 5,595,817.

[361] U. A. K. Sorathia and V. Castelli, "Fire-resistant barriers for composite materials," Aug. 1993, U.S. Patent no. 5,236,773.

[362] C. Sourdet, "Fire-resistant cowls, particularly for aircraft engines," Apr. 1988, U.S. Patent no. 4,735,841.

[363] U. Sorathia, C. M. Rollhauser, and W. A. Hughes, "Improved Fire Safety of Composites for Naval Applications," *Fire and Materials*, vol. 16, no. 3, pp. 119–125, 1992.

[364] J. G. R. Hansen and B. J. Frame, "Flame penetration and burn testing of fire blanket materials," *Fire and Materials*, vol. 32, no. 8, pp. 457–483, 2008.

[365] K. D. Tran, "Burn-through Resistance of Fibre/Felt Materials for Aircraft Fuselage Insulation Blankets," *Fire and Materials*, vol. 26, no. 1, pp. 1–6, 2002.

[366] A. G. Gibson *et al.*, "Modeling composite high temperature behavior and fire response under load," *Journal of Composite Materials*, vol. 46, no. 16, pp. 2005–2022, 2012.

[367] T. Pelzmann *et al.*, "Surface temperature and emissivity measurement for materials exposed to a flame through two-color ir-thermography," *arXiv preprint arXiv:2203.09689*, 2022.

[368] P. Chávez Gómez *et al.*, "Fuel Effect on the Tensile Strength Evolution of Carbon Fibres under Direct Flame Attack," in *22nd International Conference on Composite Materials (ICCM22), Melbourne, Australia, August 11–16*. International Committee on Composite Materials, 2019.

[369] Q. Zhang *et al.*, "Effects of structural parameters on the thermal insulation properties of coated carbon fiber fabrics," *Textile Research Journal*, vol. 90, no. 13-14, pp. 1549–1557, 2020.

[370] T. R. Marker, "A Comparison of Propane and Kerosene Burners for Cargo Compartment Burnthrough Testing," Federal Aviation Administration, Tech. Rep., 1987, DOT/FAA/CT-TN87/45.

[371] S. Le Neve and G. Marlair, "Alternative jets fuels: effect of a fuel change on aircraft fire safety," in *EASA Headquarters/International Aircraft Systems Fire Protection Working Group Meeting (IASFPWG)*, 2012.

[372] C. Sauder, J. Lamon, and R. Pailler, "Thermomechanical properties of carbon fibres at high temperatures (up to 2000 °C)," *Composites Science and Technology*, vol. 62, no. 4, pp. 499–504, 2002.

[373] C. Sauder, J. Lamon, and R. Pailler, "The tensile behavior of carbon fibers at high temperatures up to 2400 °C," *Carbon*, vol. 42, no. 4, pp. 715–725, 2004.

[374] H. Rennhofer *et al.*, "Structural development of PAN-based carbon fibers studied by in situ X-ray scattering at high temperatures under load," *Carbon*, vol. 48, no. 4, pp. 964–971, 2010.

[375] H. Rennhofer *et al.*, "The structural evolution of multi-layer graphene stacks in carbon fibers under load at high temperature–A synchrotron radiation study," *Carbon*, vol. 80, pp. 373–381, 2014.

[376] L. Liu *et al.*, "On the Oxidative Ablation and Mechanical Properties of T300 Carbon Fibers at Elevated Temperatures," *Materials Performance and Characterization*, vol. 7, no. 1, pp. 113–125, 2018.

[377] *HexTow® AS4 Carbon Fiber Product Data Sheet*, Hexcel Corp., CTA 311 JA20. [Online]. Available: https://www.hexcel.com/user_area/content_media/raw/AS4_HexTow_DataSheet.pdf

[378] *HexTow® IM7 Carbon Fiber Product Data Sheet*, Hexcel Corp., CTA 351 NV20. [Online]. Available: https://www.hexcel.com/user_area/content_media/raw/IM7_HexTow_DataSheet.pdf

[379] *HexTow® HM63 Carbon Fiber Product Data Sheet*, Hexcel Corp., CTA 355 NV20. [Online]. Available: https://www.hexcel.com/user_area/content_media/raw/HM63_Aerospace_HexTow_DataSheet.pdf

[380] P. Weigand, R. Lückerath, and W. Meier, "Documentation of flat premixed laminar CH4/air standard flames: Temperatures and species concentrations," 2003, [Online; accessed May 7, 2020]. [Online]. Available: http://www.dlr.de/vt/datenarchiv

[381] ASTM International, "Standard Terminology Relating to Thermal Analysis and Rheology," 2022, E473-22.

[382] W. Jiang *et al.*, "Thermal analysis of the oxidation of natural graphite—-effect of particle size," *Thermochimica Acta*, vol. 351, no. 1-2, pp. 85–93, 2000.

[383] E. R. Trumbauer, J. R. Hellmann, and L. E. Jones, "Oriented microchannel membranes via oxidation of carbon-fiber-reinforced glass composites," *Carbon*, vol. 30, no. 6, pp. 873–882, 1992.

[384] J. Langot *et al.*, "Modeling the thermal decomposition and residual mass of a carbon fiber epoxy matrix composite with a phenomenological approach: effect of the reaction scheme," *Fire and Materials*, vol. 46, pp. 262–276, 2022.

[385] M. T. Konnik, F. Panerai, and K. A. Stephani, "The role of impurities and degradation on the thermal conductivity of carbon fiber and amorphous carbon," *Carbon Trends*, p. 100151, 2022.

[386] X. Yang *et al.*, "Temperature and OH concentration measurements by ultraviolet broadband absorption of OH(X) in laminar methane/air premixed flames," *Fuel*, vol. 288, p. 119666, 2021.

[387] H. Kroto, "Space, Stars, C_{60}, and Soot," *Science*, vol. 242, no. 4882, pp. 1139–1145, 1988.

[388] J. B. Howard *et al.*, "Fullerenes C_{60} and C_{70} in flames," *Nature*, vol. 352, no. 6331, pp. 139–141, 1991.

[389] P. Salatino, F. Miccio, and L. Massimilla, "Combustion and Percolative Fragmentation of Carbons," *Combustion and Flame*, vol. 95, no. 4, pp. 342–350, 1993.

[390] F. Panerai *et al.*, "Experimental measurements of the high-temperature oxidation of carbon fibers," *International Journal of Heat and Mass Transfer*, vol. 136, pp. 972–986, 2019.

[391] S. Gandhi, R. Lyon, and L. Speitel, "Potential health hazards from burning aircraft composites," *Journal of Fire Sciences*, vol. 17, no. 1, pp. 20–41, 1999.

[392] A. P. Mourtiz, "Review of Smoke Toxicity of Fiber-Polymer Composites Used in Aircraft," *Journal of Aircraft*, vol. 46, no. 3, pp. 737–745, 2009.

[393] R. Perret and W. Ruland, "The Microstructure of PAN-Base Carbon Fibres," *Journal of Applied Crystallography*, vol. 3, no. 6, pp. 525–532, 1970.

[394] L. Shi *et al.*, "High-temperature oxidation of carbon fiber and char by molecular dynamics simulation," *Carbon*, vol. 185, pp. 449–463, 2021.

[395] F. S. Kachold *et al.*, "Mechanical Properties, Surface Structure, and Morphology of Carbon Fibers Pre-heated for Liquid Aluminum Infiltration," *Journal of Materials Engineering and Performance*, vol. 25, no. 4, pp. 1502–1507, 2016.

[396] I. M. Pickup, B. McEnaney, and R. G. Cooke, "Fracture processes in graphite and the effects of oxidation," *Carbon*, vol. 24, no. 5, pp. 535–543, 1986.

[397] R. T. K. Baker, "In Situ Electron Microscopy Studies of Catalyst Particle Behavior," *Catalysis Reviews—Science and Engineering*, vol. 19, no. 2, pp. 161–209, 1979.

[398] L. E. Jones and P. A. Thrower, "Influence of boron on carbon fiber microstructure, physical properties, and oxidation behavior," *Carbon*, vol. 29, no. 2, pp. 251–269, 1991.

[399] W. P. Hoffman, "Scanning probe microscopy of carbon fiber surfaces," *Carbon*, vol. 30, no. 3, pp. 315–331, 1992.

[400] P. Serp and J. L. Figueiredo, "An investigation of vapor-grown carbon fiber behavior towards air oxidation," *Carbon*, vol. 35, no. 5, pp. 675–683, 1997.

[401] D. Cho *et al.*, "Microscopic Behavior on the Protection of Polyacrylonitrile-based Carbon Fibers from Thermal Oxidation," *Polymer Journal*, vol. 29, no. 12, pp. 959–963, 1997.

[402] S.-S. Tzeng *et al.*, "Study of Oxidation of Carbon Fibers Using Resistance Measurement," *Journal of Materials Engineering and Performance*, vol. 19, no. 9, pp. 1352–1356, 2010.

[403] F. Panerai *et al.*, "Flow-tube Oxidation Experiments on the Carbon Preform of PICA," in 44^{th} *AIAA Thermophysics Conference, San Diego, CA, June 24–27.* American Institute of Aeronautics and Astronautics, 2013.

[404] F. Stevens, L. A. Kolodny, and T. P. Beebe Jr., "Kinetics of Graphite Oxidation: Monolayer and Multilayer Etch Pits in HOPG Studied by STM," *The Journal of Physical Chemistry B*, vol. 102, no. 52, pp. 10 799–10 804, 1998.

[405] K. T. Nicholson, T. K. Minton, and S. J. Sibener, "Temperature-dependent morphological evolution of HOPG graphite upon exposure to hyperthermal O(^{3}P) atoms," *Progress in Organic Coatings*, vol. 47, no. 3-4, pp. 443–447, 2003.

[406] V. Johánek *et al.*, "Real-time observation of graphene oxidation on Pt(111) by low-energy electron microscopy," *Surface Science*, vol. 644, pp. 165–169, 2016.

[407] A. Tomita and Y. Tamai, "An optical microscopic study on the catalytic hydrogenation of graphite," *The Journal of Physical Chemistry*, vol. 78, no. 22, pp. 2254–2258, 1974.

[408] V. J. Murray, E. J. Smoll Jr., and T. K. Minton, "Dynamics of Graphite Oxidation at High Temperature," *The Journal of Physical Chemistry C*, vol. 122, no. 12, pp. 6602–6617, 2018.

[409] B. McCarroll and D. W. McKee, "Interaction of atomic hydrogen and nitrogen with graphite surfaces," *Nature*, vol. 225, no. 5234, pp. 722–723, 1970.

[410] C. A. Schneider, W. S. Rasband, and K. W. Eliceiri, "NIH Image to ImageJ: 25 years of image analysis," *Nature methods*, vol. 9, no. 7, pp. 671–675, 2012.

[411] B. M. Townes and J. W. Hilborn, "The SLOWPOKE-2 reactor with low enrichment uranium oxide fuel," Atomic Energy of Canada Ltd., Tech. Rep., 1985.

[412] M. Abdollahi Neisiani *et al.*, "Novel approach in k_0-NAA for highly concentrated REE Samples," *Talanta*, vol. 180, pp. 403–409, 2018.

[413] C. A. Gaulin and H. A. Katzman, "Enhanced carbon fiber combustion using a catalyst," 11 1985, uS Patent 4,551,487.

[414] J. P. A. Neeft, M. Makkee, and J. A. Moulijn, "Catalytic oxidation of carbon black-—I. Activity of catalysts and classification of oxidation profiles," *Fuel*, vol. 77, no. 3, pp. 111–119, 1998.

[415] D. W. McKee and D. Chatterji, "The catalytic behavior of alkali metal carbonates and oxides in graphite oxidation reactions," *Carbon*, vol. 13, no. 5, pp. 381–390, 1975.

[416] A. Yoshida, Y. Hishiyama, and M. Inagaki, "Exfoliation of vapor-grown graphite fibers as studied by scanning electron microscope," *Carbon*, vol. 28, no. 4, pp. 539–543, 1990.

[417] A. Takaku and M. Shioya, "X-ray measurements and the structure of polyacrylonitrile- and pitch-based carbon fibres," *Journal of Materials Science*, vol. 25, no. 11, pp. 4873–4879, 1990.

[418] J. Rouquerol *et al.*, "Recommendations for the characterization of porous solids (Technical Report)," *Pure and Applied Chemistry*, vol. 66, no. 8, pp. 1739–1758, 1994.

[419] G. A. Hazelrigg, "A Framework for Decision-Based Engineering Design," *Journal of Mechanical Design*, vol. 120, no. 4, pp. 653–658, December 1998.

[420] G. A. Hazelrigg, "An Axiomatic Framework for Engineering Design," *Journal of Mechanical Design*, vol. 121, no. 3, pp. 342–347, September 1999.

[421] E. K. Antonsson and K. N. Otto, "Imprecision in Engineering Design," *Journal of Vibration and Acoustics*, vol. 117, no. B, pp. 25–32, 1995.

[422] Z. Li *et al.*, "Microstructural evolution during oxidative ablation in air for polyacrylonitrile based carbon fibers with different graphite degrees," *Surface and Interface Analysis*, vol. 45, no. 4, pp. 787–792, 2013.

APPENDIX A SUPPLEMENTARY MATERIAL OF ARTICLE #3

A.1 Elemental analysis: NAA results

Table A.1 shows the impurity concentrations determined by Neutron Activation Analysis (NAA) for each fiber type. Values shown as XXX (XXX) denote concentration and uncertainty of confirmed elements. Values preceded by $<$ correspond to elements that were not possible to be confirmed, although their presence is possible at lower concentrations. For instance, silicon (Si) concentration was not possible to be determined. It could represent the second impurity in terms of prevalence for the three fibers. Its exact concentrations remains undetermined although Figs. A.1b A.3b reveal its presence in amorphous residues over damaged areas, supporting the main article's observations.

Table A.1 Fiber impurity levels obtained by Neutron Activation Analysis (NAA).

Element	Concentration [ppm]		
	AS4	IM7	HM63
Na	1024 (41)	1079 (43)	11.9 (0.5)
Mg	2.74 (0.75)	3.19 (0.74)	2.70 (0.24)
Al	9.20 (0.40)	12.2 (0.5)	5.63 (0.24)
Si	< 420	< 450	< 120
S	< 320	< 360	< 60
Cl	4.72 (0.34)	6.57 (0.42)	18.6 (0.8)
K	< 70	< 40	< 20
Ca	16.2 (2.2)	14.1 (2.6)	20.1 (1.3)
Sc	< 0.007	< 0.008	< 0.003
Ti	< 2	< 1	0.698 (0.107)
V	< 0.007	< 0.008	0.103 (0.004)
Cr	< 0.5	< 0.9	< 0.4
Mn	0.0447 (0.0029)	0.0713 (0.0200)	0.0381 (0.0040)
Fe	< 70	< 70	< 20
Co	< 0.2	< 0.2	< 0.07
Ni	< 20	< 8	< 20
Cu	< 0.5	< 0.9	0.150 (0.039)
Zn	< 8	< 7	< 2
As	< 0.02	< 0.02	< 0.006
Se	< 0.4	< 0.4	< 0.4
Br	0.0815 (0.0166)	0.180 (0.019)	0.064 (0.005)
Rb	< 2	< 2	< 0.4
Zr	< 50	< 30	< 20
Mo	< 0.2	< 0.09	< 0.08
Ag	< 0.3	< 0.4	< 0.09
Cd	< 0.2	< 0.2	< 0.09
In	< 0.001	< 0.0008	< 0.0002
Sn	< 0.7	< 0.5	< 0.2
Sb	0.0126 (0.0019)	0.0361 (0.0023)	0.0089 (0.00088)
I	0.0440 (0.0056)	0.0781 (0.0072)	1.54 (0.06)
Cs	< 0.08	< 0.06	< 0.02
Ba	< 6	< 5	< 2
La	< 0.008	< 0.01	< 0.006
Hf	< 0.04	< 0.04	< 0.02
W	< 0.03	< 0.04	< 0.04
Au	< 0.0002	< 0.0003	< 0.0002
Hg	0.266 (0.055)	0.113 (0.057)	< 0.05
Th	< 0.03	< 0.3	< 0.02
U	< 0.02	< 0.02	< 0.02

Concentration (Uncertainty)

A.2 Elemental analysis: EDS spectra

The following figures show additional EDS spectra of some of the same fibers shown in the main text. Relatively clean and impurity-rich regions yield contrasting elemental signatures.

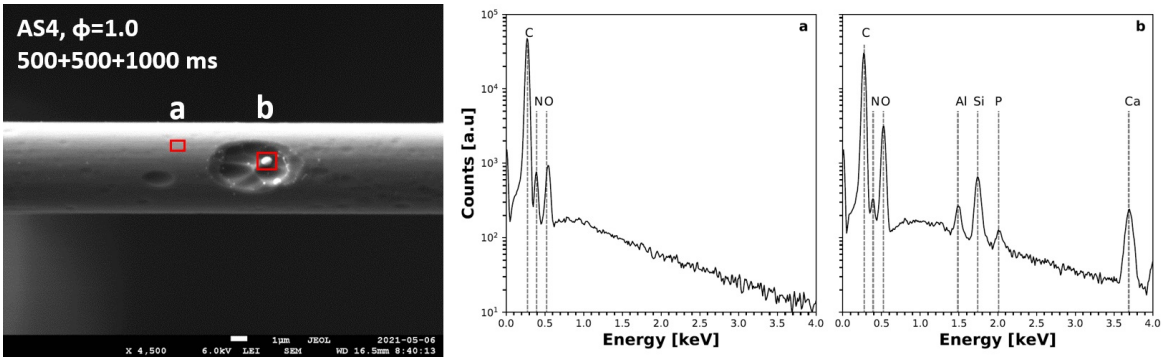

Figure A.1 AS4 fiber's SEM image (left) with EDS spectra from: a) smooth skin region and b) mega pit with residue and internal sub-pits.

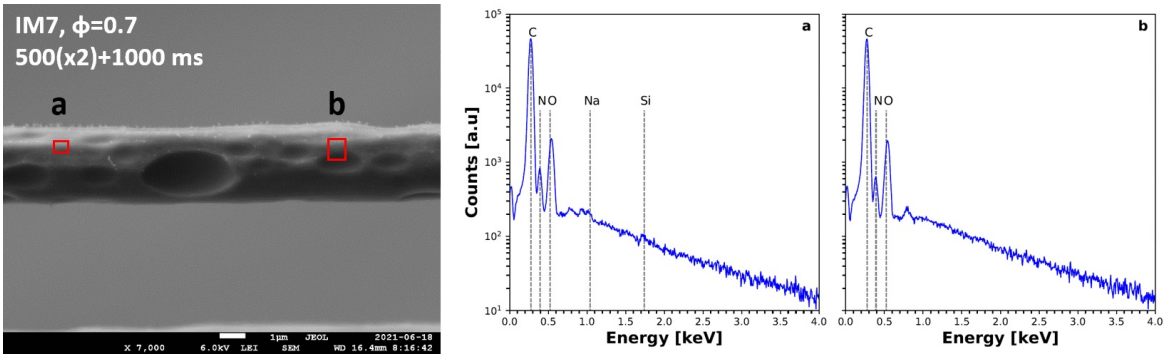

Figure A.2 IM7 fiber's SEM image (left) with EDS spectra from: a) smooth fiber portion and b) large pit inner and outer portions.

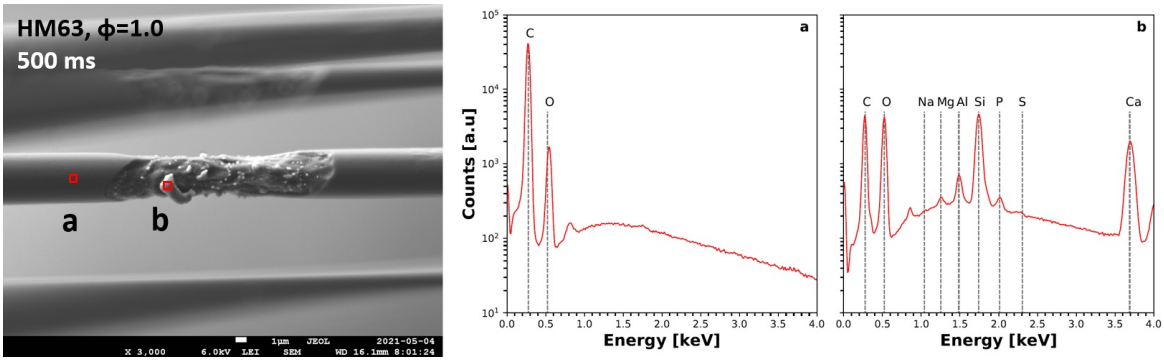

Figure A.3 HM63 fiber's SEM image (left) with EDS spectra from: a) smooth skin region and b) Si-based flake within the hourglass-like damaged region.

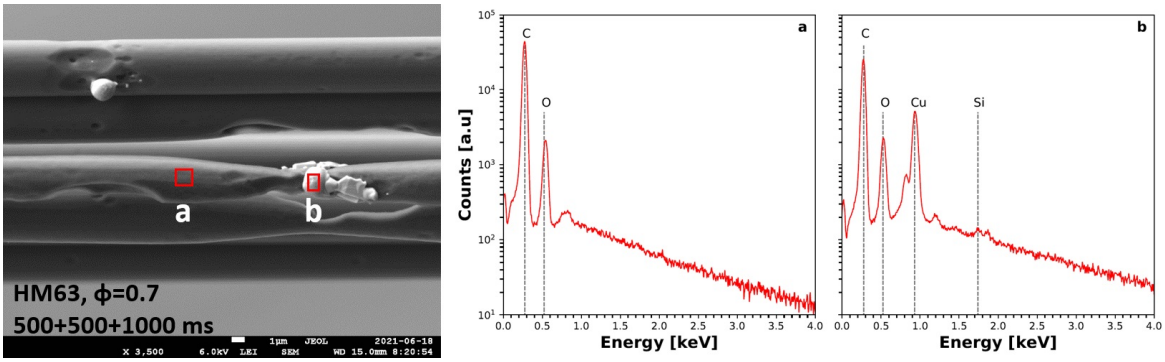

Figure A.4 HM63 fiber's SEM image (left) with EDS spectra from: a) smooth skin region and b) amorphous Cu-based impurity within the hourglass-like damaged region.

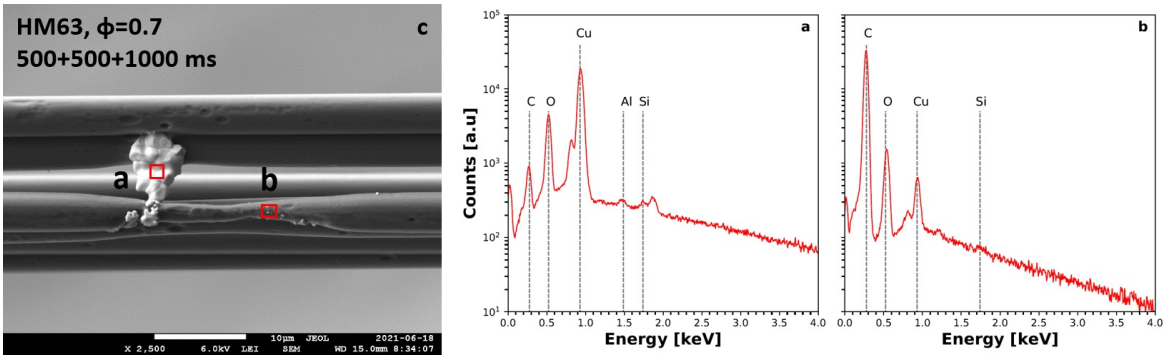

Figure A.5 HM63 fiber's SEM image (left) with EDS spectra from: a) amorphous Cu-based impurity seemingly stuck between fibers and b) thinned region within the hourglass-like damaged region.

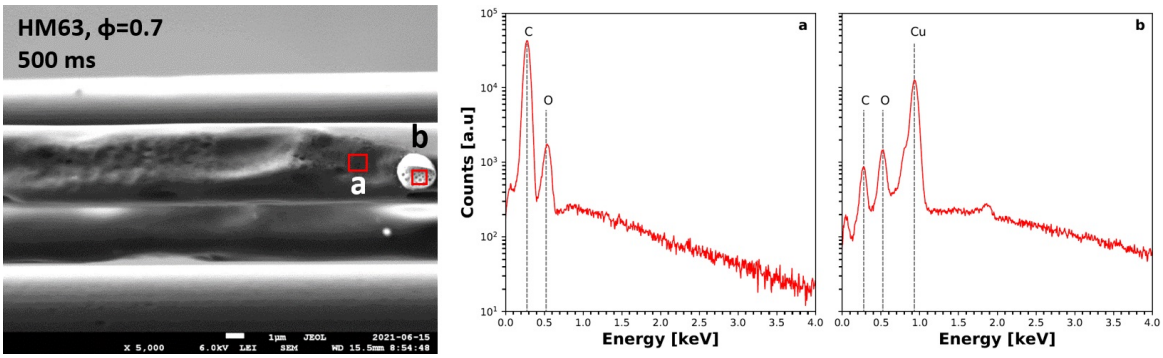

Figure A.6 HM63 fiber's SEM image (left) with EDS spectra from: a) damaged region by mobile impurity and b) Cu-based mobile impurity.